THE UNIVERSITY
of EDINBURGH

Developing a patient-derived induced pluripotent stem cell model to understand the clinical and pathological changes in macular degeneration

Shyamanga Borooah

Submitted in satisfaction of the requirements for the degree of

PhD

University of Edinburgh

2016

Declaration

I certify:

(a) that the thesis has been composed by me, and

(b) either that the work is my own, or, where I have been a member of a research group, that I have made a substantial contribution to the work, such contribution being clearly indicated, and

(c) that the work has not been submitted for any other degree or professional qualification except as specified.

Shyamanga Borooah

Acknowledgements

During the course of the work for this thesis I have been fortunate enough to meet a variety of wonderful people who have provided support and guidance.
Firstly, I would like to thank my supervisors Professor Siddharthan Chandran and Professor Baljean Dhillon and collaborators Professor Alan Wright, Professor Sir Ian Wilmut and Professor Paul Barlow for guiding me through various stages of the work presented.
I am also grateful to my resident laboratory team in particular Dr Karen Burr, David Story, Dr Bhuvaneish Thangar, Dr Navneet Vasistha, Dr Nina Rzechozek, Chen Zhao, Dr Dario Magnani, Elaine Cleary, Dr Bilada Bilican and Ghazal Haghi for their assistance with technical details throughout the work. There were also many others without swhose help the project would not be completed at differente universities. I would like to acknowledge their contribution.
University of Edinburgh: Dr Chloe Stanton, Stephen Mitchell, Dr Andy Herbert, Dr Pierre Bagnaninchi, Tyson Reutz, Dr Andrew Smith, Dr James Cameron, Professor James Ironside, Dr Wesam Gamal
University of Wisconsin, Madison: Professor David Gamm, Kyle Wallace, Dr Wei Shen, Dr Ruchira Singh and Dr Joseph Philips.
University of Cambridge: Professor Ludovic Vallier, Imbisaat Geti, Filipa Soares
University College London: Dr Anai Gonzalez-Cordero, Professor Robin Ali, Professor James Bainbridge, Dr Rachel Pearson and Yanai Duran.
University of California San Diego: Professor Radha Ayyagari

In addition, I would like to thank the funders of the research including the Wellcome Trust under the Scottish Translational Medicine and Therapeutics initiative and the Eyecare trust without whom the research would not have been possible.

Finally, I would like to give my thanks to my wife Prarthana Goswami for her patience during these studies and my mother Mrs Geeta Borooah and sister Ms Meenakhi Borooah for their ongoing support during this project.

Abstract

Late-onset retinal macular degeneration (L-ORMD) is a fully penetrant autosomal dominant macular degeneration resulting from a Ser163Arg substitution in the gene encoding the protein C1QTNF5. Clinically L-ORMD results in dark adaptation delay in the fifth decade, central visual loss in the sixth decade and further progressive visual field loss in successive decades of life. Pathologically the disease results in thick sub-retinal deposits, which have a similar composition to drusen seen in AMD, retinal pigment epithelial (RPE) loss, and neuro-retinal atrophy. The function of C1QTNF5 is incompletely understood however within the eye it is expressed most strongly by the RPE cells.

An *in vitro* model for L-ORMD was developed using human induced pluripotent stem cells (hiPSCs) derived from patients and with stem cells from patient's unaffected siblings used as controls. The hiPSCs were differentiated to RPE (hiPSC-RPE). L-ORMD hiPSC-RPE shared baseline characteristics with sibling control hiPSC-RPE. In order to model *in vivo* conditions hiPSC-RPE were grown on permeable supports in human serum enriched media. Case hiPSC-RPE cell lines were found to activate the complement pathway resulting in increased deposition of the terminal complement complex (TCC) C5b-9 when compared to control hiPSC-RPE. Using depleted serum, deposition was not affected by depletion of classical and lectin pathway components but was reduced by depletion of alternative complement pathway components. Depletion of complement components C3 and C5 abolished TCC deposition. The addition of a monoclonal antibody against C5 also reduced TCC deposition.

The role of complement dysregulation in L-ORMD pathogenesis was confirmed by immunostaining of L-ORMD and age-matched control human donor retinal sections. L-ORMD retinal sections displayed increased C3d and C5b-9 deposition. Using mutant and wild type-protein generated from a bacterial expression system it was found that the mutant protein was less stable than the wild-type. In addition the wild type protein formed multimers whilst the mutant was mainly monomeric. A surface plasmon resonance (SPR) study showed an increased affinity of wild-type C1QTNF5, especially in multimeric form for complement factor H (CFH), a key regulator of the alternative complement pathway when compared to mutant protein.

Taken together these studies implicate dysfunction of the alternative complement pathway in L-ORMD disease mechanism and have suggested a role for C1QTNF5 in the extracellular matrix. The studies also show that L-ORMD and AMD share a pathogenic and clinical similarities.

Lay Summary

Age-related macular degeneration (AMD) is the commonest cause of blindness in the developed world. The number of people suffering with AMD continues to increase placing burdens on health and social care systems worldwide. There are two main forms of AMD. The first is wet AMD in which leakage from blood vessels at the back of the eye results in visual loss. The second and commonest form of AMD is dry AMD, which results from deposits forming under the retina. In dry AMD there is a slow loss of retinal cells eventually leading to visual loss. Currently there are no treatments to modify the progression of dry AMD. Understanding AMD disease mechanism and the development of new treatments has been hampered by the lack of clinically relevant models This highlights the need to develop new platforms that adequately model human disease in order to develop new treatments for AMD. However, AMD is a highly variable disease which makes it difficult to study.

Late-onset retinal macular degeneration (L-ORMD) is a severe inherited form of macular degeneration resulting from the mutation in the gene that codes the protein C1QTNF5. Unlike AMD all patients who carry the gene mutation associated with L-ORMD undergo retinal degeneration in a step-wise manner. The disease recapitulates key clinical and pathological characteristics of AMD, which make it a good model disorder for AMD.

In this dissertation, I describe how I developed a model for macular degeneration using stem cells derived from patients with L-ORMD. The model implicated dysfunction in regulation of an innate immune pathway known as the complement system in L-ORMD disease mechanism. This suggests that AMD and L-ORMD share a common disease mechanism. The finding was verified in both a mouse model of L-ORMD and in human L-ORMD retinal donor samples. An interaction was found between C1QTNF5, the protein mutated in L-ORMD and one of the key regulators of the complement pathway an innate immune system, suggesting a role for L-ORMD in the eye. Complement was found tot be abnormally activated in L-ORMD eyes. By targeting components of the complement pathway, it was possible to abolish the abnormal complement system activity and restore normal cell function highlighting a potential target for treating both AMD and L-ORMD.

Contents

List of abbreviations

ABC…….….. Ammonium Bicarbonate
ABCA4…….….. ATP-binding cassette, sub-family A, member 4
ACN……..……..…….….. Acetonitrile
aHUS……..…Atypical haemolytic-uraemic syndrome
AMD…….…Age-related macular degeneration
APOE……..Apolipoprotein E
ARM……...Age-related maculopathy
ARMS2…….Age-related maculopathy susceptibility 2
ATP……..….Adenosine-5'-triphosphate
BlamD…….…Basal laminar deposits
BlinD……..Basal linear deposits
BM…….....…..Bruch's membrane
BSA……Bovine serum albumin
C1QTNF5……..……C1q and tumour necrosis factor related protein 5
CCL-2…….Chemokine ligand-2
CCR-2…….....Chemokine receptor-2
cDNA……...Complementary DNA
CFD……Factor D
CFI……Factor I
CFH……..Complement factor H
CFHR……...……Complement factor H-related
CNV…….…Choroidal neovascularisation
CRALBP……...Cellular retinaldehyde-binding protein
CRP……C-reactive protein
DAF……...…….Decay accelerating factor
DAPI……..4',6-diamidino-2-phenylindole
ddH_2O…….…….Distilled water
DMEM…….…….Dulbecco’s modified Eagle Medium
DMSO…….....…….Dimethyl sulfoxide
DNA……Deoxyribonucleic acid
DTT……...Dithiothreitol

ECM……..……...Extracellular matrix

EDTA…….....Ethylenediaminetetraacetic acid

ER……..Endoplasmic reticulum

ERG…….Electroretinography

FAK……...……..Focal adhesion kinase

FB……..Factor B

FCS……..…Foetal calf serum

FFA…….Fundus fluorescein angiogram

FHL-1…….……Factor H-like protein 1

FITC…….....Fluorescein isothiocyanate

FITC-ROS…….……..FITC-labelled ROS

GAG……..……...…Glycosaminoglycan

GCL……...…Ganglion cell layer

GA……..…….…Geographic atrophy

GFP……Green fluorescent protein

HEPES…….……4- (2-hydroxyethyl)-1-piperazineethanesulfonic acid

HiPSC……Human induced pluripotent stem cell

HiPSC-RPE…… ……...…….Human induced pluripotent stem cell derived RPE

His-C1QTNF5……...……..C-terminal hexa-histidine-tagged C1QTNF5

His-gC1q……C-terminal hexa-histidine-tagged gC1q

HRP…….…….Horse radish peroxidise

HTRA1……..……High temperature requirement serine protease

ICG…….…..…Indocyanine green

ICL…….Inner collagenous layer

IgG……..…..Immunoglobulin G

IL……...……....Interleukin

INF-γ……Interferon-γ

IPM……...Inter photoreceptor matrix

IPTG…….Isopropyl β-D-1-thiogalactopyranoside

iPS……..…….Induced pluripotent stem cell

IRBP……..Interstitial retinal binding protein

ITC……..…….Isothermal titration calorimetry

LB……...Lauria broth

L-ORMD……...……....Late-onset retinal macular degeneration

LRAT……...…….……Lecithin retinol acyltransferase

MAC…….……...……..Membrane attack complex

MALDI-TOF MS……

……Matrix-assisted laser desorption/ionisation time of flight mass spectrometry

MBL…….……Mannose-binding lectin

MASP…….…..Mannose-binding lectin-associated protease

MCP-1……..Monocyte chemoattractant protein-1

MerTK……...C-mer proto-oncogene tyrosine kinase

MFG-E8……..…….……...……Milk fat globule E8

MFRP……...……Membrane-type frizzled-related protein

MMP……..……..Matrix metalloprotease

MPGNII…….……...Membranoproliferative glomerulanephritis type II

NHS……..……...*N*-Hydroxysuccinimide

NGS……..…….....Normal goat serum

OCL……..……..…Outer collagenous layer

OCT…….……..…Ocular coherence tomography

ONL…….…….Outer nuclear layer

OPL…….……...……Outer plexiform layer

OR…….…….…….Odds ratio

OS…….…….……Outer segments

PFA…….……Paraformaldehyde

PAGE…….……..Polyacrylamide gel electrophoresis

PBS…….……....Phosphate buffered saline

PCR…….…….…..Polymerase chain reaction

PEDF…….……Pigment epithelium-derived factor

qRT-PCR……..…….……. quantitative real time polymerase chain reaction

ROS……..……Reactive oxygen species

RPE……..…….Retinal pigment epithelium

RPE65……...….. Retinal pigment epithelium-specific protein 65kDa

RPM……..…….……..Revolutions per minute

SCR……..……...….Short consensus repeat

SDS…….…..……Sodium dodecyl sulphate

siRNA…….……..……..Small interfering ribonucleic acid

SLO……..……..…Scanning laser ophthalmoscope

SNP…….……..……Single nucleotide polymorphism

SPR……..Surface plasmon resonance

TBE……...Tris/Borate/EDTA

TCC……..……Terminal complement complex

TGF-β…….…….Transforming growth factor β

TIMP……..…..Tissue inhibitor of metalloproteinase

TNF-α……..Tumour necrosis factor-α

TUNEL…….……Terminal deoxynucleotidyl transferase dUTP nick end labelling

VEGF…….…….Vascular endothelial growth factor

ZO-1……Zona occludens 1

List of figures

List of tables

CHAPTER 1

1. Introduction

1.1 Age-related macular degeneration

1.1.1 AMD background

Age-related macular degeneration (AMD) is the most common cause of irreversible vision loss in those aged over 50 in the developed world (Evans and Wormald, 1996, Friedman et al., 2004). It is the third most common cause of all blindness worldwide (Pascolini et al., 2004). Clinically, there are two main forms of AMD, an exudative "wet" form or neovascular AMD (nvAMD) and a non-exudative "dry" form. NvAMD results in acute onset of leakage of fluid, resulting in acute blindness, whilst dry AMD results in slow onset of visual loss (Davis et al., 2005). Ninety percent of acute registerable blindness results from nvAMD although only 20% of total cases of AMD are attributable to nvAMD (Evans and Wormald, 1996). Although the morphology of the diseases is different, the disease processes are not distinct and 10-15% of dry AMD patients eventually develop the nvAMD form.

AMD does not usually present clinically prior to 55 years of age (Klein et al., 2004). As the average age of populations continues to increase and life expectancy increases the prevalence of AMD is expected to increase further with an ageing population (Minassian et al., 2011). The prevalence of AMD in Europe is around 1.5% in those aged over 40 but increases to between 7 to 10% in those aged over 75 (Augood et al., 2006). Similar trends are likely in other developed countries and consequently, the worldwide burden of blindness of AMD is projected to increase from 196 million in 2020 to 288 million in 2040 (Wong et al., 2014).

Visual loss in AMD has been linked to a number of other sequelae that reduce quality of life Late-stage AMD has been linked with a loss of independence and depression and in the older age group with multiple sensory impairment (Lin et al., 2004, Rovner et al., 2002, Berman and Brodaty, 2006). Patients are also likely to be placed under an increasing financial burden due to lack of income. AMD also places a heavy financial burden on health and social care systems. In the United Kingdom in 2000 it was estimated that costs from visual aid provision, tax allowances, residential care, community care and social security benefits was £6455 per person during the first year and £6295 per person during each subsequent year {Meads, 2003 #203}. Meanwhile the cost of treating nvAMD was estimated to be £300 million per year for new patients alone (Smith, 2010, Raftery et al., 2007). These costs are likely to rise with an ageing population.

1.1.2 AMD clinical features

AMD presents with different features at different stages of disease. The disease mainly effects the macula which is responsible for central vision (figure 1.1). In the early stages, it is difficult to differentiate AMD from normal ageing (Sarks et al., 1999). In early disease, AMD is characterised by a number of deposits. Sub-retinal drusenoid deposits (SDD) also known as reticular pseudodrusen are found in between the photoreceptors and RPE layer (Zweifel et al., 2010) (figure 1.2). They are small and faint (125-250um) and therefore difficult to view on clinical examination and with fundus colour photography. SDD are thought to develop early in the disease process as they have been linked with early drusen (De Bats et al., 2013). In addition, SDD have been linked with choroidal thinning and the reduction in size of photoreceptor outer segments. Since the SDD are located in the peri-fovea it is thought that SDD are likely to initially affect rods, which have their highest concentration in this region (Curcio et al., 2013). Rods appear to be affected more than cones in early AMD. This supported by both histopathological and dark adaptation studies.

Figure 1.1 Fundus photograph labelled with foveal (f), para-foveal (Pa) and peri-foveal (Pe) measures.

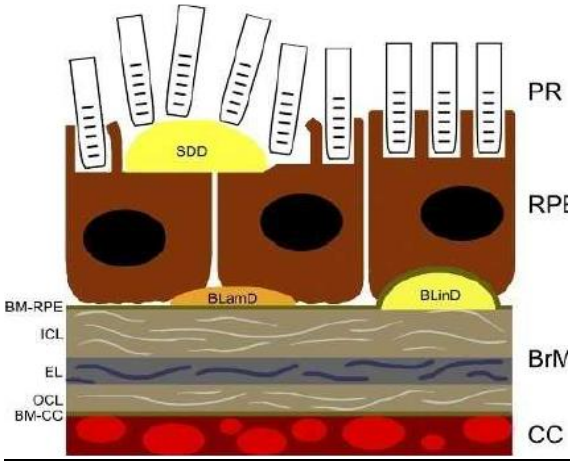

Figure 1.2 Diagram illustrating different forms of drusen with location in the outer retina. Pseudodrusen (SDD) is found adjacent to the photoreceptors (PR) and above the RPE. Basal Laminar deposit (BLamD) is found above Bruch's membrane (BrM) whilst basal linear deposit (BLinD) is found outside the basement membrane of the RPE. (Nivison-Smith, L., Milston, R., Madigan, M. and Kalloniatis, M., 2014. Age-related macular degeneration: linking clinical presentation to pathology.*Optometry & Vision Science*, *91*(8), pp.832-848.)

Deposits basal to the RPE include drusen. Drusen are focal nodules found between the RPE and Bruch's membrane (BM). They are described by their outline and size. They present as discrete nodules in hard drusen or yellowy plaques with less distinct boundaries in the form of soft drusen. Fundus photography is still the gold standard for imaging drusen. Drusen are perhaps the best clinical indicator of progression to AMD. The age-related eye disease study (AREDS) initially classified drusen into 9 types (Davis et al., 2005). This was later simplified to a 5 stage severity scale which in combination with pigmentation provided a prognostic indicator of progression of AMD (Ferris et al., 2005) (Table 1.1). Small drusen were classed as smaller than 63 um, intermediate drusen 63 to 125um and large drusen as greater than 125um but less than 250um and very large drusen are greater than 250um. Intermediate, large and very large drusen were characteristic of early AMD and conferred greater risk of progression whilst small drusen could normally also be seen in ageing. Soft drusen indicate a later stage of disease as they lift the RPE and consequently the edges are less distinct as they are not bounded by RPE adhesion to BM. On ocular coherence tomography (OCT) they appear as flatter lesions occasionally with a space in the sub-RPE on either side whilst hard drusen are usually more raised. Fundus autofluorescence (FAF) shows increased fluorescence to the edges of drusen suggesting that RPE on the edge are under stress perhaps from direct pressure (Bindewald et al., 2005). Drusen stain early during

fundus fluorescein angiogram (FFA) and increase in fluorescence with time. This can be differentiated from leaking vessels as the size of hyperfluorescence due to drusen does not change.

AMD classification	Definition
No ageing changes	No drusen or pigmentary changes
Normal ageing changes	No pigmentary changes. Only small drusen (<63um)
Early AMD	Medium drusen (>63um), no pigmentary changes
Intermediate AMD	Large drusen (>125um) and/or any pigmentary changes
Late AMD	Neovascular AMD and/or geographic atrophy

Table 1.1 Classification of AMD from the AREDS study based on drusen and pigmentary changes (adapted from Ferris et al., 2005)

Cuticular drusen are a particular form of drusen appearing in large numbers from the peri-fovea to the mid peripheral macula. They are very small in size (25-75um) and hence difficult to see clearly on fundus examination especially in their early stages. Cuticular drusen are also found sub-RPE and above BM and have similar composition to soft drusen (Leng et al., 2009, Spaide and Curcio, 2010). They show early fluorescence with fluorescein angiography. ICG shows cuticular lesions as raised lesions. Using FAF, Cuticular drusen show reduced fluorescence at their centres surrounded by a ring of increased autofluorescence. Early AMD is also clinically associated with pigmentary changes at the macula. These are mainly associated with clumping and migration of RPE which are more easily seen with OCT (Okubo et al., 1999).

In late-stage AMD, patients lose visual acuity as the foveal photoreceptors are lost (Sunness, 1999, Kim et al., 2002). Approximately 15% of advanced and late stage AMD patients can suffer from geographic atrophy (GA). In GA, large areas of RPE are lost with associated loss of overlying photoreceptors and underlying atrophy of the choriocapillaris. Although geographic atrophy can be clearly seen with fundus photography, the edges are often poorly defined. Recently, FAF and infra-red (IR) have enabled better delineation of areas of GA which has allowed for better monitoring of progression. FAF has no autofluorescence in areas of GA and often increased FAF in areas at the edge of GA lesions providing high contrast. OCT shows thinning in areas of atrophy and loss of the RPE, photoreceptor or in later stages all the neuro-retina (Curcio et al., 1996). IR reflectivity shows increased reflectivity from the atrophic lesion as the RPE no longer mask the IR generated by the choroid.

10-15% of patients who suffer with late-stage dry AMD develop nvAMD (Chew et al., 2014). In nvAMD, new blood vessels develop in the choroid under the BM known as choroidal new vessels (CNV). Type I CNV remain below the RPE whilst type II CNV penetrate the RPE. The new blood vessels are fragile and may leak a lipid-rich fluid and hence the term exudative AMD is often used interchangeably. The new vessels can also bleed and result in haemorrhagic macular degeneration. However, the neuro-retinal RPE interface is usually maintained until late in disease and therefore vision is stable until late in the disease in type I CNV. In type II CNV any leakage disrupts photoreceptor function and results in a more acute loss of vision (Grossniklaus and Green, 2004). Bleeds and lipid exudation are easily identifiable by fundus photography, however early CNV are more subtle and may appear as greyish membranes in the macula. Angiography is the best way to visualise CNV. Angiographically, type I membranes are described as occult. As vessels grow sub-RPE they are flat, leakage is protected by overlying RPE, and therefore there is a slow spreading hyperfluorescence Type II CNV leak early and produce a lacy network following the new vascular network. Type II CNV result in a classic pattern of hyperfluorescence. Type II lesions are more clearly seen with indocyanine green angiography (ICG) which highlights the choroidal to retinal circulatory link (Grossniklaus and Green, 2004).

.

1.1.3 AMD pathology

AMD is a complex polygenic and multifactorial disease with marked clinical variability. The variability makes AMD difficult to study. The variation results from an interplay between multiple genes, environmental risk factors and alterations in the local microenvironment in the neuro-retinal, RPE, BM and choroid complex. Although many factors have now been identified as risks for AMD a clear understanding of initial injury in early disease and an understanding of how these pathways lead to disease is still unclear. This section will briefly summarise the current understanding of pathogenesis and demonstrate the difficulty in studying the disease.

Whilst managing AMD clinicians noted that AMD had familial clustering (Gass, 1972). However many of the identified traits did not show clear Mendelian inheritance. As many of the associations with AMD result from single nucleotide polymorphisms (SNPs), identifying genes has been difficult with traditional linkage analysis. However, recent genome wide association studies (GWAS) have been able to identify common allelic variants in the DNA of large patient cohorts with AMD. The most common and important SNPs that have been found and replicated in a wide variety of populations relate to components of the complement pathway, an innate immune system. The complement pathway is discussed in more detail in section 1.4. However, other SNPs have

also been found related to the immune system, extracellular matrix (ECM), oxidative stress, cellular function and neovascular cytokines which are discussed below.

Defects in extracellular matrix turnover are implicated in macular degeneration. HTRA1 (10q26) gene is associated with AMD. It is involved in the breakdown of ECM proteins including complement terminal component regulators clusterin, vitronectin and fibromudulin (Kanda et al., 2007, Fritsche et al., 2008). HTRA is also found in drusen (Yang et al., 2006). A meta-analysis showed that HTRA1 was strongly associated with AMD giving a 7.46 times increased risk (Tang et al., 2009). The HTRA gene is located close to the ARMS2 gene, which is also implicated in AMD. Fibulin 5 (14q31.1) is also associated with AMD and is involved in ECM turnover. It assists in the polymerisation of elastin fibres. In normal eyes fibulin 5 expression is localised to the BM and the choroid. In AMD it is also localised to sub-RPE deposits including drusen (Tang et al., 2009). Fibulin 5 may be downstream of HTRA1 in helping modulate elastin in Bruch's membrane (Clausen et al., 2011). COL8A1 (3q12.3) and COL10A1 (6q21-q22) code for collagen XIII and X respectively. Neither of these collagens is thought to play a major role in the sub-RPE or BM. Consequently, their roles in pathogenesis have not been clearly defined. The collagens have been proposed to play a part in ECM integrity and neovascularisation (Yu et al., 2011, Rooney et al., 1993).

In addition to extracellular matrix turnover, genes associated with lipid metabolism have also been associated with AMD. APOE (19q13.2) codes for Apoliprotein E (ApoE). ApoE is involved in lipid metabolism and transport. Mice deficient in ApoE were found to show signs of cellular stress. Cells from these mice expressed proteins associated with ageing and cells had reduced reserves of antioxidants (Bonomini et al., 2010). ApoE has three isoforms: Epsilon 2 (Ɛ2), Epsilon 3 (Ɛ3) and Epsilon 4 (Ɛ4). Patients carrying Ɛ2 alleles were found to have increased risk of AMD whilst those carrying Ɛ4 were found to have a reduced risk (Baird et al., 2004, Souied et al., 1998). A meta-analysis of studies on ApoE and risk in AMD found that there was a 20% risk of AMD attributable to the Ɛ2 isoform and a 40% protective effect associated with the Ɛ4 isoform (Thakkinstian et al., 2006). This suggests that lipid metabolism may play a part in AMD pathogenesis. Lipids are also found in the basal deposits in early AMD and may be due to early cellular dysfunction. Another associated gene involved in lipid transport is the VLDLR (9p24) gene that codes for a receptor for the very low density lipoprotein. Case-control and familial studies have implicated the VLDLR gene in risk for AMD (Haines et al., 2006). VLDL not only transports lipids but is also thought to have a direct response in reducing angiogenesis (Chen et al., 2007). VLDL receptor knockout mice were found to have marked sub-retinal neovascularisation (Li et al., 2007).

ARMS2 (10q26) is closely located to the HTRA1 gene. The exact function of ARMS2 is not known however, it is thought to play a part in mitochondrial function (Kanda et al., 2007). ARMS2 protein has been localised to mitochondrial membranes implicating the protein in mitochondrial metabolism. This relationship was further strengthened when cigarette smoking was found to further increase susceptibility to AMD in patients with ARMS2 polymorphisms (Schmidt et al., 2006). ARMS2 greatly increases the risk of AMD and patients homozygous for SNPs in ARMS2 were found to be eight times more likely to develop AMD (Rivera et al., 2005).

Looking at specific risk factors for nvAMD, VEGFA (6p12) has been associated with nvAMD. This gene codes for vascular endothelial growth factor (VEGF). VEGF is a growth factor that is important in generation of new blood vessels. Polymorphisms in VEGFA have been shown to increase AMD risk particularly in late-stage neovascular disease (Haines et al., 2006, Churchill et al., 2006). SERPINF1 (17p13.3) codes for pigment epithelial derived factor (PEDF). PEDF has several functional roles. It is anti-angiogenic, neurotrophic and inhibits tumour growth. An allelic variant of PEDF is associated with nvAMD (Lin et al., 2008). Previously vitreous PEDF levels have been found to be lower in AMD patients suggesting that PEDF has a protective role in nvAMD (Holekamp et al., 2002).

Looking at the immune system TLR3 (4q35) and TLR4 (9q33.1) code for toll like receptors. These are part of the innate immune system and activate a range of pathways in the immune system. TLR3 is linked to apoptosis in cellular stress response. TLR3 SNPs have been shown to reduce the risk of AMD (Yang et al., 2008). TLR4 recognises lipopolysaccharides and it is a mediator of the stress response. TLR4 SNPs have been shown to increase the risk of AMD in one non-replicated study (Zareparsi et al., 2005).

In addition to genetic risk factors for AMD environmental factors are also thought to contribute to AMD pathogenesis. Large population based studies have highlighted environmental and lifestyle associations with AMD. Chakravarthy *et al.* recently performed a meta-analysis of these studies and number of other similar studies from across the globe. The 26 studies included 94, 058 patients. 16 factors were identified. 3,178 patients suffered from end-stage AMD. In all studies, there was a strong association with age. Changes during ageing have already been described in the natural history section (Chakravarthy et al., 2010).

Oxidative stress is implicated in AMD. Amongst lifestyle factors associated with AMD, cigarette smoking has the strongest association. Cigarette smoke is made up of a number of constituents and it is not known which of the components of smoke is important in pathogenesis. However, it is thought that smoking alters the inflammatory balance within the retina. As a result patients with AMD risk alleles in the complement factor H (CFH) gene are placed at additional risk of developing AMD above that of the normal population (DeAngelis et al., 2007). In addition, smoking is thought to induce oxidative stress. Oxidative stress is already implicated in disease pathogenesis. Diet also suggests a role for oxidative stress in the progression to late-stage AMD. Studies have found a beneficial effect from using beta-carotene, vitamin C and vitamin E and zinc supplements, which reduced the risk of losing visual acuity. Meanwhile ultraviolet light, a suggested source of photo-oxidative stress in the retina, has been associated with AMD. A meta-analysis of fourteen studies identified an increasing risk of AMD with greater sunlight exposure. Even the non-population based studies identified a significant risk when the data was pooled ($p=0.004$) (Sui et al., 2013).

At a cellular and molecular level a number of processes have been found to result in AMD progression. Firstly, a number of cellular pathways, which play a part in normal retinal physiology, have been found to dysfunction. One of the primary roles of RPE cells is photoreceptor homeostasis. RPE phagocytose photoreceptor outer segments (OSs). Lipofuscin accumulates within RPE with age and is thought to be a by-product of incomplete lysosymal digestion of photoreceptor OS (Sui et al., 2013). One of the components of lipofuscin is N-retinylidene-N-retinyl-ethanolamine (A2E). A2E has been shown to affect RPE function by reducing degradation and processing of lipids (Holz et al., 1999, Finnemann et al., 2002, Lakkaraju et al., 2007). It also sensitizes RPE to light induced damage and induces innate immune system activation. As a result, A2E is likely to be a mediator of RPE cell death and is associated with AMD (Sparrow and Cai, 2001). Apolipoprotein E (Apo-E) has been noted in drusen and variant Ɛ2 is a risk for AMD (McKay et al., 2011).

Inflammation has been implicated as one of the initial causes of injury in AMD. The first studies that identified inflammatory mediators were histopathology studies from AMD patients. In early AMD, immunoglobulins have been identified in drusen (Newsome et al., 1987, Johnson et al., 2000, Mullins et al., 2000a). Various inflammatory mediators have also been found including c-reactive protein. A cell-mediated response is also triggered with dendritic cells found to be in direct contact with drusen.

Cell-mediated inflammation was thought to be the primary mechanism of cell injury as mononuclear cells, multinucleated giant cells, active microglia and dendritic cells all identified in AMD (Hageman et al., 2001, Anderson et al., 2002, Penfold et al., 1986, Penfold et al., 1985). In addition, a humoral response with retinal autoantibodies have been detected in the sera of patients (Gurne et al., 1991). The retina, which is normally relatively immune privileged, loses some of this privilege during inflammation partly due to breakdown of the blood-retinal barrier (Ohta et al., 1999, Ohta et al., 2000). It is unclear what may trigger this but several infectious agents have been implicated in causing the initial inflammatory response (Ishida et al., 2003, Kalayoglu et al., 2005). The most compelling evidence that chronic inflammation plays a central role in AMD comes from the finding of activated complement pathway components in drusen. There is also an increased risk of AMD in allelic variants of genes involved in the complement pathway. The complement pathway will be discussed in more detail in the complement pathway chapter.

Taken together the information in this section illustrates that there are a multitude of factors which may contribute to the development of AMD. This provides not only marked inter-individual differences but also differences in phenotype and pathology in the eyes of individuals. Consequently studies of AMD require large numbers to confirm phenotype correlations.

1.1.4 Animal models of macular degeneration

A number of animal models have been developed in order to recapitulate AMD in the laboratory setting. The majority of animal models of AMD are murine. Animal models allow the study of the interaction between neuro-retina, RPE, BM and choroid complex with systemic modulators of disease. Murine models have shown phenotypes in mutations of human genes related to AMD and have therefore been proposed (Mishima and Kondo, 1981) as a good way of modelling AMD (Elizabeth Rakoczy et al., 2006). There are however several limitations with the use of rodent models. Firstly, rodents do not have a macula (Zeiss, 2010). There is no cone rich region in rodents unlike porcine or primate models. A further point is that rodent physiology appears to be different from human retinal physiology . For example, the models do not appear to have any drusen like sub-RPE deposit with some evidence that lysosomes are exocytosed apically rather than basally as in human RPE (Mishima and Kondo, 1981). As a result, findings from animal studies have to be interpreted within this context of several limitations for modelling of human AMD. This section looks at animal models of different stages of AMD.

One of the earliest changes in AMD is the development of deposits in BM. The deposits found between the RPE basement membrane and inner collagenous layer are known as BLinD. The

deposits developing between the RPE and the RPE basement membrane and are known as BLamD. BLinD formation is associated with AMD. BM is also known to thicken with age. Ageing in different mice strains is thought to result in similar changes (Ramkumar et al., 2010, Dithmar et al., 2001). Mice fed with a high glucose or fat diet also have BM thickening. APOE has three main allelic variants that confer differing risk of AMD. These are Ɛ4, Ɛ3 and Ɛ2 respectively in decreasing risk of AMD. ApoE null mice develop thickened BM with both sub-RPE lipid and intra-BM lipid deposits. Knock-in mice have also been developed with the various risk alleles. These mice all develop BM thickening and sub-RPE deposits when provided a high fat diet (Malek et al., 2005). Whilst the Ɛ4 allele is protective in humans, it appears to cause the most severe disease in these murine models (Malek et al., 2005). Low density lipoprotein (LDL) receptor knockout mouse also have thickened BM. In a similar manner to the APOE knockout mice they have raised triglyceride levels. CD36 knockout mice also develop BM thickening. CD36 binds oxidised phospholipids on RPE (Picard et al., 2010). Both mice require feeding on a high fat diet to develop their phenotypes. These studies highlight the potential role of aberrant lipid metabolism in early AMD.

Drusen is a feature of early AMD. A number of mouse models develop white drusenoid deposits. Studies demonstrate that drusenoid deposits are unlikely to be composed of constituents of drusen and are likely to be due to microglia or macrophages (Luhmann et al., 2009). Additionally, the RD8 mutation has been found to cause white lesions in the retina in several models of retinal disease (Chang et al., 2013). The RD8 mutation does not conform to any human gene mutation associated with AMD. Modelling drusen using rodent models has proven difficult. However, primates have a macula region with a fovea and a retina that appears to have RPE with basal exocytosis of lysosomal material (Ishibashi et al., 1986, Gouras et al., 2008). Both Rhesus monkeys and Macaques have been reported to develop drusen (Gouras et al., 2008, Umeda et al., 2005). Thirty-two percent developed drusen, which contained ApoE, amyloid P, C5 and C5b-9 however this required 16.9 years on average making experimental design difficult (Umeda et al., 2005). However, primate models have failed to recapitulate later disease features such as geographic atrophy or CNV.

Oxidative stress has been implicated in AMD as a potential source of initial RPE injury with incomplete digestion of photoreceptor OS. One of the products of OS digestion is docosahexaenoic acid (DHA). An oxidised product from DHA is carboxy-ethylpyrole (CEP). When mice were innoculated with CEP they developed AMD related phenotypes including deposition of complement components in sub-RPE deposits followed by loss of overlying RPE. The model highlighted interactions between the complement pathway and oxidative stress

(Hollyfield et al., 2008). Superoxide dismutase (SOD) is one of the main regulators of reactive oxygen species (ROS) in the RPE. In mice however, the knockout of SOD1 has resulted in BM thickening and drusen-like deposit, RPE loss and CNV in mice aged greater than 10 months (Imamura et al., 2006). Similarly, knockdown of SOD2 resulted in RPE degeneration, BM thickening and photoreceptor loss (Justilien et al., 2007).

A number of allelic variants for genes encoding the components of the complement system and the alternative complement pathway in particular have been associated with AMD. The complement system is discussed in more detail below. Perhaps the most studied gene in AMD is CFH, a negative regulator of the alternative complement pathway. A CFH null mouse has been generated which developed a mild neuro-retinal degeneration. However, the mouse did not develop BM thickening or sub-RPE deposits. It also developed autofluorescent lesions in the retina. Thus far, this model has not been checked for the RD8 mutation, which can also result in similar changes (Coffey et al., 2007).

Chemokines direct immune cells to sites of inflammation. Ccl2, also known as monocyte chemoattractant protein, is raised in AMD patients (Sennlaub et al., 2013). In Ccl2 knockout mice there was an increase in BM thickness, drusen like deposits and complement component deposition by 9 months (Ambati et al., 2003). Older mice also developed CNV. However, there is some debate over the phenotype of this mouse with a further study noting no progression of deposit (Luhmann et al., 2009). This suggests that in mice the clearance of deposits may be performed by macrophages as these deposits also contained the OS fragments A2E (Ambati et al., 2003). Meanwhile Cx3cr-1 null mice have an accumulation of microglia in the sub-retina. Fundoscopy reveals drusen like lesions at corresponding sites. However, further detailed study following removal of any RD8 mutations failed to replicate the phenotype (Luhmann et al., 2009).

Geographic atrophy and CNV are the hallmarks of late-stage AMD. A GA pattern is found in Dicer1 knockout mice with downstream signalling similar to that found in humans (Tarallo et al., 2012). There have been a number of animal species used for modelling CNV using lasers (Ryan, 1979, Criswell et al., 2004). Neovascularisation peaks at approximately 4-6 weeks with regression of vessels starting as early as 3 weeks (Ohkuma and Ryan, 1983, Ryan, 1982).

In summary, there are a variety of potential animal models for AMD. The majority of these are murine and require some manipulation in order to show features of AMD. However, the lack of phenotypes in murine mutants of key macular degeneration associated genes suggests that murine pathophysiology is different to that in man. This

points to the need to develop a humanized model of macular degeneration.

1.1.5 Studying complex disorders using monogenic disease

Our knowledge of many common complex diseases has been generated from the initial study of rare inherited forms of these common conditions that have highlighted critical pathways in disease pathogenesis. This section will briefly review some diseases in which this approach has benefitted understanding of more common disease.

Perhaps the best example of mechanistic determination from rare familial forms comes from the study of Alzheimer's disease (AD). Approximately only 1-6% of AD is early onset (Rocca et al., 1991). Autosomal dominant inheritance is rare making up only 13% of inherited types of early onset AD (Campion et al., 1999). The inherited forms have altered the processing of amyloid precursor protein (APP). The identification of the role of presenilins and APP in the formation of deposits in AD helped in the understanding of plaque formation in AD.

In diabetes mellitus (DM), maturity onset diabetes young (MODY) is a form of diabetes has certain traits of type 2 diabetes but occurs in the young (<25). MODY is a cause of less than five percent of DM (Ledermann, 1995). Currently six genes are known to cause MODY. All have an autosomal dominant inheritance pattern. Some of the MODY mutations are linked to abnormalities in glucokinase function and have provided insights into beta islet cell dysfunction and in understanding the pathophysiology in DM (McCarthy, 2004).

As in AD, the final critical pathways for hypertension have also been made clear by investigation of Mendelian inherited forms of hypertension. Although population studies have highlighted how ageing, body mass index, diet, lack of exercise and salt intake are risk factors for the disease the molecular mediators of hypertension were not clear. Studies of gene defects in the epithelial sodium channels in the cortical collecting tubule can cause severe hypertension as in Liddle's syndrome (Knight et al., 2006). Further studies from autosomal dominant inherited hypertension have highlighted the importance of the renin-aldosterone and angiotensin system and provided targets for treatment of essential hypertension (Snyder, 2002).

Rare Mendelian inherited diseases, which share traits with more common complex diseases, provide a platform to study disease mechanisms and can highlight common pathogenic pathways. Using rarer inherited monogenic forms of macular degeneration may also provide a suitable approach for studying critical pathways in the pathogenesis of AMD.

1.2 Late-onset retinal macular degeneration

AMD is a common complex and highly variable disease, which can result in severe visual disability. Although there are treatments for certain forms of late-stage AMD there is a need to develop early preventative treatments for all AMD. Understanding early disease pathogenesis has been hampered by the dearth of models replicating human pathophysiology and this in turn has limited the developments of new treatments. This points towards the need to develop a reliable humanised model of macular degeneration. The use of monogenic diseases with key characteristics of AMD may provide a pathway for the better understanding AMD.

L-ORMD is a rare monogenic disorder of the retina resulting from a mutation in the gene C1QTNF5. It is dominantly inherited and fully penetrant. Patients carrying the gene progress through a series of signs and symptoms in various stages of the disease. It shares key clinical and pathological characteristics with age-related macular degeneration and has consequently been proposed as a good model for macular degeneration (table 1.2). This section summarises clinical and pathologic characteristics of the disease from the literature.

	L-ORMD	AMD
Age of onset	50-60 years old	70-80 years old
Central phenotype	Early peri-foveal yellow dots and pigmentation, later atrophy and choroidal neovascularisation	Varied forms of drusen including soft, hard, reticular pseudodrusen and cuticular drusen
Peripheral phenotype	Marked scalloped atrophy in later disease extending to far periphery	Normal
Dark adaptation	Delay most sensitive 15 degrees temporal to the fovea	Delay most sensitive at the fovea
Full field ERG	Reduction in amplitude and increased latency in late-stage disease	Usually normal
Visual field	Field field loss starting centrally extending to the far periphery in late disease.	Automated usually normal with mild changes in extensive AMD
Anterior segment	Long anterior zonules, and peripupillary atrophy	Normal

Table 1.2: A comparison of phenotypic features in L-ORMD and AMD.

1.2.1 L-ORMD clinical characteristics

Patients are asymptomatic during the first four decades of their life. However, they do exhibit phenotypic signs of L-ORMD. On dilatation, patients are noted to have long anterior zonules on their lenses (Ayyagari et al., 2005). The youngest patient reported was aged 24 years. Patients may also display iris atrophy particularly in the peripupillary ruff and mid periphery and some may develop pigmentary secondary glaucoma (Ayyagari et al., 2000, Ayyagari et al., 2005, Subrayan et al., 2005).

L-ORMD has been classified to three main stages (table 1.3). The first symptoms described by patients usually occur in their fifth decade of life. Patients describe dark adaptation difficulties. Examination shows early drusenoid changes with yellow dots in their peripheral macula (Milam et al., 2000). Dark adaptation investigations show early latency although there is some variability

(Ayyagari et al., 2005). Other investigations including kinetic perimetry and electroretinography (ERG) are normal in the early stage of the disease. As the disease progresses areas of neuro-retinal atrophy develop in the peripheral macula and gradually increasing in size initially sparing the fovea (Milam et al., 2000). Consequently best-corrected visual acuity (BCVA) may be relatively well preserved till late in the disease. Visual field testing may show abnormalities from 10 to 40 degrees from the central vision (Milam et al., 2000).

Stage	Age	Phenotypic features
1	0-40	Normal fundus Long anterior zonules
2	40-60	Normal best corrected visual acuity Dark adaptation delay Peri-foveal yellow dots Pigmentation in the macula Early atrophy sparing the fovea
3	>60	Reduced best corrected visual acuity Atrophy involving the fovea Neovascularisation Scalloped atrophy of the peripheral retina Scotomas on perimetry Reduced full field ERG

Table 1.3: Summary of clinical findings at each stage of L-ORMD

In late-stage disease, the fovea also becomes affected resulting in a marked loss of central vision (Kuntz et al., 1996). Additionally, CNV may develop which rapidly involute to form gliotic scars (Ayyagari et al., 2005). Areas of atrophy are well demarcated and mid-peripheral bone spicule changes occur (Kuntz et al., 1996, Duvall et al., 1986). Interestingly, these cases reported sharply demarcated lines between healthy and atrophic retina as the prominent feature of affected eyes as well as mid-peripheral bone spicule pigmentation. More recent clinical studies using spectral domain ocular coherence tomography (SD-OCT) have revealed a loss of photoreceptors and thinning of the neuro-retina in atrophic and peri-atrophic areas (Vincent et al., 2012, Soumplis et

al., 2013). At this stage full field ERG is reduced showing prominent rod-cone dystrophy (Vincent et al., 2012).

The disease continues to progress beyond the macula and in the ninth and tenth decades patients have almost full field visual loss with an atrophic retina resembling retinitis pigmentosa.

1.2.2 L-ORMD pathology

Light microscopy of donor L-ORMD eyes revealed thick sub-RPE deposits extending from the *ora serrata* to the macula and were approximately 50um thick (figure 1.3). The deposits extended from the basal lamina of the RPE to the inner collagenous layer of Bruch's membrane. At the macula there was disruption of photoreceptors, RPE and Bruch's membrane, although the anterior retina was not affected (Milam et al., 2000, Kuntz et al., 1996). Rod outer segments were shortened with disorganised disc membranes especially at the macula (Duvall et al., 1986). New blood vessels were formed extending from the choriocapillaris through Bruch's membrane, and disciform scarring was also observed indicating old CNV (Milam et al., 2000, Kuntz et al., 1996).

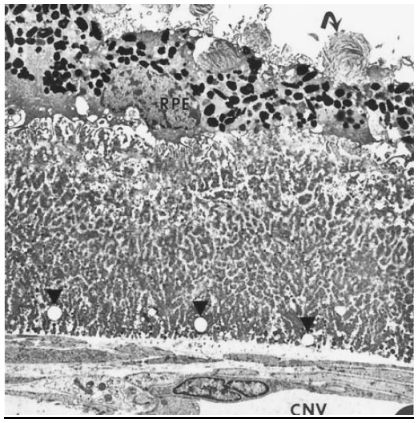

Figure 1.3 Electron micrograph image of a L-ORMD post-mortem donor retina. The image shows a thick heterogeneous deposit below the RPE. The outer layer of the deposit has lipid globules which have been extracted during the preparation of the sample (Arrowheads). Below the deposit above the elastic lamina of Bruch's membrane is a new fibrovascular layer with a CNV. Apically photoreceptor outer segments are visible (curved arrowheads). This image is modified from (Milam *et al. 2000*)

Immunohistochemistry of the deposits revealed collagen, lipids, amyloid P, lysozyme, elastin, apolipoprotein B-100, calcium, esterified and unesterified cholesterol and rhodopsin, with Muller cell processes also observed in some regions (Kuntz et al., 1996, Milam et al., 2000). Autofluorescence studies have also found marked lipofuscin autofluorescence in L-ORMD RPE

(Duvall et al., 1986).

Electron microscopy demonstrated fibrous growth, with deposits anteriorly showing amorphous material with electron dense material inclusions and posteriorly showing more granular material and possible macrophages. There was apical displacement of RPE by spherical deposits, which consisted of basal lamina-like surface shells and cores containing wide-spaced collagen.

1.2.3 Hypotheses of C1QTNF5-mediated pathogenesis

The C1Q and tumour necrosis factor 5 *(C1QTNF5)* gene is located on chromosomal region 11q23. *C1QTNF5* is translated from 3 exons. The whole gene is found within a 3' untranslated region of the mouse frizzled-related protein (*MFRP*) gene. The gene is conserved across vertebrate species (Hayward et al., 2003). The mutation responsible for L-ORMD occurs from a C to G substitution in the third exon. C1QTNF5 protein is composed of a globular C1Q domain, a collagen like domain and signal peptide at the nitrile end. The protein has a molecular weight of 25kDa (Kishore et al., 2004, Tu and Palczewski, 2012). The mutation codes for an amino acids within the globular C1Q domain (gC1Q).

The exact function of C1QTNF5 has yet to be established. In the eye, C1QTNF5 is most highly expressed in the baso-lateral RPE and the ciliary body epithelium (Ayyagari et al., 2005). A systemic expression analysis revealed that C1QTNF5 was most highly expressed in the stromal cells of adipose tissue as well as having lower expression in brain and testes (Wong et al., 2008). It has been hypothesised that C1QTNF5 plays a role in lipid metabolism because of a similarity in structure to adiponectin. C1QTNF5 was suggested to act as a circulating adipokine particularly in the absence of other members of the C1QTNF family and in insulin resistance (Schmid et al., 2013). Meanwhile a role in glucose metabolism was proposed because serum levels of C1QTNF5 were raised in insulin resistant rodents (Park et al., 2009). Additionally, in human studies, levels of C1QTNF5 reduced as insulin resistance decreased following exercise (Lim et al., 2012). C1QTNF5 was shown to phosphorylate 5' adenosine monophosphate-activated protein kinase (AMPK) leading to increased cell surface recruitment of glucose transporter type 4 (GLUT4) receptors to increase glucose uptake (Park et al., 2009). MFRP and C1QTNF5 also interact, suggesting a functional relationship between the two proteins. MFRP is a transmembrane protein containing N-terminal cytoplasmic region, a transmembrane domain, and an extracellular region with tandem repeats of two cubulin domains, low-density lipoprotein receptor related sequence, and a cysteine rich domain at the C terminus. The exact function of MFRP is also currently unclear

(Katoh, 2001).

It is also unclear how mutant C1QTNF5 causes pathology in L-ORMD. Mutant C1QTNF5-expressing transfected cells showed significantly reduced adhesion when compared with the wild-type C1QTNF5 expressing transfected cells. There was a differential adhesion with reduced binding to laminin but no difference with fibronectin (Shu et al., 2006b). One proposed mechanism of deposit formation was through reduced adhesion of RPE to Bruch's membrane resulting in an increased ECM deposition in the sub-RPE space.

Mutation in C1QTNF5 results in an alteration of transport and processing of the protein. In studies using stably transfected cell lines wild-type C1QTNF5 was found to be secreted whilst mutant protein was not (Shu et al., 2006b). A western blot of the conditioned media showed good migration of wild type protein but not the mutant suggesting that aggregation of the mutant play a role in dysfunction. C1QTNF5 was found in cell lysates as well as the secretome of transfected cells. However, mutant protein was only found in the cell lysates (Mandal et al., 2006a) Staining of C1QTNF5 suggested a co-localisation with ER markers (Shu et al., 2006b). Taken together the evidence points to mutant C1QTNF5 not being secreted and retained as aggregates in the endoplasmic reticulum potentially causing a disorder of protein degradation. It is not clear whether L-ORMD results in a gain of function from cellular stress or whether this causes a loss of function from reduced secretion of wild type protein.

1.2.4 Mouse models of L-ORMD

Thus far, only one heterozygous knock in mouse model of L-ORMD has been published (Chavali et al., 2011). These mice replicate many of the changes found in humans. They demonstrate early slow rod-B wave recovery on ERG which is similar to the dark adaptation delay seen in patients. In addition, they have retinal white spots, RPE abnormalities, sub-RPE deposit vascular leakage and photoreceptor loss. From 10 months onwards mice developed hyperfluorescent white spots which increased with age. However, histopathology revealed only pynknotic photoreceptor nuclei at 12 months with swollen inner segments by 15 months with cells loss only being identified at 21 months. Expression of C1QTNF5 and rhodopsin was significantly reduced by twelve months. These findings were consistent even after removal of RD8 mutations from the mice (Sahu et al., 2015).

Dinculescu *et al.* also attempted to produce a murine model of L-ORMD by delivering mutant C1QTNF5 using an AAV vector with expression driven by a BEST1 promoter (Dinculescu et al., 2015). One eye of the C57BL/6 mice received 1ul 1 x 10^{12} genome copies/ml. The other eye was

left as an untreated control. Two months post procedure expression of AAV C1QTNF5 was found throughout the RPE. Mutant C1QTNF5 was found to be retained within RPE forming large spherical aggregates. The mutant also secreted towards the basal side forming a sub-RPE layer whilst wild type C1QTNF5 was also found on the apical RPE. Nine months post procedure mice showed RPE loss and photoreceptor and neuro-retinal layer thinning. The deposits were found to contain high levels of mutant C1QTNF5.

In summary, L-ORMD is a fully penetrant disease in which all patients carrying the mutation develop pathology. The pathology occurs earlier and is more severe than AMD. Additionally, L-ORMD displays many of the traits of AMD. There is a good animal model of disease for potentially translation and to date transfected non-retinal cell models have suggested pathological mechanisms. Taken together these suggest that L-ORMD is a good disease to model macular degeneration.

1.3 The Complement System

The complement system is part of the innate immune system. The complement system plays several roles including defence against pathogens, removal of apoptotic cells and debris, clearance of immune complexes and stimulation of adaptive immune responses (Walport, 2001). The pathway is an amplification cascade. It is composed of over 40 proteins with three main triggering arms which culminate in a final common pathway leading to the formation of a membrane attack complex (C5b-9). The main aim of this section is to provide background information regarding the normal role of the pathway including a more detailed look at the principle components and regulators and in particular complement factor H. Although there is a large amount of evidence for the role of the complement pathway in AMD pathogenesis it is still unclear whether complement dysfunction is the initiating mechanism for disease or whether the complement propagates AMD. In addition, it is still unclear why a system whose primary role is to protect the body from attack does itself appear to cause localised activation and injury.

1.3.1 The activation and regulation of complement activity

The complement cascade is initiated by three main pathways; the classical, the lectin and the alternative pathway (Walport, 2001)(figure 1.4). Each pathway has its own particular set of triggers to initiate the cascade. The classical pathway is activated when C1q binds to the Fc portion of IgM or IgG complexes or to CRP, beta-amyloid and low density lipoprotein. In addition, C1Q can be activated by binding to apoptotic cells (Gaboriaud et al., 2004). C1q activates the enzyme C1r which then cleaves C1s. C1s activates C2 to C2a and C2b and activates C4 to release C4a and C4b

(Nauta et al., 2002). C2b and C4b form a complex, which acts as a C3 convertase. The lectin pathway is initiated when the molecules mannose-binding lectin (MBL) and ficolins (L, H and M) bind to bacterial surfaces (Thiel, 2007). This complex activates serine proteases which in turn cleaves thioester bonds on C2 and C4 resulting in the formation of C2a and C2b in addition to C4a and C4b. C4b and C2b then form a complex, which acts as a C3 convertase.

The alternative complement pathway has a continuous tickover (Pangburn et al., 1981). It is activated by the hydrolysis of C3 to form C3 (H_2O). When this molecule binds with Bb from the CFD mediated cleavage of CFB it forms a C3 convertase C3 (H2O)Bb (Pangburn et al., 1981). All three C3 convertases convert C3 to C3a an anaphylatoxin and C3b an opsonin. This activates the major amplification loop of the complement system. C3b binds to CFB, which is cleaved by CFD to Bb and Ba (Montes et al., 2009). The Bb fragment remains bound to C3b, which forms a C3 convertase to produce further C3b, thereby, increasing the number of C3b molecules in the amplification loop. Generated C3b binds to the C3 convertase C3bBb to form C3bBb3b in the alternative pathway. C3b also binds to C4b2b generated from the classical and lectin pathways. The addition of an extra C3b to these complexes forms a C5 convertase, which cleaves C5 to C5a an anaphylatoxin and C5b. C5b binds to C6, C7, C8 and C9 to form the terminal complement complex (TCC). Multiple C9s bind to the complex and form a ring on the cell membrane to create a perforation in the membrane.

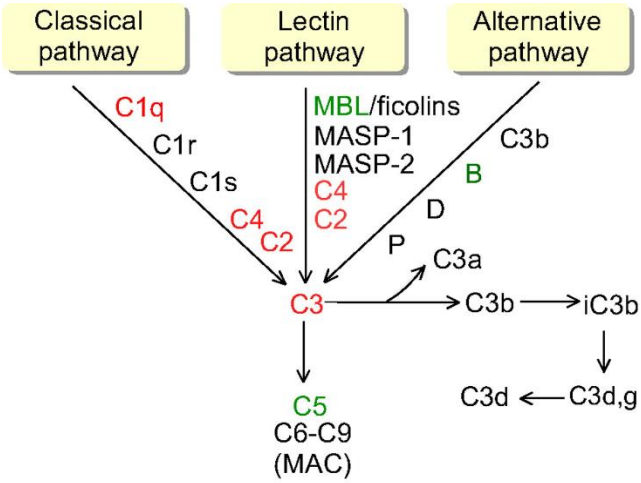

Figure 1.4 Schematic of the complement pathway. The diagram shows that three main pathways exist which converge on C3. C3b cleavage from C3 leads to the formation of C5 convertases which cleaves C5b. This complexes with factors C6, C7, C8 and C9 to form a terminal complement complex C5b-9 also known as the membrane attack complex. Rutemark, C., Alicot, E., Bergman, A., Ma, M., Getahun, A., Ellmerich, S., Carroll, M.C. and Heyman, B., 2011. Requirement for complement in antibody responses is not explained by the classic pathway activator IgM.*Proceedings of the National Academy of Sciences*, *108*(43), pp.E934-E942.

The complement cascade has several regulators in order to prevent widespread destruction from deposition of MAC complexes. The classical and lectin pathways are inhibited by C1 esterase inhibitor. A C2 receptor inhibitor also prevents the activation of C2 by C1s (Inal et al., 2005). The main regulator of the tickover loop of the alternative complement pathway is complement factor H (CFH). The role of CFH is regulation is discussed in more detail below. However, it is thought that in the fluid phase CFH-related proteins (CFHR) may also help inhibit the alternative complement pathway CFHR-1 has been shown to both assist the decay of C3 convertases and help inactivate C3b to iC3b in a similar manner to CFH. The CFHR is thought to act mainly in the fluid phase as it lacks many of the cell surface binding components of CFH (Jozsi et al., 2007). The further breakdown of iC3b leads to the cleavage of C3d the surface bound thioester domain of C3. The equivalent inhibitor of the lectin and classical pathways is C4b-binding protein. Together CFH, CFHR and C4b-binding proteins also help recognise self-glycosaminosglycans (GAGs) and self-sialic acids and prevent attack on self-cell surfaces.CFHR-1 protein also binds to C5 convertases to inhibit their function (Heinen et al., 2009). Cells also express decay accelerators which help the breakdown of convertases including CD55 a decay accelerating factor (DAF) and membrane co-factor protein also known as CD46 (Persson et al., 2010). The TCC formation is also regulated by a cell surface regulator CD59 that prevents the formation on cell surfaces. CD59 prevents C9 polymerising on cell membranes and in so doing prevents MAC formation. Soluble regulators such as vitronectin and clusterin are able to bind to formed complexes in the extracellular matrix to prevent the formation of the TCC complex. There is also some evidence that these compounds decay MAC itself (Johnson et al., 2011).

1.3.5 Complement dysregulation in AMD pathogenesis

Drusen is one of the first clinical hallmarks of early AMD. Various studies have identified complement components in drusen suggesting that complement may be involved early in AMD pathogenesis. Early components of the complement pathway CFB and anaphlyatoxins C3a andC5a have been found in drusen (Gold et al., 2006). Meanwhile terminal pathway component C5 and C5b-9 were found to be at the core of drusen (Mullins et al., 2000a). Additionally regulators of the complement pathway including CFH, vitronectin, clusterin and MCP have also been shown to be present (Johnson et al., 2001, Hageman et al., 2006).

Cadaveric samples from AMD patients showed raised levels of complement pathway proteins in the BM and choroid when compared with control eyes (Yuan et al., 2010). The expression levels were greatest at the macula. The vitreous of patients also showed raised levels of complement

pathway C3, CFB and CFD in the vitreous of advanced disease when comparing levels to patients with early disease (Loyet et al., 2012). Additionally, MAC complex deposition was greatest in the RPE/choroid of AMD patients (Hageman et al., 2005). Regulators of complement pathway activation have also been shown to be abnormal in human cadaveric studies. MCP was reduced in early AMD and CD59 expression was reduced in the RPE of AMD patients (Vogt et al., 2011, Ebrahimi et al., 2013). In late stage disease, CNV removed at the time of surgery showed C3a, C5a and C5b-9 immunostaining of these vessels suggesting activation of complement pathways (Lommatzsch et al., 2008). Examples of damage caused by complement dysregulation in other systems include systemic lupus erythematosus (SLE), atypical haemolytic uraemic syndrome (aHUS) and dense deposit disease (DDD) (Manderson et al., 2004, Kavanagh et al., 2012, Martinez-Barricarte et al., 2010). Similarly, complement dysregulation may lead to pathogenesis in AMD.

It is still not completely clear whether the increase in complement component deposition seen in AMD is due to localised or systemic factors. Bb, C3, C3d, iC3b, and CFD were all raised in patients with AMD (Reynolds et al., 2009, Scholl et al., 2008). C3d, CFB, Ba and CFD were also raised at greater levels in advanced AMD. In addition, these complement components could be combined with genotypic information to accurately predict AMD in up to 79% of cases (Hecker et al., 2010). A single standard deviation increase in levels of these products increased the risk of AMD 5 fold. The link between CFH serum levels and AMD has been more mixed (Hakobyan et al., 2008, Hecker et al., 2010). However, CFH autoantibodies are reduced in AMD patients (Dhillon et al., 2010).

Genetic studies have also exposed an association between allelic variants of complement pathway components and AMD. The first single nucleotide polymorphism (SNP) found to be associated with AMD was discovered in *CFH* (1q32) gene (Haines et al., 2005, Hageman et al., 2005, Klein et al., 2005, Edwards et al., 2005). CFH is a negative regulator of the alternative complement pathway. The discovery of the Y402H polymorphism has been replicated in different populations (Haines et al., 2005, Hageman et al., 2005, Klein et al., 2005, Edwards et al., 2005). The polymorphism is thought to have a 25% to 50% attributable risk. Additionally it was found to result in patients showing signs of AMD 7 years earlier than AMD patients without the polymorphism and it also increased the rate of disease progression (Mori et al., 2007, Baird et al., 2006). A mouse model for human Y402H was developed which developed some changes similar to AMD including sub-retinal deposit. The SNP codes for a region of component compound module (CCP) 7 on CFH. This region binds heparin, CRP and necrotic cells (Clark et al., 2006, Laine et al., 2007, Ormsby et al., 2008). Further studies on CFH have revealed many more allelic

variants with strong associations with AMD (Li et al., 2006). The *C2/CFB* (6p21.3) gene codes for complement component C2. SNPs in C2 and CFB had a protective effect on AMD (Sun et al., 2012). The protective variant of CFB was shown to have four times less affinity with C3b. Therefore the C2 allelic variant was less likely to form the C3 convertase in the amplification loop (Montes et al., 2009). Another protective variant in the CFB gene was found in the cleaved signal peptide region and has been proposed to alter the secretion of CFB (Gold et al., 2006). C3 is encoded by the *C3/CFD* (19p13.3-p13.2) gene. C3 polymorphisms are associated with an increased attributable risk of AMD. A substitution of arginine to glycine at position 102 in the C3 protein results in a 2.6 fold increase in AMD risk for those homozygous for the variant. The population attributable risk for CFD in AMD is low but a meta-analysis of studies does show an association for AMD in CFD SNPs (Stanton et al., 2011). Patients with AMD also have higher levels of CFD.

CFI is encoded by the *CFI* (4q25) gene. *CFI* has an association with AMD (Yu et al., 2011). The allelic variant associated with AMD is found in an intronic region of the gene and is therefore thought to affect the promoter region of *CFI*. *SERPING1* (11q12-q13.1) codes for a naturally occurring inhibitor of C1, which prevents its activation in the classical complement pathway. Polymorphisms were found to be associated with AMD and later confirmed with a case control study (Ennis et al., 2008). The finding is relatively surprising in the light of all the previous associations with the alternative complement pathway.

In summary, there is strong evidence for a role for the complement pathway in AMD pathogenesis. This suggests value of investigating the complement pathway in a model of macular degeneration.

1.4 Human induced pluripotent stem cells (hiPSCs) and disease modelling

1.4.1 Retinal pigment epithelium, Bruch's membrane and choroid

The RPE is the primary cell type expressing C1QTNF5 within the eye. The RPE is also known to

show disorganisation and is lost in L-ORMD. There is evidence from transfected cell studies that RPE dysfunction also plays a role in L-ORMD disease mechanism. As a result, the RPE is likely to play a central role in a good model of AMD. This section briefly reviews the role of the RPE in normal physiology.

The RPE layer is a pigmented, polarised, polygonal monolayer of cells. It is a cuboidal epithelium found between the photoreceptor outer segments and the Bruch's membrane below it. RPE cells are relatively flat with height of approximately 10-12um and a width of approximately 14um at the macula. In the periphery, the width of cells increases to approximately 60um. The RPE are polarized cells with an apical-basal polarity (Marshall, 1987, Streeten, 1969). At its apical surface the RPE is in contact with an extracellular matrix known as the interphotoreceptor matrix. In order to make contact with photoreceptors the RPE project microvilli. These small microvilli are important for phagocytosis and form sheaths around the photoreceptors (Bairati and Orzalesi, 1963, Spitznas and Hogan, 1970). The basal surface develops multiple infoldings that increase the absorptive and secretive surface area. The apical portion of the lateral walls are important for cell to cell adhesion and contain tight junctions and occasional gap junctions (Rahner et al., 2004, Konari et al., 1995). These junctions are important in maintaining the integrity of the monolayer and controlling the passage of molecules. Thus the majority of apical basal flow is controlled by the RPE cell itself and therefore enables the cell to modify the composition of the interphotoreceptor matrix to maintain the photoreceptor microenvironment. Although the junctions between RPE cells are tight, they are not in the same order of function as other tight junctions for instance the blood brain barrier. There have been various reports of transepithelial resistance (TER) from approximately 850 Ω/cm^2 to 200 Ω/cm^2 (Hu and Bok, 2001). Cells located in the blood brain barrier are reported to have a TER between 1000-2000 Ω/cm^2 (Rizzolo, 2007).

The RPE cell is itself packed full of organelles. The organelles have a polarised organisation. The apical surface is dense with melanosomes. The nucleus, Golgi body and mitochondria are found towards the basal surface. In keeping with its phagocytic role and anti-oxidative role the RPE has many phagosomes which are mobilised using a microtubular intermediate filament architecture. The RPE has a high number of mitochondria suggesting high metabolic function.

The RPE is known to have a number of functional roles in the healthy retina including light absorption, photoreceptor outer segment phagocytosis, control of oxidative stress, recycling of photoreceptor pigment, control of extra cellular composition and growth factor secretion. These roles are discussed below as dysfunction in these properties has been linked to various diseases.

The RPE is placed under large amounts of oxidative stress. Within the eye, light is focused on to the macula and the fovea in particular. Ultraviolet is filtered by the cornea and lens and consequently blue light cause the greatest damage to the retina and result in photo-oxidative stress. RPE also contain large numbers of mitochondria involved in normal generation of adenosyl

triphosphate (ATP) to provide the cell with energy. The nicotinamide adenine dinucleotide phosphate (NADPH) dependent oxidases found in organelles also produce large quantities of (reactive oxygen species) ROS (Brown and Griendling, 2009). Other enzymatic pathways that lead to ROS formation include the cyclo-oxygenase, lipoxygenase and cytochrome p450 pathways. Organelles also produce ROS during normal cellular housekeeping including peroxisomes, which manage large chain fatty acids from the membranes and endoplasmic reticulum which degrade misfolded protein (Dixon and Stockwell, 2014). The burden of oxidative stress is increased further by the phagocytosis of photoreceptor outer segments (discussed below). The enzymatic cascade that results from the breakdown products of phagocytosis results in the formation of lipofuscin. Following phagocytosis the outer segments are transported to the Golgi body in phagosomes. In the phagosomes NADPH-oxidase dependent oxidation results in the generation of hydrogen peroxide (H_2O_2) (Tate et al., 1995).

In order to combat oxidative stress the RPE has a number of adaptations. Melanosomes are organelles that make and store melanin (Raposo and Marks, 2007). Melanosomes also contain a range of anti-oxidant enzymes whilst their membranes contain ion channels. These functional elements within melanosomes play a part in scavenging reactive oxygen species (Simon et al., 2008, Hu et al., 2008). To catalyse the breakdown of H_2O_2 the RPE upregulates the generation of catalase (Tate et al., 1995). The RPE also contains a number of other non-enzymatic antioxidants. These include carotenoids, zeaxanthin, lutein, α tocopherol and carotene (Liles et al., 1991).

In order for photoreceptors to function properly they have to regenerate new outer segment (OS) discs and remove used discs. Rods regenerate their outer segments within a fortnight (Young and Droz, 1968). Each RPE is in contact with approximately 300 OSs and phagocytoses between 20-30,000 discs daily (Young and Bok, 1969). The physiological regulation of phagocytosis is regulated by the light/dark cycle and temperature. RPE perform two main types of phagocytosis; specific and non-specific. Specific phagocytosis requires several steps. αVβ5 integrin on apical microvilli recognises photoreceptor OS packets and activates downstream players in phagocytosis including MerTK (Finnemann et al., 1997). The MerTK activated complex interacts with myosin IIa. Together this results in the formation of a phagocytic cup, which enables the microvilli to engulf OS. Invagination is thought to be (cAMP) mediated (Edwards and Flaherty, 1986). Non-specific phagocytosis is similar to pathways found elsewhere in the body and exhibited by phagocytic cells such as macrophages.

The RPE also recycles photoreceptor visual pigments, which are essential for phototransduction. Light causes the change in 11 cis retinal to all-*trans* retinal via several intermediates including meta-rhodopsin II (Hargrave, 2001). This activates transducin and induces a hyperpolarisation of

the photoreceptor and an alteration of neurotransmitter release to bipolar cells, which effectively transduces light energy to produce a neural response. In rods, all-*trans* retinal is released from the membrane of photoreceptor discs into the lumen. It then binds with N-retinlidene-phosphatidylethanolamine (N-ret-PE) (Liu et al., 2000). The complex then joins ABCA4, a large transmembrane transporter that transfers the complex into the cytoplasm of the outer segment (Allikmets et al., 1998). Retinol dehydrogenase (RDH) converts all-*trans* retinal to all-*trans* retinol that subsequently binds to interphotoreceptor binding protein (IRBP) and transfers all-trans retinol to the retinal pigment epithelium (Rattner et al., 2000). Once in the RPE, all-trans retinol is released and binds to cellular retinol binding protein (CRBP) which moves into the endoplasmic reticulum (ER) where it is esterified by lecithin:retinol acyl transferase (LRAT) (Fong et al., 1984). RPE-65 hydrolyses retinyl esters to 11-*cis* retinol, which is bound to cellular retinaldehyde binding protein (CRALBP) (Hamel et al., 1993, Moiseyev et al., 2006). LRAT esterifies the 11-cis retinol to 11-*cis* retinyl ester for storage if required (Ruiz et al., 1999). 11-*cis* retinol is then converted to 11-*cis* retinal by RDH 5 and 11. CRALBP binds 11-*cis* retinal before transferring it to IRBP, which transfers 11-cis retinal to replenish photoreceptors (Bunt-Milam and Saari, 1983).

The RPE maintains the ECM for photoreceptor homeostasis by enabling transport through cellular transporters or by paracellular transport. Water flows from apical to basal through the cell via a number of transport mechanisms (Hughes et al., 1984, Chihara and Nao-i, 1985). Glucose and substances required by the photoreceptor such as DHA are transported from basal to apical (Kita and Marmor, 1992, Bazan et al., 1992, Hsu and Molday, 1994). Conversely, waste products from the photoreceptors such as lactic acid are transported in the opposite direction (Hamann et al., 2000). The RPE also controls extracellular pH by modulating bicarbonate levels. In order to support photoreceptors the RPE secretes fibroblast growth factor (FGF) (Khaliq et al., 1995). The RPE also secretes a number of other factors including transforming growth factor beta (TGF-β), ciliary neurotrophic factor (CNTF), insulin like growth factor and platelet derived growth factor (PDGF) (Khaliq et al., 1995, Cao et al., 1997, Campochiaro et al., 1994). Pigment epithelium derived factor (PEDF) maintains the stability of the choroidal blood vessel cells and prevents proliferation of these cells and hence neo-vascularisation (Dawson et al., 1999). It also protects the neuro-retina from stress-induced damage (Cao et al., 2001). VEGF is secreted at low levels by the RPE mainly basally (Adamis et al., 1993). Its role in normal function is to maintain choriocapillaris vascular endothelial cell viability (Burns and Hartz, 1992). Thus the RPE plays a role in maintaining the local homeostasis of the outer retina.

The RPE layer is attached on its basal surface to the BM. This acellular pentalaminar structure lies between the retinal pigment epithelium and choroid. Histologically the BM can be divided into five

layers with a total thickness of only approximately 3.2um that varies according to location within the retina. The outer most layer is the basement membrane of the choriocapillaris. The middle layer is an elastin layer that is sandwiched in between two collagenous layers known as the outer and inner collagenous layer. The inner most layer of BM is the RPE basement membrane.

Looking at each of these layers starting with the outermost layer the choriocapillaris basement membrane is mainly composed of type IV, V and VI collagen in addition to laminin and heparan sulphate and is 0.14um thick (Aisenbrey et al., 2006). Collagen type VI forms the majority of this layer and forms microfibrils onto which other structures adhere. The outer collagenous layer of BM is composed of collagen type I, II and V which arrange themselves into a grid covered with a range of active molecules including glycosaminosglycans (GAGs), molecules involved in the coagulation cascade and complement cascade components (Marmor, 1998). It is approximately 0.7um thick. The elastin layer is approximately the same thickness as the outer collagenous layer at 0.8 um and is several times thinner at the macula than the periphery (Chong et al., 2005). It contains elastin fibres, collagen type IV and fibronectin. The elastin fibres contain small spaces sized at approximately 1um to enable the passage of substances through the layer (Marmor, 1998). The inner collagenous layer is double the thickness of the outer collagenous layer at 1.4 um but otherwise the structures and composition are almost identical (Marmor, 1998). Finally, the inner most layer is the RPE basement membrane. This layer is approximately 0.15 um thick. The structure of BM is thought to help cell adhesion, migration, differentiation, control of substances transported across the BM and the prevention of choroidal vascularisation of the neuro-retina.

Blood supply to the RPE is provided by the choroid. This is a vascular layer found outside of the Bruch's membrane-RPE complex. In humans, the choroid is thickest at birth. It decreases in thickness with age from approximately 200um at birth to 80 um by the ninth decade (Ramrattan et al., 1994). The choroid is thickest at the fovea reducing in thickness at the periphery. The Choroid is made up of several layers. The choriocapillaris, which lies just outside the Bruch's membrane, is a thin network of fenestrated capillaries. The choriocapillaris is only 10um thick at the fovea and thins more peripherally to approximately 7 um. The diameter of the capillaries varies between 20-40um which is larger than normal capillary diameter (Bill et al., 1983). Sattler's layer sits outside the choriocapillaris and contains small to medium sized vessels (Hayreh, 1975). The vessels supply and drain the choriocapillaris. Haller's layer contains larger medium to large vessels that in turn supply and drain the Sattler's layer (Hayreh, 1975). In between the vessels lies elastin and collagen to maintain choroidal structure. The immune cells of the retina also reside in these layers.

1.4.2 Human induced pluripotent stem cells (hiPSCs)

After conception, the developing zygote divides to form the morula and blastocyst. These cells continue to divide into an inner cell mass and an outer layer of cells known as the epiblast. Cells from the inner cell mass were first isolated and grown in 1998 and were called human embryonic stem cells (hESCs) (Thomson et al., 1998). HESCs were said to be pluripotent stem cells. Stem cells have the ability to self-renew and differentiate to other cell types. Cell potency describes the ability of a cell to differentiate into other cells. Pluripotent cells are able to differentiate to cells of the three germ layers, which include the endoderm, ectoderm and mesoderm. With each successive differentiation, cells lose their ability to differentiate to other cell types. However, an increasing body of evidence pointed to the fact that under the correct conditions even terminally differentiated somatic cells could be reprogrammed back to a pluripotent state (Gurdon, 1962, Wilmut et al., 1997). Takahashi *et al.* further interrogated the factors responsible for somatic cellular reprogramming and were able to distil these down to four transcription factors. Using these factors, they were able to reprogram first mouse fibroblast cells to a pluripotent state (Takahashi and Yamanaka, 2006) and later human fibroblasts to a pluripotent state (Takahashi et al., 2007). The resultant cells were called human induced pluripotent stem cells (hiPSCs) as they shared properties with other pluripotent cells such as hESCs.

1.4.3 Retinal differentiation of hiPSCs

Retinal differentiation of hiPSCs can be divided generally in to either default differentiation or directed differentiation protocols. Default methods generate RPE without the addition of exogenous transcription factors. The protocols utilise the tendency of pluripotent cells to differentiate to neural lineages in the absence of other factors (Munoz-Sanjuan and Brivanlou, 2002). However, the technique is not efficient and produces mixed populations of cells. Additionally, some lines may not have an intrinsic capacity for retinal differentiation, which may be dependent on endogenous expression of retinal differentiation genes (Mellough et al., 2012).

In contrast, directed differentiation uses exogenous transcription factors, proteins or small molecules to help to recapitulate early embryological development. For retinal differentiation cells are directed through a step wise differentiation through pluripotent cells to primitive anterior neural phenotype, retinal progenitor before terminal differentiation in to either RPE or neuro-retinal lineages. Directed differentiation protocols had initially been optimised using hESCs (Klimanskaya et al., 2004, Lamba et al., 2006, Meyer et al., 2009, Osakada et al., 2008). Fibroblast growth factor was shown to be a key regulator of pluripotency in human pluripotent cells (Vallier et al., 2005). Removing basic FGF from pluripotent cell maintenance media initiated differentiation (Reubinoff

et al., 2001). Neuroectodermal induction requires suppression of other differentiation pathways including mesodermal and endodermal cell fates. Suppression of bone morphogenetic protein can induce a neuroectodermal like stage (Tropepe et al., 2001). Inhibition of *SMAD* signalling increased neural enrichment to over 90% from 10% (Chambers et al., 2009). A subset of neurally differentiated cells were shown to develop an eye field specification and form retinal cells via a retinal progenitor stage (Vugler et al., 2008). Neural progenitors can be directed to a retinal cell fate by substances that increase *MITF* expression such as Activin A (Meyer et al., 2011). Neuro-retinal progenitors can in turn be patterned to either RPE or neuro-retinal fate by a number of different mediators (Hirami et al., 2009, Jin et al., 2011, Lamba et al., 2010, Mellough et al., 2012, Osakada et al., 2009b).

1.4.4 Disease modelling using hiPSCs

With increasing evidence that hiPSC derived cells recapitulate key physiological and functional *in vivo* characteristics there has been a shift in focus from optimising differentiation protocols to modelling retinal disease. The study of retinal disease has been hampered by the limited availability of disease causing cell types, which is difficult to obtain from patients. HiPSCs provide a valuable alternative. With the correct differentiation protocols hiPSCs can provide an almost limitless supply of disease specific cell lines to model human disease. This approach has been used successfully to model diseases from a variety of conditions affecting a number of different organ systems. Examples of diseases successfully modelled which have provided insights into disease mechanism include amyotrophic lateral sclerosis, long QT syndrome, Alzheimer's disease, sickle cell disease and Friedrich's ataxia (Bellin et al., 2012, Malan et al., 2011, Yahata et al., 2011, Zou et al., 2011, Liu et al., 2011).

Looking specifically at modelling diseases of the RPE using hiPSC-RPE several diseases have already been studied using this approach. HiPSC-RPE derived from a patient with gyrate atrophy revealed potentially translatable patient specific findings. Gyrate atrophy results from reduced activity of the enzyme ornithine aminotransferase (OAT). Rare variants are able to be corrected using vitamin B6 (Meyer et al., 2011). The study identified that vitamin B6 was able to increase OAT activity in the cell lines derived from the patient. The findings could be directly applicable to the care of the donor patient. HiPSC-RPE derived from patients with Best vitelliform macular dystrophy discovered that mutant RPE developed several types of metabolic dysfunction when compared with control RPE including build-up of lipofuscin on feeding of cells, abnormal fluid flux, delayed degradation of photoreceptor outer segments and increased oxidative stress after feeding (Singh et al., 2013b). Subcellular localisation studies identified an endoplasmic reticulum

localisation of BEST1 protein suggesting that abnormal BEST1 has a role in regulating intracellular calcium flux. HiPSC have also been generated from patients with AMD. HiPSC-RPE derived from patients with ARMS2/HTRA1 associated with AMD were found on unbiased proteomic screening to have increased levels of SOD2 and markers of oxidative stress when compared to cells derived from controls with protective risk alleles suggesting a role for inherent vulnerability to oxidative stress in RPE cells in disease pathogenesis (Yang et al., 2014a).

There are however several limitations to modelling disease using hiPSCs. When comparing hiPSCs to hESCs transcriptional differences have been noted (Liao et al., 2010). HiPSCs have been shown to retain some of the epigenetic background of the original cell of the parent cell despite complete reprogramming (Bar-Nur et al., 2011, Kim et al., 2010). HiPSCs contained differentially methylated DNA regions that were related to the cell of origin (Kim et al., 2010). Additionally, X-reactivation does not readily occur when generating hiPSCs (Pomp et al., 2011, Tchieu et al., 2010). Failure of transcriptional activation of epigenetically silenced regions can limit the impact of using hiPSCs particularly when genes of interest are in transcriptionally silenced regions (Urbach et al., 2010).

During hiPSC generation and maintenance, a number of genetic changes may occur in hiPSCs when compared to the donor cell of origin. These changes may limit interpretation of the effect of the disease causing mutations. First generation reprogramming methods generated hiPSCs by insertion of transgenes in to the genome. These insertions could not only silence host cell genes but also lead to non-silenced transgene expression (Soldner et al., 2009). Prolonged culture and passaging of hiPSCs has been shown to result in an accumulation of genetic mutations and karyotypic abnormalities which may lead to significant differences in gene expression which are not related to the disease phenotype (Ben-David et al., 2011, Laurent et al., 2011). These factors can be mitigated by thorough validation.

Additionally not all diseases are suitable for modelling using hiPSCs. Firstly, the terminally differentiated cells generated in culture from hiPSCs are matured for only a short time and may reflect functionally immature cells (Kuzmenkin et al., 2009, Peng et al., 2010). This may be beneficial when studying developmental diseases or when cell maturity is not relevant to the study of a disease mechanism (Itzhaki et al., 2011), but may hamper the study of chronic disease. However, hiPSC derived RPE also show phenotypes of functionally mature cells including high TER, photoreceptor OS phagocytosis, functional release of growth factors, fluid flux and ATP induced calcium release (Kokkinaki et al., 2011). This suggests that hiPSC-RPE can be used to study adult disease. A further limitation in modelling certain diseases is the inherent variation in

generation of hiPSCs and differentiation of disease specific cell lines. Disease phenotypes need to be robust to enable the identification of *in vitro* phenotypes. Finally, the study of complex diseases which are not confined to cell autonomous disease mechanisms, may be challenging but may be overcome with the use of experimental design such as co-culture to recapitulate *in vivo* conditions (Di Giorgio et al., 2007).

In summary, increasing evidence points to the utility of hiPSC disease modelling within the context of limitations of the platform. Many of the limitations can now be mitigated against by using newer hiPSC protocols and by using good experimental design. This points to the use of hiPSC-RPE generated from L-ORMD patients and controls in order to model L-ORMD.

1.5 Rationale, Aims and Hypotheses

There has been a rapid development in therapy for both AMD and inherited retinal disease. Some of the treatments used for AMD are potentially applicable to L-ORMD (Aye et al., 2010). In order to monitor disease progression there needs to be an understanding of natural history and phenotype of disease to provide clinical biomarkers. This first aim of this part of the study is to refine the phenotype of L-ORMD using multimodal imaging and to investigate tools to monitor progression in L-ORMD using an observational study to investigate a cohort of L-ORMD patients.

Although studies have established causal factors in AMD pathogenesis, understanding of the stepwise sequence of events that leads to AMD is still unclear. Currently, it is difficult to identify patients who will develop AMD and consequently the study of early AMD has been limited. Additionally, it is still unclear what causes the initial injury in macular degeneration. L-ORMD is a good model of AMD as it replicates key clinical and pathological features of AMD. Unlike AMD, L-ORMD has Mendelian inheritance and therefore it is possible to identify patients by genetic testing early or prior to clinical disease onset. This provides an opportunity to study disease processes in early macular degeneration.

Pathology studies have shown that drusen, an early marker of AMD, contains activated complement components. Additionally, genetic studies have demonstrated that mutations in complement pathway components lead to an increased risk for the development of AMD. Taken together this provides evidence that complement dysfunction plays a role in early macular degeneration. The second aim of the study is to see whether complement dysfunction also plays a role in L-ORMD. The hypothesis is that localised complement dysregulation also plays a role in L-ORMD pathogenesis. In order to demonstrate complement pathway involvement in L-ORMD

disease mechanism I firstly use *in vivo* retinal samples from a L-ORMD mouse model and later human L-ORMD donors to study complement activation.

Developments in cell biology now enable the generation of stem cells from patients with inherited diseases. The step-wise differentiation of these stem cells with defined protocols provides a virtually unlimited source of cells carrying disease-causing mutations. RPE cells have been proposed to play a central role in L-ORMD disease pathogenesis. I aimed to generate RPE from L-ORMD patients and their unaffected siblings in order to develop an *in vitro* model for L-ORMD. The initial hypothesis of this part of the studies was that RPE generated from cases would show cell autonomous differences from that generated from sibling controls. I next aimed to study whether any differences in complement activation identified during the *in vivo* studies could be recapitulated using the cell model. The hypothesis was that localised complement dysregulation could be identified in case RPE when compared to control RPE.

CFH is a regulator of the alternative complement pathway. Allelic variants of CFH are associated with AMD. In previous work performed by Dr Xinhua Shu (unpublished) an interaction between C1QTNF5, the protein affected in L-ORMD, and CFH has been identified. The aim is to generate wild-type and mutant protein and to test the affinity of the mutant and wild-type with purified CFH. The hypothesis is that the mutation alters the affinity of C1QTNF5 for CFH.

Taken together the overall aim is to provide a greater understanding of L-ORMD clinical characteristics and to better understand the disease mechanisms that cause the clinical phenotypes. It is hoped that findings from this series of studies will provide insights not only for L-ORMD disease mechanism but also for other deposit forming macular degenerations.

CHAPTER 2

2. L-ORMD *in vivo* studies

2.1 Introduction and rationale

L-ORMD exhibits many clinical similarities with AMD in early disease and has been proposed as a good model for AMD. Clinical similarities include dark adaptation delay, drusen like deposits, pigmentation, choroidal neovascularisation and neuro-retinal atrophy (Jacobson et al., 2001, Milam et al., 2000, Ayyagari et al., 2005) (Table 2.1). Recently, the rapid development of newer devices have enabled more detailed investigation of both the retinal structure and function. Although L-ORMD is a rare condition, one of the largest cohorts of L-ORMD patients resides in South East Scotland and North East England. These patients have not been phenotyped previously. Consequently, the initial aim is to compare the phenotype of our cohort with previous reports in the literature (table 2.1). Although genetic testing is now available to identify L-ORMD, it is often difficult to differentiate L-ORMD clinically from other conditions in the early stages. This study provides an opportunity to update the L-ORMD phenotype using a multimodal approach. The study aims to look at structural changes in early L-ORMD and to see how this correlates with clinical presentation. The hypothesis is that using newer multimodal imaging techniques L-ORMD patients will show features similar to AMD.

Authors	Year published	Number of family members investigated	Numbers presumed/confirmed to be affected	Studies
Kuntz et el.	1996	5	3	Automated perimetry
Milam et al.	2000	7	6	Goldman perimetry, ERG, DA
Ayyagari et al.	2000	10	9	Colour vision, ERG, Goldman perimetry, DA
Jacobsen et al.	2001	23	12	Goldman perimetry, ERG, DA
Moroi et al.	2003	15	7	Anterior segment exam
Ayyagari et al.	2005	55	38	ERG, DA
Vincent et al.	2012	4	4	SD-OCT, ERG, EOG
Soumplis et al.	2013	4	4	SD-OCT, ERG
Jacobsen et al.	2014	2	2	SD-OCT, 2 colour rod sensitivity
Papastavrou et al.	2015	9	9	Dark adapted ERG

Table 2.1 Summary of previous clinical studies and investigations.

SD-OCT= spectral domain ocular coherence tomography, DA= Dark adaptometry, RG=Electroretinography, EOG=Electro-oculogram

The earliest histological changes in AMD include basal deposits in Bruch's membrane. Depending on the layer of the deposit the terms basal linear deposit (BLinD) and basal laminar deposit (BLamD) have been used (Sarks et al., 1980). BLinD are found below the basement membrane layer of the RPE in Bruch's memebrane and above the inner collagenous layer whilst BLamD are found in between the RPE membrane and RPE basement membrane. BLinD are composed of vitronectin, apolipoprotein B and E and neutral lipids such as cholesterol (Curcio and Millican, 1999). BLamD contain wide spaced collagen and amorphous material (Curcio and Millican, 1999, Spraul et al., 1999). BLamD can occur with normal ageing whilst BLindD is more specific for AMD (Green and Enger, 1993, Loffler and Lee, 1986). Drusen are also a hallmark of early AMD but are also seen in senescence. BLamD have been found to contain activated complement pathway components in a similar manner to drusen (Anderson et al., 2002). Drusen consist of vitronectin, apolipoprotein B and E, neutral lipids and alpha-crystallins (Crabb et al., 2002, Malek et al., 2003). They have been particularly linked with the complement cascade. They contain compounds such as c-reactive protein, cholesterol and amyloid which can activate the complement cascade (Farkas et al., 1971). Additionally they also contain activated complement components including the final common pathway of the complement system the membrane attack complex (Mullins et al., 2001). Histopathological investigation of L-ORMD retina has previously revealed that the sub-RPE deposit in L-ORMD results forms a bilayer (Duvall, J. et el., 1986). The outer layer is mainly composed of lipids whilst the inner layer consists of wide-spaced collagen. The deposit also contains amyloid P, lysozyme, elastin, apolipoprotein B-100, calcium, cholesterol and rhodopsin in a similar manner to drusen.

Although localised complement dysregulation has been implicated in macular degenerations the role of the complement pathway has not been investigated in L-ORMD. The aim of the histopathological section of the study was to see if there was a difference in complement activation between L-ORMD retina and controls. Recently, a mouse model for L-ORMD was characterised. As human donor retinal samples for L-ORMD were rare, I first used the retina of a recently generated mouse model. Next investigated complement deposition using human L-ORMD retinal samples. The hypothesis was that complement dysregulation contributes to L-ORMD disease pathogenesis.

2.2 Methods

Shyamanga Borooah (University of Edinburgh) or Vasileois Papastavrou (Newcastle University) designed, recruited all patients and performed all visual acuity and microperimetry studies. The medical photography department of the Princess Alexandra eye pavilion and the Royal Victoria

infirmary Newcastle performed fundus photography, SLO, FFA and ICG. James Cameron (University of Edinburgh) performed OCT on AMD patients and on a subset of L-ORMD patients. For recording of details images were reviewed by at least two ophthalmologists including Dr Ashraf Khan, Dr James Cameron and Professor Baljean Dhillon (University of Edinburgh). The electrodiagnostics department of Greater Glasgow and Clyde NHS performed multifocal ERG. Shyamanga Borooah (University of Edinburgh) performed all statistical analyses.

For the immunohistochemistry experiments, all studies were performed by Dr Shyamanga Borooah with guidance from staff of the shared university research facility (University of Edinburgh). Human donor samples from Edinburgh were fixed and paraffin embedded blocks by Professor James Ironside. Human donor samples from San Diego were fixed and paraffin embedded blocks by Professor Christine Curcio (university of Alabama). Mice retinal samples were obtained from mice generated by Professor Radha Ayyagari (University of San Diego). The mice were generated, bred, grown and culled with samples fixed and embedded by Professor Ayyagari's team.

The data analysis for this dissertation was generated using the Real Statistics Resource Pack software (Release 4.3). This was used to provide summary data including arithmetic mean and standard deviation (SD). Standard error (SE) was calculated and used for graphs where three or more samples were used. For comparative statistics, two groups were first individually checked for normality in distribution using the Shapiro-Wilk test of normality. If deemed normal, a t-test was used. If the data was not normally distributed then a non-parametric test such as the Mann Whitney U-test was used for comparison.

2.2.1 Patients

Patients were included if they had been confirmed to carry the Ser163Arg mutation and were at least in stage 2 L-ORMD i.e. having some changes at the macula visible on ophthalmoscopy. Patients were excluded if they had had previous retinal surgery, diabetic retinopathy or retinal laser surgery. Additionally, patients were excluded if they did not have a clear optical view of the fundus due to media opacities. We examined 20 eyes of 10 patients from a large cohort of L-ORMD patients.

Patients were at various stages of L-ORMD disease process after stage 2. The patients were stratified according to severity of disease

The study was reviewed by the institutional ethics board of Newcastle University Hospitals NHS trust and given a REC number: 11/NE/0199

2.2.2 Clinical vision studies

Distance visual acuity testing was performed at 4m using a standardised backlit 4m ETDRS LogMAR chart (Precision vision, La Salle, Illinois) with a diffuser. This method has been used previously been shown to be repeatable with good intra class correlation in macular degeneration patients (Aslam et al., 2014). Standardised charts were changed for each eye being tested in order to prevent patients memorising letters. Patients wore their latest optometric prescription in trial frames. Each line had five letters. Patients were asked to read each letter starting with letters on the top row. Patients were asked to continue until they were unable to read a complete line. If patients were unsure of letters, they were asked to best guess. The LogMAR score was calculated by assigning each letter correctly identified a score of 0.02 (Ferris et al., 1982). Patient's left eye and right eye visual acuity were tested and responses noted on a scoring sheet.

Near visual acuity was measured using a Bailey-Lovie reading chart (Bailey and Lovie, 1980). The test uses lines of 5 unrelated words of equal standard letter size starting with the largest letters on the top line. There is a logarithmic reduction in size of letters with each line (N80-N2). Testing was performed under standard lighting conditions at 25 cm with the patients wearing a +4.00 reading correction over the most recent prescription. The chart has previously been shown to be repeatable in AMD patients and appears to correlate well with measures of visual acuity related to normal activities of daily living (Aslam et al., 2014, McClure et al., 2000).

2.2.3 Clinical imaging

For colour fundus photography a TRC-501X (Topcon medical systems, New Jersey, U.S.A) was used. This device has a 50 degree lens. Patients were dilated with 1 drop of tropicamide 1% (Bausch and Lomb ltd, U.K.) to each eye at least thirty minutes prior to examination. Following which each eye was photographed. Focus, contrast and white balance were adjusted manually by a trained medical photographer. Images were captured on a Nikon D90 (Nikon, Japan) digital camera. This modality of digital imaging is not a new imaging format however, was used to provide true colour images representations in a close format to that provided by newer imaging formats described below.

Fluorescein sodium is a water soluble molecule (354 Daltons). It is 20 percent in solution and 80% protein bound. Fluorescein fluoresces at approximately 520nm. It diffuses into tissues staining them and if there is any break of the blood retinal barrier fluorescein readily leaks. The dye is masked by the retinal pigment epithelium except in early choroidal filling. A bolus of 4ml of 20% fluorescein sodium (Martindale pharmaceuticals, Essex) was injected through an intravenous line. Images were capture from 5 seconds with lates performed at 5, 10 and 30 minutes where possible.

ICG is a molecule of size 775 Daltons and, unlike fluorescein (354 Daltons) the molecule is almost completely protein bound and does not normally escape from retinal vasculature with its blood-retinal barrier. However, the choroidal vasculature with its fenestrated capillaries does permit a slow leak of ICG (Bouchenaki et al., 2002). The staining of the choroidal structures can be masked providing areas of hypofluorescence or absent fluorescence. ICG fluoresces at 830nm, which enables it to be easily imaged using infra-red imaging devices at a different spectrum to fluorescein and therefore allows simultaneous imaging. 25 mg of ICG-Pulsion powder (Pulsion medical systems, Germany) was reconstituted to5mg/ml in 5ml of water for injection. A bolus of the ICG was injected through an intravenous line.

Studies have now shown the utility of using SLO images to study AMD and in particular GA. A SLO is able to measure *in vivo* fluorescence generated from fluorophores in the retinal pigment epithelium (Feeney-Burns et al., 1980, Katz, 2002) thought to be produced from photoreceptor outer segment metabolism in the RPE which could only previously be studied *in vitro* (von Ruckmann et al., 1995, Delori et al., 1995, Bellmann et al., 1997). Reduced autofluorescence may signify reduced functioning photoreceptor-RPE activity reducing retinal sensitivity. Increased fluorescence may signify a prognostic indicator of future photoreceptor-RPE death and has been used for prognosis in GA (Scholl et al., 2004, Holz et al., 2007).

Confocal SLO images were obtained for fundus autofluorescence (wavelength=480 nm) using the Spectralis SLO machine (Heidelberg Engineering, Heidelberg, Germany). Central fixation was attempted and images of the central 30 degrees field of view were taken at a resolution of 768 x768 pixels. This was similar to settings previously used in geographic atrophy (Schmitz-Valckenberg et al., 2008). As some of the L-ORMD patients had poor central fixation the automatic eye tracking software (Automatic real-time (ART)) packaged with the Spectralis was used with a score of 20. This showed the average of 20 B-scan confocal SLO images. To measure the size of areas of atrophy semi-automated software was used (Heidelberg eye explorer v6.0c, Heidelberg Engineering). An initial pilot study was performed with two masked ophthalmologists given 10 images from L-ORMD patients. The ophthalmologists were asked to measure the area of atrophy. A Cronbach's statistic of agreement was calculated to measure the amount of agreement. In order to measure the rate of increase at least two images were chosen greater than one year apart for each patient.

Spectral domain OCT imaging was carried out using a Heidelberg Spectralis SD OCT (Heidelberg Engineering, Heidelberg, Germany) with 870 nm wavelength (Helb et al., 2010). The Spectralis

has an acquisition speed of 40,000 A-scans per second and scans to a depth of 2.8 mm. The resolution of images is approximately 4µm per pixel. To obtain images of the posterior pole 61 scans were taken covering an area of 9 x 7.5mm. Each scan was averaged with an ART of at least 9. To assess the foveal morphology the number of B scans averaged was increased to 100 using ART settings in concordance with recent papers on structure functional assessments of GA (Pilotto et al., 2015). Images were also taken of the choroid using the enhanced depth imaging (EDI) function on the Spectralis. Analysis was made using Heidelberg eye explorer software (version 6.0c) which automatically segmented retinal layers providing thickness measurements. Measurements were taken at the fovea to use a landmark as in recent publications. In addition, 8 participants who were age-matched were selected and used as age-matched controls for measures of retinal volume, neuro-retinal thickness and choroidal thickness. Further semi-automated segmentation was made of the choroid using Heidelberg eye explorer to separate the Sattler and the Haller layer using a recently validated method (Sim et al., 2013). The thickness of both these layers was then measured using the fovea as a landmark. For deposit measurements the fovea was again used as a landmark. A cross section OCT of the fovea was taken. The image was inverted to black on white to enhance contrast in order to visualise the sub-RPE deposit (figure 2.1). The manual measuring tool on the Heidelberg Spectralis software was then used in the 1:1 µm mode in order to measure the deposit height at the fovea. The readings were validated initially by two masked graders. A Cronbach's alpha analysis was used to see the correlation of measures using this system with 18 test images from patients.

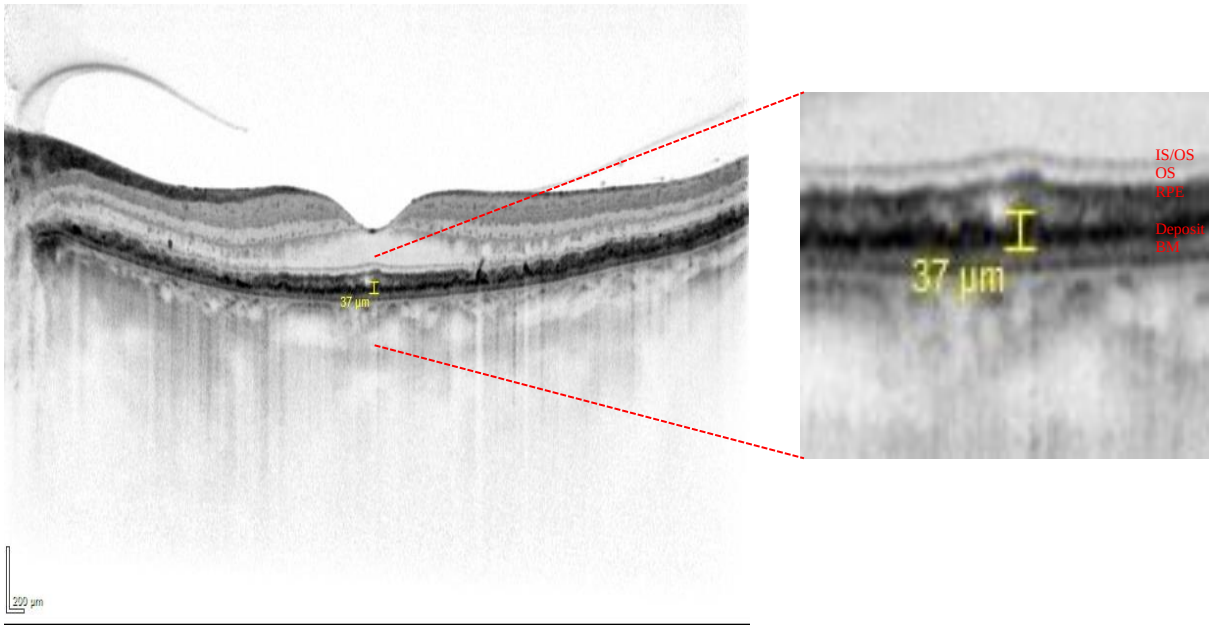

Figure 2.1: Measuring deposit thickness

The image on the left shows a low magnification OCT cross section of the retina in black on white format in order to highlight the sub-RPE deposit. The image on the right shows the deposit (deep black layer) measured using Heidelberg Spectralis software. red arrows signify the thickness of the deposit. The deposits were measured by a scale generated by Heidelberg Spectralis software. The images are labelled with photoreceptor inner segment (IS), the photoreceptor inner and outer segment junction (IS/OS), photoreceptor outer segment (OS), the retinal pigment epithelium layer (RPE), deposit and Bruch's membrane (BM).

2.2.4 Multifocal electroretinography

The conventional ERG uses different stimuli including flash and flicker to elicit a response in the retina. The response of the whole retina is then recorded. However, the recording of global responses may mask more subtle regional changes as found in early macular disease (Palmowski et al., 1999, Heinemann-Vernaleken et al., 2001). Multifocal ERG overcomes some of these shortcomings by independently recording responses from multiple regions of the retina. Different areas of the retina are stimulated by a pseudo-random binary system. A three dimensional plot is then generated from the final amplitudes from the recordings of the different retinal regions.

L-ORMD patients were placed 32 cm from a stimulus monitor, which displayed 61 hexagons covering a visual field of 25 degrees. A cross was used to maintain central fixation and a steady background illuminance was provided. Each of the hexagons alternated between black and white. A ground electrode was placed on the patient's forehead with reference electrodes on the patient's

outer canthi and monopolar loop scleral electrodes were used to make the recordings. Amplitudes and latencies were determined for each region. A scalar product method using a multiplication and summation was used to measure local response. The median scalar product was compared with the normative database using Wilcoxon matched pair methodology (Parks et al., 1996).

2.2.5 Microperimetry

Microperimetry was performed using a similar method to those used previously in AMD patients (Pilotto et al., 2015). Two factors were altered for L-ORMD cases. In order to avoid dark adaptation abnormalities affecting readings the patient's readings were dark adapted for 30 minutes prior to the test rather than the test being performed under mesopic conditions. Additionally, as L-ORMD can cause scotomas beyond the fovea and perifoveal regions the central 40 degrees was tested centred on the fovea. A patch was used to cover the untested eye. The MP1 microperimeter was used (Nidek, Gamagori, Japan). This test was only suitable for stage 2 patients as a central fixation cross was used. A 4-2 double staircase threshold strategy was used using a Goldman size III target, which was presented for 200ms. A monochromatic background was set at 2.27 cd/m2 (=4 asb).

2.2.6 Histopathology

Human samples were kindly donated from the University of Edinburgh tissue bank by Professor James Ironside and from the Professor Ayyagari (University of California, San Diego). Full consent for donation was obtained from the institutional review boards of NHS Lothian, University of Washington and University of Pennsylvania. Eyes were donated within 12 hours of death and stored in a mixture of 10% formalin saline and fixed for at least 6 hours before dehydrating in a series of increasingly concentrated alcohols prior to embedding into paraffin.

The murine C1QTNF5 heterozygous, C1QTNF5 knockout and control sections were from C57BL/6J mice and were a kind donation from Professor Radha Ayyagari (University of California, San Diego). The maintenance, culling and subsequent use of retinal samples was approved by the University of California, San Diego Institutional animal care and use committee. After the animals were sacrificed, the eyes were removed, cornea punctured, and lens removed. The eyes were immersed for fixation overnight in 2% paraformaldehyde and 2% glutaraldehyde. The next day the eyes were washed in phosphate buffered saline (PBS) and then embedded in 30% sucrose/OCT in preparation and frozen in preparation for sectioning.

For human paraffin blocks were dewaxed in xylene for 10 minutes, rehydrated in ethanol (absolute, 90%, 80% and then 70%), and washed in ddH_2O. Antigen retrieval was performed using citrate based retrieval buffer at pH6 (Leica) in a decloaking chamber, slides were heated to 90^oC for 20 mins then allowed to cool to 80^oC before washing in water. Sections were either prepared manually or later using the automated Leica Bond immunostaining using the Leica Refine HRP polymer detection system using similar timings. Slides were washed three times for 5 minutes in PBS. Following this, endogenous peroxidase activity was blocked by incubating the slides for 10 minutes in Bloxall (Vector laboratories, Burlingame, California, USA) in PBS, 0.05% Tween to block endogenous peroxidase activity. Slides were washed twice in PBS for 5 minutes prior to incubating the sections for half an hour in 20% normal goat serum (NGS) in PBS. The slides were the incubated for 2 hours at room temperature in primary antibody diluted in 20% NGS in PBS. Slides were then washed in PBS three times for 15 minutes before staining for 30 minutes with biotinylated secondary antibody. The slides were then washed twice in PBS and incubated for 30 minutes with VECTASTAIN® ABC kit (Vector laboratories) with a final stain of 3,3'diaminobenzidine (DAB) or Vector® Red Alkaline Phosphatase Substrate until staining became clearly visible before rinsing in tap water. The slides were then counterstained in Haematoxylin for approximately five minutes until nuclei were clearly counterstained before a final wash with tap water and mounting on slides with pertex mounting medium (Histolab, Gothenburg, Sweden). A negative control, where the primary antibody was omitted was included in each run.

To identify Bruch's membrane collagen and elastin staining was performed. After dewaxing and rehydrating slides through a series of alcohols. For collagen staining a 50 mL of 0.1% Fast Green, 50mL of 0.1% Direct Red, 900mL of Picric Acid Solution was made. The solution was incubated on slides for two hours before slides were washed with tap water and dehydrated through a graded series of alcohols. For elastin staining slides were incubated with solution composed from 20ml 5% Alcoholic haematoxylin, 8ml 10% Ferric Chloride solution and 8mL Lugol's Iodine for 30 minutes. The slides were then washed in tap water prior to incubation with a further solution made from 20mL 10% ferric Chloride Solution and 80ml ddH_2O. Van Gieson stain was then used to counterstain for 20 seconds prior to the slides being dehydrated in 100% ethanol and mounted.

Mouse sections were cut on a cryostat at 18 microns (Gonzalez-Cordero et al., 2013). Slides were blocked with 5% NGS and 1% BSA in PBS. The primary antibody was then incubated overnight in the same blocking solution. After three washes with PBS the slides were incubated with the secondary antibody for 2 hours at room temperature before a final wash and then counterstaining

with DAPI (sigma-Aldrich). A coverslip was placed onto the slides using mounting medium FluoSave (Merck-Millipore).

In order to see if the changes noted in the L-ORMD samples were different from normal ageing a number of aged eye samples were also tested. Some of these samples were also noted to have early drusen. These specimens were kindly donated by Dr Luminita Paraoan, (Liverpool University).

2.3 Results

2.3.1 Summary of patient cohort

Patients carrying the Ser163Arg mutation in C1QTNF5 are known to progress through a number of stages of disease. All patients were confirmed through sequencing to have L-ORMD in 2010 and actively attending the Princess Alexandra eye pavilion, Edinburgh were recruited from the Edinburgh arm of the study. Similarly, in Newcastle, patients with known L-ORMD who were actively being monitored by the Royal Victoria Infirmary were recruited in to the study. Consequently, 7 patients were recruited from Edinburgh and 10 patients from Newcastle were recruited at various stages of disease . It was understood that this is a relatively small group of patients with the condition however the numbers compared favourably with the largest cohort studies using older methods of investigation and was far larger than the most recent studies using similar methodology including spectral domain OCT. As a result, the study should provide some valuable insights into the clinical phenotype as well as confirming that the patients in this cohort have similar characteristics to previously described cohorts with established phenotypic characteristics. A summary of the patient cohort can be found in table 2.2.

Case	Age	Sex	Stage	BCVA (Right, Left)	Medical history	Medicines	Fundus features
1	57	Male	2	63,63	Hypertension, Hypercholesterolaemia	Lisinopril Amlodipine Simvastatin	Drusenoid deposits in the para-fovea, peri-fovea and temporal retina. Marked pigmentation in peri-fovea temporally
2	58	Male	3	38, 48	Polymyalgia rheumatica	Vitamin A Prednisolone 2mg	Marked atrophy of temporal peri-fovea, fovea and temporal retina. Minimal nasal foveal sparing
3	51	Female	2	81,84	Nil	Nil	Large drusenoid deposits throughout the peri-fovea and temporal retina. Some pigmentation inferiorly in the peri-fovea.
4	54	Male	2	94,90	Splenectomy	Vitamin A Simvastatin Penicillin V	Small drusen throughout peri-fovea and temporal retina with foveal sparing.
5	65	Male	2	83,83	Nil	Simvastatin	Large drusen with pigmentation in peri-fovea and temporal retina. Some temporal atrophy
6	50	Female	2	85,84	Hypothyroid	Thyroxine	Medium sized drusen in the peri-fovea and temporal retina

7	60	Male	2	84,85	Nil	Vitamin A Simvastatin	Small drusenoid deposits in the para-fovea, peri-fovea and temporal retina with peri-foveal pigmentation
8	60	Male	2	73,10	Diabetes type 2 Smokes 7 a day	Amitryptilline Simvastatin Aspirin Novorapid Lanctus	Large drusenoid deposits marked atrophy with foveal sparing
9	74	Female	3	62,4	Diabetes type 2, Hypothyroidism, Hypercholesterolaemia	Bendroflua methiazide, Atenolol Levothyroxine Simvastatin	Marked central atrophy with temporal haemorrhage on the right eye. Pigmetation surrounding atrophy
10	66	Female	3	11, 79	Bladder Ca, Hypercholesterolaemia, TIA	Atorvastatin Clopidogrel	Marked confluent atrophy from disc to temporal macula and near temporal retina with pigmentation
11	55	Male	2	83, 85	Hypertension, Diabetes type 2	Candesartan Simvastatin	Marked soft drusenoid deposits in the para, peri – foveal region into the temporal retina
12	68	Female	3	4,2	Nil	Calcichew	Widespread atrophy with marked pigment clumps in the macula and smaller amounts of pigmentation peripherally
13	57	Male	2	76,85	Hypercholesterolaemia TIA	Aspirin Bisoprolol Amlodipine Atorvastatin	Small discrete drusenoid deposits scattered throughout the

							macula with larger softer deposits in the temporal retina
14	66	Female	3	24,3	Diabetes type 2, Atrial fibrillation	Atenolol Amlodipine Digoxin Levothyroxine	Marked areas of atrophy including the fovea and the temporal retina with some surrounding drusenoid deposit
15	67	Female	2	74, 74	Hypothyroid	Thyroxine Venflaxine	Marked soft drusenoid deposit throughout the macula and early temporal retina sparing the central fovea. Some atrophy temporal to the fovea
16	71	Female	3	30, 12	Nil	Calcichew Levothyroxine Losartan Omeprazole Pravastatin	Severe atrophy with large pigment clumps centrally
17	63	Male	3	18,11	Hypertension	Atenolol	Marked confluent atrophy from the disc to the early temporal retina including the fovea. Some soft drusenoid deposits surrounding this atrophy

Table 2.2 Summary of L-ORMD patient cohort in this study

Although imaging was performed on all individuals, I decided to concentrate primarily on stage 2 disease patients. These patients present with the most clinical diagnostic difficulty and therefore phenotyping will potentially provide the most benefit in the diagnosis and management for these patients. In addition, little is known about the progression of the disease at this stage. If future trials for therapy are envisaged there need to be clear phenotypic markers of progression. The differential diagnoses at this stage include geographic atrophy and other inherited deposit diseases including Sorsby fundus dystrophy and dominant drusen. Stage 3 patients develop gross changes. The main question was to see whether stage 2 L-ORMD had distinct clinical characteristics or whether early L-ORMD shared characteristics with more common diseases such as early macular degeneration.

2.3.2 L-ORMD phenotype

In order to start phenotyping the patients I first planned to repeat previous studies on my cohort of patients. Together with Dr Papastavrou (Newcastle University) we designed a longitudinal study to encompass older and newer technology for monitoring these patients. As far as I was aware this cohort of patients had never previously been phenotyped.

To start with we planned to repeat basic studies performed in previous studies for our cohort to ensure that findings in our cohort were not markedly different from findings in previous reports for L-ORMD (table 2.1). These included visual acuity and colour fundus photography (table 2.3). This was important, as later studies would be dependent on cells derived from patients in this cohort. We next wanted to identify new structural features using newer technology including near infra-red reflectance, scanning laser ophthalmoscopy. Some of these studies had been already been performed on smaller cohorts (Jacobson et al., 2014, Soumplis et al., 2013). Fundus fluorescein angiogram (FFA) and indocyanine green angiography (ICG) have previously been used to identify focal deposits in AMD (Arnold et al., 1997, Bottoni et al., 1994, Querques et al., 2013, Souied et al., 2006). In order to better understand the early drusenoid picture seen in L-ORMD these studies were performed on stage-2 patients. Finally, we looked to compare structure with function by using microperimetry and multifocal ERG. Patients were staged into either group 3 if the fovea was involved on autofluorescence or stage 2 if the fovea remained intact (table 1.3).

List of investigations for the L-ORMD cohort
Visual acuity
Colour fundus photography/ wide field colour scanning laser ophthalmoscopy
Scanning laser ophthalmoscopy autofluorescence
Near-infra-red reflectance
FFA
ICG
Microperimetry
Multifocal ERG

Table 2.3 Summary of clinical studies performed on patients

17 patients were recruited into the cohort. The mean age of patients was 61.3 with 8 female and 9 male patients. 10 Patients were in stage 2 and 7 patients were in stage 3. The mean age of stage 2 patients was 57.6 years (SD=1.75) and the mean age of stage three patients was 68.0 (SD=1.61). Best corrected visual acuity findings were as expected with stage 2 patients having a mean ETDRS letter score of 77.7 letters (SD= 4.08) whilst the stage 3 patients had a mean ETDRS letter score of 23.7 letters (SD= 6.85) significantly less ($P<0.001$).

The cohort seemed to be representative of previous descriptions of L-ORMD (Borooah et al., 2009). All patients showed anterior segment characteristics including long anterior zonules and iris atrophy (figure 2.2). Progression appeared to be similar to previous reports with most having spared central vision till their seventh decade. Colour fundus photography findings showed an expected phenotype of progression with age and stage (figure 2.3). Early stage 2 patients had relatively few features on colour fundus photography. Close inspection identified fine drusenoid spots in the para and peri-fovea. These were most marked temporally. There were no signs of atrophy or neovascularisation. Later stage 2 patients showed more prominent drusenoid lesions which were scattered across the macula but concentrated in the temporal macula. This was similar to a previous report (Vincent et al., 2012). Pigmentation was noted in the peri-foveal region. There were also signs of early atrophy sparing the fovea in the temporal macula. Stage 3 disease showed changes in the fovea with atrophy, pigmentation and occasionally choroidal neovascular scarring. The peripheral retina showed marked scalloped areas of atrophy with some associated pigmentation. These atrophic areas extended to the Ora Serrata in late stage 3 patients (figure 2.3).

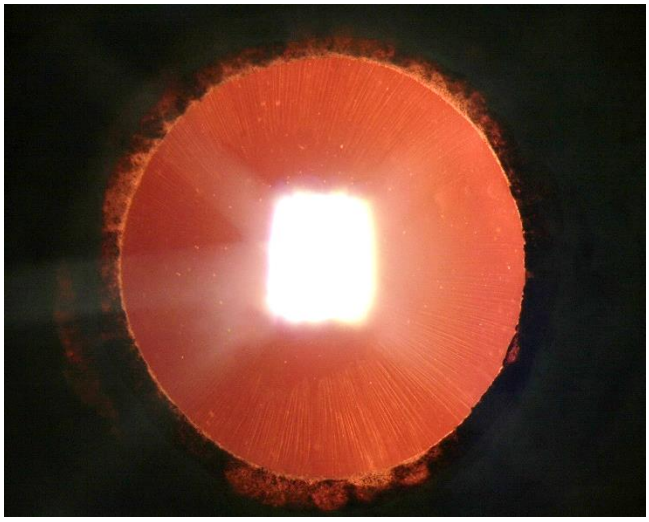

Figure 2.2 Anterior segment photograph.

The photograph of the left eye shows long anterior zonules extending beyond the pupillary margin. Pupillary atrophy at the pupillary ruff.

Figure 2.3: Fundus images from different stages of L-ORMD.

(A) Early stage 2: Colour fundus photograph. Fine drusenoid deposits visible in the macula with a concentration in the temporal macula. Little or no foveal involvement.
(B) Late stage 2: Colour fundus photograph. Neuro-retinal atrophy in the macula with foveal sparing. The fovea also demonstrate drusenoid changes with early pigmentation.
(C) Stage 3: Widefield scanning laser ophthalmoscope image demonstrating complete atrophy of the macula with marked pigmentary changes at the fovea. In the periphery, there are scalloped areas of atrophy extending to the far peripheral fundus.

Looking more closely at the colour fundus photographs of stage 2 patients, there appeared to be a regional difference in the shape and type of drusenoid deposit (figure 2.4). The peri and para-foveal deposits were small discrete and sharply demarcated. This pattern was also seen in the temporal deposits however, in some cases the deposits were larger with a softer edges more similar to soft drusen. This was only seen in later stage 2 patients suggesting that this feature may be a

progression.

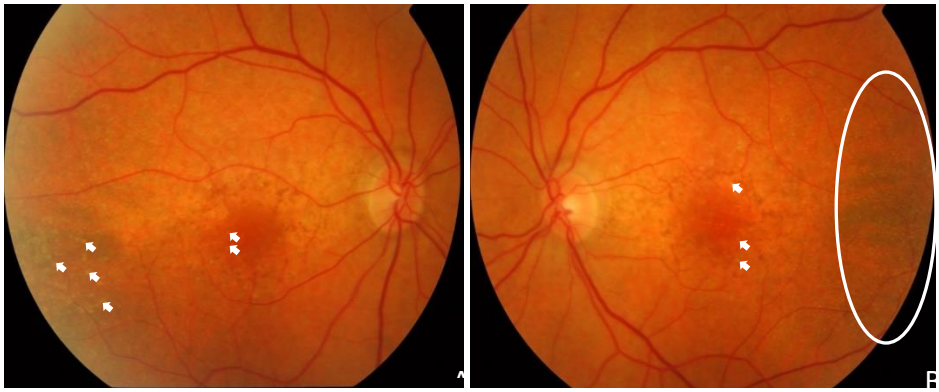

Figure 2.4 : Colour fundus photographs from a L-ORMD patient with stage 2 disease.

(A) The image shows the right fundus. The white arrows highlight areas of drusenoid change. The deposits are more reticular in the peri-foveal region with a more distinct larger appearance in the temporal macula.
(B) The image shows the left fundus. The arrows highlight small, discrete round drusenoid deposits in the peri-fovea. The white oval encloses a region of the temporal macula with large quantities of reticular drusen.

Newer imaging techniques have highlighted different forms of drusen in AMD. I wanted to use similar techniques to see if the drusenoid deposits seen in L-ORMD resembled those previously described in AMD. The small punctate drusen seen in the early stage 2 patients were sized <150um and resembled cuticular drusen. The temporal drusen seen in later stage 2 patients resembled softer drusen. I sought to further delineate the drusenoid deposits noted on colour fundus photography by using infra-red reflectance, SLO autofluorescence and SD-OCT. Infra-red reflectance has previously highlighted a mottled appearance in the peri-fovea in L-ORMD patients (Jacobson et al., 2014). Additionally, infra-red imaging has previously highlighted drusen which may not be clearly be visible on colour fundus photography. FAF can be used to highlight regions in which sub-RPE deposits form (Vincent et al., 2012). FAF can also help differentiate reticular pseudo-drusen. Only three studies have used SD-OCT to study L-ORMD patients. Of these only two have used the Spectralis platform which provides the greatest resolution. OCT can help delineate the type of drusen by size and location. Hard drusen, soft drusen and cuticular drusen are all found sub-RPE whilst reticular pseudo-drusen is found above the RPE. In addition, hard drusen are smaller (<83um), whilst soft drusen tend to be larger (>125um). Cuticular drusen are small and occur in groups often giving a sawtooth appearance.

The infra-red reflectance revealed marked scattered pinpoint increased infra-red reflectance which

were not visible on colour fundus photography. The distribution mainly spared the fovea and was concentrated in the temporal retina and temporal macula (figure 2.5). The lesions are small (<100um) (figure 2.6). FAF revealed little or no change in early stage 2 disease. In later stage 2 disease, there were marked areas of mottled increased FAF surround the fovea in the rod-rich regions which extends into the temporal retina (figure 2.7). On closer inspection of the peri-fovea, pigmentation on colour fundus photography corresponds to areas of increased FAF (figure 2.8).

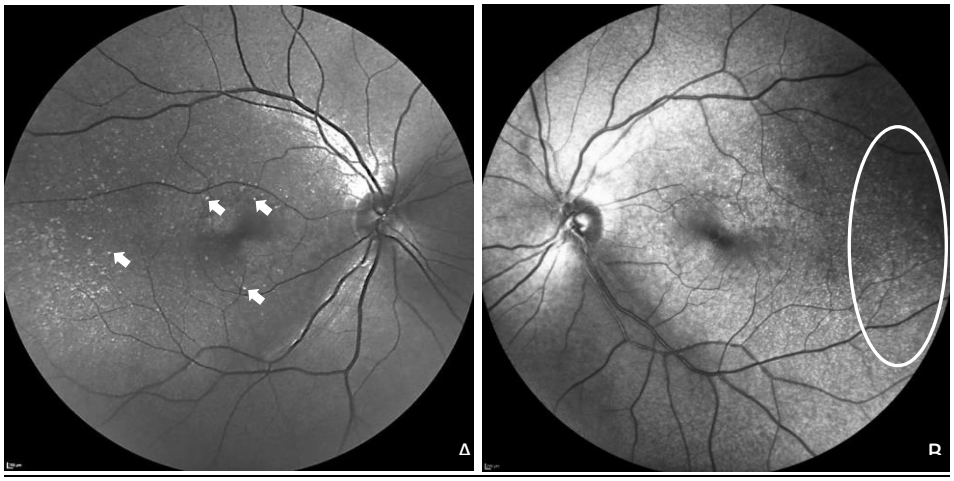

Figure 2.5: Infra-red reflectance images from the fundus of a stage-2 L-ORMD patient.

(A) Right fundus image. The image shows scattered discrete small areas of reflectance <100um (white arrows) in diameter in the macula and temporal fundus.

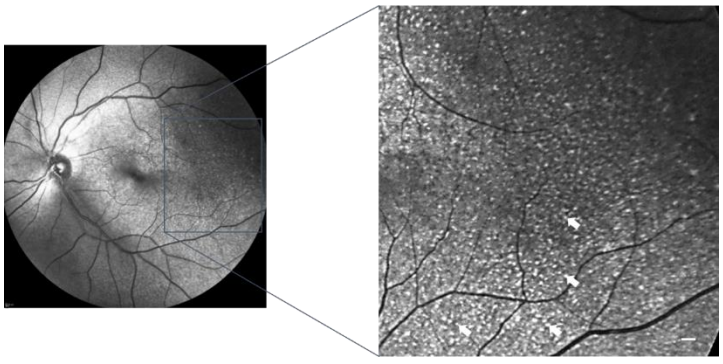

(B)

Figure 2.6: High magnification infra-red reflectance image (820nm) from stage-2 L-ORMD patient. Multiple discrete punctate high reflectance spots in the sub-retina. Their small size (<100um) and central bright infra-red reflectance suggest they are similar to cuticular drusen seen in AMD. (Scale = 400um)

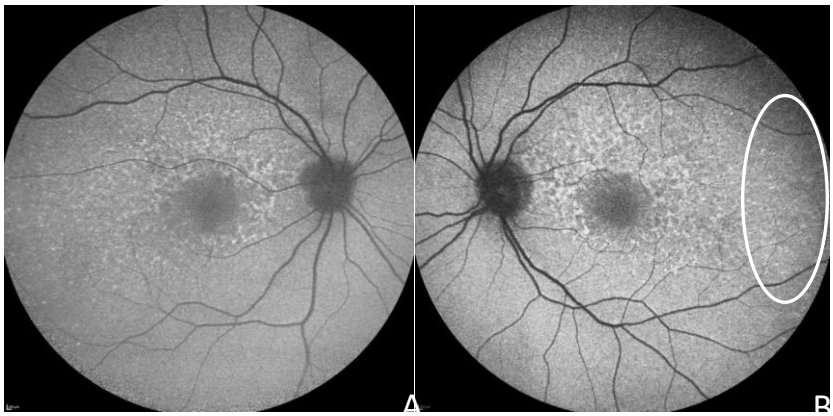

Figure 2.7: Fundus autofluorescence images (488nm) from a stage 2 L-ORMD.

Images show mottled increased autofluorescence in the para and peri-foveal regions with some increased autofluorescence in the temporal fundus. There are relatively few hypoautofluorescent areas.

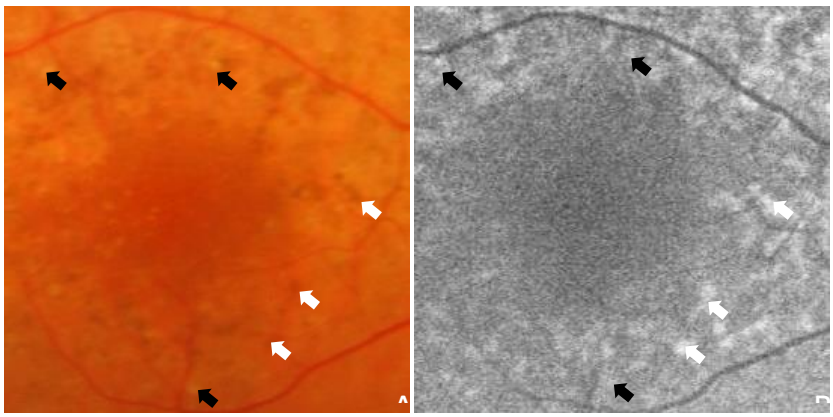

Figure 2.8: Foveal autofluorescence images from a stage 2 L-ORMD.

(A) Colour fundus photograph. Photograph shows para-foveal pigmentation (white arrows) and yellow drusenoid deposits (black arrow).
(B) Fundus autofluorescence image. Both areas of pigmentation and drusenoid change are associated with increased autofluorescence (white and black arrows).

Left fundus image. The image shows multiple discrete sub-retinal areas of high reflectance. SD-OCT imaging revealed a variety of different forms of drusen in the same patient. The sub-RPE deposit was found throughout the retina in all patients (figure 2.1). It was thickest under the temporal macula and retina (figure 2.9). It led to a saw tooth pattern forming associated with

cuticular drusen in the temporal region. In the same retina in the peri-foveal region there were also changes above the RPE which disrupted the IS-OS junction but left the RPE layer intact. Looking at other retina it was clear that these lesions were associated with changes on FAF and were akin to reticular pseudodrusen, which lie adjacent to photoreceptor outer segments (figure 2.10).

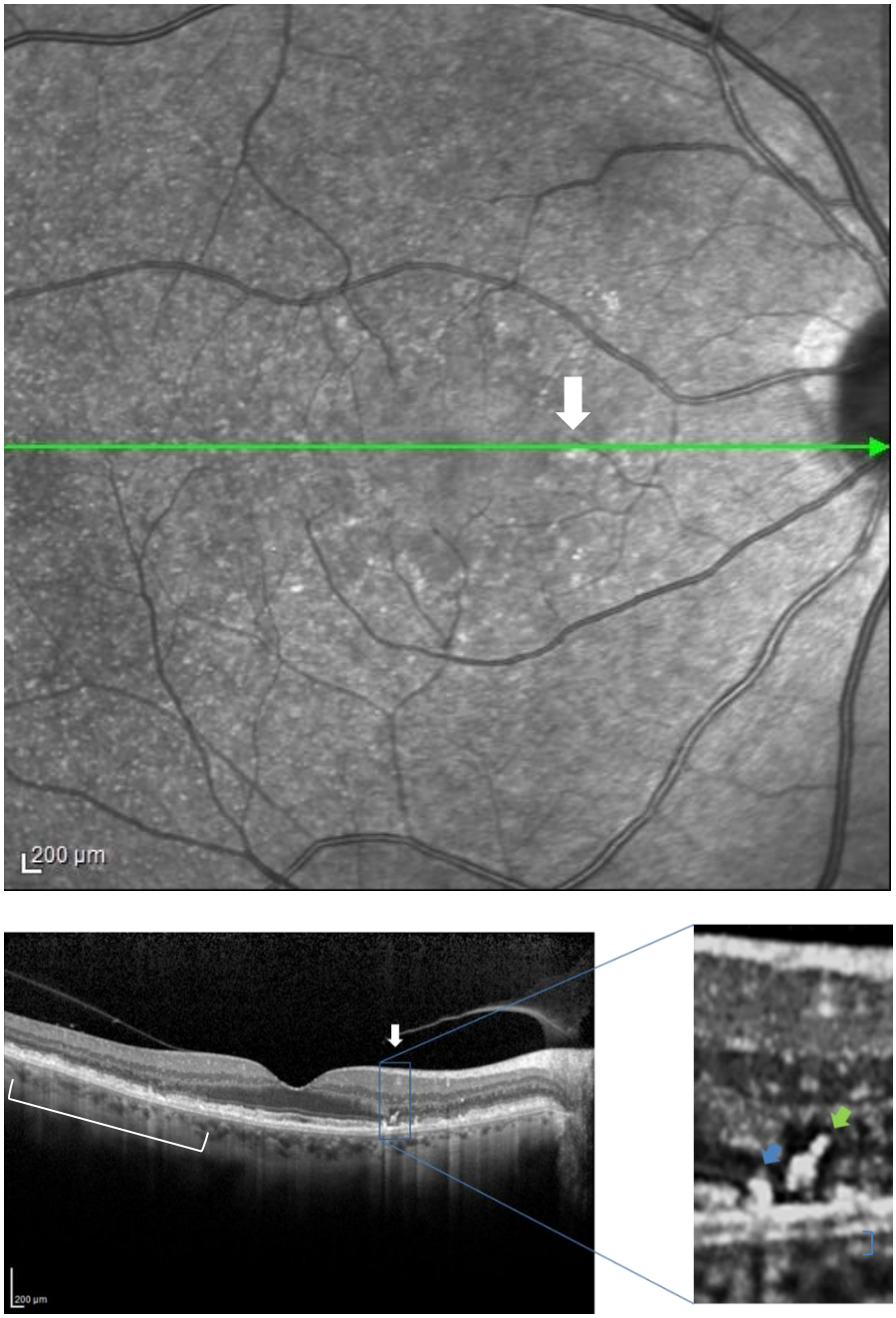

Figure 2.9: OCT Images from a stage-2 L-ORMD patient. The upper image shows an en-face SLO image of the right fundus. The green line identifies the cross-section for the OCT images. There are focal areas of increased autofluorescence (white arrow).The lower images show the OCT cross section of the retina. The white arrow corresponds to the location of the white arrow on the en-face image. There is increased variable thickening of the sub-RPE (white bracket). The magnified image highlights a region of disruption of the RPE and IS/OS junction. There are areas of increased intensity above the RPE. This is similar to reticular pseudo-drusen. The white bracket highlights the increased sub-RPE thickness.

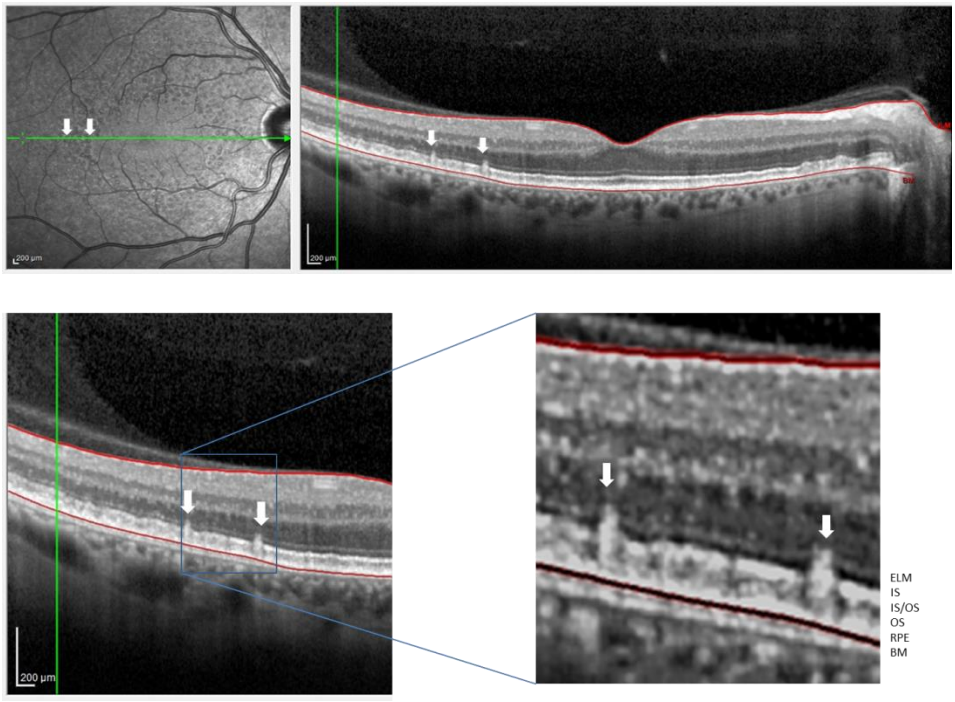

Figure 2.10: OCT images form the right fundus of a stage 2 L-ORMD patient.

The upper image shows the en-face OCT (left) from the right fundus. The image shows multiple discrete lesions with increased central autofluorescence surrounded by areas of decreased autofluorescence. The green line signifies the cross section for the OCT. The white arrows highlight two areas of increased autofluorescence surrounded by decreased autofluorescence. The OCT cross section (right) shows two lesions disrupting the IS/OS junction. The magnified images (bottom images) show that the lesions appear above the RPE similar to reticular pseudodrusen in AMD. The image is labelled with external limiting membrane (ELM), photoreceptor inner segment (IS), the photoreceptor inner and outer segment junction (IS/OS), photoreceptor outer segment (OS), the retinal pigment epithelium layer (RPE) and Bruch's membrane (BM).

We had identified that even in early stage 2 the sub-retinal deposits were found throughout the retina. However, this did not match the focal lesions seen on fundus photography. As a result, in these early stage 2 patients we decided to perform FFA and ICG to see if there was any specific staining or leakage pattern associated with these lesions (table 2.4). Although neovascularisation has been reported in L-ORMD cases previously (Vincent et al., 2012), we did not note any leakage from neovascularisation in our cohort at the time of investigation. The red free images highlighted the areas of drusen (fig 2.15). Early FFAs revealed little except for mottled choroidal filling in all cases. Late FFA however showed increasing hyperfluorescence of deposits, which were almost confluent in nature in the temporal retina and macula. These regions coincided with the increased thickness of deposit and the cuticular region of deposit (figure 2.12). The ICG showed more marked changes. As the ICG progressed, there were clear areas of discrete decreased fluorescence

which were found in the temporal macula and temporal retina. There was also a clear demarcation from the start of the hypofluorescent region and the area showing normal background fluorescence (figure 2.13). This suggests that there was likely to be focal masking of the choroidal fluorescence in the temporal fundus and that although there was a diffuse sub-retinal deposit there were also focal changes. In addition, although the large choroidal vessels were clearly seen in the periphery in early ICG images, foveal region developed what appeared to be an opaque plaque really in the ICG runs with no clear vasculature visible.

Case	FFA features	ICG features
1	• Marked staining of the temporal region in late sequences	• Marked hypofluorescent discrete areas in late images
2	• Marked window defect centrally and temporally • Late staining of deposits around areas of atrophy	• Marked confluent area of increased fluorescence at macula with some areas of hypofluorescence
4	• Marked staining temporally	• Marked hypofluorescent areas temporally • Central areas of increased fluorescence
5	• Window defect temporally • Marked late staining especially temporally	• Marked hypofluorescent areas temporally • Central plaque-like increased staining
7	• Marked late staining across macula but especially temporally	• Marked discrete hypo and hyperfluorescent areas

Table 2.4 Summary of FFA and ICG characteristics of stage 2 patients who consented to dye imaging

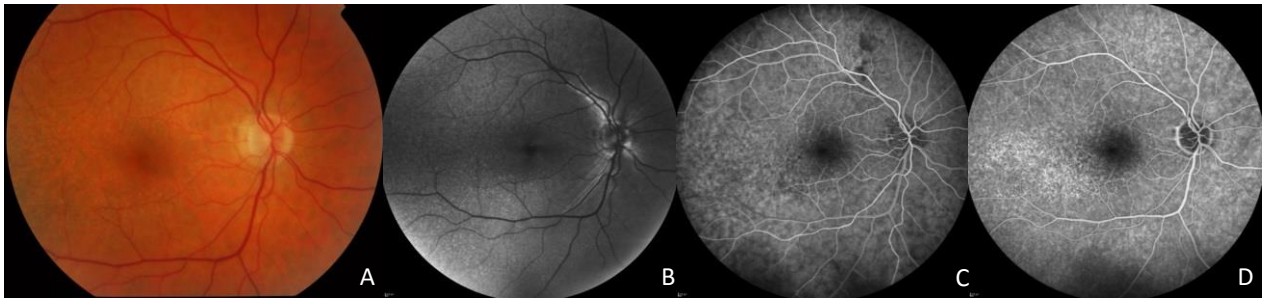

Figure 2.11: Images form the right fundus of an early stage 2 L-ORMD patient.

(A) Colour fundus photograph. The photograph shows scattered drusenoid change in the peri-fovea and temporal retina.
(B) Red free image. The red-free image shows scattered pale areas in the peri-fovea, peripheral macular and in the temporal fundus particularly in the temporal region.
(C) Venous phase FFA (29 seconds). Image shows patchy background choroidal fluorescence. Early increased fluorescence in the area temporal to the fovea.
(D) Late FFA (1 minute 55 seconds). Marked hyperfluorescence in the temporal macula with staining of discrete dots coalescing in many areas. There is no manifest leakage of fluorescein.

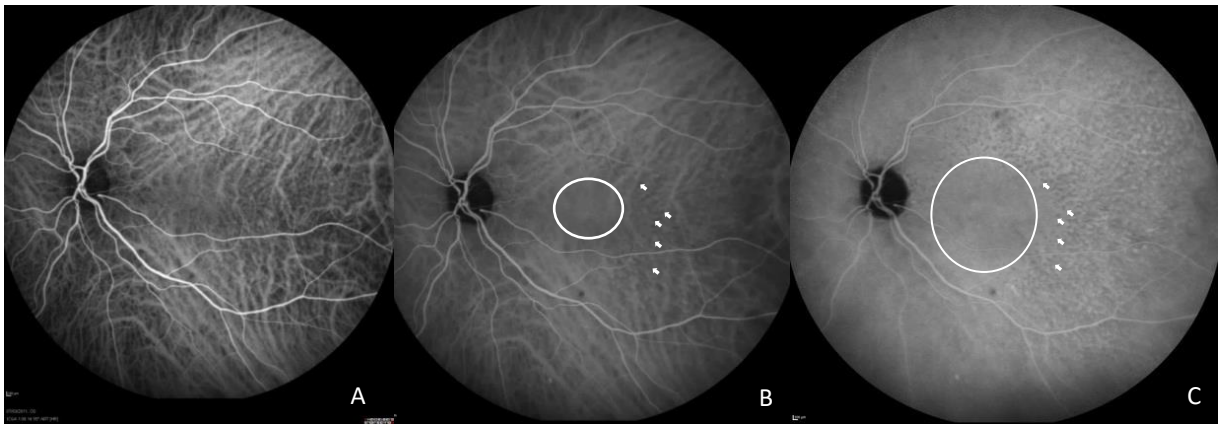

Figure 2.12: Indocyanine green images from the fundus of an early stage 2 L-ORMD.

(A) Early ICG image (1 minute). The image shows good choroidal filling and no clear abnormalities in the intra-retinal vasculature.
(B) Late ICG image (5 minutes). The image shows early hypofluorescence masking choroidal fluorescence (white arrows) and early generalized staining of the fovea (white oval).
(C) Late ICG image (11 minutes 30 seconds). The image shows increased contrast of scattered discrete areas of hypofluorescence (white arrows). There is a discrete boundary between the foveal and peri-foveal fluorescence (white oval) and the mottled peripheral fovea and temporal retina.

OCT provides a measure of structure of the retina. However, to measure function, perimetry could be used. L-ORMD patients have previously been studied using full field perimetry (Milam et al., 2000, Vincent et al., 2012). In our experience this did not show any differences until late stage disease. A pilot of this was tested on some of the stage 2 patients. Consequently, we decided to test microperimetry. This offers a more detailed look at macula function and has previously been used in macular degeneration looking at the central 45 degrees of the macula and combining function with a colour fundus image (Pilotto et al., 2013, Midena et al., 2007). The microperimetry was performed on all our patients. Patients with very early stage 2 showed no loss of retinal function (figure 2.14). However, later stage 2 patients showed an early dense scotoma beginning temporally at approximately 15 degrees from the fovea (figure 2.15). The microperimetry findings matched the FAF findings. However, interestingly, in later stage 2 patients there was a small deficit noted in areas beyond the main areas of atrophy.

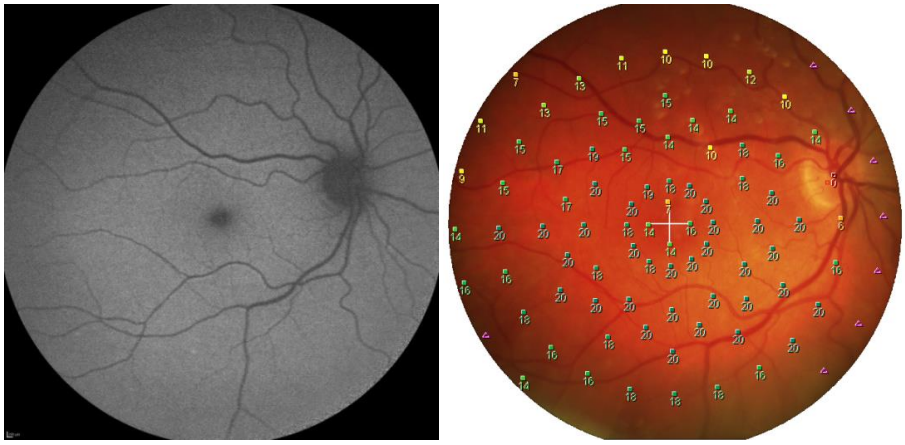

Figure 2.13: Microperimetry of an early stage 2 fundus

The scanning laser ophthalmoscope image (left) shows little aberration in fluorescence. The microperimetry image (right) shows the microperimetry results superimposed on a colour fundus image of e the right eye. The readings show near normal field results using an absolute scale where 20 is the most sensitive and 0 the least sensitive region of the retina. The colour fundus photograph shows scattered drusenoid lesions in the peri-fovea indicative of early stage 2 disease.

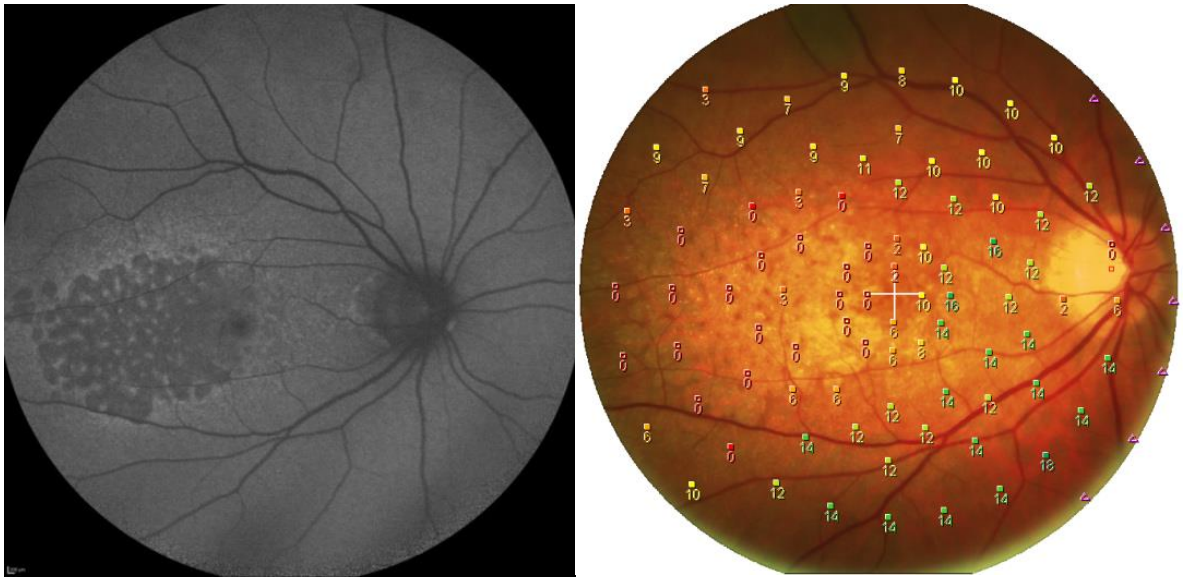

Figure 2.14: Scanning laser ophthalmoscope image and microperimetry recording from an early stage 3 L-ORMD patient

The scanning laser ophthalmoscope image (left) shows areas of marked scalloped reduced fluorescence temporal to the fovea. These scalloped areas are surrounded by a cuff of increased autofluorescence. The microperimetry scoring (left) is superimposed on the colour fundus photograph. There is a clear reduction in sensitivity in the areas of atrophy which also correspond to areas of reduced autofluorescence.

Multifocal ERG has also been used in AMD (Park et al., 2011, Moschos et al., 2004). The functional findings in the multifocal ERG closely matched those of the microperimetry with few changes in early disease but significant deficits once atrophy was apparent temporal to the fovea (figure 2.16). Again there were subtle focal deficits beyond this temporal region. In both the microperimetry and multifocal ERG studies the fovea was relatively spared despite marked deficits elsewhere.

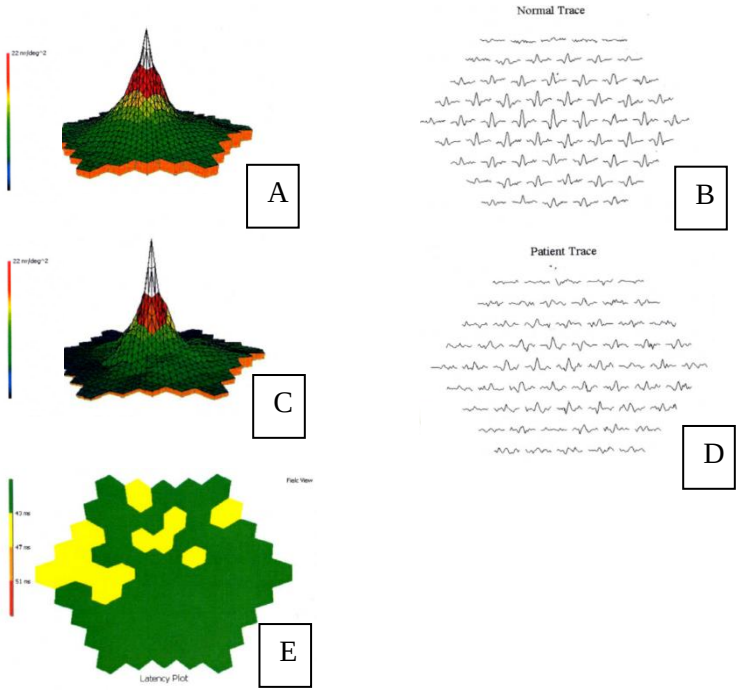

Figure 2.15: Multifocal ERG.

(A) Normal response density amplitude plot.
(B) Normal trace array.
(C) Response density plot from the right eye of the patient described in figure 2.19. Note the central foveal sparing with similar amplitudes centrally to the normal plot.
(D) Patient trace array. Note that although the central foveal traces have a similar amplitude to the normal area there is a marked reduction in amplitude away from the fovea particularly in the temporal retinal traces.
(E) Latency plot. The latency plot shows that the temporal and peri-foveal retina in particular show increased latency. These areas partly correspond to the microperimetric areas of reduced sensitivity.

2.3.3 L-ORMD case-control comparison

Having noted the changes at the fovea on the ICG and the generalised patchy choroidal filling on the FFA in L-ORMD patients I wanted examine the choroidal vasculature in more detail. During the course of my studies two main developments occurred that enabled me to examine choroidal structure more deeply. Firstly, software updates to the Heidelberg Spectralis OCT enabled the investigation of deeper structures using an enhanced depth imaging function (EDI). Secondly, a further update to the software allowed autosegmentation of structures including the choroid. The addition of manual segmentation with measurements provided a way to examine the choroid in detail.

Using the EDI function, I was able to visualise the choroidal vessels clearly from the BM to the sclera. Early on in these studies I noticed choroidal thinning in early stage 2 patients. Additionally, the vessels in the choroid appeared larger and more prominent. Recent publications have noted

choroidal thinning in early AMD (Whitmore et al., 2015). I suspected that choroidal thinning was also occurring early in L-ORMD patients. In order to investigate this I recruited all early stage 2 patients who had little or no atrophy on FAF. I compared the choroidal scans of these patients with those from randomly selected from a database of control patients held at the Anne Rowling clinic, Edinburgh. The images of the choroid were autosegmented using default Heidelberg software to provide a choroidal thickness (figure 2.17). To ensure that there was a landmark, choroidal measurements were taken at the fovea. The measurements were performed by a masked ophthalmologist grader. The measurements had been previously validated by two masked ophthalmologists using 20 test images with good agreement (Cronbach's alpha=0.97).

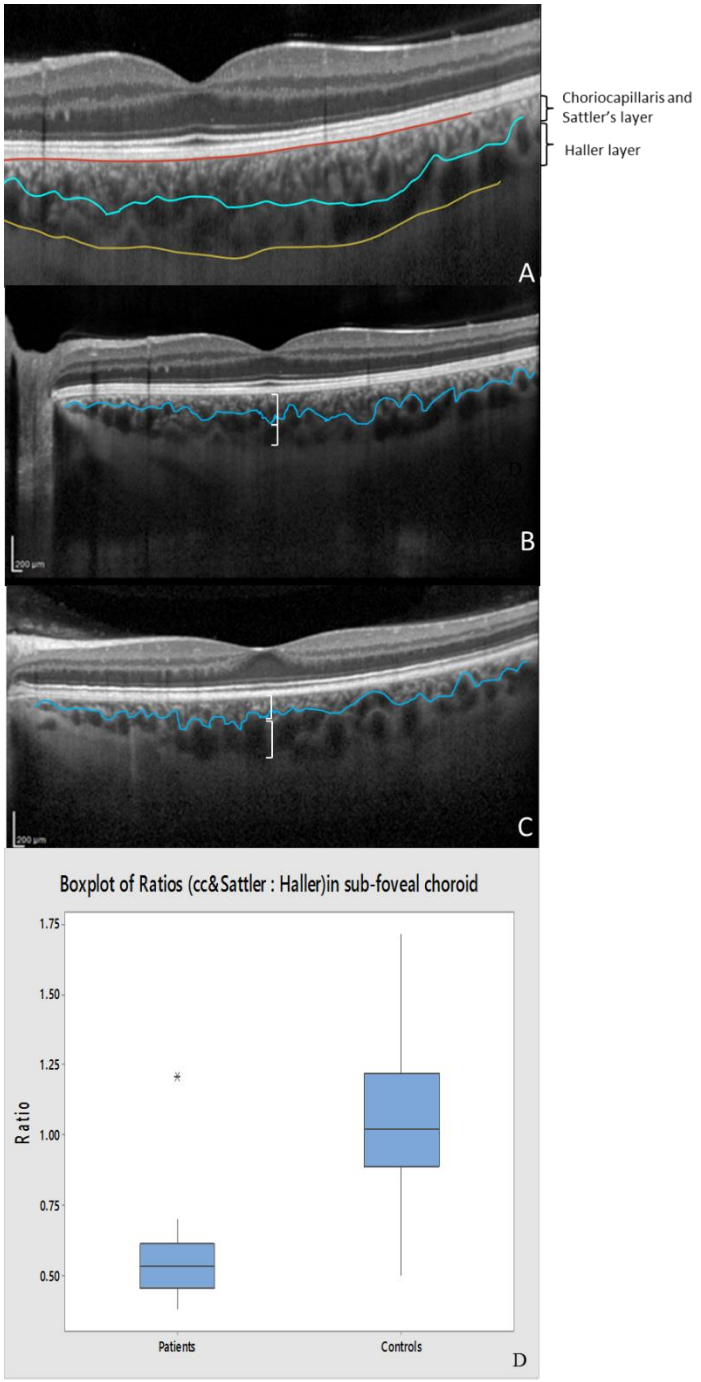

Figure 2.16: Retinal cross section OCTs using enhanced depth imaging to measure choroidal thickness.

(A) The image depicts the semi-automated quantification of choroidal thickness. The Bruch's membrane (red line) and outer choroidal boundary is generated automatically by Heidelberg Spectralis segmentation software. The blue line is generated manually to separate the larger vessels of the Haller layer from the smaller vessels of the Sattler's layer. Total choroidal thickness is also measured. The measurements were taken at the fovea using Heidelberg Spectralis software generated scale (not shown).

(B) A representative image from the fundus of a control patient. The Sattler and choriocapillaris is relatively thick compared with Haller's layer.

(C) A representative image from an early stage-2 L-ORMD patient. The Haller layer is relatively enlarged compared with the Sattler layer and choriocapillaris. The neuro-retina shows no obvious atrophy.

(D) Box plot of the Sattler:Haller ratio. When comparing the ratio of Sattler to Haller layers in the cases and controls the box plots show that there is a relative sparing of the Haller layer compared to the Sattler layer although the controls do show a wide range of ratios.

In the case group 22 eyes were examined. The average age of the stage 2 patients was 57.6 years, with 4 females and 7 males. In the control group 18 eyes were examined. The average age of the controls grouped was 57.9 years with 5 males and 3 females. The respective refraction of the patients is shown in table 2.5. The choroid was significantly thinner in LORMD patients (mean=218.8uM, SD=72.5) when compared to controls (mean=278.8um, SD=73.7) ($P<0.05$) when measured at the fovea (figure 2.17). No significant difference was found in the neuro-retinal

thickness between cases (mean=237.9um, SD=36.3) and controls (mean=236.4um ,SD=9.5). The early treatment of diabetic retinopathy study (ETDRS) divided the macula up into 9 regions with the fovea at the centre. To confirm that the neuro-retinal thickness was not significantly different between patients and controls the neuro-retinal volumes in the ETDRS macular regions were also investigated separately. Again no significant difference between cases (mean=8.4mm^3, SD=0.9) and controls (mean=8.6mm^3, SD=0.3) were noted.

Case	Spherical equivalent refraction (OD,OS) dioptres
Ctrl 1	0.75, 0.75
Ctrl 2	2.5, 2.25
Ctrl 3	2.5, 2
Ctrl 4	-2,-2
Ctrl 5	0.5,0.75
Ctrl 6	1,1
Ctrl 7	-1,-1
Ctrl 8	-4.5,-4
Case 1	-4.5, -4.0
Case 2	0, 0.5
Case 3	0, 0
Case 4	-2,-2
Case 5	0,0
Case 6	0,0
Case 7	0,0

Table 2.5 Spherical equivalent refraction of the left and right eye of cases and controls undergoing imaging for choroidal thickness measurements

This suggests that choroidal changes may occur prior to neuro-retinal changes. Looking more closely at which layer is most affected by the apparent loss in thickness a masked ophthalmologist manually segmented the inner choriocapillaris and Sattler layer from the outer Haller layer which has larger vessels. A method for defining the thickness of the inner and outer choroid under the fovea was first validated by two masked ophthalmologists using 20 test images from cases and controls. This had an extremely high agreement with a Cronbach's alpha of 0.98. Using this approach, an ophthalmologist masked to the diagnosis found a significantly greater proportion of the thickness reduced at the fovea due to Sattler layer loss in L-ORMD than in controls (figure 2.21). The average thickness of Sattler's layer in the stage 2 cases was 51um (SD=29.6) and 138.7um (SD=37.8) in the control group. This was a significant difference ($p<0.0001$). The average thickness for the Haller layers were 89.1um (SD=45.1) for the cases and 136um for the controls (SD=39.6). The Haller layers were also significantly thinner in the case when compared to age-matched controls ($p<0.01$). This suggests that the smaller and medium sized choroidal

vessels are initially more vulnerable in L-ORMD than the larger choroidal vessels found in Haller's layer (figure 2.17D).

2.3.4 Assessing the progression of L-ORMD

Having identified that the temporal macula and retina showed the most marked sub-retinal deposit, I wanted to investigate whether this was also the site of initial atrophy. This would help differentiate L-ORMD from early geographic atrophy, which would tend to be more central. In order to investigate early atrophic disease, I included stage 2 patients (patients affected prior to full foveal involvement but with fundus signs of disease). Software on the Heidelberg Spectralis superimposed an ETDRS chart on to the FAF image for the patients. A count was made for the number of times an area of reduced FAF was seen in a particular ETDRS region. The methodology used was similar to that described for foveal sparing geographic atrophy in AMD (Schmitz-Valckenberg et al., 2009).

The outer temporal macula was found to have the highest percentage of reduced autofluorescence (90%) followed by the outer inferior macula (figure 2.18). This suggested that in L-ORMD disease started temporal to the fovea before progressing towards the centre. This study divided patients into stage 2 and stage 3 but did not perform a longitudinal study looking at regional progression of disease.

Another recent software update enabled regions of atrophy to be measured on the SD-OCT using FAF images (figure 2.19). This technique had recently been used to monitor geographic atrophy progression. This technique had not previously been used in L-ORMD patients. As a result, the measurements were first validated by masking two ophthalmologists who then generated measurements of atrophy from 20 sample images from L-ORMD patients. The pilot study showed good agreement (Cronbach's alpha=0.98). A masked ophthalmologist then used this technique to measure images from stage 2 patients with atrophy. Images were taken at least one year apart.

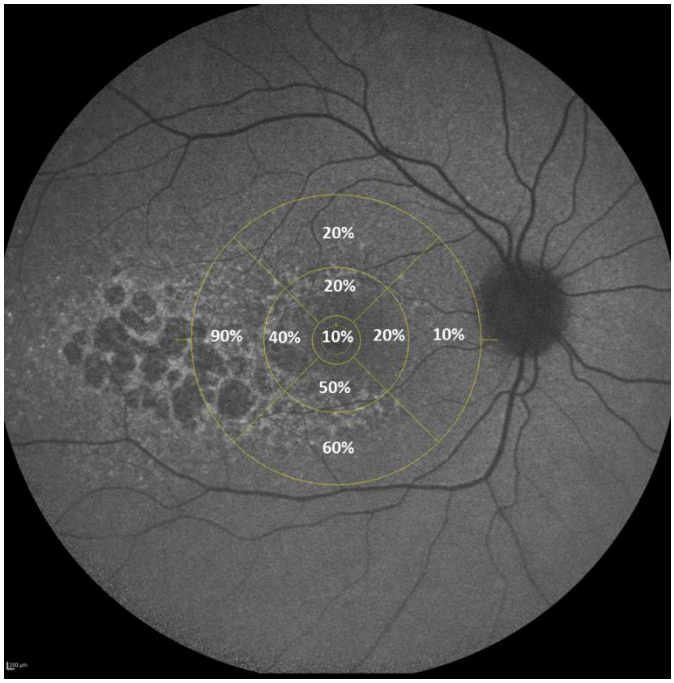

Figure 2.17: Topography of atrophy in stage 2 L-ORMD.

An automatically generated ETDRS topography grid was generated and overlaid by Heidelberg Spectralis software on to stage 2 case FAF images. The images were then analysed to see how many times reduced FAF was seen in each ETDRS region. The image depicts the percentage of times FAF was seen in each region for stage 2 patients. This shows a preponderance of the outer temporal region.

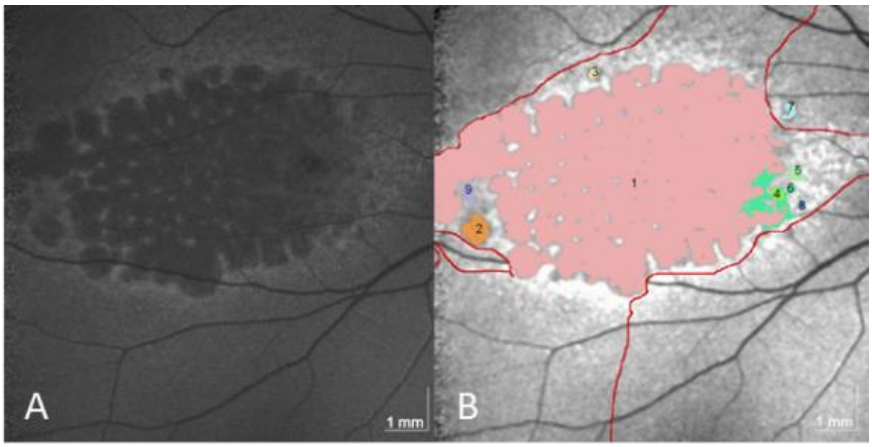

Figure 2.18: Assessing progression in L-ORMD.

(A) Fundus autofluorescence images (820nm) of the right macula. There are clear areas of reduced autofluorescence surrounded by areas of increased autofluorescence similar to geographic atrophy.

(B) Heidelberg regionfinder software is used to map areas of reduced autofluorescence. Each number represents a seed point for semi-automated generation of areas. The red lines signify boundaries within which measurements are generated. The software produces an area table of each seeding area for analysis.

Measuring the areas of atrophy in LORMD with Heidelberg Region finder software showed good agreement Cronbach's α=0.98 using 2 masked observers. The average size of hypofluorescent areas at baselines was 3.6 mm^2. There was poor correlation between age and size of areas at baseline (R=0.12). The rate of progression was 2.5mm^2/year (SD=2.1mm^2) in stage 2 patients.

The deposit thickness was also measured in all patients. This was measured manually using the Heidelberg Spectralis software to assign a size. Again, a validation study was performed using 20 test images and two ophthalmologists masked to the diagnosis of the images. A very high agreement of 0.99 using Cronbach's alpha test was achieved. Measurements were performed under the fovea to provide a reference landmark for calculations. The average deposit in all patients was 16.6 um (SD=1.65). There was no significant increase in deposit size over two years. In addition, there was no significant difference in deposit thickness at the fovea between stage 2 and stage 3 patient (p=0.82). This study will however be limited by the resolution of the SD-OCT machine which is approximately 4 µm.

2.3.5 C1QTNF5 localisation immunohistochemistry

The OCT scans highlighted several types of drusen formation. I wanted to investigate these further using histopathology. In addition, I wanted to investigate the composition of deposits in detail. Previous studies have examined sub-RPE deposits in L-ORMD (Malek et al., 2003, Kuntz et al., 1996). However, these studies were performed prior to identification of the causal gene. It has been proposed that mutant C1QTNF5 forms aggregates (Shu et al., 2006a). However, to date there have been no studies examining whether C1QTNF5 protein is found in the deposit. One hypothesis is that the deposit is also composed of the mutant protein.

Human post-mortem L-ORMD eyes were rare. A single human donor sample was located in the University of Edinburgh. Two further samples were later donated by Professor Radha Ayyagari (University of California, San Diego) in order to confirm my findings. Three patient samples were provided:

1) An 80 year old male patient with confirmed L-ORMD. The samples had previously been described by Duvall et al (Duvall et al., 1986).

2) A 82 years old patient previously described by Milam *et al.* (Milam et al., 2000)The FFB donor number is: 566

3) A 80 years old patient described by Kuntz et al(Kuntz et al., 1996). The FFB donor number is: 356.

The initial immunohistochemistry was performed using DAB staining on these paraffin embedded samples. After the initial immunohistochemistry it was realised that the brown colour of the DAB staining was not clear again the pigmentation of the RPE and choroid. Consequently, a red refine stain (Sigma) was used in later sections. The samples were reviewed with a histopathologist, Dr Colin Smith (University of Edinburgh) who was masked to the diagnosis. The L-ORMD post mortem samples showed marked staining of the sub-retinal deposit for C1QTNF5 (figure 2.20).The staining pattern was slightly different between samples. L-ORMD donor 1showed marked sub-RPE staining with staining extending to the middle of the deposit. L-ORMD donor II samples showed marked staining of the inner deposit. Staining was most marked in the centre of the deposit. Donor III showed staining throughout the deposit. In all three samples, the immune staining was not homogeneous.

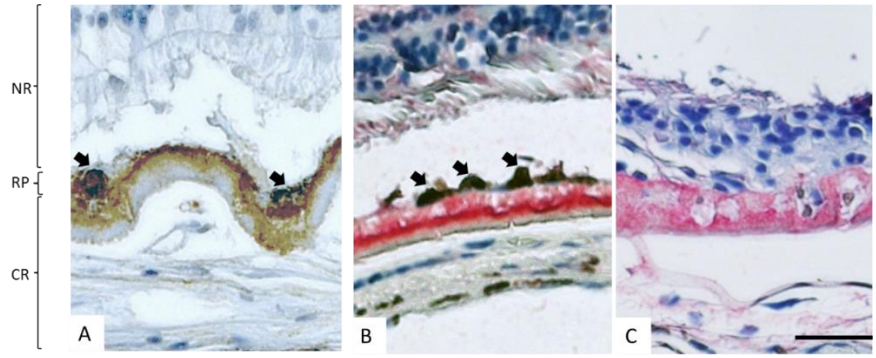

Figure 2.19 L-ORMD human donor retinal sections immunostained with anti-C1QTNF5 antibody (1:200).
The photographs show heavy immunostaining in all samples in the deposit. There is also marked loss and disorganization of the RPE (black arrows). In case I and II, the immunostaining is greatest in the inner deposit with secondary staining enhancement with DAB and red refine respectively (figures 2.24 A and B). In figure 2.24C the whole deposit is immunostained for the deposit visualized with red refine. (scale=25 µm). NR= neuro-retina, RP=retinal pigment epithelium, CR=choroid.

In order to confirm that the sub-RPE immunostaining phenotype for C1QTNF5 was specific to L-ORMD I also performed similar staining on 7 control samples from elderly patients with no known eye pathology. In addition, a further sample from a patient with early AMD was used (table 2.7). Both the histopathologist and myself were masked to the diagnosis of the samples. In these samples there was only faint immunostaining directly sub-RPE for C1QTNF5 (figure 2.21). The AMD patient showed no staining of sub-RPE drusen (figure 2.21). In order to confirm the finding that C1QTNF5 I wanted a further positive control.

Identification	Age of donor (years)	sex	Eye/medical history
CTRL1	85	F	No eye path noted/hypertension
CTRL2	71	M	Drusen/Parkinson's, hypertension
CTRL3	72	F	Dementia, cataract surgery
CTRL4	91	F	Cardiac arrest
CTRL5	78	M	Bronchial cancer
CTRL6	88	M	Acute pancreatitis
CTRL7	35	M	Pneumonia, carcinomatosis
CTRL8	81	F	COAD peritonitis
CTRL9	71	M	Carcinomatosis

Table 2.6 Details of patients from whom post-mortem donor control retina were donated for histopathological studies.

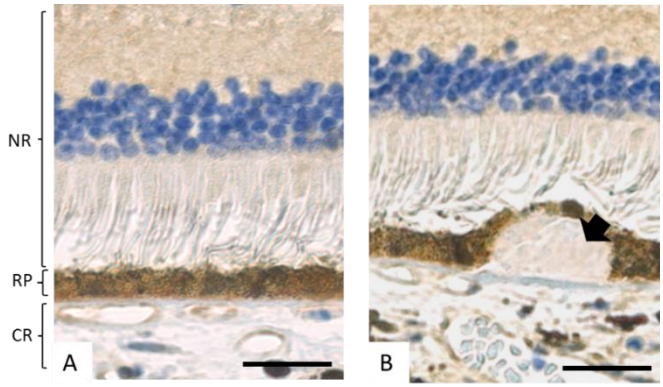

Figure 2.20: Images of retinal sections from an aged control patient and a patient with early AMD.
The retinal sections are from a 78 year old male patient with no known eye disease (A) and 71 year old male patient with early AMD (B). The sections were immunostained with C1QTNF5 antibody 1:200 and DAB secondary. There was only minimal staining of the basal RPE. Drusen remained unstained for C1QTNF5 (black arrow). (scale=25 µm) NR= neuro-retina, RP=retinal pigment epithelium, CR=choroid.

Recently a mouse model of L-ORMD had been generated. The mouse also developed sub-RPE deposits. I predicted that the mouse model would also show evidence of C1QTNF5 deposition in a similar manner to human L-ORMD retina. The finding again showed that the mutant mice had marked staining of the deposit for C1QTNF5 much like the human L-ORMD post mortem samples (figure 2.22) whilst the wild-type control had only faint sub-RPE staining (figures 2.22 and 2.23). Consequently, I initially wanted to test this hypothesis by using samples from the recently generated murine model for L-ORMD (Chavali et al., 2012). These samples were kindly donated by Professor Radha Ayyaagri (University of California, San Diego) (table 2.7).

Genotype	Age	RD8 geno
CTRP5 Hom KO	19 mo	+/+
CTRP5 Hom KO	19 mo	+/+
CTRP5 Hom KO	19 mo	+/+
CTRP5 Het KI	20 mo	-/-
CTRP5 Het KI	20 mo	-/-
CTRP5 Het KI	20 mo	-/-

Table 2.7 Summary of mice genotypes used for murine histopathological studies.

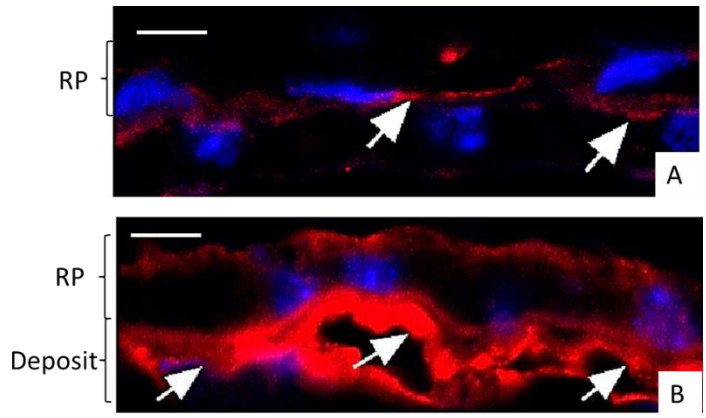

Figure 2.21 Immunofluorescence images of mouse retinal sections immunostained with anti C1QTNF5 The sections were stained with C1QTNF5 antibody (1:200) with secondary staining (555 µm). The image from a wild-type mouse retina show minimal amounts of staining of the basal RPE membrane (A). The image from the heterozygous C1QTNF5 mutant knock in shows a marked sub-RPE deposit. The deposit shows dense staining for C1QTNF5 (B) (scale=10 µm). RP=RPE

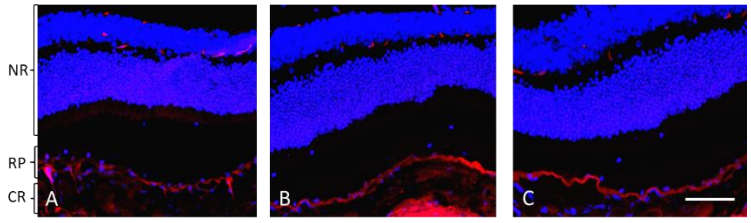

Figure 2.22 Wide-field immunofluorescence images of retinal sections from three heterozygous mutant C1QTNF5 knock in 19 month mice immunostained for anti C1TQNF5 antibody 1:200. The images show staining with DAPI for nuclei (blue) and C1QTNF5 (red). A primary of anti-C1QTNF5 was used with an Alexa-fluor secondary fluorescing at 555nm for the secondary. The images show strong staining of the sub-RPE deposit. There is also autofluorescence in the neuro-retina, choroid and sclera. (scale=200 µm)

2.3.6 Complement immunohistochemistry

Complement dysfunction has been implicated in the macular degenerations (Anderson et al., 2002, Fernandez-Godino et al., 2015). However, immunohistochemistry had never been performed on L-ORMD retina previously. I predicted that complement dysfunction also played a role in L-ORMD pathogenesis. L-ORMD human donor retina is rare. Consequently, I initially wanted to test this hypothesis by using samples from the recently generated murine model for L-ORMD (Chavali et al., 2011). These samples were kindly donated by Professor Radha Ayyaagri (University of California, San Diego).

I prepared sections of similar species of mice (C57BL/6) as controls in order to optimise the staining method. The mice were noted to have not only pigmented RPE but also a pigmented choroid. Initially I attempted to perform immunohistochemistry on the samples using fluorescence. However, the marked autofluorescence at 488nm and 555nm wavelengths precluded a clear image of staining in controls for C1QTNF5 As a result I switched to using red refine (Sigma) and brightfield microscopy for images. Recently, Professor Eric Pierce's group (Harvard university) have published on a mouse model of another inherited retinal dystrophy, Malattia Leventinese (Fernandez-Godino et al., 2015). They were able to demonstrate complement component deposition in the retina of these mice, which was increased when compared to controls. I proposed using a similar approach and contacted Prof Pierce's group who kindly provided information about antibodies.

C3d is a breakdown product of C3b after lysis by CFH. It is a marker for complement activation. After performing immunohistochemistry for C3d, the slides were reviewed by a consultant histopathologist who was masked to the genetic status of the mice. C5b-9 is the TCC of the complement pathway. Positive staining would suggest that complement was not only active but also incompletely controlled as c5b-9 can cause cellular damage with membrane pore formation. Staining for C5b-9 has previously been reported in both inherited and age-related macular degenerations (Fernandez-Godino et al., 2015, Anderson et al., 2002).

Looking firstly at the murine retinal samples, strong C3d immunostaining was noted in the sub-retinal deposit of the heterozygote knock in mouse with some faint staining of the choroid (figure 2.24). In the knockout C1QTNF5 mouse not only was there no staining for C1QTNF5 but also for C3d with no discernible sub-retinal deposit (figure 2.25). There was a lack of C5b-9 immunostaining either the heterozygous C1QTNF5 L-ORMD mutant strain or the control (figure 2.26).

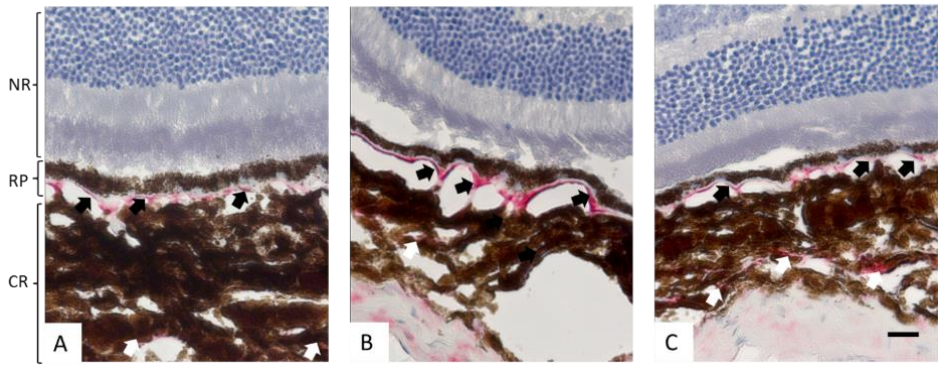

Figure 2.23 Sections from retina of three 20 month old heterozygous mutant mice immunostained with antibody to anti-C3d. Sections were initially incubated with a primary of anti C3d. A secondary of anti-rabbit was used and highlighted using a red-refine stain.(red). All three retinal sections show red refine staining of the sub-RPE deposit (black arrows). There is also minimal staining of the pigmented choroid which is most clearly seen in image C. (scale=20 µm)

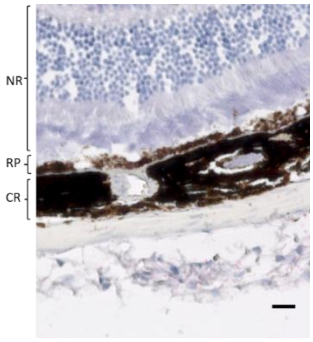

Figure 2.24 Image of a retinal section from a 19 month old C1QTNF5 knockout mouse immunostained with antibody to C3d. The knockout mouse section was prepared in a a similar manner to the sections shown in figure 2.23. The image shows that there is no sub-deposit. In addition, there is no staining of the retina or choroid for c3d.. (scale= 20 µm)

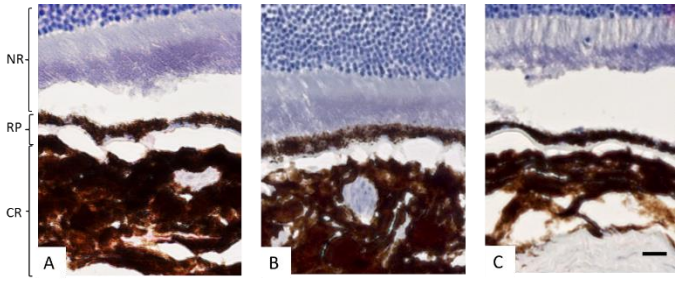

Figure 2.25: Sections from the retina of three 20 month old heterozygous mutant mice immunostained with antibody to anti-C5b-9. The sections were initially incubated with anti-C5b-9 antibody. A secondary of anti-rabbit was used and red refine used to highlight any staining. The images show a clear sub-RPE deposit. However, there is no staining of the neuro-retina, RPE, deposit or choroid using this primary antibody. (scale=20 µm)

Building on the findings that the deposit in mouse model stained for C3d, I next optimised staining for C3d and C5b-9 using control human retinal samples (figure 2.27). The normal aged control and the AMD control both showed immunostaining of the inner choroid for C3d. In addition, the drusen seen in the AMD control showed dense staining for C3d in a similar manner to the sub-RPE deposits in L-ORMD mice. After optimisation, I immunostained L-ORMD donor post-mortem samples. All three L-ORMD samples showed staining for C3d in the sub-RPE deposit and the inner choroid (figure 2.28). The pattern of staining was mainly on the inner and outer part of the deposit with relative sparing of the central deposit. All the aged human retinal samples also showed similar choroidal staining with staining most prominent directly below the RPE (figure 2.31). This suggested that findings complement dysregulation identified in AMD and on the L-ORMD mouse model may also be present in human L-ORMD.

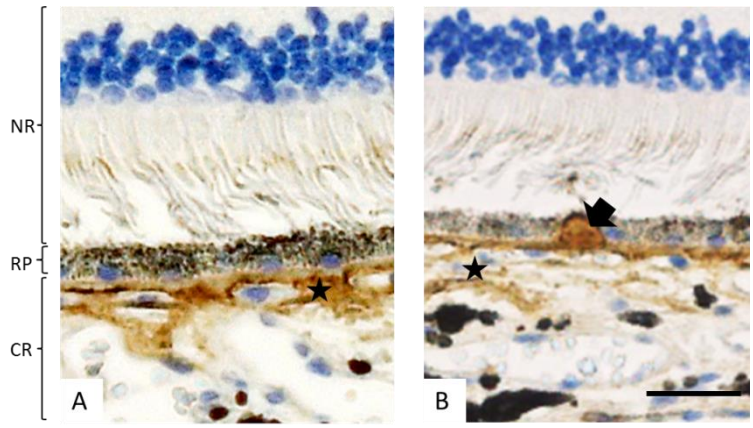

Figure 2.26 Sections from the retina of a 72 year old control post-mortem donor (A) and 71 year old post-mortem donor with early AMD (B) immunostained with anti-C3d antibody. The sections were initially incubated with anti-C3d antibody primary and DAB secondary. Both sections show marked brown immunostaining of the inner choroid (black star). In image (B) the druse is also shows heavy staining for C3d (black arrow). (scale=25 μm)

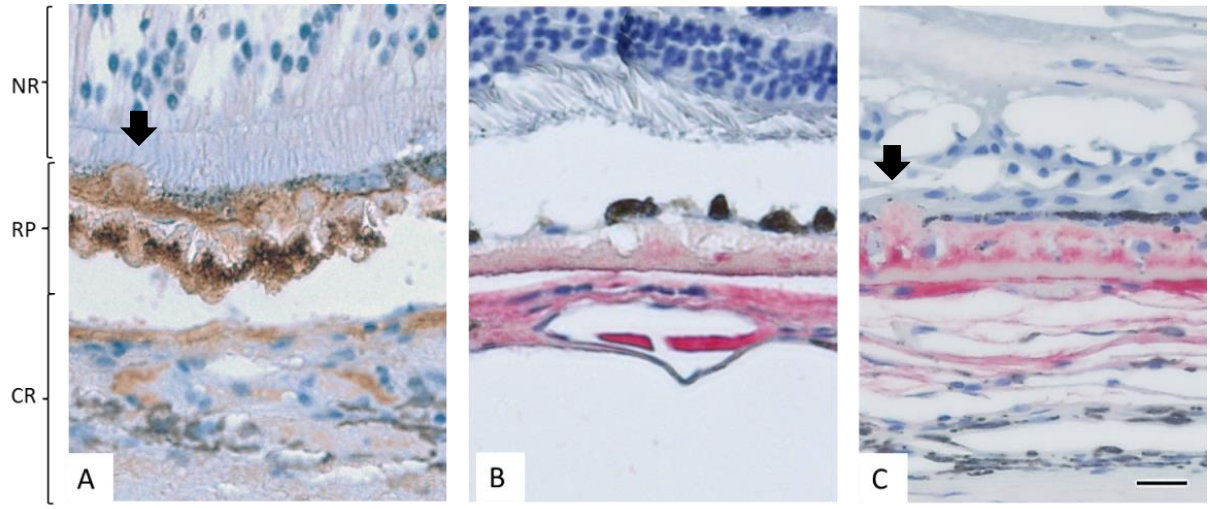

Figure 2.27 Sections from the post mortem retinas of three L-ORMD cases immunostained with anti-C3d antibody.

The sections were all incubated with anti-C3d human primary. In figure 2.27A DAB was used as a secondary. In figures 2.27B and 2.27C red refine was used to highlight primary immunostaining. (A) There is marked immunostaining of the deposit (brown) particularly in the inner deposit and outer deposit. There is also lighter staining of the choroid. Focal areas of protrusion of the deposit through the RPE which appear similar to the OCT images in figure 2.14 (B) Marked red immunostaining of the choroid and focal areas of the outer deposit. (C) Strong immunostaining of the inner and outer sub-RPE deposit. The image also shows strong staining of the inner choroid. The black arrow highlights an area of deposit protrusion. (scale=25 μm)

Although the mouse staining showed no obvious staining for C5b-9, I repeated the staining in the human post mortem samples to see if there was any difference in TCC deposition. The L-ORMD samples stained positively for C5b-9 in the deposit and the choroid (figure 2.29). The pattern of staining was slightly different between the cases. Case I showed staining in the middle of the deposit (figure 2.29A). Case II showed staining in the central and outer half of the deposit sparing the outer most part of the deposit (figure 2.29B). Case III showed only faint staining of the outer half of the deposit (figure 2.29C). The control lines showed little or no immunostaining for C5b-9 (figure 2.30). However, the early AMD post mortem sample showed marked staining of the sub-RPE drusen. Again this suggested that the complement dysregulation seen in the deposit may have similarities to AMD drusen. This variation was likely due to the different stage of disease found within the biopsy samples with the case III sample obtained at a very late stage 3.

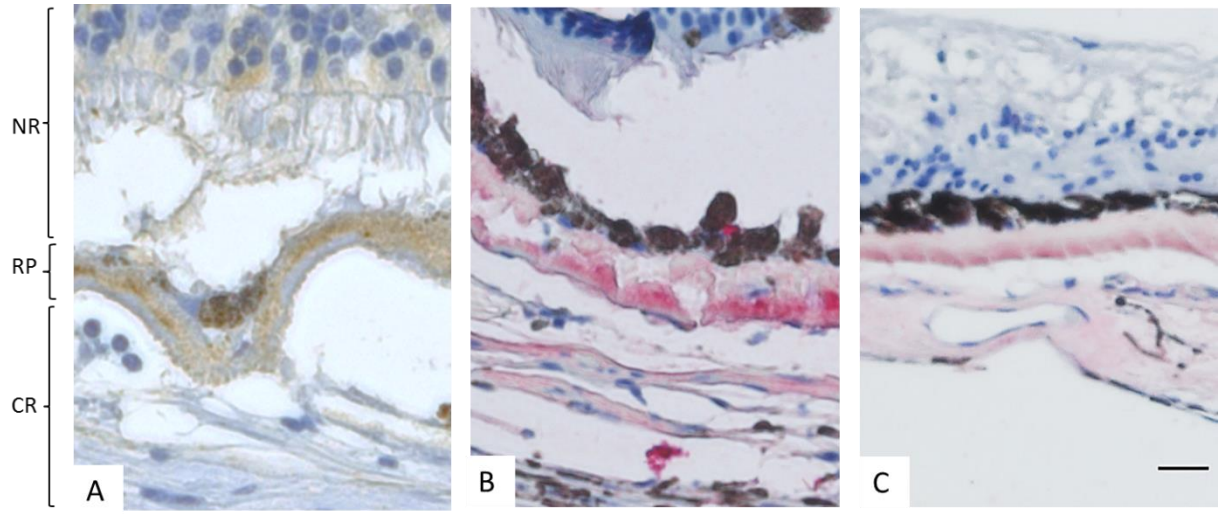

Figure 2.28: Sections from the post mortem retinas of three L-ORMD cases immunostained with anti-C5b-9 antibody.

(A) Brown immunostaining of the deposit particularly in a band in the centre of the deposit. (B) Red immunostaining of the deposit and choroid with some focal areas of staining in between RPE. (C) Faint staining of outer deposit and choroid. (scale= 20 µm)

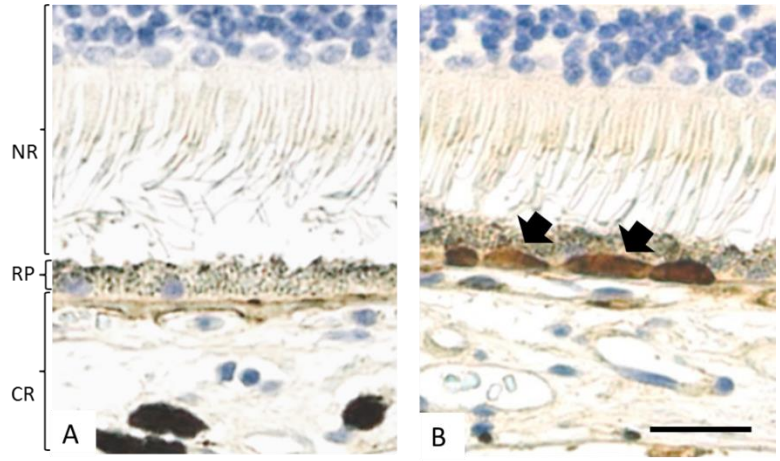

Figure 2.29: Sections from the retina of a 72 year old control post-mortem donor (A) and 71 year old post-mortem donor with early AMD (B) immunostained with anti-C5b-9 antibody. (A) shows only minimal staining in the sub-RPE. (B) Little staining of the neuro-retina or choroid with heavy focal immunostaining of drusen (black arrows) (scale=25 µm)

2.4 Discussion

In this study, clinical phenotyping of L-ORMD patients revealed that in early patients central visual acuity remained normal until late stage 2 disease. This was mirrored by functional

investigations with multifocal ERG and microperimetry also showing normal measurements at the fovea. The earliest changes in this cohort occurred in the temporal macula where deposits were also thickest. Choroidal thickness was reduced in particular in the inner small to medium sized vessels in L-ORMD patients prior to neuro-retinal atrophy when compared to normal controls. In addition, the rate of growth of geographic atrophy could be monitored using semi-automated system, which would provide a method of monitoring disease progression in stage 2 disease. OCT studies highlighted an early reticular pattern of drusen formation, which was highlighted by FFA and late ICG studies. However, drusenoid deposits were heterogeneous. Some reticular and cuticular type drusen were see in early stage 2 disease in addition to thickening of the sub-RPE deposits. All these forms of drusen are also associated with AMD. However, unlike AMD, L-ORMD deposits predominate in the temporal retina and macula in early disease and this can distinguish the disease from AMD. In addition, drusenoid deposits also commonly develop beyond the retinal vascular arcades which is rare in AMD.

Novel findings in this set of studies include the use of automated segmentation software on the OCT to help delineate the choroid with the addition of manual segmentation to look at specific layers within the choroid in L-ORMD. Additionally, the use of multifocal ERG and microperimetry can be used to highlight reduced function. The reduced amplitude and increased latency in the multifocal ERG correspond to early atrophic damage in the temporal region of the macula. Finally, histopathology studies of heterozygous C1QTNF5 mutant mouse retina and from human L-ORMD retina have demonstrated immunostaining suggesting increased complement activation in both the sub-RPE deposit and inner choroid of L-ORMD samples a when compared with control retinal samples.

Previously, Jacobsen *et al.* had shown that in patients suspected to have L-ORMD, dark adaptometry abnormalities were observed prior to retinal findings (Jacobson et al., 2001). The dark adaptation delay was most sensitive at 15 degrees from foveal fixation. In this study we have shown that deposit thickness varies but is initially greatest temporal to the fovea. Additionally, the initial site of atrophy occurs just temporal to the fovea. Some forms of GA also have demonstrate early foveal sparing (Schmitz-Valckenberg et al., 2009). Published rates of progression for GA vary from 0.74-1.68mm^2/year (Schmitz-Valckenberg et al., 2009, Steinberg et al., 2013, Fleckenstein et al., 2011, Fleckenstein et al., 2010). However, the rate of progression for early L-ORMD is greater than that for GA. It would be interesting to also compare figures for later disease as L-ORMD continues to progress beyond the macula whilst GA is usually confined to the macula.

In this study, we identified changes above the RPE in early disease. These pseudodrusen masked

ICG fluorescence and were stained by fluorescein. These changes were also visible on SLO and IR. The deposits resembled reticular pseudodrusen (RPD) which have recently been described in early AMD (Spaide and Curcio, 2010, Finger et al., 2014). As RPD are found between the RPE and photoreceptors, it has been hypothesised that they cause damage to adjacent photoreceptors earlier than sub RPE drusen. This may account for the loss of rod function in the mid-peripheral macular seen in L-ORMD patients. Similarly, in AMD, RPD is associated with early field loss on microperimetry (Wu et al., 2015, Ooto et al., 2013, Querques et al., 2014).

RPD in AMD has been associated with choroidal thinning. There is increasing evidence that choroidal changes may precede changes in the RPE or neuro-retina in AMD (Whitmore et al., 2015). As L-ORMD is a peripherally progressive disease, it allows the study of changes prior to RPE or neuro-retinal loss. In this study, the histopathology specimens showed increased deposition of complement pathway components in L-ORMD eyes when compared to age matched controls suggesting a role for complement pathway dysfunction in early disease. Staining for these components was also seen in the inner choroid, a region of the choroid we have identified as most greatly affected in L-ORMD patients. Similar findings are also beginning to emerge in AMD (Whitmore et al., 2015, Whitmore et al., 2014, Mullins et al., 2014a).

The key histopathology findings are the demonstration that the deposits in both the mouse and the human stain for C1QTNF5 protein. Secondly, both the mouse and human L-ORMD retinal samples show evidence of complement dysregulation when compared to similarly aged control retinal sections. Recently, another deposit Malattia Leventinese or Doyne's honeycomb retinal dystrophy results from a mutation in the *EFEMP1* gene. In the mouse model, deposit formation was demonstrated (Fu et al., 2007). The deposit contained increased quantities of extra-cellular matrix material and also immunostained for Efemp1 protein (Fernandez-Godino et al., 2015, Garland et al., 2014a). Similarly deposit in the L-ORMD samples stained for C1QTNF5. Studies in AMD have demonstrated a number of components in sub-RPE deposits including basal laminar deposits and drusen (Hageman and Mullins, 1999a). These include CFB, CFH, C3, C3d, C3b, C5, C6, C7, C8, C9 and C5b-9 (Mullins et al., 2000a, Gold et al., 2006, Crabb et al., 2002, Anderson et al., 2002). Immunohistochemistry and expression analyses of the RPE-Bruch's membrane-choroid complex reveal that the choroid together with the RPE are able to generate most of the components of the complement pathway in order to activate the TCC (Anderson et al., 2010). This suggests that there is a localised complement dysregulation. The findings from this series of studies fit in well with those from the other studies. However, one difference is found in the pattern of immunostaining. Whilst drusen appear to be uniformly immunostained for C3d and C5b-9, the deposit in L-ORMD appears to be more heterogeneous with variable staining of the inner middle

and outer deposit. This difference in immunostaining may result from differences in composition of the deposit which has been shown to be a bilayer with wide-spaced collagen and ECM deposition on the inner deposit and lipid composition in the outer deposit (Kuntz et al., 1996).

In summary, the phenotyping of L-ORMD has revealed several tools to identify and monitor L-ORMD. Additionally, the multi-modal approach has highlighted several changes in L-ORMD, which are similar to changes in early AMD. Together with histopathology investigations, this suggests that the initial site of injury may also involve the choroid and implicates dysregulation of the complement pathway in L-ORMD disease pathogenesis. Similarities between the findings in L-ORMD and AMD further confirm that L-ORMD is a good model for AMD and demonstrate the utility of using L-ORMD to investigate disease mechanisms in early macular degeneration.

CHAPTER 3

3. Generating retinal pigment epithelium (RPE) from human induced pluripotent stem cells (hiPSCs)

3.1 Introduction and rationale

The earliest changes in AMD occur at the level of the RPE and BM. It is likely that RPE cellular injury initiates AMD although the exact mechanism is still unclear (Hogan, 1972, Dorey et al., 1989). Obtaining diseased RPE for investigation of early disease mechanism would be useful. However, obtaining intraocular samples of RPE in sufficient quantity is problematic due to the potential risks of organ damage. HiPSCs offer a potential solution. They have been used to model a number of diseases by differentiating hiSPCs to cell types implicated in disease (Tucker et al., 2015, Johnson et al., 2015, Yang et al., 2014a, Jin et al., 2012, Singh et al., 2013b). By reprogramming patients' cells carrying harbouring mutations and then differentiating these to hiPSC-RPE to disease causing cell types it is potentially possible to generate an unlimited supply of RPE for investigation of disease mechanisms *in vitro*.

There has been a rapid evolution of protocols for reprogramming cells to hiPSCs. The original reprogramming strategies used two different sets of transcription factors (Takahashi *et al.*, 2007) (Yu *et al.*, 2007). Both initial protocols used OCT4 and SOX2 but Takahashi *et al.* used KLF4 and c-MYC whereas Yu *et al.* used NANOG and LIN28. Both groups used retroviral vectors with a plasmid backbone that integrated in to the host cell genome. For reprogramming to occur a number of different criteria are required to be fulfilled. Firstly, the genes encoding the transcription factors have to be integrated and expressed. The expression is limited to within a relatively narrow stochastic window. Finally, following reprogramming the expression of transcription factors should be silenced to enable differentiation. This results in a relatively low reprogramming efficiency (Hanna *et al.*, 2009). Additional limitations include the generation of partially reprogrammed cells which reduce efficiency and the need to use irradiated mouse embryonic fibroblasts (MEFs)which increase variability in culture (Mikkelsen *et al.*, 2008)(Chan *et al.*, 2009). MEFs were the original platform for maintaining pluripotent cells. However, this technology has now been superseded by defined media used to maintain pluripotency.

During the course of my doctoral studies a number of new protocols were standardised that used non integrating expression of transcription factors. Initially the use of non-integrating viral vectors was used successfully including adenovirus, adeno-associated virus and Sendai virus. However, the

use of these vectors was still limited because the viruses may remain in the cells for several passages (Rashid et al., 2010). A further step change resulted from episomal reprogramming which combined the benefits of a non-integrative methodology, the use of non-biologically active vectors and the use of a feeder free system (Takahashi *et al.*, 2007 , Yu *et al.*, 2007; Lowry *et al.*, 2008, Okita *et al.*, 2008, Fusaki *et al.*, 2009, Si-Tayeb *et al.*, 2010 and Nakanishi and Otsu, 2012).

RPE differentiation from pluripotent stem cells was optimised firstly using hESCs (Vugler et al., 2008, Gamm et al., 2008, Klimanskaya et al., 2004, Idelson et al., 2009) and latterly with hiPSCs (Meyer et al., 2011, Buchholz et al., 2009, Osakada et al., 2009a). A well-characterised differentiation protocol replicating embryology was published by Meyer *et al*.(Meyer et al., 2009). Following a period of training in the laboratory of Professor David Gamm. this protocol was adopted, with adaptations, as the primary protocol for hiPSC-RPE differentiation in these doctoral studies. The differentiation and subsequent validation of hiPSC and hiPSC-RPE lines is described below.

3.2 Methods

Patient and sibling recruitment was performed by Dr Shyamanga Borooah. All fibroblast biopsies and cultures were performed by Dr Shyamanga Borooah. HiPSC reprogramming for case lines 1 and control lines 1 and 2 was performed by Dr Shyamanga Borooah in the laboratory of Dr Ludovic Vallier (University of Cambridge), with the guidance of Ms Imbisaat Geti (University of Cambridge). Generation of episomal case lines 2 and 3 was performed at the MRC centre for regenerative medicine under the supervision of Dr Karen Burr (University of Edinburgh). Validation of hiPSCs was performed by Dr Shyamanga Borooah with the assistance of Dr Karen Burr (University of Edinburgh). HiPSC maintenance was performed initially by Dr Shyamanga Borooah and later by the core stem cell team in Professor Chandran's laboratory. Dr Nina Rzercheck and Dr Bhuvaneish Thangar (University of Edinburgh) provided advice for western blot optimisation.
HiPSC differentiation to RPE was performed by Dr Shyamanga Borooah. In addition, Dr Shyamanga Borooah performed all characterisation including microscopy, electron microscopy, PCR, western blot, immunohistochemistry, phagocytosis assay, electron microscopy. Time was spent in the laboratory of Dr David Gamm (University of Wisconsin, Madison) who provided advice regarding hiPSC differentiation.

3.2.1 Generation and maintenance of case and control hiPSCs

In order to obtain patient cells for cellular reprogramming to hiPSCs a fibroblast sample was taken from cases and controls. Procedures were performed following informed consent and covered by NHS Lothian ethics committee approval (REC 08/S1101/1). Subcutaneous 2% xylocaine with adrenaline 1:100,000 (Astra-Zeneca) was allowed to take effect on the forearm of donors for 10 minutes. A 3.5 mm punch biopsy was then taken. The area was cauterised to provide haemostasis before 5/0 prolene purse string suture (Ethicon) was used to close the wound. The punch biopsy sample was placed in DMEM + 10% FBS and placed in ice for transport prior to further processing.

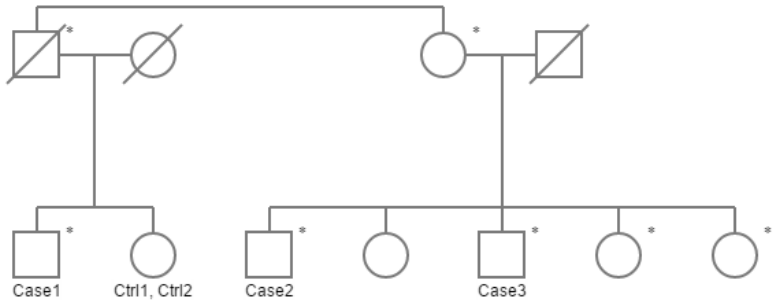

Figure 3.1 L-ORMD family pedigree *=affected

The biopsy sample was carefully dissected under a microscope to remove the epidermis and sub-cutaneous fat. The fibroblast layer was then placed in a 100mm plate with a coverslip placed on top before 10% FBS DMEM was carefully added to cover the biopsy. Outgrowth of fibroblasts from the biopsy sample occurred between 3 to 7 days.

After a further two weeks when fibroblasts were near confluent, the cells were removed using 0.05% trypsin/EDTA (Gibco) and decanted into a 15 ml conical tube. 10% FCS+ DMEM (Gibco) was added to neutralise the trypsin and then the cells were spun at 1500g to remove excess trypsin. The cells were then resuspended in 10% FCS+ DMEM before being plated in a T25 flask. After a week, the same process was performed to plate cells into three T75 flasks. Once confluent, the cell were stored in cryovials in 10% DMSO+DMEM freezing solution and stored in liquid nitrogen for long-term storage.

Three main methods were used for fibroblast reprogramming. Different methods were used because of the rapid development in reprogramming technologies during the course of the doctoral work. Each of the methods are outlined below: 1) Lentiviral reprogramming using a lentiviral backbone, 2) Sendai virus reprogramming and 3) Episomal reprogramming.

Lentiviral reprogramming was performed as previously described (Banito et al., 2009). Briefly, Fibroblasts were thawed into a 6 well plate in 10% FBS+ DMEM. When cells reached 80% confluence the medium the cells were lifted to single cells by incubating in 0.05% trypsin for 5 minutes at 37°C. Cells were resuspended in 5 mls MEF medium and the counted using a haemocytometer. 10^5 cells were plated into 1well of a 6well plate. Cells were incubated at 37ºC 5% CO_2 for 24 hours. Yamanaka factors *OCT4, SOX2, KLF4* and *c-MYC* (Vectalys,Toulouse, France) at MOI 10 were used to transduce the cells for 24 hours and the cells were incubated. On the fifth day, cells were split into single cells using trypsin 0.05% incubation for five minutes before being transferred to a 100MM plate with irradiated MEFs and grown for a further 2 days. After day 9, cells were grown in standard hESC culture medium. The first hiPSC colonies appeared approximately fifteen days later and were picked approximately five days after appearing. Individual colonies were picked and transferred to a 12 well plates containing MEFs feeders in KSR + FGF. Colonies were expanded by enzymatic dissociation

Sendai virus reprogramming was performed as previously described (Rashid et al., 2010). Fibroblasts were plated in wells of a 6 well plate at 1 X 10^5 two days prior to transduction in fibroblast medium. When cells reached 80% confluency, the Sendai reprogramming kit was used (Cytotune, invtirogen) by transducing using Sendai virus expressing Yamanaka factors at recommended concentrations to reach the target MOI within the kit. Virus was added to the medium at the calculated concentration to 1 ml of fibroblast medium. The fibroblasts were transduced under incubation at 37ºC for 24 hours before medium was replaced with fresh fibroblast medium. Cells were cultured for a further 6 days before enzymatic dissociation on to radiated MEF 100mm culture dishes at a concentration of 2 x10^5 cells per plate. Cells were maintained in hESC medium for approximately three further weeks before hiPSC colonies appeared. Colonies were picked manually using a microscope and placed individually into MEF 24 well culture plates prior to further culture and expansion.

The episomal protocol used was a variation on that already published (Okita et al., 2011). 0.2% gelatin (Sigma) coated 5 x 10^5 fibroblasts were harvested using enzymatic dissociation and counted using a haemocytometer. 18ul Amaxa supplement1 and 82ul nucleofection solution were mixed to create a transfection solution. Fibroblasts were spun down in a centrifuge at 300g for 3 minutes before the dried cell pellet was resuspended in the transfection solution. 1.7 µg of three episomal DNA suspensions OCT3/4/shP53, Sox2/Klf4 and L-Myc/Lin28 episomal vectors (Addgene) were added. The electroporation was performed using an Amaxa 4D-nucleofector (Lonza). Following transfection the fibroblasts were plated into one well of a 1 in 60 matrigel coated six well plate containing fibroblast media before the plate was placed in an incubator under standard incubation

conditions. Media was replaced every 2 days. After one week when fibroblasts were nearly confluent cells were harvested using 0.05% trypsin/EDTA (Gibco) before being replated onto 100mm Geltrex (Thermo Fisher scientific) coated plates in fibroblast media. After a further two days media was switched to pluripotent cell medium (E6+bFGF) (Stem cell technologies). Media was changed every two days. Colonies emerged from the third week and were mechanically picked and placed into 24 well plates coated with matrigel and covered in E8 media (Stem cell technologies).

For maintenance all cells were transitioned to feeder free E8 media on to 1:60 matrigel (BD bioscience) coated plates. Every 7 days as cells became confluent cells were passaged to single cells using dispase and collagenase (1:1). Cells were left under standard incubation conditions for approximately 15 minutes till cells dissociated from the plates. The cell colonies from all wells of a six well plate were then aspirated into a 15 ml tube and allowed to settle. The colonies were allowed to settle and the media aspirated. The cells were then washed in 10 mls of PBS. After 5 minutes, the media was aspirated and replaced with 1 ml E8 media. The cells were then aspirated repeatedly with a 1000ul pipette to break colonies in to single cells. A further 5 mls of E8 was added before 500ul of media form the tube was placed in each well of a fresh matrigel coated six well plate. A further 1.5 ml of E8 was added to each well. The plates were transferred to an incubator and shaken in a figure of eight to evenly spread cells across the well. The plate was incubated under standard conditions and media was completely replaced with 2mls fresh E8 on a daily basis. For the experiments, only cells from passage number 15 to 65 were used.

HiPSC validation included immunostaining, PCR, DNA sequencing, karyotyping and confirmation of 3 germ layer differentiation. In order to confirm mutant and wild type genes in case and control lines DNA was extracted from the lines using the Wizard SV genomic DNA kit (Promega) according to kit instructions using spin columns. To briefly summarise the protocol. Cell pellets from a well of a six well plate were sheared by passing them through a 20 gauge needle ten times attached to a 1ml syringe. The entire sample was transferred to spin-column containing sample lysate and the column spun for 1minute at 12000g. The flow through was discarded. The kit wash solution was added to the spin column and the membrane washed by centrifuging at 12000g for 1 minute and the flow through once again discarded. These steps were repeated a total of three times. A final spin of 12000g for 2 minutes was perfomed in order to dry the membrane. The spin column was placed into a 1.5 ml microfuge tube. RNAase solution was added and nuclease free water was added to elute the membrane. The column was spun for a final time at 12,000g for 1 minute. Confirmation of DNA content was made using a NanoDrop (Thermo fisher scientific). The microfuge tube containing the eluent was then used directly for amplification. A mastermix was made up using the high fidelity Q5 TAQ polymerase kit (New England Bioscience). Amplification was performed at 65C for 40 cycles.

To check amplicon size the product was run on 2% agarose gel for half an hour at 100V. After confirmation, the DNA was cleaned up using ChargeSwitch® gDNA Mini Tissue Kit (Thermo Fisher scientific). A final check on a NanoDrop for a concentration of at least 1ng/ul per 100 base pairs was performed on a NanoDrop (Thermo Fisher scientific). Sanger sequencing was performed by source bioscience (Nottingham, United Kingdom). Information about primers is available in the appendix.

For karyotyping 0.2 ml colcemid (Sigma) at a working solution of 0.1ug/ml was added to the media of each well of a six well plate. The plates were then placed under standard incubation conditions for 2 hours. Cells were then enzymatically dissociated with 0.05% trypsin. The cells were transferred to a 15 ml conical flask and then spun at 1200 RPM for 5 minutes. The supernatant was discarded and the cells resuspended in 5ml KCl. A 75%methanol 25% acetic acid fixative was prepared and added dropwise to the conical flask to a volume of 3ml. The fixed cell suspension was then frozen at –20ºC and sent to the cytogenetics laboratory for formal screening under microscopy (Addenbrookes, hospital, Cambridge, United Kingdom)

For three germ layer differentiation cells were split onto new six well matrigel coated plates as per normal passaging of hiPSCs and fed with 2 mls of E8 before incubation overnight. For mesodermal differentiation, a three-day protocol was used. The cells were fed with chemically defined media (CDM) with the addition of Activin (10ug/ml), FGF2 (4 µg/ml) BMP4 (10ug/ml), Ly (10mM) and CHIR (3mM). Media was completely replaced every day for three days. For endodermal differentiation, a 3-day protocol was used. On day 1 cells were fed with CDM containing activin (10ug/ml), FGF2 (4ug/ml), BMP4 (10ug/ml), Ly (10mM) and CHIR 3mM. ON day 2 the cells were fed with day 1 media minus CHIR. On day 3 cells were fed with CDM with the addition of activing (10ug/ml), FGF2 (4ug/ml) and B27 (1:50). For neuroectodermal differentiation cells were fed with CDM with SB (1ul/ml), FGF2 (4ug/ml), and LDN (1ul/ml). The cells were maintained in this media for 12 days and fed on alternate days. After differentiation protocols were complete cells were wither harvested for PCR studies or fixed for staining. Methods for these procedures are described below.

3.2.2 Generation of case and control retinal pigment epithelium (RPE) from hiPSCs

Differentiation of case and control hiPSC-RPE was performed using a previously published method (Meyer et al., 2011). HiPSCs were enzymatically lifted using dispase (1mg/ml) (Life Technologies, 17105-041). Following washing, the cells were grown as embryoid bodies in E8 medium for 4 days in a 100mm plate and placed on a shaker under normal incubation conditions.

During days 2-4 the cells were incubated with 100 ng/ml Noggin (or Dorsomorphin) and XAV939 (Tocris) added to basal media. On day 5 media was changed to neural induction medium (NIM). After 6 days, the aggregates were plated onto laminin-coated 6 well plates. Media was changed every 2 days. On day 16 media was changed to retinal differentiation media (RDM) without retinoic acid with B27. From days 20-40 Activin A (100 ng/ml) (kind donation from Marko Hyvonen, University of Cambridge) was added to RDM from day 20–40. Pigmented RPE gradually developed from day 21. At day 50 RPE were manually picked under microscopy. Collected cells were enzymatically dissociated into single cells and replated at 50,000 cells per cm^2 onto laminin coated 6 well plates initially in 10% FCS+RDM before being transitioned over one week to RDM. Cells were maintained in RDM for four weeks prior to use in experiments. RDM media was changed thrice weekly for maintenance. In order to optimise the protocol advice was obtained from Prof David Gamm, Dr Wei Shen and Dr Ruchira Singh (University of Wisconsin, Madison). A summary of hiPSC-RPE differentiation protocol is shown in figure 3.2.

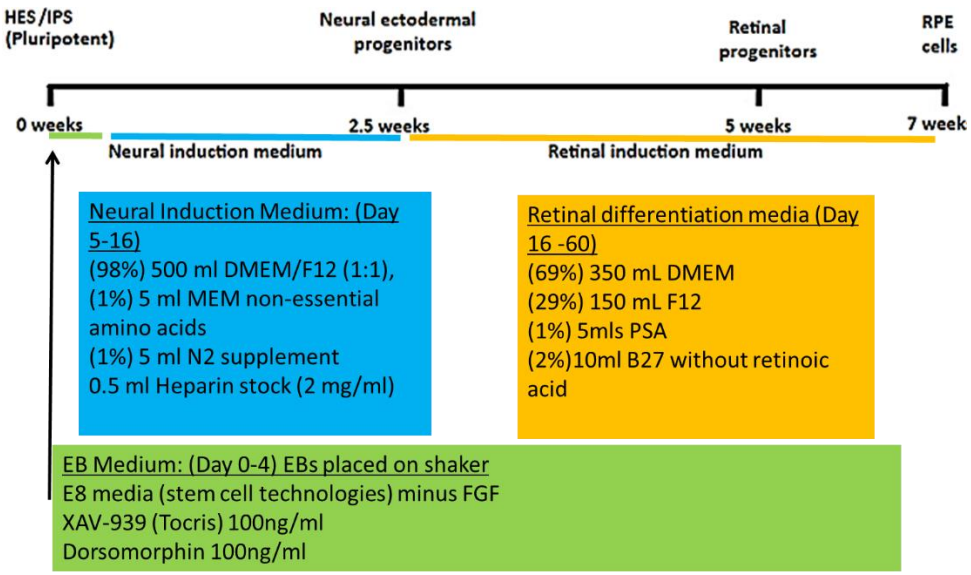

Figure 3.2: Diagram depicting the differentiation protocol from hiPSC to hiPSC-RPE. Differentiation occurs in three main phases. Firstly neural cell specification of pluripotent cells in EB medium minus FGF. Neural induction in neural induction medium to promote the growth of primitive anterior neural cells. Finally retinal differentiation. Activin A is added (100ng/ml) from day 20 to 40 to enrich the pigmented RPE population. After approximately 50 days colonies of pigmented cells are manually selected for expansion.

3.2.3 Immunohistochemistry

For immunohistochemistry followed standard procedures which have been previously published for RPE (Singh et al., 2013a). Media was aspirated and washed two times with PBS (Gibco). The cells were then incubated at room temperature with 4% PFA for half an hour. After a further wash

with PBS the cells were permabialised with 3% TritonX-100 in PBS for 15 minutes. Cells were then blocked in 3% normal goat serum (Dako) in PBS for one hour. Primary antibody was prepared to the appropriate concentration in blocking solution. (For a full list of antibodies please see the appendix.) Cells were incubated a 4^{o}C overnight with the primary antibody. After three washes in PBS with 0.01% Triton-X100 the cells were incubated in Alexafluor (Invitrogen) secondary antibodies for 30 minutes. The cells had a final staining with DAPI (1:500). After a final three washes in PBS the cells were mounted in Fluorsave (Merck-EMD Millipore) mounting medium.

The same technique was used for immunohistochemistry hiPSCs with some minor modifications. Cells were blocked for 10 minutes in 4% PFA, 0.1% Triton x-100 was used to permabialise the cells and DAPI (1:2500) for 5 minutes was used to counterstain the cells.

3.2.4 Transmission electron microscopy

For electron microscopy, samples were fixed in 3% glutaraldehyde in 0.1M Sodium Cacodylate buffer; pH 7.3, for 2 hours then washed in three 10 minute changes of 0.1M Sodium Cacodylate. Specimens were then post-fixed in 1% Osmium Tetroxide in 0.1M Sodium Cacodylate for 45 minutes, then washed in three 10 minute changes of 0.1M Sodium Cacodylate buffer. These samples were then dehydrated in 50%, 70%, 90% and 100% normal grade acetone for 10 minutes each, then for a further two 10-minute changes in acetone. Samples were then embedded in Araldite resin.

3.2.5 Trans-epithelial resistance

The transepithelial resistance (TER) was measured using a previously established protocol (Sonoda et al., 2009). Measurements were made using an epithelial voltohmeter EVOM2 (World precision instruments, Sarasota, Florida).All measurements were performed in the cell culture hood within 3 minutes of removal from the incubator. The electrode heads were placed inside the well and outside the well in the media of a 24 well transwell (Corning). Measurements of TER were made. To obtain a resistance per well the resistance of a blank laminin coated well was subtracted and the result multiplied by the growth area of the well (0.33CM^{2}).

3.2.6 Phagocytosis assay

Phagocytosis assays were performed as a modification of existing assays (Mao and Finnemann, 2013). Bovine photoreceptor rod outer segments (OS) were commercially prepared under dim

light from Bovine retina (InVision Bioresources, Seattle, USA). In order to fluorescently label the OS the OS were washed in a wash solution composed of 10% sucrose, 20 mM phosphate buffer pH 7.2, 5 mM taurine. After three washes the OS were resuspended in 5ml of the same solution in a 15ml tube. A FITC working solution was made by dissolving 10 mg FITC isomer I (Invitrogen) in 5 mL 0.1 M sodium-carbonate buffer at pH 9.5. 1.5 ml of the working solution was added to the 5ml OS suspension. The suspension was rotated for 1 hour in the dark. The OS were then washed in the wash suspension twice and then twice in 2.5% sucrose DMEM before being resuspended in 2.5% sucrose DMEM in the appropriate concentration. Counts of OS were made using a haemocytometer.

For the phagocytosis assays, RPE were plated in 96 well plates at 50,000 cells per cm^2. At least three replicates were plated for each experimental condition. 50 POS per cell were calculated (Singh et al., 2013b, Singh et al., 2013a). 50ul of suspension at the appropriate concentration were added to each well for varying lengths of time. In order to terminate phagocytosis the wells were washed three times with PBS. In order to detect only internalised OS the cells were then incubated in 0.4% trypan blue for ten minutes to stain any external OS before a two final washes with PBS. The wells were then fixed in 4% PFA for 30 minutes. 3% Triton PBS was added for 30 minutes and then DAPI 1 in 500 was placed on the cells for ten minutes. The wells were then coated in mounting medium Fluorsave (Merck-Millipore). Cells were imaged on a Zeiss fluorescent microscope and the number of OS per cell analysed using imageJ.

3.3 Results

In chapter 2, it had been established that the cohort developed L-ORMD in a similar manner to previous reports of the disease. For further studies a smaller family of patients were identified who had unaffected siblings. Five cases were initially identified and two controls for donating fibroblasts. Sibling cases and controls were chosen to provide the closest relationship between case and control lines. This would mean the genetic background would have as little variation between cases and controls. Therefore any differences between lines could more confidently be attributed to mutations in C1QTNF5. These fibroblast lines were labelled 1 to 7 (table 3.1). The cases had previously been identified by the regional genetics unit to carry the mutation and were part of the cohort described in chapter 2 who were shown to have clinical signs of stage 2 L-ORMD. The fibroblasts grew from all punch biopsy samples (figure 3.3) Fibroblasts were stored at low passage (<4) as previously senescence had been shown to impair reprogramming (Banito et al., 2009). Initially, fibroblast lines 1, 2, 5 and 7 were reprogrammed. During the course of the studies, reprogramming techniques were constantly evolving from retroviral integration based methods to non-integrated viral and finally non-integrated episomal techniques. Therefore a

variety of different techniques were used to reprogram the fibroblasts to hiPSCs. The first set of fibroblasts were reprogrammed using retroviral and Sendai virus (table 3.2). Reprogramming generated several clones from each fibroblast line. A minimum of two clones were stored for each line. A further two fibroblasts were from lines 3 and 4 were reprogrammed separately at a later date using episomal methods and validated similarly.

Fibroblast cell line details	Patient details	Case/Control
Line 1	58 year old male	Case
Line 2	56 year old female	Control
Line 3	51 year old male	Case
Line 4	54 year old male	Case
Line 5	54 year old male	Case
Line 6	57 year old male	Case
Line 7	54 year old female	Control

Table 3.1: Summary of the source of donor fibroblast lines.

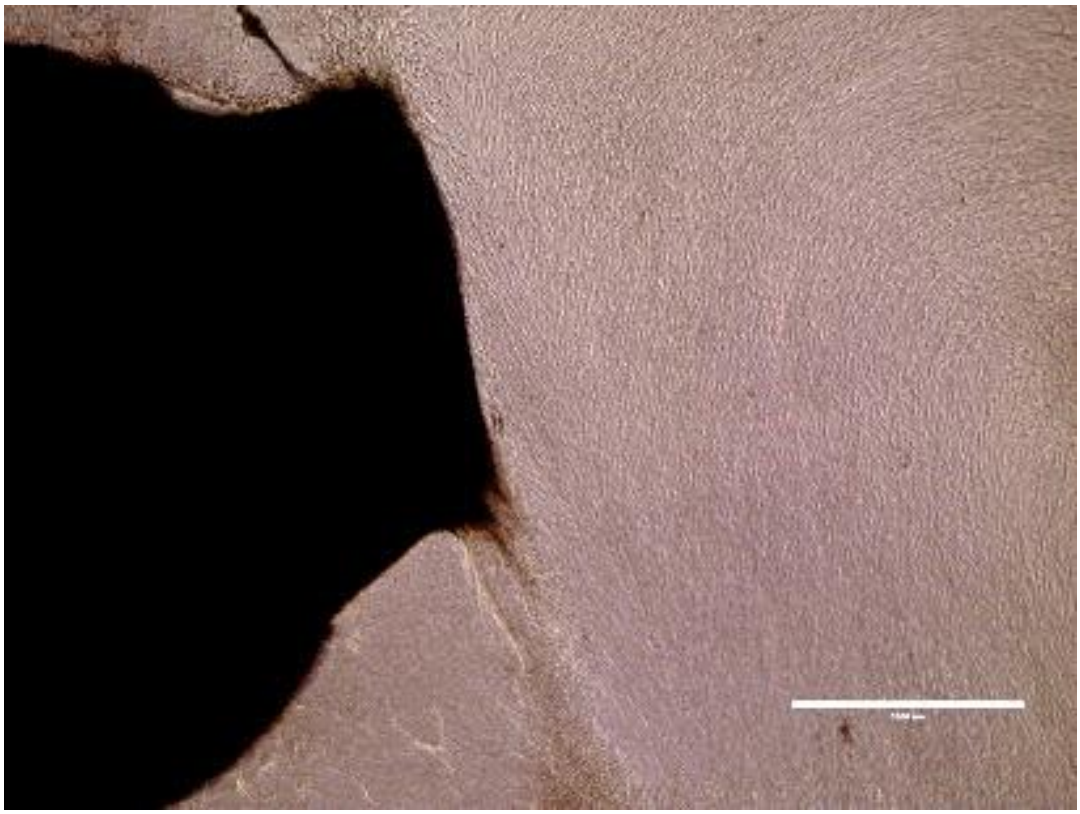

Figure 3.3: Brightfield image of fibroblasts growing in fibroblast culture media from punch biopsy (dark object). (scale =1000 μm)

Fibroblast origin	Stem cell	Type
Line 1(case)	Clone 0.5	Sendai
	Clone 1	Sendai
	Clone 3*	Sendai
	Clone 5	Sendai
Line 2(Control)	Clone 1	Sendai
	Clone 2*	Sendai
	Clone 6*	Retroviral
Line 3(Case)	Clone 1*	Episomal
	Clone 2	Episomal
Line 4(Case)	Clone 1*	Episomal
	Clone 2	Episomal
Line 5(Case)	Clone 3	Sendai
Line 6(case)	Clone 1	Retroviral
	Clone 2	Retroviral
Line 7(Control)	Clone 1	Sendai
	Clone 3	Sendai

Table 3.2 : Summary table of hiPSC clones generated by reprogramming. The asterisks highlight the clones used in these studies.

In order to validate the generation of hiPSCs from patients and controls, established validation criteria were investigated (Takahashi et al., 2007). Cells were first investigated for morphology. All cell types revealed cells with large nuclei forming densely packed colonies with retractile edges which is similar to that described form pluripotent cells (figure 3.4) (Takahashi et al., 2007, Thomson et al., 1998). The cells expressed and immunostained for markers of pluripotency (figure 3.5 and 3.6). To fulfil criteria of pluripotency the cells were all differentiated to the three germ layers using protocols optimised previously (Rashid et al., 2010). PCR using primers for neuro-ectoderm, mesoderm and endoderm showed expression of relevant markers identified by immunohistochemistry (figure 3.7). This showed that the cells were pluripotent. Cells were cryopreserved after approximately passage 10 to 20 as a bank for later studies once the hiPSC phenotype had stabilised.

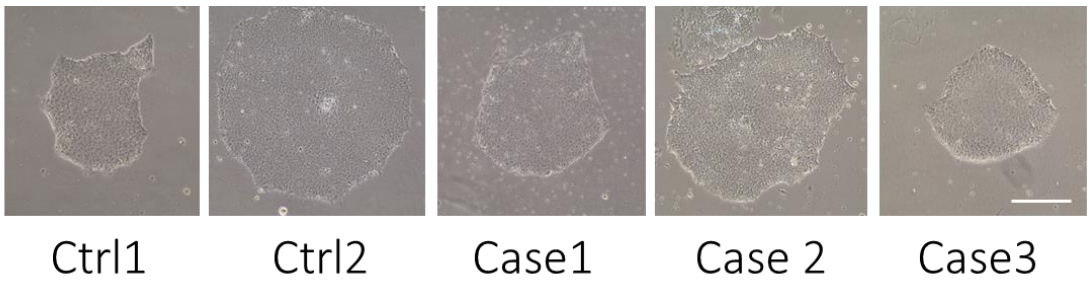

Figure 3.4: Brightfield images of hiPSC lines. The images show features commonly seen in pluripotent cells including densely packed colonies of cell with large nuclei. The colonies have refractile edges. (scale=200 µm)

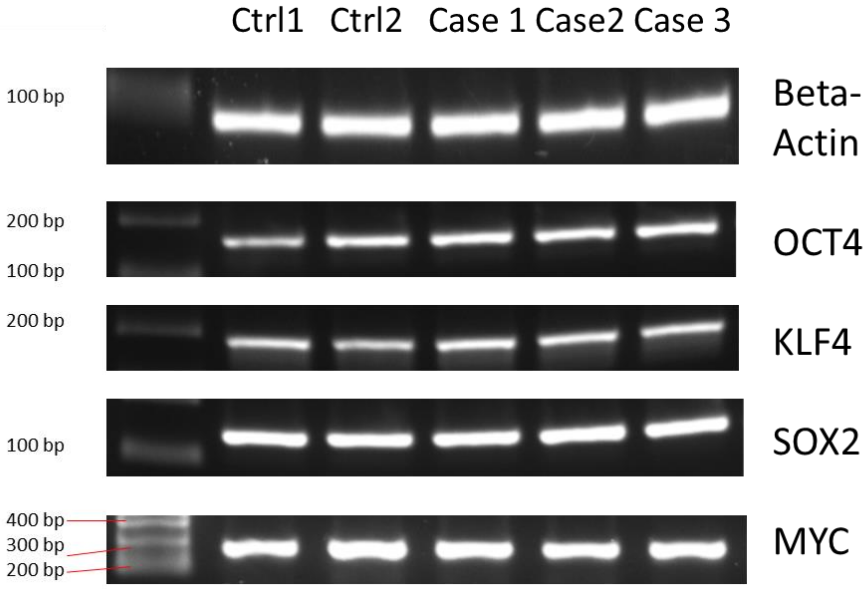

Figure 3.5: Imaging from agarose gels of PCR products for pluripotency gene expression. All cases and controls show endogenous expression of pluripotency related genes

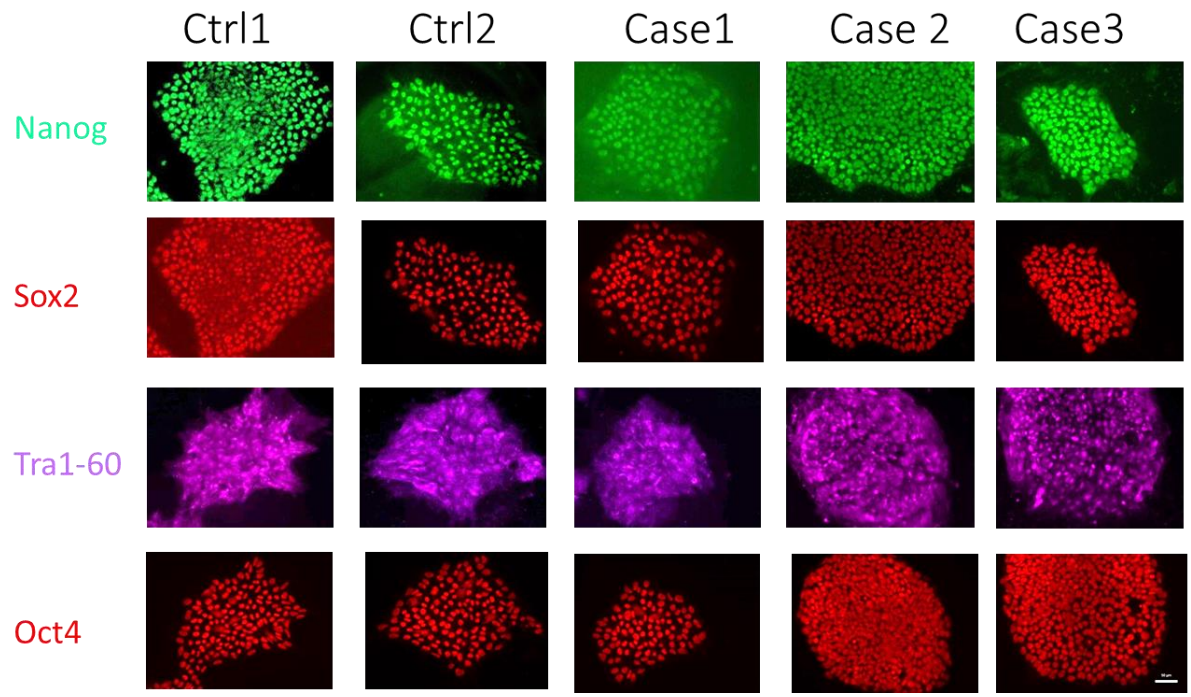

Figure 3.6: Immunofluorescent images of hiPSC colonies The images show that all cell lines express markers of pluripotency including Nanog (green), Sox2 (red), Tra 1-60 (purple) and Oct4 (red). Unlike the other markers Tra 1-60 is a surface antigen and therefore less clearly defined. (scale = 50 µm)

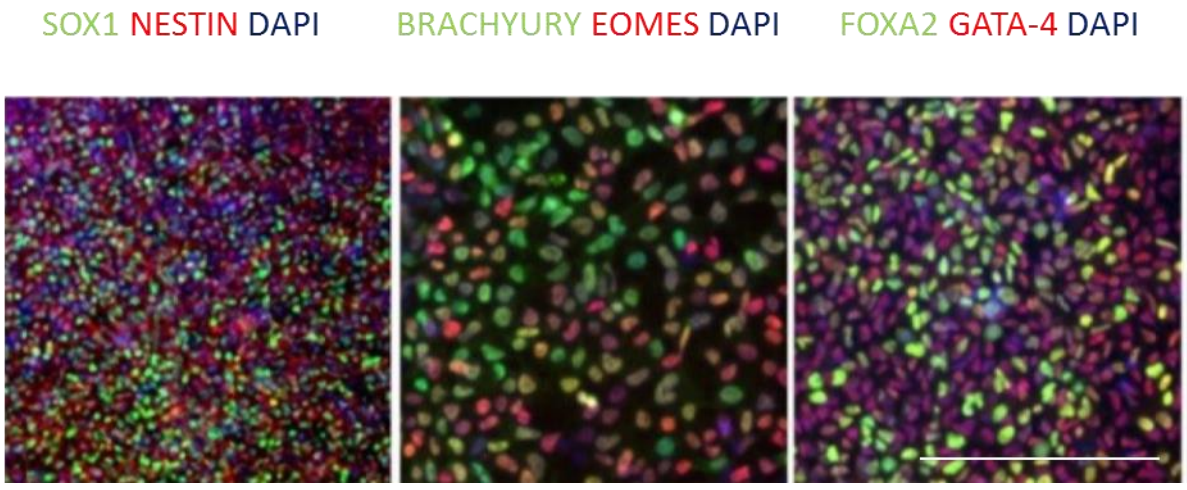

Figure 3.7 Immunohistochemistry of three germ layer differentiation hiPSCs. Markers include neuroectoderm (SOX1 and nestin); mesoderm (brachyury and Eomes); and endoderm (FOXA2 and GATA-4op row is from CTRL1 and the bottom (scale =50µm). The representative images are from Ctrl1 hiPSCs.

Prior to differentiating the cells, I also wanted to ensure chromosomal and genetic integrity. I initially prepared G-banded karyotyping which was performed by Addenbrooke's hospital cytogenetics unit 83.7). At this stage two cell lines were rejected from fibroblast line 5 and 7. The hiPSCs generated from fibroblast line 5 was noted to have a balanced translocation between the short arm of chromosome 12 and the long arm of chromosome 15 whilst those generated from fibroblast line 7 were noted to have a 48 XXX karyotype. However, karyotyping of the fibroblasts also revealed the same mutations. In order to quality control the reprogramming of the cell lines an initial fibroblast karyotyping step was performed prior to reprogramming. For the final experiments case lines 1, 2, 3 and control lines 1 and 2 had a normal karyotype. In order to check that the mutation had transferred correctly, I performed sequencing analysis of the primer product including the mutation. All cases were confirmed to be heterozygote for the mutation and all the controls were found to be homozygote for the wild type (figure 3.9).

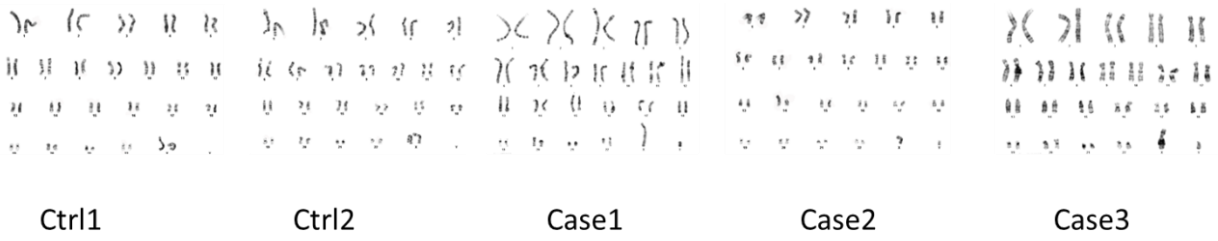

Figure 3.8: Digital photographs of G-banded karyotyping performed on case and control lines. Case lines all show 46 XY phenotype whilst the control lines show a 46 XX phenotype.

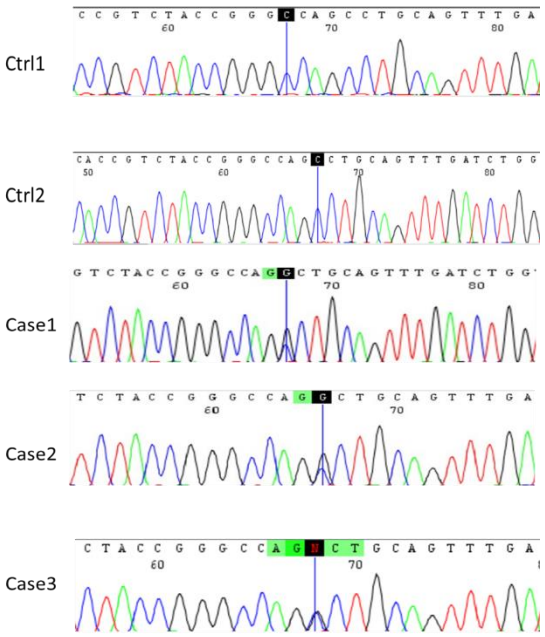

Fig 3.9: Direct sequencing of case and control lines

The sequencing analysis shows that at base 686 in the gene (line) there is a homozygous cytosine in the control lines. In the mutant lines at the same point there is a mixed guanosine and cytosine suggesting heterozygosity with insertion of the mutant allele caused by a C>G substitution resulting in the p.Ser163Arg

HiPSC differentiation to RPE was performed using a modification of a protocol learnt at the University of Wisconsin under Dr David Gamm (Meyer et al., 2011). The protocol was limited because of the inability to increase the yield of RPE with a proliferation stage. In order to increase the amount of RPE generated with each differentiation I trialled different plating techniques. An attempt to keep the hiPSCs in suspension throughout the differentiation successfully led to an increase yield of RPE with greater proliferation of cells. However, the cells formed 3 dimensional organoids which made it difficult to manually dissect the pigmented RPE. This resulted in a lower final yield of RPE. Instead the plates were placed on an orbital shaker from day 0 to day 7. This enabled large amounts of hiPSCs to be differentiated in one 100mm dish resulting in larger amounts of RPE with each differentiation although the efficiency was likely unchanged. The protocol generated pigmented colonies of RPE after 25 days (figure 3.10).

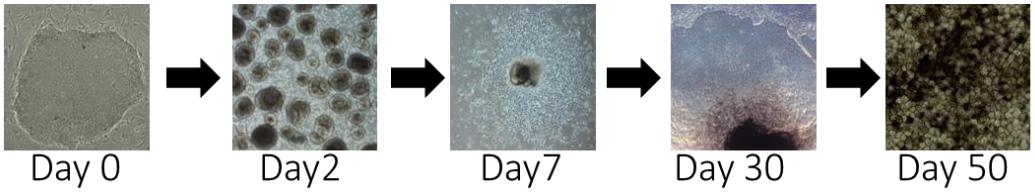

Figure 3.10: Brightfield images illustrating hiPSC differentiation to hiPSC-RPE. Day 0 shows a hiPSC colony with typical close packed cell morphology. Day 2 shows embryoid bodies (EBs) which are maintained on an orbital shaker. These are clumps of differentiating hiPSCs in suspension and simulate the blastocyst. Day 7 shows an EB 2 days after plating onto a laminin coated plate which simulates implantation. There is early evidence of neural induction with the sprouting of small neurites. This is because cells transition through a primitive anterior neural stage prior to eyefield specification. Day 30 shows early pigmentation of a colony of retinal progenitors. Day 50 shows deep pigmentation of a colony of hiPSC-RPE which are ready for manual dissection.

In order to validate the RPE a number of phenotypic investigations were performed looking for gene expression and markers of mature RPE function (Singh et al., 2013a). The pigmented colonies were firstly examined under light microscopy (figure 3.11). Examination revealed a pigmented, polygonal monolayer of cells. Electron microscopy showed cells with a characteristic apical basal polarisation (figures 3.12 and 3.13). These included apical microvilli, mitochondria and melanosomes within the cells, tight junctions and basal infoldings and an RPE basement membrane forming. A western blot showed protein expression for proteins found in RPE (figure 3.14). Immunostaining showed expression of RPE specific markers (figure 3.11). The basic characterisation did not show any phenotypic differences between case and control cells.

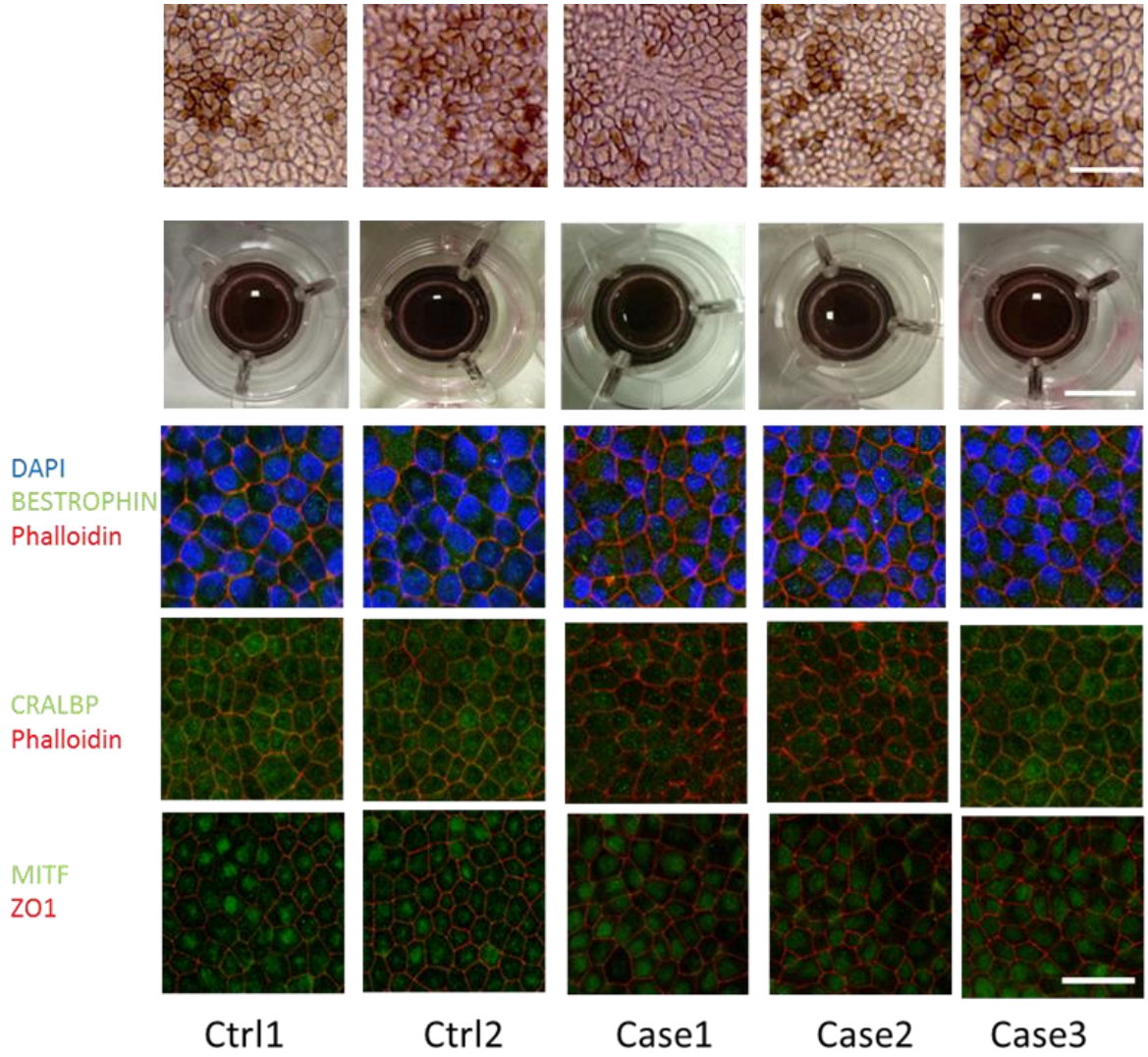

Figure 3.11: Images of case and control lines showing characteristics of RPE cells

The top row show brightfield images of pigmented RPE grown in a 24 well plate showing a classical polygonal, pigmented monolayer. The second row of images show deeply pigmented RPE grown on membrane inserts. The third row of images show fluorescence images showing classical RPE morphology highlighted by phalloidin. They also show membrane immunostaining for RPE specific marker Bestrophin. The fourth row of images show immunofluorescence images highlighting staining for RPE specific marker CRALBP. The fifth row of images show immunofluorescent images for Mitf a marker for melanocytic cells.

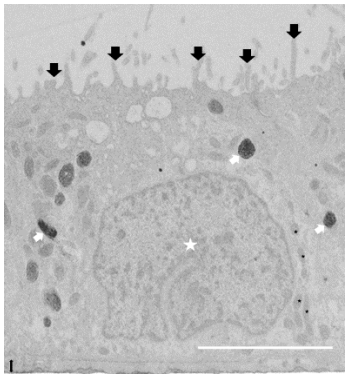

Figure 3.12 : Electron micrograph image of Ctrl1 hiPSC-RPE on a membrane insert. The image shows classical features attributed to a polarized RPE including apical microvilli (black arrows), melanosomes (white arrows), mitochondria and a basal lamina membrane. (scale= 5 µm)

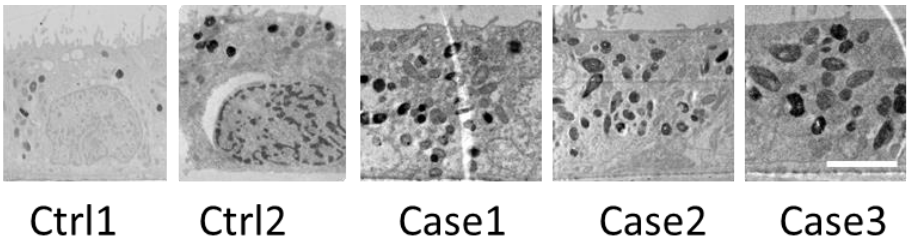

Figure 3.13: Electron micrograph images of case and control hiPSC-RPE. Images show that all the case and control hiPSC-RPE demonstrate the features of RPE cells. (scale = 5 µm)

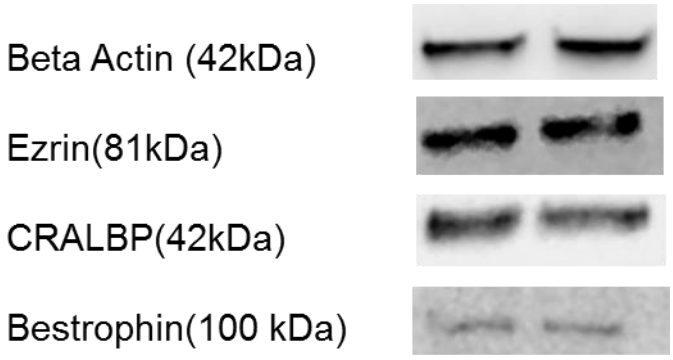

Figure 3.14: Western blot of RPE markers. The western blot of Ctrl1 (left) and Case1 (right) identifies similar expression of standard RPE markers Bestrophin, CRALBP and Ezrin in both the case and control lines.

In order to investigate whether the cells were functional and resembled previous report of *in vitro* culture of human primary cultured RPE functional studies were performed. The first functional study was to investigate Transepithelial resistance (TER) (figure 3.15). This was performed using a technique previously described on primary human RPE culture. The results revealed no significant difference between case and control lines between cases and control lines when samples

were pooled. All cell lines produced a TER of >150 Ω/cm^2. RPE also perform phagocytosis of photoreceptor OS on a daily basis. The phagocytosis assay was performed and revealed an increased phagocytosis in the case line than the control lines (figure 3.16).

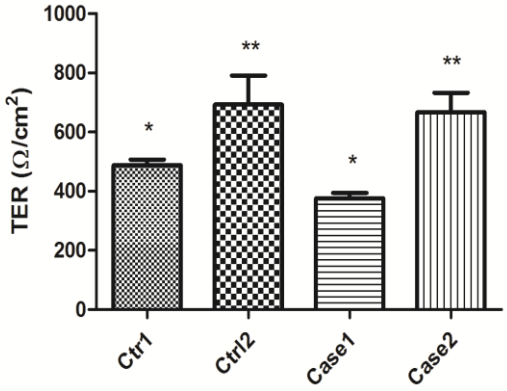

Figure 3.15 : Graph showing transepithelial resistance measurements for case and control hiPSC-RPE from membranes with confluent hiPSC-RPE monolayers. The results show that the hiPSC-RPE attain high TER values four weeks after plating. There was no significant difference in basal TER between case and control lines with line to line variation. The values shown are the calculations after subtracting the value of resistance obtained from a control well with the same media but no cells with standard error bars. (*= mean TER of 3 inserts, **=mean TER of 6 inserts). A value of 150 Ohms per square centimeter Is taken as the standard minimum for *in vivo* RPE.

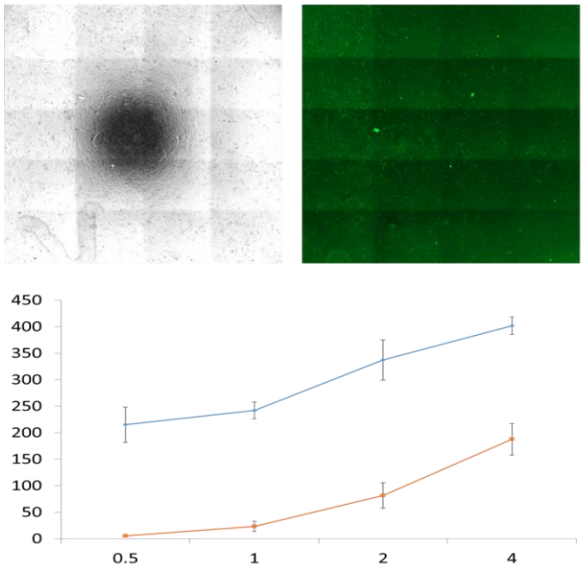

Figure 3.16: Phagocytosis assay. Top left image is a tiled brightfield image of RPE in a 96 well. The cells were stained for DAPI to aid cell counting. Top right image is an autofluorescent image in the 488 channel highlighting FITC-OS. The number OS were counted using automated software

and the count divided by the number of cells in each image. The graph shows the number of OS ingested per cell (y axis) at 0.5, 1, 2 and 4 hours (x-axis). The graph shows standard error bars from 3 wells at each condition.

Another important property of RPE is that they do not continue to proliferate for instance in tumour lines or some immortalized cell lines. Ki67 is a marker of cell proliferation. Cells which had been plated for only one week continued to express ki67. However, cells which had been plated for approximately four weeks not only developed traditional RPE structure but also stopped expression of ki67 suggesting that monolayer had stopped proliferating (figure 3.17).

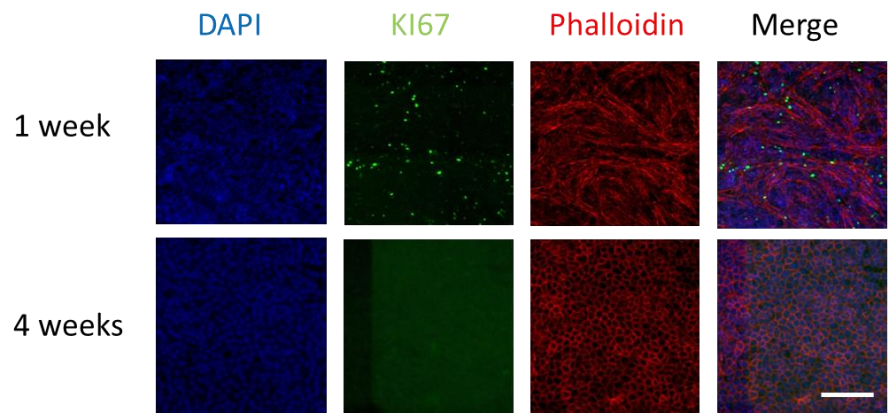

Figure 3.17: Tiled Immunofluorescence imaging of a control hiPSC-RPE to test for proliferation. The top set of images show cells 1 week after plating. There is marked ki67 staining suggesting that there is continuing proliferation of cells. Additionally the disorganized phalloidin staining suggests that the monolayer is remodeling.

The bottom set of images shows cells 4 weeks after plating. There is no ki67 staining suggesting that the monolayer is not proliferating. The phalloidin staining shows a clear RPE like polygonal structure associated with mature RPE. Cells used for experiments were plated for at least 4 weeks.

For the experiments used in the studies eventually hiPSCs from fibroblast lines 1, 3 and 4 were used as cases and two clones of fibroblast line 2, reprogrammed separately using different techniques, were used as controls (table 3.2).

3.4 Discussion

HiPSC-RPE have now been well characterised (Mekala et al., 2013, Carr et al., 2009, Singh et al., 2013a) have been found to resemble native RPE in functional characteristics and protein expression profile (Blenkinsop et al., 2015). The hiPSC-RPE generated in this study fulfil the key phenotypic characteristics of RPE. Morphologically they resemble RPE being pigmented and polygonal. Electron microscopy also reveals that they grow apical microvilli, contain melanosomes and develop basal infoldings that resemble native RPE (Singh et al., 2013a, Carr et al., 2009). They express tight junction marker ZO-1. In addition, they express RPE specific proteins including Bestrophin and CRALBP (Mekala et al., 2013). The hiPSC-RPE in this study show apical basal polarity on electron micrograph (Singh et al., 2013a).

Additionally, hiPSC-RPE appear functionally similar to mature RPE. Monolayer cultures have been used in experiments when they have a TER of at least 200Ω/cm^2 based on studies showing that TER of human RPE monolayers *in vivo* is 150Ω/cm^2 (Maminishkis et al., 2006, Quinn and Miller, 1992). One of the primary roles of RPE is the phagocytosis of POS. Phagocytosis had been studied *in vitro* using immunohistochemistry, western blot and FACS (Buchholz et al., 2009, Singh et al., 2013b, Westenskow et al., 2012). In this study, immunohistochemistry was used to confirm ROS phagocytosis by hiPSC-RPE.

An important characteristic of terminally differentiated cells that do not show tumour potential is that they do no continue to proliferate and are post mitotic. HiPSC-RPE have previously been shown to downregulate proliferation marker KI67 after long term culture (Reichman et al., 2014, Kanemura et al., 2014). The cells in this study also appear to downregulate KI67 after approximately four weeks of plating.

In summary, the hiPSC-RPE generated from case and controls show standard functional and expression profiles for mature RPE. This suggests that the cells are suitable for investigating early *in vitro* disease phenotypes in L-ORMD.

Chapter 4

4. Investigating *in vitro* differences between C1QTNF5 mutant and control hiPSC-RPE

4.1 Introduction and rationale

HiPSC-RPE provide a platform for the *in vitro* study of human retinal disease. This method has already been used to study a number of RPE diseases including Best vitelliform maculopathy (Singh et al., 2015, Singh et al., 2013b), retinitis pigmentosa (Li et al., 2014), choroideraemia (Cereso et al., 2014) and gyrate atrophy (Meyer et al., 2011).

C1QTNF5 is predominantly expressed by the RPE and ciliary body within the eye (Mandal et al., 2006b). C1QTNF5 is secreted and then is located on cell membranes in the outer retina (Mandal et al., 2006b). Several lines of evidence point to dysfunction in the RPE occurring early in the disease process including histological samples showing RPE disorganisation (Duvall et al., 1986). Transfected cell studies showed that mutant C1QTNF5 formed high order aggregates which accumulated within the ER (Shu et al., 2006b). Therefore the RPE is thought to be a key mediator of disease. We have shown that hiPSC-RPE generated from patients and sibling controls show mature phenotypes and properties of mature physiological function in chapter 3. Taken together the above suggests investigating L-ORMD using hiPSC-RPE generated from cases and controls. The initial aim of this series of studies was to characterise an *in vitro* phenotype comparing hiPSC-RPE generated from cases with hiPSC-RPE generated from an unaffected control. The hypothesis was that cells harbouring the C1QTNF5 mutation would demonstrate cell autonomous differences in standard tests of RPE function.

4.2 Methods

All the experiments in this section were performed by Dr Shyamanga Borooah at the University of Edinburgh.

4.2.1 Cell viability

To assess cell viability a lactate dehydrogenase cytotoxicity kit was used as an adaptation of an existing protocol (Yang et al., 2014b). HiPSC-RPE were plated at a density of 50,000 cells per cm^2 on laminin coated 96 well microtitre plates. Cells were initially fed for two days with 10% FCS in RDM, followed by 7 days in 2% FCS in RDM before reverting to plain RDM for a minimum of three weeks prior to experiments.

A LDH cytotoxicity assay kit (Thermo Scientific) was used according to kit instructions.

For each condition, cells were plated in triplicate. In further experiments cells were incubated with 100ul RDM. For a set of triplicates 10ul lysis buffer was added to the media to act as a positive control 45 minutes prior to harvesting the supernatant and 10ul of sterile water was added to other wells. 50 ul of the supernatant was transferred to a fresh flat-bottomed microtitre plate. 50ul reaction mixture was added to each well. These were mixed for 3 seconds in a plate reader and the incubated in the plate reader for 30 minutes at 25ºC. 50ul stop solution was added and the plate measured at absorbance 490nm and 680nm. The 680nm absorbance value was subtracted from the 490nm value to minus the background. To calculate the LDH activity LDH activity from the plain media was subtracted from cell supernatant absorbance. Data from the plate readers was transferred to Excel 2013 (Microsoft corporation, Redmond, USA).

4.2.2 OS processing

To investigate the build-up of autofluorescent material in hiPSC-RPE following long term feeding with ROS a previously published protocol by Singh et al was used (Singh et al., 2013b). HiPSC-RPE were plated at a density of 50,000 cells/cm^2 onto laminin coated µ-slide 8 chamber glass bottom slide wells. After two days media was changed to 2%FCS in RDM. After one week media was changed to RDM. Cells were fed every two days with 50 ROS per RPE cell in RDM for a total of two months. After two months, the cells were reverted back to RDM only feeding for one week. The cells were fixed in 4% PFA for 30 minutes and then mounted in fluorsave (Merck-Millipore). The plates were imaged at 555nm and 488nm wavelengths in order to image lipofuscin (Sparrow and Boulton, 2005). ImageJ was used to analyse the area of fluorescent material per cell.

4.3 Results

4.3.1 Expression of C1QTNF5 protein

Studies using transfected cell lines showed that C1QTNF5 was secreted (Shu et al., 2006b). The mutant protein was not secreted and accumulated within the ER (Shu et al., 2006b). The histopathology investigations performed in chapter 2 suggested that C1QTNF5 was secreted and deposited particularly in the inner deposit adjacent to the RPE cells in the case donor retina. To see if there was a difference in secretion of C1QTNF5 between case and control, conditioned media was obtained. Conditioned media was generated by maintaining RPE in the same media for 5 days. The media was tested using western blot and showed clear differences in the pattern of staining between the case and

control lines (figure 4.1). The conditioned media showed a far greater amount of staining for C1QTNF5. In addition, in the non-reduced sample the C1QTNF5 formed more high order multimers. It appears that the normal arrangement of multimeric bouquets suggested by protein studies is inhibited by the mutant protein (Tu and Palczewski, 2014). The western blot also shows that the multimers are not exact multiples in molecular weight of the predicted monomeric predicted weight of 26 kDa. Next, I wanted to see if the multimers could be reduced to a monomeric species. The C1QTNF5 generated from the control hiPSC-RPE could be reduced to monomers. However, in the protein secreted by the control hiPSC-RPE heterogeneous multimers are still present. Next I wanted to see if there was a difference in localisation of C1QTNF5 within the cell. A western blot of cell lysate showed a difference in C1QTNF5 localisation within the cell. (figure 4.2). Again the wild type protein alone seemed able to easily form multimers in the non-reduced state whilst the addition of the mutant appeared to reduce formation of multimers, leaving mainly a monomeric form under non-reducing conditions.

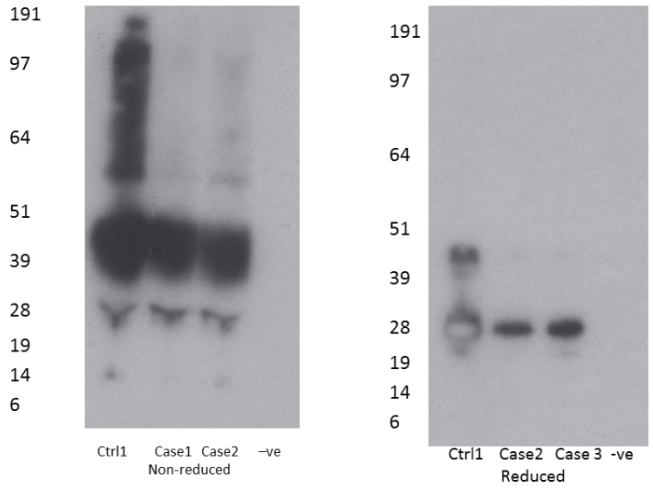

Figure 4.1: Western blots of conditioned media from case and control hiPSC-RPE lines under non-reduced and reduced conditions. Under non-reducing conditions (left) the media from the control line appeared to produce marked multimers. The media from the two case lines formed fewer multimers and instead resulted in monomers and dimers. Under reduced conditions (right) the media from the control line was still not reduced completely to a monomeric form whilst the case lines appeared only at the predicted monomeric molecular weight of 28kDa.

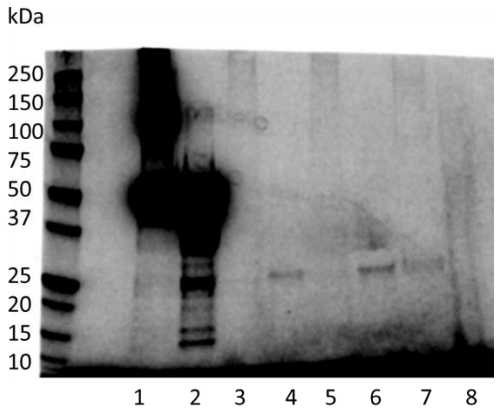

Figure 4.2: Western blot with antibody to C1QTNF5. The image shows the results of a western blot for non-reduced recombinant wild type full length C1QTNF5 (Lane 1), reduced recombinant wild type C1QTNF5 (lane 2), Non-reduced cell lysate from Ctrl1 (lane 3), reduced cell lysate from Ctrl1 (lane 4), non-reduced cell lysate from Case1 (lane 6) reduced cell lysate from Case1 (lane 7) and a negative control of HEK cell lysate (lane 8). The cell lysates were controlled for GAPDH. There is evidence that when wild type C1QTNF5 is in a non-reduced state it forms multimers (lane 1). This is still maintained even after strong reduction with dimers and trimers visible (lane 2). Non-reduced cell lysate from Ctrl1 surprisingly shows little staining except some faint staining as a multimers. This could suggest that multimers occur (lane 3). However, when reduced a strong monomeric band at approximately 26 kDA is seen (lane 4). Meanwhile both the non-reduced and reduced lysates of the case provide a strong band at the predicted monomer (lane 6 and 7) suggesting that polymerization of C1QTNF5 is reduced in the case. Finally, the negative control fails to show a specific band (lane 8)

In order to investigate differences between the case and control lines further an immunostaining experiment for C1QTNF5 was performed on case and control lines (figure 4.3). The immunohistochemistry study showed that in the control cell line C1QTNF5 was localised both apically and basally in the membrane with little intracellular staining. Both the case and control lines showed some staining apically and intracellularly although the case lines appeared to have more intracellular staining. In addition, the case lines had marked immunostaining basally in the sub-RPE in the membrane. This is somewhat similar to the staining seen *in vivo* of the deposit (figure 2.24).

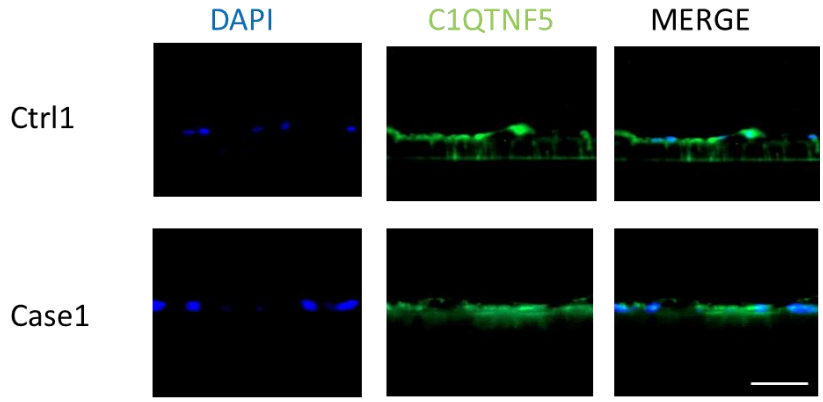

Figure 4.3 : Immunocytochemistry for C1QTNF5. The figure shows cross sections of membrane and stained with DAPI and immunostained with anti-C1QTNF5 antibody. There is intra-cellular immunostaining of both case and control lines. There is also some staining of the membrane inset below the cells in the control and more marked staining of the membrane in the case line. (scale= 50 µm)

4.3.2 Comparison of TEM basal deposit in mutant and control lines

One of the key phenotypic characteristics in L-ORMD is a thick sub-RPE deposit. I next sought to replicate conditions seen in the outer retina by growing the cells on membrane inserts. Previously, Amin *et al* had shown that sub-RPE deposits could be modified (Amin et al., 2004). Cells were grown for two months on membrane inserts in RDM and then fixed using glutaraldehyde and prepared for electron microscopy. The size of the sub-RPE deposit between the RPE and the membrane was measured. Three membrane inserts were measured for a case line and a control line (figure 4.4). No significant difference between the deposit thickness measured in three different places was found between the case and control line when cells were maintained in RDM for at least 2 months.

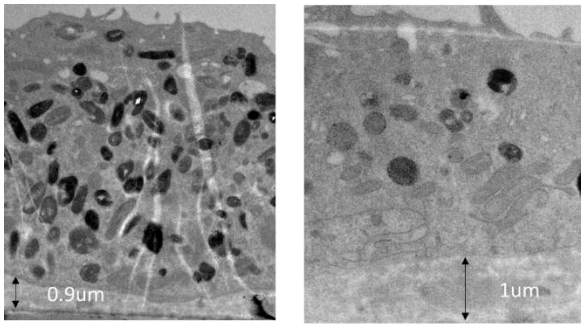

Figure 4.4 : Transmission electron microscopy images of sub-RPE deposit. Representative images of sub-RPE deposit in control line 2 (left) and case line 1(right). There was no significant difference in deposit thickness between cases and controls.

4.3.3 Comparison of TER in mutant and control lines

TER has been routinely used to test the function of the RPE monolayer in *in vitro* experiments (Maminishkis et al., 2006, Singh et al., 2013a). Recently, it was found that TER could provide phenotypic differences between different cell types in studies performed by one of our collaborators. The initial experiments looked to see if there was a difference in TER between the case and control hiPSC-RPE in RDM. There was a variability in TER in all lines. There was no significant difference between case and control lines when the results were pooled.

A further set of studies was performed to test the cells before and after the addition of 40% serum to more closely simulate findings in the outer retina. Georgianikkis *et al.* found that an increase in TER after serum and with increased C5b-9 staining. No significant differences were found in the TER pre and post serum in the case or control hiPSC-RPE cell lines (figure 3.14).

4.3.4 Comparison of ROS phagocytosis in mutant and control lines

A previous unpublished study (Dr Fern Slingsby, University of Edinburgh) using transfected ARPE-19 cells transfected to overexpress either wild type protein or mutant protein showed a phagocytosis deficit with the mutant transfected cell lines compared with the wild–type cell lines. This pointed towards a role for C1QTNF5 in phagocytosis. The strong apical staining in the control hiPSC-RPE lines suggested that C1QTNF5 was located in the correct part of the RPE to potentially modify phagocytic interactions.

Consequently, we compared mutant and wild type RPE lines initially with one case and control line to see if these findings were replicate in hiPSC-RPE with more physiological levels of RPE protein expression. The studies used a case and control hiPSC-RPE line differentiated at the same time and plated under the same conditions into a 96 well plate. The tests were performed at the same time under the same conditions with 3 repeats and the wells fixed at set time points. Hoescht stain was added to label nuclei. The FITC-ROS were then imaged using fluorescent microscopy counted using imageJ and normalised for cell numbers labelled with Hoescht stain. The assay found a significantly increased number of phagocytosed FITC-ROS ($p<0.05$) at the half an hour, one hour, two hours and four hours after the addition of FITC-ROS respectively (figure 3.15).

4.3.5 Comparison of OS processing in case and control lines

Having found differences in the phagocytosis rate between case and control lines. I wanted to see if this also led to downstream differences in OS processing. Singh *et al.* had shown that in the hiPSC-RPE derived from patients with mutations coding for Best vitelliform dystrophy there was an increased build up of lipofuscin in the case lines when compared with control lines (Singh et al., 2013b). Similarly, both case and control L-ORMD lines were fed OS for two months and then investigated for autofluorescence using confocal microscopy at 488nm and 555nm wavelengths (figure 4.5). Nine confluent wells of each cell line were tested. A 500 um by 500 um image was chosen of each well under brightfield conditions. Autofluorescence z-stack images were then taken at 488 and 555nm wavelengths and a DAPI image taken to count cell numbers. The area of lipofuscin was then measured on maximal intensity images of combined z-stacks. Both case and control lines had increased autofluorescence compared with a control line that was maintained for the same length of time but not fed with OS. When statistical analysis was performed although the mean fluorescence of the case lines was greater than the control hiPSC-RPE there was no significant difference ($p=0.59$) between the amount of autofluorescent material in each cell line.

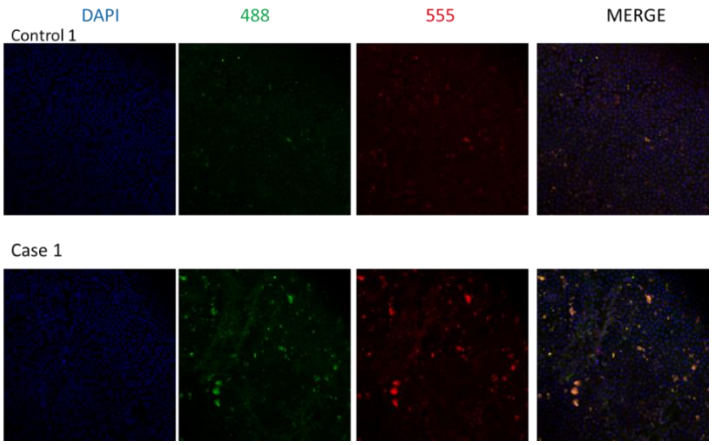

Figure 4.5 : Confocal images looking for autofluorescence in hiPSC-RPE lines. Representative images showing a buildup of intra-cellular autofluorescent material measured at 488 and 555nm wavelength after 2 months feeding with OS laden media. Although there appeared increased autofluorescence in the case line when statistical analysis was performed there was no significant difference between the lines when analyzed by automated pixel density measurements. This suggested that there was no significant difference in lipofuscin formation between the case and control line following long-term feeding with ROS.

4.4 Discussion

In this set of studies C1QTNF5 protein was found to be expressed in greater quantity in the control lines when compared with the case lines. Secretion of C1QTNF5 was also found to be greater in the control lines when compared to the case lines. Examination of sub-RPE deposit using TEM showed that the deposit was significantly greater in case lines compared with control lines. However, there was no difference in TER in case lines when compared with control lines. There was also a significantly increased generation of lipofuscin in case lines when compared with control lines following long term feeding with ROS.

Hayward *et al.* (2003) demonstrated that C1QTNF5 is expressed by RPE and is predicted to be secreted (Hayward et al., 2003). In order to investigate C1QTNF5 secretion HEK293-EBNA cells were stably transfected with wild-type or mutant His-tagged C1QTNF5 (Shu *et al.*, 2006b). His tagged protein was found in the cell lysates of both cells transfected with mutant and wild type plasmids however, protein was only found to be secreted in control cell lines. Mandal *et al*, similarly transfected COS-7 cells with V5-tagged wild type and mutant C1QTNF5 with similar outcomes. Immunostaining found co-localisation of the mutant protein with ER markers (Mandal et al., 2006b). Polyacrylamide gel electrophoresis (PAGE) showed that only the wild type protein migrated whilst the mutant did not under non-reducing conditions however the proteins formed

monomers under reducing conditions. Taken to together this suggested that mutant C1QTNF5 formed high order aggregates that were retained within the cell and not secreted. The findings are similar to those in this study. The findings were slightly different from this study which showed that C1QTNF5 was found in the media of control and case lines. However, the media from the control lines, containing wild-type C1QTNF5 readily formed high order multimers. Whilst the media from the mutant lines showed that C1QTNF5 formed mainly monomers and dimers.

L-ORMD retina are known to have a thick sub-RPE deposit (Duvall et al., 1986, Kuntz et al., 1996, Malek et al., 2003). We found that both case and control RPE produced a sub-RPE deposit. The case lines appeared to produce a deposit of greater thickness. Staining of L-ORMD deposits have shown that the sub-RPE deposit is a bilayer. The inner layer is composed of components similar to those found in other degenerative diseases. We also found that the inner layer stained well for C1QTNF5 on immunohistochemistry.

The formation of deposits *in vitro* has been reported in another inherited macular degeneration. Murine RPE harbouring a mutation in the gene *EFEMP1* responsible for the retinal degeneration Malattia Leventinese grown on transwells also resulted in sub-RPE deposits (Fernandez-Godino et al., 2015). The deposits were found to contain the extracellular membrane components collagen I, elastin, TIMP-3, fibrillin-1 and fibronectin in abnormal amounts. In addition, the deposits from the case lines contained increased amounts of EFEMP1. To see if substances secreted by the mutant RPE cells were responsible for deposit formation wild type cells were incubated in conditioned media from mutant cells. The wild type cells also proceeded to develop a deposit. Analysis of the condition media revealed C3a as a potential stimulator of deposit formation. This was confirmed by a dose dependent reduction of deposit formation when the cells were incubated in media containing C3a-neutralising antibodies. The studies suggested that in a model Malattia Leventinese complement activation is required for deposit formation. Antibodies neutralising C5 however did not appear to reduce deposits. We also showed that the use of C3 depleted serum abolished c5b-9 staining. However, in contrast to Fernandez-Godino *et al*. we noted that the use of C5 depleted sera also abolished TCC deposition whilst C5 neutralising antibody reduced TCC deposition in a dose-dependent manner (see section 2.3.6). We suspect that the EFEMP1 model may not be mediated by dysfunction of later regulators of the complement pathway as in our model. Levels of C3d a marker of C3b degradation by CFH were found to be the same between case and control lines. Additionally although TCC deposition was detected, there was no significant difference between case and control.

In phagocytosis experiments case hiPSC-RPE were found to have a higher rate of phagocytosis when compared with control hiPSC-RPE. In addition, we noted increased autofluorescence in case hiPSC-RPE when compared to control hiPSC-RPE following long term feeding with ROS although this was not significantly different. The increased phagocytosis rate in case lines is difficult to explain. In unpublished data Dr Xinhua Shu and Dr Fern Slingsby performed ROS phagocytosis experiments using transfected HRPE-1 cells. Cells transfected with mutant C1QTNF5 were found to have a reduced rate of phagocytosis when compared with cells transfected with wild type C1QTNF5. Singh *et al*, investigated phagocytosis in both short term and long term culture of hiPSC-RPE from patients with a mutation in *BEST1 (Singh et al., 2013b).* After long term feeding with ROS the RPE were found to have increased autofluorescence. In this series of studies, however long term feeding with OS did result in increased autofluorescence although there was no significant difference in the amount of autofluorescent material generated between the case and control line. This may reflect different disease pathogenesis. Lipofuscin builds early within and below the cell in Best vitelliform dystrophy disease whereas in L-ORMD FAF is noted to increase late in the disease and is especially noted to occur in areas adjacent to existing neuro-retinal atrophy. Interestingly, Singh et al. also noted an increased phagocytosis rate for FITC-labelled POS at the 4 hour time point in case hiPSC-RPE when compared to control hiPSC-RPE. However, the differences were lost at 24 hours (Singh et al., 2013b). In our experiments we did not assess phagocytosis at the 24 hour time point.

Chapter 5

5. Investigating interactions between control and mutant C1QTNF5 hiPSC-RPE and the complement pathway

5.1 Introduction and rationale

Oxidative stress has been implicated in AMD disease mechanism (Hollyfield et al., 2008). Different stressors have previously been used to investigate oxidative stress in RPE cell lines (Rabin et al., 2013, Garcia et al., 2015, Cano et al., 2014, Joseph et al., 2013, Klettner, 2012, Lu et al., 2006). Incubating cells in hydrogen peroxide provides a simple method of assessing the effects of oxidative stress *in vitro* (Hsiung et al., 2015). We hypothesise that the addition of hydrogen peroxide to media will expose an increased vulnerability of hiPSC-RPE cell lines to cell death.

Complement pathway dysfunction has been implicated in AMD. Amongst the earliest histopathological signs of AMD are sub-RPE deposits (Curcio et al., 2013). These deposits have been shown to contain components of the complement pathway and in addition, many activated components of the pathway suggesting that inflammation plays a part in early macular degeneration (Anderson et al., 2002, Crabb et al., 2002, Mullins et al., 2001). Allelic variants in complement pathway components have been found to increase the risk of AMD (Hageman et al., 2005, Seddon et al., 2011). Taken together this implicates complement pathway dysfunction in early macular degeneration.

We have already shown that localised complement pathway deposition may also be involved in L-ORMD pathogenesis using both a mouse model of L-ORMD and donor retina from L-ORMD patients. Recently, several groups had reported systems to study complement activation on different types of RPE cells *in vitro* using complement containing media (Johnson et al., 2011, Lueck et al., 2015, Georgiannakis et al., 2015). RPE cells were grown on permeable membrane supports recapitulating RPE Bruch's membrane interactions. L-ORMD hiPSC-RPE display phenotypic and physiologic characteristics resembling mature RPE. Combining the use of L-ORMD hiPSC-RPE in a system that mimics the outer retinal microenvironment would allow the interrogation of early *in vitro* disease phenotypes in L-ORMD. Although RPE have already been shown to generate the majority of components of the complement pathway human serum containing active complement components was added to enable formation of the terminal complement complex (TCC). The hypothesis is that mutant C1QTNF5 hiPSC-RPE would show signs of complement dysfunction resulting in increased TCC deposition when compared to control hiPSC-RPE.

5.2 Methods

All the studies presented within this chapter were performed by Dr Shyamanga Borooah except FACS studies which were performed by Dr Anai Gonzalez-Cordeiro (University College, London). Advice for live cell microscopy was sought from Dr Dario Magnani (University of Edinburgh). Advice of setting up the complement serum studies on membrane inserts was sought from Professor Stephen Moss and his PhD student Apostolos Georgianikkis (University College London).

5.2.1 Oxidative stress studies

After initial cell viability studies showed no significant difference in cell death between case and control lines we investigated whether factors implicate in AMD pathology may differentially increase the vulnerability of hiPSC-RPE carrying mutations when compared to controls. Oxidative stress has been previously shown to induce differences between cell lines in a model of AMD (Radu et al., 2014). For oxidative stress experiments, protocols previously used on RPE were optimised for hiPSC-RPE having previously been optimised for other cell lines (Rzechorzek et al., 2016, Yang et al., 2014b). HiPSC-RPE cells were plated onto laminin coated 96 well plates at a density of 50,000 cells per cm^2. Cells were initially fed with 10% FCS RDM for two days, and then 2% FCS in RDM for one week before reverting to RDM for a further two weeks. One week prior to studies the hiPSC-RPE were fed with standard RDM with B27 supplement minus antioxidants (Gibco). At the start of the experiment, media was switched to RDM minus antioxidants containing different concentrations of hydrogen peroxide (Sigma) and 1 :5000 SYTOX® green membrane dead cell stain (molecular probes, life technologies) as per kit instructions. Triplicates were prepared for each condition. Cells were placed in a live cell imaging platform and maintained for 12 hours under standard incubation conditions. They were imaged at set timepoints using an automated setup on a Zeiss fluorescent microscope. ImageJ was used to analyse the tiled image from each well. Three non-overlapping fields from each well were used for analyses. The average of three wells were used to produce a mean and standard error for each condition. For ROS identification 500um hydrogen peroxide was added to cells for 6 hours in order to gain maximal chance of ROS production. The cellROX® ROS identification kit was used as per instructions in order to identify ROS generated intracellularly. The cells were imaged at 488 wavelength as per the kit on a fluorescent microscope.

5.2.2 Human complement serum studies

Human complement serum assays were performed on transwell plates and generated as per previously published protocols (Singh et al., 2013a). The investigation of complement activation of RPE cells on membranes was performed using modifications of previously published protocols (Johnson et al., 2011). RPE cells from confluent monolayers were dissociated into single cells using 0.5% trypsin/EDTA. 24 well transwell membranes were coated with 1% laminin in DMEM 5 hours prior to plating and then incubated under standard conditions. Half an hour prior to plating the membranes were incubated with 10% FBS in RDM. HiPSC-RPE were then plated at a density of 50,000 cells per cm^2. The cells were maintained in 10% FBS RDM for two days before being switched to 2% FBS RDM for 7 days. After this, the cells were maintained for a minimum of three weeks in serum free RDM prior to any experiments.

For initial complement serum studies human complement serum (HCS) (Complement technologies incorporated, Tyler, USA) was incubated at various concentrations of HCS in RDM for 12 hours. For timecourse studies hiPSC-RPE were incubated under standard conditions in 40% HCS in RDM over varying lengths of time. For HCS quantification and depletion studies hiPSC-RPE cells were incubated for 12 hours in 40% HCS in RDM or 40% depleted serum in RDM. For treatment studies case hiPSC-RPE were incubated in 40% HCS in RDM with varying concentrations of anti-complement C5.

For all studies, the experiments were terminated by washing membranes three times in PBS and then fixing the membranes for 30 minutes in 4% PFA in PBS. The membranes were then incubated in 3% Triton X100 in PBS for 30 minutes prior to blocking in 2% NGS and 1% BSA in PBS for one hour. Membranes were then removed and placed in 50ul of primary antibody was added in blocking solution for overnight incubation at 4^{o}C. The antibody primarily used for the assays was anti-C5b-9 1:100 (DAKO, Ely, United Kingdom) however a full list of antibodies used can be found in the appendix. The following day after three washes in PBS an Alexafluor secondary antibody (Invitrogen) was added for 30 minutes. After a further three washes in PBS DAPI 1:500 and Rhodamine phalloidin (Invitrogen) 1:2500 we were added for 10 minutes. After a final wash in PBS the membranes were dried and mounted on slides cell side up and mounted with coverslips using fluorsave (Merck-Millipore). The membranes were imaged using Zeiss confocal microscopy. A minimum of three fields of 100uM x 100uM were selected from each membrane and three repeats of each condition were imaged for analyses. The mean intensity density of the fields was calculated in the channel of the C5b-9 staining using imageJ. Advice from Professor Stephen Moss and Dr Apostolos Georgiannakis (University College London) was obtained to optimise the methodology regarding plating, staining and imaging of membranes.

5.3 Results

5.3.1 Comparing cell viability following oxidative stress insult in case and control lines

In the human donor pathology samples there was RPE disorganisation and loss in the L-ORMD cases. I hypothesised that L-ORMD hiPSC-RPE would also show a differential vulnerability *in vitro* when compared to control hiPSC-RPE. To test this hypothesis a live dead cell assay was used initially under basal conditions (Prajapati et al., 2015, Berner et al., 2014, Yang et al., 2014c)(Figure 5.1). Neither case lines nor control lines showed marked signs of cell death and there was no significant difference in cell death between the lines at baseline (figure 5.2).

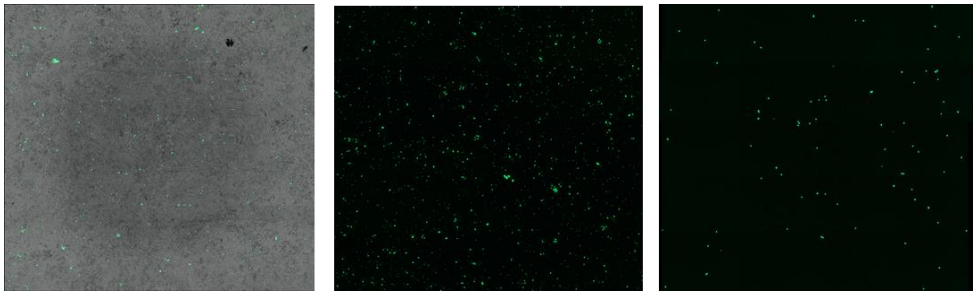

Figure 5.1: Oxidative stress studies. The left image is merged image of brightfield and channel 488nm wavelength from a 96 well plate. The middle image shows the SYTOX green immunofluorescence staining in a case line after 3 hours of 500 µm hydrogen peroxide. The image on the right shows SYTOX green immunofluorescence staining in a control line after 3 hours of 500 µm hydrogen peroxide.

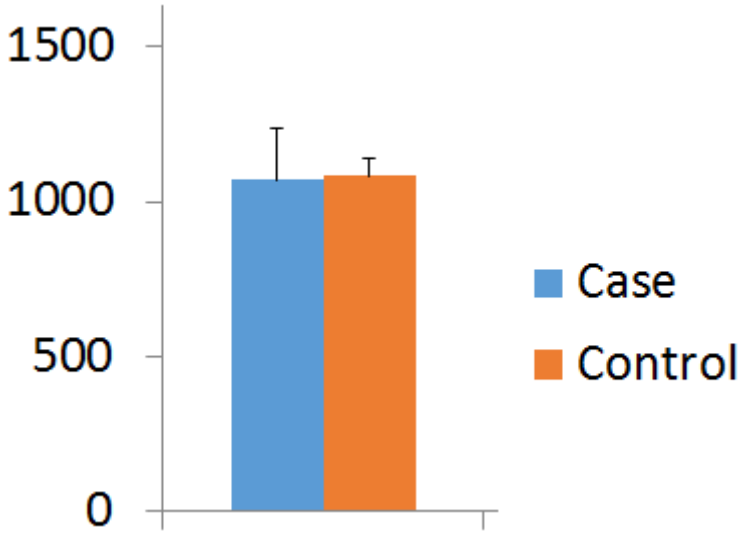

Figure 5.2: Live cell viability studies. Ctrl2 and Case1 were studied under basal condition to see if there was any difference in viability under basal conditions. No significant difference was found.

In order to investigate what potential stressors the cells may be vulnerable to I chose to perform a targeted RNA screen of cellular stress and toxicity comparing case and control lines. The screen showed that there were several genes with variable expression of greater than two fold between cases and control lines after normalisation to GAPDH expression (figure 5.3). From the genes identified the highest differences in expression were found in genes involved with oxidative stress catalase (14.1 fold higher in the case). Catalase is an enzyme found in the peroxisome of human cells and is a key regulator of oxidative stress. It converts hydrogen peroxide to water and oxygen. It has been found to be upregulated in a number of cell lines to protect against hydrogen peroxide induced oxidative stress and ageing (Alcendor et al., 2007, Hasegawa et al., 2008).

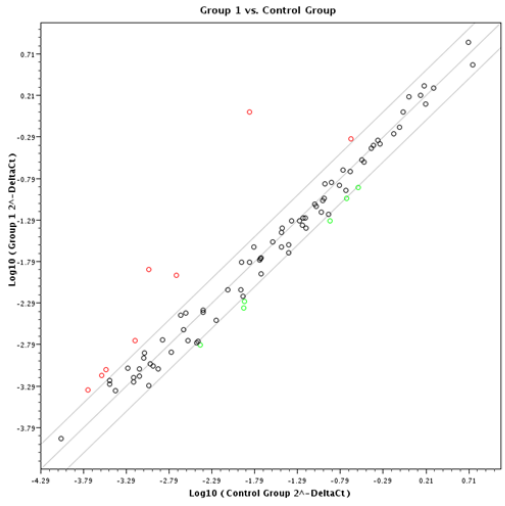

Gene	Fold Regulation
CASP10	2.6371
CAT	14.0866
CCL4	2.7184
CSF2	2.5353
HMOX1	2.2454
HSPA2	5.5543
HSPA6	2.7541

Gene	Fold Regulation
CDKN1A	-2.0458
CYP2E1	-2.3447
HSPA4	-2.4467
IL18	-2.286
RAD50	-2.6634
SOD2	-2.0716

Figure 5.3 : Cellular stress array. Quantitative real-time PCR array with three repeats performed for each gene using cDNA from Case1 and Ctrl1 hiPSC-RPE. The graph shows how many genes showed a greater than two fold difference between case and control lines. The table on the left shows genes expressed greater in the case compared with the control. The table on the right shows genes that were expressed at less than two fold less than the control line. The most marked fold change is noted in catalase expression in the case. In addition, there is also an increase in haem oxygenase expression

To investigate a potential role for oxidative stress and hydrogen peroxide in particular on cell viability, I developed a live-cell imaging platform for testing the effect of different concentrations of hydrogen peroxide on my the hiPSC-RPE cells. Using methods previously described in studies using ARPE-19 cells in oxidative stress cells were plated into a 96 well plate (Yang et al., 2014c). The cells were imaged at 15 minutes after baseline and at 3 hours (figures 5.4 and 5.5). There was no significant difference between case and control lines with basal media at 15 minutes ($p=0.51$). However, there was a significant increase in SYTOX® staining with hydrogen peroxide at each concentration and at each time point in the case line when compared to the control lines ($p<0.05$) (figure). The SYTOX® staining appeared to increase in a dose dependent manner with hydrogen peroxide concentration. This suggested that the case hiPSC-RPE had an increased vulnerability to hydrogen peroxide mediated oxidative stress when compared to control hiPSC-RPE.

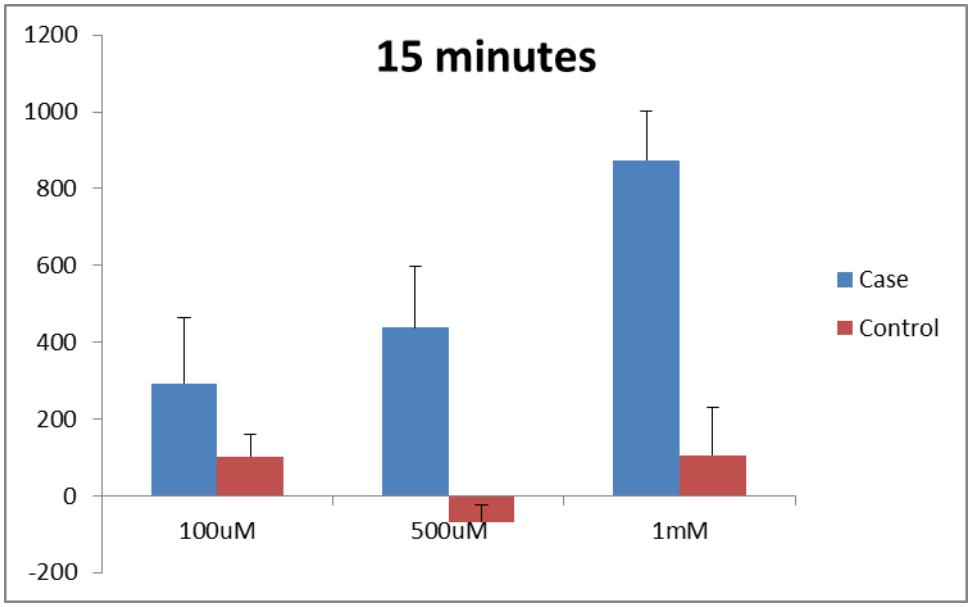

Figure 5.4: SYTOX green staining at 15 minutes in case and control hiPSC-RPE. The results show the number of cells with positive staining corrected for baseline. Each condition had three repeats with standard error bars shown. The case lines show a dose dependent increase in vulnerability when compared to control cell lines. The control cell lines do not show any increase in cell viability at this timepoint.

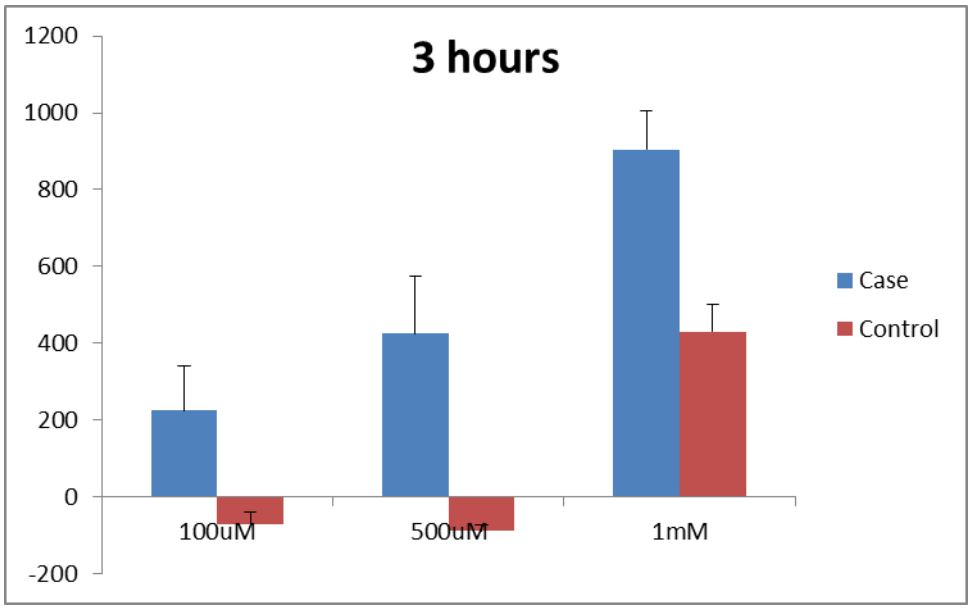

Figure 5.5 : SYTOX green staining at 3 hours in case and control hiPSC-RPE. The results show the number of cells with positive staining corrected for baseline. Each condition had three repeats with standard error bars shown. The case lines show a dose dependent increase in vulnerability when compared to control cell lines. The only control cell line to show an increased vulnerability at this timepoint is at the highest 1mM concentration.

To understand the mechanism of cell death a further set of studies were performed. Firstly, to see if cell death resulted from an apoptotic pathway activation a caspase-3 staining was performed (figure 5.6). This showed that caspase-3 staining was not increased in the case line when compared with the control lines after 3 hours of oxidative stress. This suggested that there was little change in intracellular redox state. Hydrogen peroxide has previously been shown to induce necrosis in cells in higher concentrations (Saito et al., 2006). This is thought to be an effect extracellularly at the cell membrane. To see whether hydrogen peroxide induced any ROS formation intracellularly cells were imaged using the IMAGE-IT™ assay (Thermofisher scientific) which stains for 5-(and-6)-carboxy-2',7'-dichlorodihydrofluorescein diacetate (carboxy-H_2DCFDA). Little intracellular staining was noted (figure 5.7). This together with the membrane permeability stain SYTOX® suggest that necrosis with disruption of the cell membrane may be the key mechanistic difference between the lines.

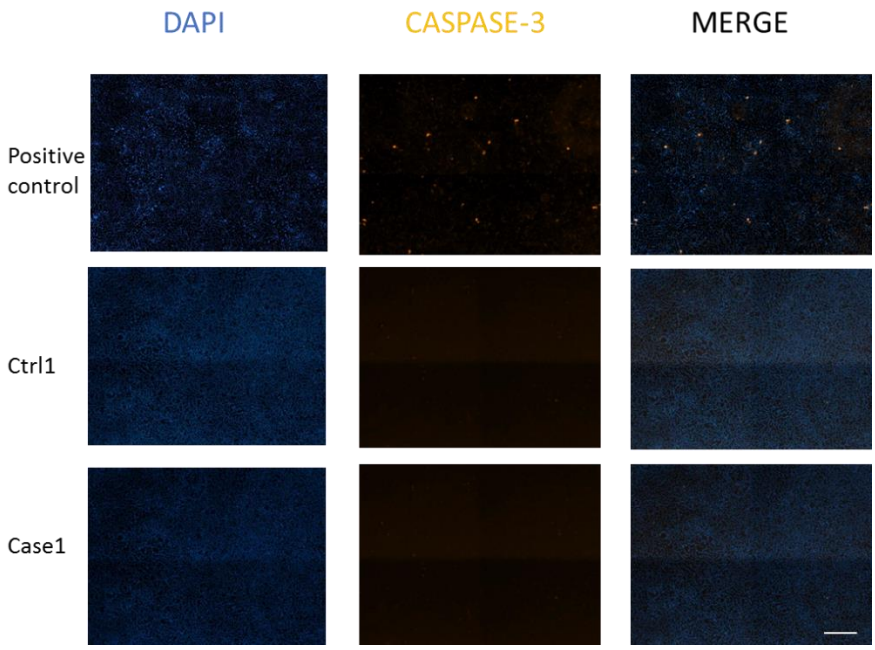

Figure 5 6: Apoptosis immunostaining. The images show fluorescent images at 647 for immunostaining for caspase-3 using a kit (BD bioscience). The top row shows images for a positive control treated with 1 x 10^{-6} M staurosporine for four hours showing small amounts of positive immunostaining. Neither the case nor the control hiPSC-RPE show any staining for caspase-3. (scale =200 µm)

Free radical and positive control

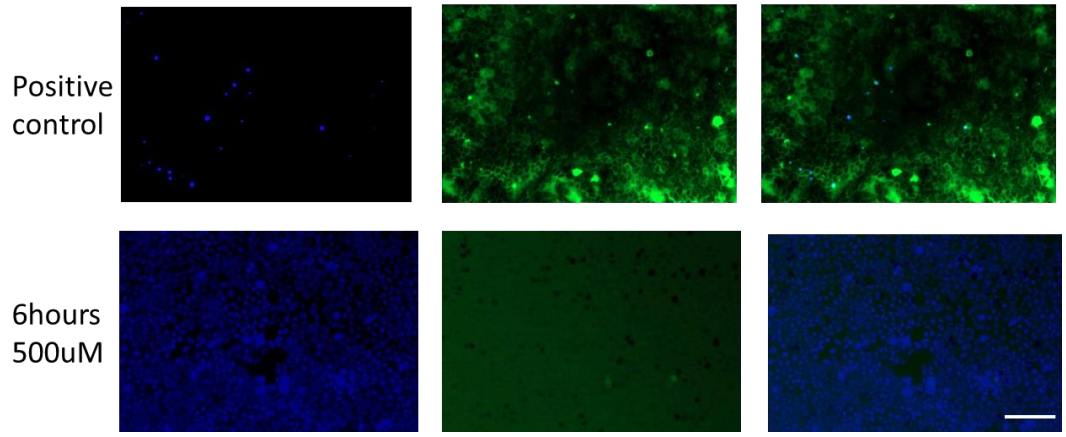

Figure 5 7: Intracellular ROS generation assay. This study was performed to investigate intracellular oxidative stress after hydrogen peroxide administration. The study was performed using the which stains for 5-(and-6)-carboxy-2',7'-dichlorodihydrofluorescein diacetate (carboxy-H_2DCFDA). A positive control was prepared with tert-butyl hydroperoxide (TBHP). The positive control shows intracellular staining. The hiPSC-RPE case line shows no intracellular staining despite 6 hours of 500 µm hydrogen peroxide. (scale = 100 µm)

5.3.2 Investigating terminal complement complex (TCC) deposition

During the histopathology studies increased complement pathway activation was noted in the case lines. This appeared to be far greater than in controls of similar age. I wanted to see if this could be replicated *in vitro* using hiPSC-RPE. The hypothesis was that case hiPSC-RPE would also activate complement at a greater level than control hiPSC-RPE. In order to test this hypothesis I optimised a cell model using inserts. Following discussion with Professor Stephen Moss' team (University College London) a membrane insert system was established with human complement serum in the basal compartment and normal RDM in the apical compartment (figure 5.8). A system was used which was similar to one published using foetal RPE cells which found some C5b-9 activation (Johnson et al., 2011). Since TCC deposition had been seen in the histopathology studies this was chosen as the initial target for studies.

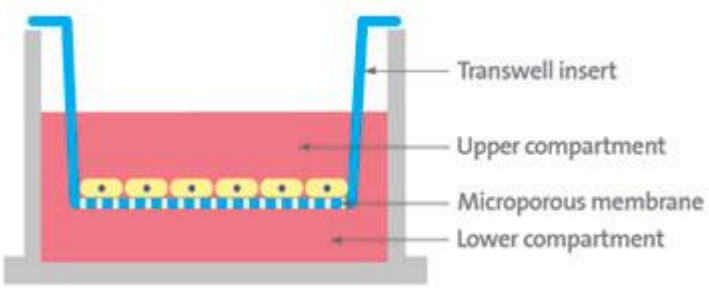

Figure 5.8. : Schematic of a membrane insert. The diagram shows a microporous polyester hanging insert used for the complement activation assay. RDM is placed in the upper compartment and the serum-RDM placed in the lower compartment. The hiPSC-RPE are grown on the membrane as a monolayer. (http://www.fishersafety.com/ecomm/servlet/cmstatic?storeId=10652&href=Scientific/scientificStandard/Features/Corning/corning-transwell-culture-supports.jsp)

Cells were plated on the membranes and maintained in 40% serum in the basal compartment to see if this would induce TCC deposition (figure 5.9). To see whether any of the apparent immunostaining was due to non-specific adherence of the antibody to elements in the system a set of case cells was treated with serum that had been heated thereby inactivating the complement proteins. The heat inactivation abolished TCC deposition (figure 5.9). There was a significantly greater deposition of TCC in the case hiPSC-RPE when compared to the control hiPSC-RPE lines (<0.01 comparing any case line to either control line)(figure 5.9). To see what was being stained I performed confocal Z-stack image capture. The Z-stacks were started at the bottom of the membrane insert and ended at the top of the cells. The predominant immunostaining in the case lines occurred below and in between hiPSC-RPE. In addition, there was a smaller but definite immunostaining of the deep membrane below the case hiPSC-RPE in all cell lines (figure 5.9). This was similar to some of the immunostaining seen in the post mortem L-ORMD samples (Figure 2.28).

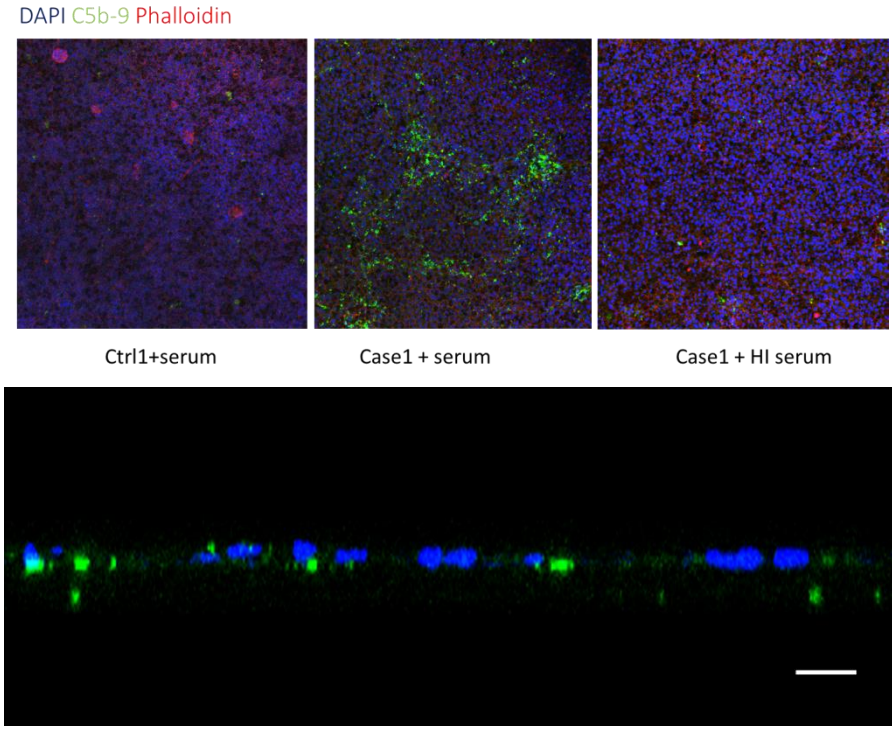

Figure 5.9: Confocal microscopy of complement activation assay. The upper left image shows little C5b-9 deposition in in a representative image from the Case1 hiPSC-RPE incubated in 40% serum–RDM for 12 hours. The middle image on the top row shows marked C5b-9 deposition across cells. The right image on the top row shows marked reduction in C5b-9 deposition with the use of heat inactivated 40% serum-RDM on Case1 hiPSC-RPE. The lower image shows a cross section generated from Z-stacks of a membrane insert. There is clear immunostaining of C5b-9 (green) on hiPSC-RPE. There is also deeper staining within the membrane.

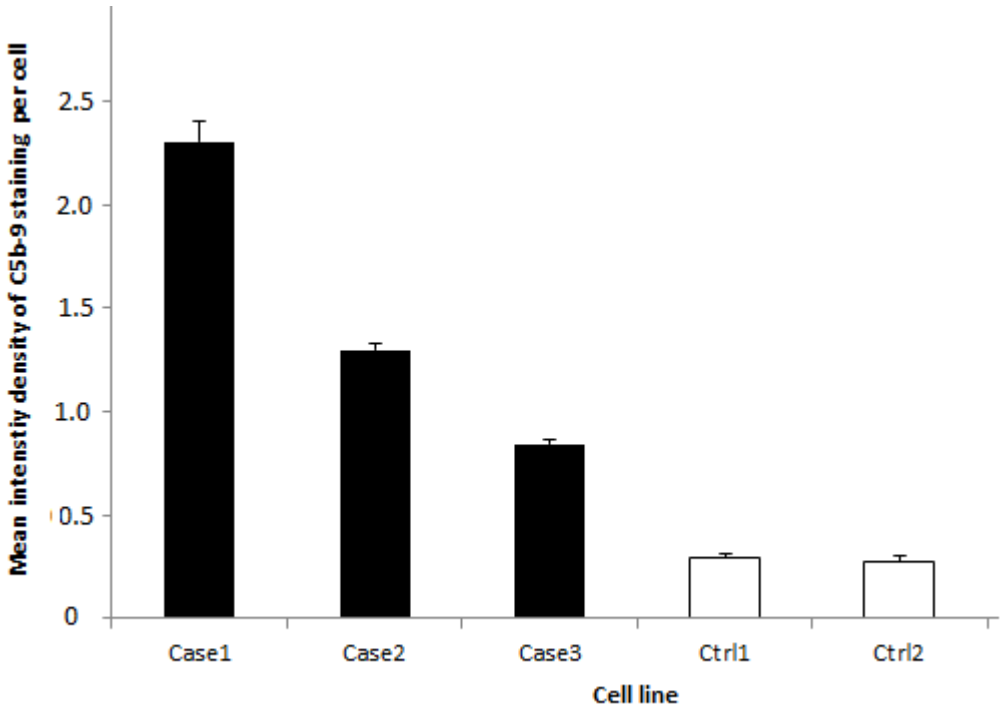

Figure 5.10: Comparison of C5b-9 staining in cases and controls. Using the model a minimum of three repeat experiments were performed on three membrane inserts. A minimum of three images were taken from each well. Standard error bars are shown. The images were analysed in each channel for mean pixel intensity density per cell. There was a significant difference between case and control lines ($P<0.01$)

After verifying that there was differential deposition of C5b-9 in the case lines when compared to the control lines, I performed timepoint and concentration experiments to optimise the model. Various concentrations of serum were used in the basal compartment. Maximal TCC deposition was found with 40% serum diluted in RDM (figure 5.11). In timepoint experiments it was found that TCC deposition was greatest at 12 hours before slowly decreasing at higher concentrations in the case line (figure 5.12).

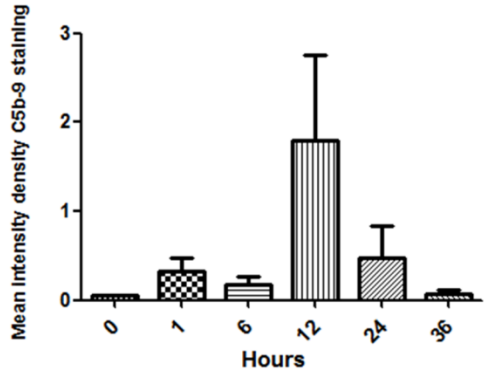

Figure 5.11 : Timepoint analysis of the c5b-9 deposition assay. Using the model a minimum of three repeats were performed and three images taken from each with standard error bars shown. The figure shows that the 12 hour timepoint appears to result in the greatest deposition of c5b-9.

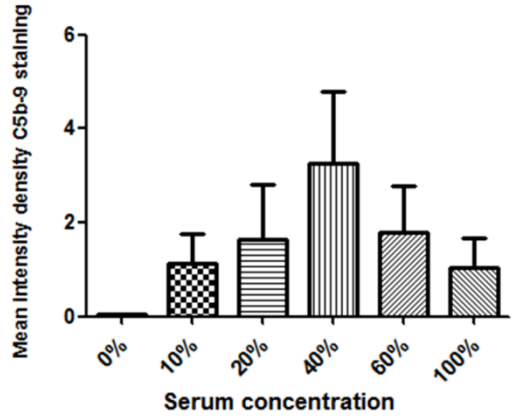

Figure 5.12 : Serum concentration analysis for C5b-9: Using the model a minimum of three repeat experiments were performed. A minimum of three images were taken from each well. Standard error bars are shown. The results show a gradual increase in C5b-9 deposition to 40% serum-RDM at the 12 hour timepoint.

Next I wanted to see if the 40% serum concentration was affecting viability. Previously (section 5.3.2) I had optimised a live dead cell permeability assay. I decided to stain the case and control lines similarly. There was a marked increased in green uptake in the case lines when compared with the control lines when the cell lines were placed in 40% serum-RDM for 12 hours (figure 5.13). This was abolished when heat inactivated serum was used suggesting that this could be a complement mediated process. A caspase-3 staining again revealed no staining suggestive of apoptosis. The C5b-9 appeared to form clusters. However, it was not clear whether there was co-staining with the SYTOX® green. To gain a better understanding of what the C5b-9 was binding to in the assay I planned a FACS experiment with Dr Anai Gonzalez-Cordeiro (University College London). She performed the FACS studies using a set of cells which had been grown in RDM

alone and a further set which had been placed in 40% RDM-serum for 12 hours as per the model. The cells were stained with annexin V, a marker for apoptosis and DRAQ7, a nuclear marker of cell death. In the untreated lines, there was a small but significant difference between Cb5b-9 staining in the cases and the control (figure 5.14). After treatment, there was a significant increase in C5b-9 immunostained cells in the case lines when compared to control lines The control line was noted to have a small increase in the percentage of C5b-9 immunostained cells after treatment with serum. When gating for necrosis the number of cells with necrotic characteristics i.e. negative for apoptosis but positive for cell death was significantly increased in the case lines when compared to control lines (figure 5.15). Taken together the studies showed that the case lines which immunostained for C5b-9 had an increased susceptibility to cell death by necrosis after the addition of serum. This suggested that necrosis was predominant in the case lines compared to the control lines.

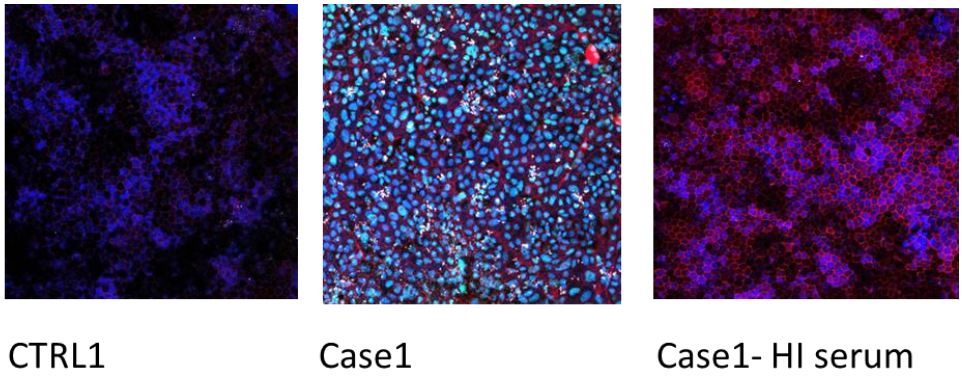

Figure 5.13: Cell viability in the model. The model was combined with cell viability/membrane permeability dye SYTOX green. In addition, C5b-9 deposition was immunostained (white). The cells were stained with DAPI (blue) and phalloidin (red). The control line showed no signs of loss of viability and membrane integrity and also no C5b-9 deposition. The case line under the same conditions showed marked loss of membrane integrity and also marked clusters of C5b-9 deposition. To test whether this resulted from serum and complement components heat inactivated serum was used. This abolished cell death and C5b-9 deposition.

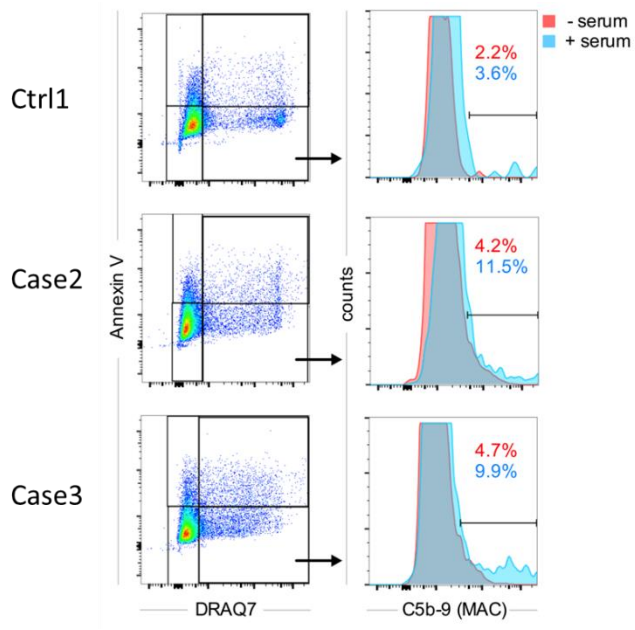

Figure 5.14 : Fluorescence activated cell sorting (FACS) analysis of C5b-9 (MAC) coated cells. HiPSCs are immunostained with anti-C5b-9 antibody and annexin V and stained with cell viability marker DRAQ7. The cells are then gated appropriately through FACS and counted. Gating for DRAQ7 +ve and annexin V –ve cell suggest necrotic cells. There is a greater percentage of C5b-9 coated cells in the case lines when serum is added than when the cells are maintained in RDM. This suggest that necrosis increases when serum is added and that C5b-9 coats necrotic cells.

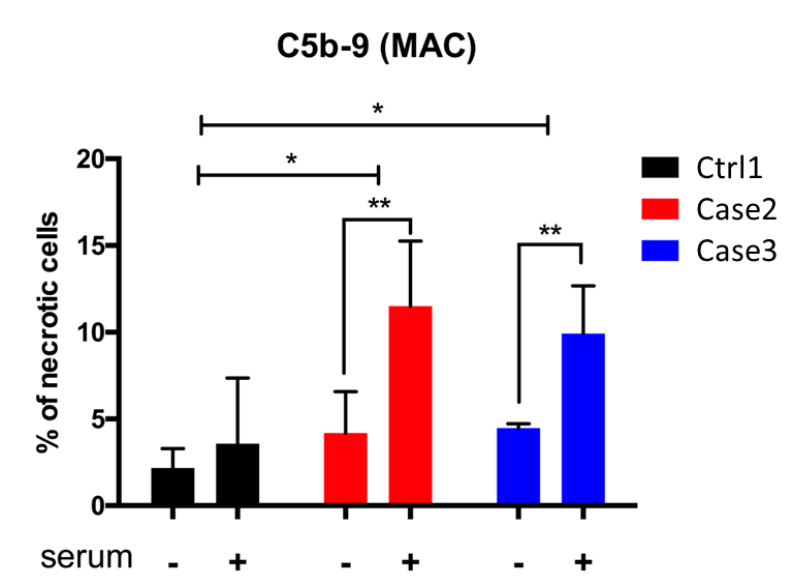

Figure 5.15 : Results of the FACS analysis of C5b-9 (MAC) coated cells. HiPSCs are immunostained with anti-C5b-9 antibody and annexin V and stained with cell viability marker DRAQ7. The cells are then gated appropriately through FACS and counted. Gating for DRAQ7 +ve and annexin V –ve cell suggest necrotic cells. There is a greater percentage of C5b-9 coated cells in the case lines when serum is added than when the cells are maintained in RDM. This suggest that necrosis increases when serum is added and that C5b-9 coats necrotic cells. Standard error bars are used and a minimum of three biological repeat tests were performed. (*= P<0.05, **=P<0.05)

5.3.3 Investigating the differential triggers for complement activation

To see which arm of the complement pathway was mediating the TCC activation in the model the serum was depleted of components from different arms of the complement pathways (figure 5.16). At least 5 membrane studies were performed per condition. The studies were all performed at the same time and immunohistochemistry was also performed at the same time with images taken under the same conditions on the confocal microscope. The results are from the pooled results of Case lines 2 and 3.

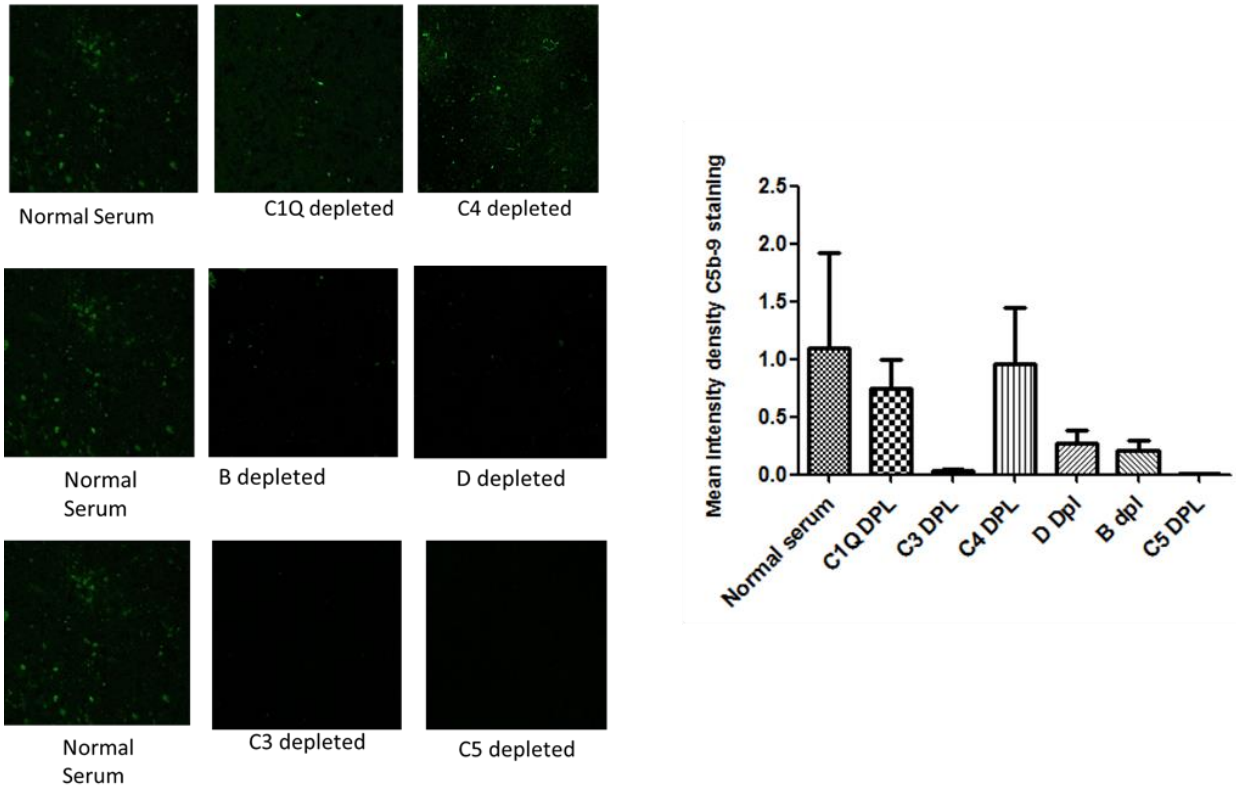

Figure 5.16: C5b-9 deposition in the model using depleted sera. Using the model a minimum of three repeat experiments were performed. A minimum of three images were taken from each well. Standard error bars are shown. The images above are representative 100 μm x 100um images from different conditions. When compared to normal serum there was a small non-significant decrease in C5b-9 deposition when classical pathway component C1Q was depleted (p=0.076). Depletion of C4, a component of both the classical and Lectin mediated pathways resulted in no difference in TCC deposition when compared to the normal serum (p=0.35). Their depletion of factors B and D, alternative pathway components, resulted in a small but significant reduction of TCC activation ($p<0.01$). Depletion of common complement pathway components C3 and C5 resulted in a significant decrease in deposition ($P<0.01$).

The depletion of C1Q a component of the classical pathway led to a small non-significant decrease in TCC deposition when compared with a two-tailed Mann-Whitney U-test (p=0.076). Depletion of C4, a component of both the classical and Lectin mediated pathways resulted in no difference in TCC deposition when compared to the normal serum (p=0.35). Factors B and D are part of the alternative complement pathway. Their depletion resulted in a small but significant reduction of TCC activation. Statistically, using non-parametric comparative analyses Factor D depleted serum resulted in significantly reduced TCC ($p<0.01$) whilst factor B depleted serum also resulted in a

significantly reduced TCC deposition (P<0.01).

However, depletion of complement components C3 and C5 which are necessary for C5b-9 formation in all pathways resulted in a near complete loss of TCC deposition (figures 5.16). Statistically, C3 depletion resulted in a significant decrease in deposition (P<0.01) whilst C5 depletion resulted in a significant reduction in TCC deposition (p<0.01). Taken together the results of the serum depletion studies suggest that in this model C5b-9 activation may be secondary to a number of pathways with the alternative complement pathway activation providing the greatest activation.

From the previous FACS on case and control hiPSC-RPE lines it appears that there is some TCC formation and deposition even without the addition of serum. I wanted to investigate whether endogenous expression of complement pathway components results in the failure to abolish TCC activation despite depletion of the different pathway components from serum. To see if the cells expressed complement pathway components I performed a quantitative real time PCR array on cDNA generated from RNA pooled from case lines using a qPCR array (figure 5.17). The analysis revealed that most complement components were expressed by the hiPSC-RPE.

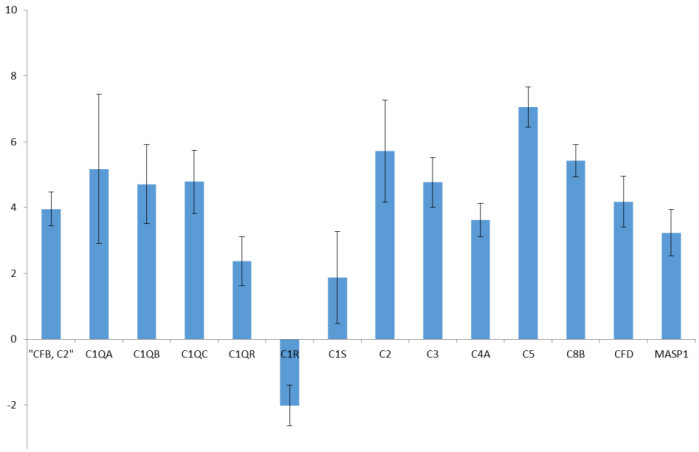

Figure 5.17 : Complement pathway expression analysis in hiPSC-RPE. The array shows the pooled results from the complement array performed on case and control hiPSC-RPE cDNA. Three repeats for each gene were performed on each cell line. Standard error bars are shown. The CT was normalized to GAPDH. The results show that there is endogenous expression in hiPSC RPE of most complement pathway components.

To see if the genotypic differences between cells in key complement regulatory genes could account for the differences in TCC activation, I sequenced the hiPSC lines for four main risk alleles for AMD as identified by a comprehensive meta-analysis of recent studies (table 5.1). The

findings were mixed with cell lines harbouring different risk alleles for AMD risk (table 5.2). This suggested that in cases and controls the risk alleles AMD did not play a significant role in altering the phenotype.

Gene	Locus	Risk allele	Chromosome	P	Odds ratio
ARMS2-HTRA1	rs10490924	T	10	$4 \times 10_{-540}$	2.76 (2.72–2.80)
CFH	rs10737680	A	1	$1 \times 10_{-434}$	2.43 (2.39–2.47)
C2-CFB	rs429608	G	6	$4 \times 10_{-89}$	1.74 (1.68–1.79)
C3	rs2230199	C	19	$1 \times 10_{-41}$	1.42 (1.37–1.47)

Table 5.1: Summary of alleles which generate the greatest risk of AMD. (AMD gene consortium)

HiPSC cell line	CFH	ARMS2-HTRA	C3	C2-CFB
Case1	+	-	-	-
Case2	-	+	-	+
Case3	+	+	-	+
Ctrl1	+	-	-	+
Ctrl2	+	-	-	+

Table 5.2 : Summary of the AMD risk status for the hiPSC lines used in the experiments.

5.3.4 Examining complement activation in the *in vitro* L-ORMD model

The TCC for complement is composed of complements C5b, C5, C7, C8 and C9. Depletion of C5 from serum had been shown to almost completely abolished TCC immunostaining in the model. This suggested a potential treatment approach to correct the C5b-9 activation phenotype on the cells. There was already a humanised monoclonal anti C5 antibody that had been used clinically to treat a number of other conditions (Hillmen et al., 2006, Radhakrishnan et al., 2012, Vivarelli et al., 2012). I wanted to see whether a monoclonal C5 antibody could be used to correct the phenotype in this model of macular degeneration.

Firstly, to confirm that C5 would be a suitable target for treating the model I repeated the C5

depletion study to ensure that only the loss of C5 resulted in a loss of C5b-9 activation. I replaced C5 to the concentration found in serum to some of the inserts containing C5 depleted serum. These studies showed that replacement of C5 returned complement activation and C5b-9 deposition on the inserts (figure 5.18). The addition of C5 to C5 depleted serum resulted in a significant increase in TCC deposition ($p<0.01$).

A suitable mouse monoclonal antibody to C5 which had previously been shown to have some efficacy in preventing complement mediated lysis of sheep red blood cells (Sandoval et al., 2000). Reports from the manufacturer had shown that this antibody had a functional effect being able to reduce lysis of sheep red blood cells by human serum. I treated the inserts containing 10% serum-RDM, with a high concentration of anti-C5 antibody (figure 5.18). There was a marked reduction in TCC deposition (figure 5.18). To investigate whether the drug was responsible for this I tested various concentrations of the monoclonal antibody in 10% serum-RDM (figure 5.19). This showed a dose-dependent reduction in TCC deposition. A concentration of 500ng/ul lead to a non-significant decrease in TCC deposition ($p=0.08$). However, a dose of 2000ng/ul led to a significant drop in TCC deposition ($p=0.03$) when compared to the 10% serum. A further significant reduction in TCC deposition resulted from 4000 ng/ul resulted in an almost complete loss of TCC deposition when compared to the 10% serum-RDM ($p<0.01$) suggesting that an anti-C5 monoclonal antibody could be used to reduce TCC deposition in the model. Ideally, I would have liked to have performed a similar experiment using an isotype control to verify that the reduction was just due to reduced function brought about by the antibody.

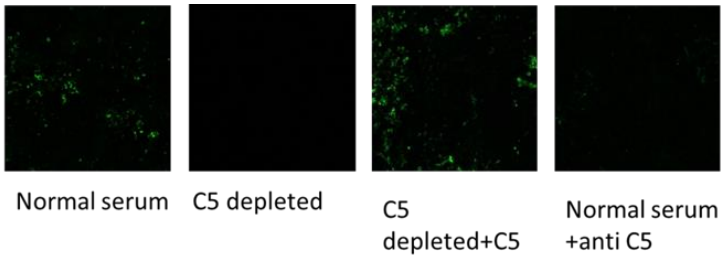

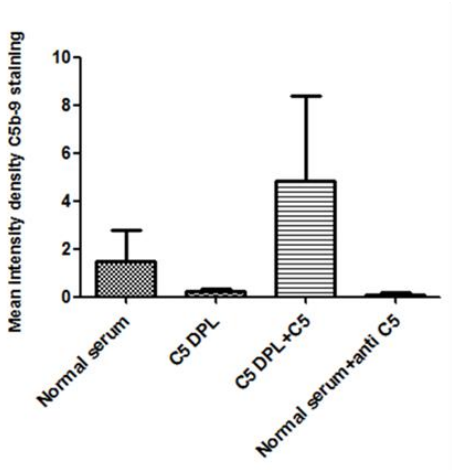

Figure 5.18 : C5b-9 deposition in the model focusing on C5. Using the model a minimum of three repeat experiments were performed. A minimum of three images were taken from each well. Standard error bars are shown. The images above are representative 100 µm x 100um images from different conditions. This depletion replacement assay confirmed the findings above. There was a significant decrease in C5b-9 deposition with C5 depletion form serum. This was reduced when C5 was replaced suggesting that the depleted serum contained all other active components except for the C5. In order to test a treatment, A 4000ng/ul dose of monoclonal anti C5 antibody was added to the serum. This resulted in a significant decrease in C5b-9 deposition ($P<0.01$).

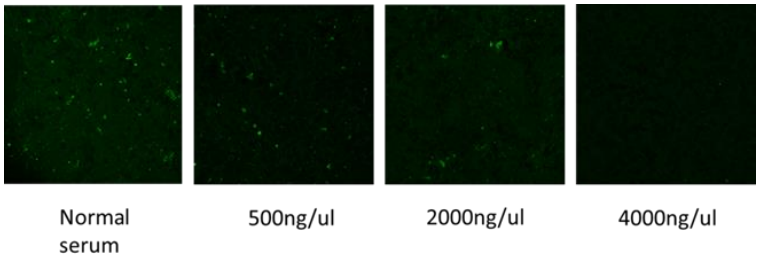

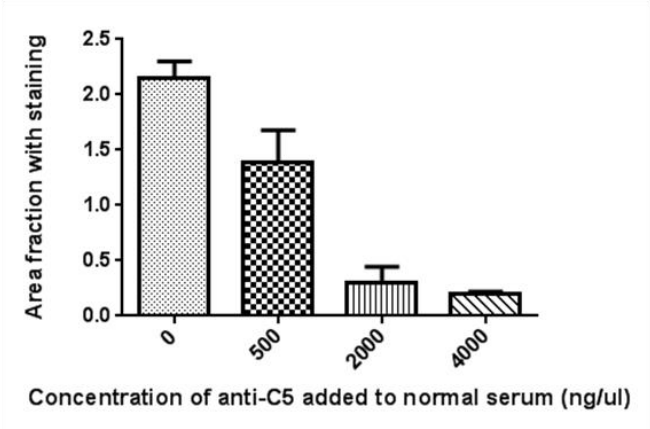

Figure 5.19 : Anti-C5 antibody dose-response. Using the model a minimum of three repeat experiments were performed. A minimum of three images were taken from each well. Standard error bars are shown. The images above are representative 100 µm x 100um images from different conditions. A decrease in C5 deposition was noted with increasing monoclonal antibody concentration. A concentration of 500ng/ul lead to a non-significant decrease in TCC deposition ($p=0.08$). However, a dose of 2000ng/ul led to a significant drop in TCC deposition ($p=0.03$) and 4000 ng/ul concentration of monoclonal antibody resulted in an almost complete loss of TCC deposition when compared to the 10% serum-RDM ($p<0.01$).

5.4 Discussion

In these set of studies we have shown that when mutant C1QTNF5 hiPSC-RPE were cultured in the presence of human serum, significantly greater TCC deposition was seen on mutant C1QTNF5 hiPSC-RPE when compared to control hiPSC-RPE. TCC deposition was time dependent an increased peaking at 12 hours. By depleting factors essential for different complement pathways TCC formation was found to be mainly alternative complement pathway dependent. These studies replicate the human *in vivo* findings described in earlier chapters.

Johnson *et al*. grew human foetal RPE on similar membrane supports (Johnson et al., 2011). When these cells were exposed to human serum they were found to develop two types of sub-RPE deposit in a similar way to the deposits in this study. The first deposit was found directly sub-RPE whilst the second deposit was found deeper within the pores of the membrane. TCC activation was

also noted however when similar complement pathway depletion studies were performed TCC formation was found to be classical pathway dependent.

Radhu *et al*. used a similar setup to examine foetal human RPE cells carrying protective and risk alleles for AMD (Radu et al., 2014). In order to stimulate complement activation the RPE were fed with ROS from ATP-dependent transporter for phosphatidylethanolamine (ABCA4) knockout mice. The ABCA4 gene encodes for a protein that binds to retinoids on photoreceptor outer segments and assists in the processing of ROS in RPE. Mutations in the gene can lead to Stargardt disease which results in lipofuscin and bisretinoids in RPE. The RPE carrying AMD predisposing risk alleles were shown to have C5b-9 deposition. The TCC formation was identified as alternative pathway dependent. The difference when compared to the system described by Johnson *et al.* suggests that different arms of the complement pathway may be activated under different conditions. Lipofuscin formation may result in activation of the alternative complement pathway.

In our study, we showed that TCC formation increased with time till approximately 12 hours. After 12 hours, there was a slow reduction in TCC deposition. TCC deposition in this model may peak at this time because of depletion of complement components in the serum inhibiting the formation of new complexes. Clearance of TCC may result from endocytosis mediated clearance by RPE cells as suggested by recent studies by Georgiannikis *et al. (Georgiannakis et al., 2015).* The long-term culture of cells in human serum was not investigated in this series of studies but may potentially propagate the complement response. This would certainly be interesting to investigate particularly as the complement response has been implicated in deposit formation (Fernandez-Godino et al., 2015).

TER was not found to be significantly different between case and control lines in the previous chapter. TER is a marker of RPE function and monolayer integrity and is maintained by tight junction formation and active ion transport . The hypothesis was that C5-9 formation would disrupt monolayer integrity and result in a lower TER. Giorgianikkis *et al*. showed c5b-9 formation on porcine RPE grown in human serum using a similar model system (Georgiannakis et al., 2015). They noted that TER increased with C5b-9 deposition suggesting that although TCC were deposited they were not resulting in cell lysis. The SYTOX® experiments revealed an increase in nuclear staining with SYTOX® in case lines compared with controls. The increased staining was exacerbated with oxidative stress and with time. However, a baseline LDH assay showed no significant difference in LDH levels between case and control lines. The findings suggest that case hiPSC-RPE have a deficit in membrane integrity making cells susceptible to oxidative damage (Kim et al., 2003). Study of apoptosis using caspase-3 also showed that apoptotic cell death was

not the primary mechanism of cell death. Kim *et al.* also showed that necrosis resulted from hydrogen peroxide exposure in a model using ARPE-19 cells (Yang et al., 2014b). Interestingly, Yang *et al*. noted SYTOX® staining when activating the alternative complement pathway on ARPE-19 cells.

Taken together the studies in this section show that the model appears to replicate *in vivo* findings of complement activation from L-ORMD human donor samples. In addition, the model also offers a method to study alternative complement pathway activation, the main complement pathway implicated in AMD.

Chapter 6

6. Investigating an interaction between C1QTNF5 and the complement pathway

6.1 Introduction and rationale

The C1QTNF5 gene encodes a 25 kDa protein (Hayward *et al.*, 2003; Mandal *et al.*, 2006; Wong *et al.*, 2008). C1QTNF5 contains three domains: a signal peptide domain (amino acids 1–15), a collagen domain (amino acids 30–98), and a gC1q domain (amino acids 103–243) (Fig. 1A) C1QTNF5 shares features with other members of the C1q family including mulitmerisation. C1QTNF5 readily forms trimers, which leads to the formation of a globular head composed of three gC1q domains (Shapiro and Scherer, 1998). C1QTNF5 can also forms octadecameric bouquets (Tu and Palczewski, 2014). The Ser163Arg mutation is found in the gC1q domain.

CFH is an important regulator of the alternative complement pathway. Mutations in CFH have already been implicated in macular degeneration. CFH is composed of 1213 amino acids. The amino acids are arranged into 20 complement control protein modules (CCPs) each of which contains approximately 60 amino acids. Each CCP is connected to its adjacent CCP by a linking region which allows marked flexibility and enables CFH to have a highly variable three dimensional structure. In unpublished data from Shu *et al*. C1QTNF5 has already been shown to bind to CFH. The hypothesis is that mutant and wild-type C1QTNF5 will have differential affinity for CFH.

In order to see if C1QTNF5 has an affinity for CFH we will first generate mutant and wild type proteins. C1QTNF5 has previously been generated from both cell and bacterial expression systems. Recently studies using a bacterial expression system were able to reliably express the gC1Q domain of both wild type and mutant C1QTNF5 (Tu and Palczewski, 2012). As the mutation was found in the globular domain the aim was to use a similar protocol to generate wild type and mutant gC1q domains.

Surface plasmon resonance (SPR) is a highly sensitive, label-free method of investigating interactions between complexes (Daghestani and Day, 2010)(figure 6.1). The method was first described in 1968 (Otto, 1968). The technique uses the understanding that electromagnetic oscillations occur when light encounters charged conducting surfaces. Plasmons represent quantum oscillations of electron clouds within a conducting material. The transverse oscillations are called surface plasmon polaritons (SPP). When vector of light waves travelling parallel to the conducting surface matches the SPP then resonance occurs. SPR only occurs at certain angles of incidence of light. SPR will cause a change in the angle of reflectivity at a reflective surface. The sensors note

the reduced incidence of light with SPR. The detectors identify change in angle of light reflection when there is new binding on the surface of the sensor. The method is useful because it only requires small concentrations of ligands to provide reliable repeatable results. SPR has been used to probe protein to ligand, protein to protein and nucleotide hybridisation (Karlsson and Falt, 1997, Moon et al., 2010). SPR has already used to understand the binding of CFH to a number of ligands (Yu et al., 2005, Weismann et al., 2011). We aim to use SPR to investigate protein-protein interactions between C1QTNF5 and CFH. The hypothesis is that CFH also interacts with C1QTNF5 and that it interacts differently to mutant C1QTNF5 protein when compared to wild type C1QTNF5.

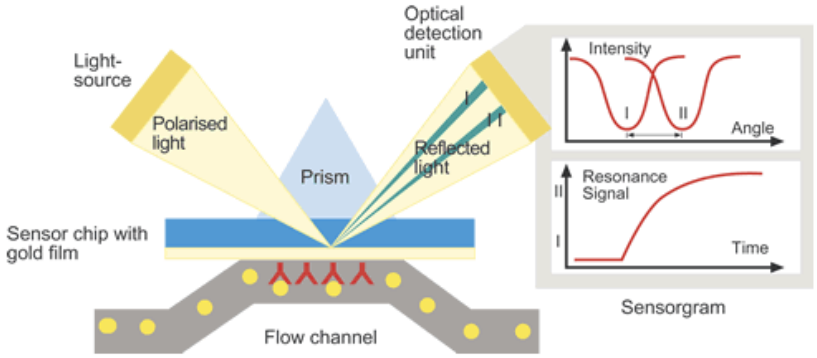

Figure 6.1 : A diagram showing surface plasmon resonance. Polarised light is incident on a gold membrane. When a substrate (red) binds to ligands (yellow circles) a resonance signal is released and this is sensed as a change in reflected light. (http://www.rci.rutgers.edu/~longhu/Biacore/)

6.2 Methods

The studies creating *E.Coli* lines, generating, purifying and analysing proteins were performed by Dr Shyamanga Borooah and Dr Chloe Stanton (University of Edinburgh) and suggested by Professor Alan Wright (University of Edinburgh). These studies were performed at the core protein facility (University of Edinburgh).

Preparation for the surface plasmon resonance experiments was performed by Dr Shyamanga Boroah and Dr Chloe Stanton (University of Edinburgh). The SPR experiments were performed by Dr Andrew Herbert (University of Edinburgh). Preparation of materials for the CFH functional strudies was performed by Drs Shyamanga Borooah and Chloe Stanton. The Coomassie was performed by Dr Chloe Stanton.

6.2.1 Creating *E.Coli* lines stably expressing wild-type gC1QTNF5 and mutant gC1QTNF5

Recombinant His-gC1q was purified from individual *E. coli* colonies grown in Luria Broth (LB) containing 0.1mg/ml ampicillin and incubated overnight at 37 ℃ with shaking and expression was induced overnight with 1 mM IPTG at 20 ℃. Cell pellets were collected by centrifugation at 10,000g for 10 minutes, then resuspended and incubated for 30 minutes in 50 mM sodium phosphate, 300 mM sodium chloride, 10 mM imidazole pH 8.0 plus 1 mg/ml lysozyme.

A codon-optimized gC1QTNF5 coding sequence was synthesised and amplified. The C-terminal also coded for His. These were made using a codon-optimised C1QTNF5 sequence for bacterial expression (GeneART), and cloned using the following primers and sequential Gateway cloning steps into pDONR221 and pDEST-14.

Step1:

C1QTNF5_gC1Q_nc C-His_F

Fwd 5'- GCT TCG AAG GAG ATA TAC ATA TG CGTAGCGCATTTAGCGCAAAACG -3'

C1QTNF5_ nc C-His _R

5'-TGA TGG TGA TGG TGA TGG CCA TC TGCAAAAACCGGACTGCTATGCC -3'

Step2:

Fwd 5'-com-GGG GAC AAG TTT GTA CAA AAA AGC AGG CTT CGA AGG AGA TAT ACA TAT G-3' (49)

Rev 5'-com-GGG GAC CAC TTT GTA CAA GAA AGC TGG GTC CTA GTG ATG GTG ATG GTG ATG GCC ATC-3' (57)

The mutants were designed similarly with the G>C substitution. Again, the mutants were made by site directed mutagenesis. This work was performed by Dr Chloe Stanton. The recombinant plasmid construction was verified by DNA sequencing (the plasmid was constructed and supplied by Dr Chloe Stanton, University of Edinburgh). The methodology used for the expression of the gC1Q protein was based on a previously published successful methodology for expressing gC1q (Tu and Palczewski, 2012). The recombinant plasmids were transformed into Rosetta™ (DE3)pLysS Competent cells (Novagen) *E.Coli*. These strains supply tRNAs for AGG, AGA, AUA, CUA, CCC, GGA codons which is otherwise limited by the codon usage of normal *E. coli*. The bacteria were initially grown out on agar plates with recombinant plasmid added to plates. Colonies were individually picked using a P200 tip and added to a cultivation tube containing 2ml Luria broth. The cells were grown for twelve hours at 37^{o}C and placed on a shaker at 250rpm. After 6 hours the broth was testedg for starting cell density using OD_{600} on a NanoDrop (Thermo-

Scientific). Wells with an optical density of 0.1-0.2 were used prior to shaking flask culture. The Enpresso B (BioSilta, Oulu, Finland) culture system was used for protein expression A 500ml shake flask was prepared with 2 tablets from the Enpresso B kit of supporting chemicals in 50 ml ddH_20. The flask was shaken for 30 minutes at 37°C until tablets were fully dissolved. Chloramphenicol was added and 2ml of the culture medium from the transformed bacteria were added before a glucose-releasing reagent was added to the flask. The flask was sealed and incubated at 30°C and shaken at 250rpm. After 15 hours a further supplement of glucose reagent and a booster supplement tablet were added from the kit. At 24 hours the cells were cooled to 16°C. 0.5 mM isopropyl β-D-1-thiogalactopyranoside (IPTG) was added to induce expression. The cells were then lysed using a Soni-Prep 150 sonicator (MES UK, London, United Kingdom) and Constant systems 1.1 kW TS cell disruptor (Constant systems limited, Daventry, United Kingdom) an automated high-pressure (40 kpsi) lysis system with temperature control. The lysed mixture was centrifuged at 10,000g for 30 minutes (Beckman Avanti) to remove cellular debris and the supernatant was retained.

The supernatant was filtered through 0.22uM Amicon® filters to remove further debris. ÅKTA Xpress - Low pressure, automated, unattended parallel lab-scale production unit (GE Healthcare) (4˚C) was used to sequester and elute protein fractions from the supernatant. The supernatant was run through a Superdex 200 10/300 GL column (GE Healthcare) bead columns using 30 mM sodium phosphate 20 mM imidazole pH 8.0, followed by the same buffer containing 50 mM imidazole pH 8.0 and His-gC1q was finally eluted using 1M imidazole pH 10. Every 10ul of eluent was collected separately. Eluents with matched spectrophotometric profiles were pooled and analysed by Coomasie gel and SDS-PAGE targeting the FLAG tag and by mass spectrometry. The molecular weight of 16KDa was predicted for the gC1Q.

In order to perform size exclusion chromatography using multi-angle light scattering (SEC-MALS) a 100ul of 1mg/ml protein in 1M imidazole pH 10 buffer was run through a Viscotek MALS-20 detector which was attached to an AKTA 10 purifier (Mogridge, 2004). The detector used an incident light beam (660 nm) to detect not only concentration of solute but also the molar mass and the system was connected to a collector to collect different fractions.

6.2.2 Thermal denaturing assay

In order to compare the stability of the generated mutant and wild type gC1Q a thermal denaturation assay was used. Protein concentrations were all standardised using quantitative spectrophotometry at 280nm using a NanoDrop (Thermo fisher scientific) to get a concentration of

0.1mg/ml. 50ul of protein diluent was placed in each well with at least three replicates in order to calculate the protein unfolding temperature (*T*m) in a 96 well plate. Fluorescent dye Sypro orange (life technologies) in a 5X concentration was added. The plates were briefly spun for 1 minute at 1000g in a centrifuge to ensure mixing of protein and Sypro orange and then sealed with optical sealing film prior to a thermal denaturation run on a Biorad iQ5 iCycler set up to detect fluorescence from the Sypro orange. As proteins unfolded due to increasing temperatures, the dye exposed large hydrophobic regions, resulting in a large increase in fluorescence (ex/em 485/575) measured by the iCycler. The iCycler was set to run from 20 to 80^{o}C with a hold of 30 seconds at each temperature and ramping at 1^{o}C increments. Data was exported onto excel (2013 Microsoft, Redmond, USA) for analysis. The melting temperature (*T*m) was taken as the peak inflexion of the denaturation curve.

6.2.3 Surface plasmon resonance (SPR)

All SPR experiments were carried out using a Biacore T100 machine by Dr Andrew Herbert (University of Edinburgh). Preparation of substrates and media for each run was performed by Drs Shyamanga Borooah and Chloe Stanton (University of Edinburgh). T100 software was used for pH scouting, coating the chips and kinetic assays. All buffers, protein samples and the Biacore sample compartment and operating temperatures were maintained at 25°C. The running buffer was 10 mM HEPES pH 7.4, 150 mM sodium chloride, 0.005% P20 (Biacore, Little Chalfont, UK). The optimal conditions were 25 ^{o}C 0.01 M HEPES pH 7.4, 0.15 M NaCl, 0.005% v/v Surfactant P20 + 50uM EDTA. Immobilisation of His-C1QTNF5 to the NTA chips was carried out through the His tag via nickel on a nitrilotriacetic acid (NTA) biacore chip. This was performed by flowing 100um $NiCl_2$ over the cells initially prior to flowing the proteins. The stability of the nickel-protein complexes were initially verified by measuring resonance after multiple cycles of buffer flow. For the experiments, the injection times were for 180 seconds with different concentrations of CFH flowing over the chip with dissociation times allowed for 600 seconds with only running buffer flowing over the chip. These parameters were set after initial test runs with both proteins. An internal repeat was carried out for each run, taking a mid-range dilution. There was also a reference cell coated just with nickel to see if there was any binding of CFH to the substrate. One experiment was run on at least one chip loaded with wild-type and mutant His-C1QTNF5. Six injections of increasing concentrations of CFH in buffer were performed for 180 second with a flow rate of 30ul/second. Each injection had a concentration of CFH which was double the concentration of the previous injection. Data was analysed with Biacore evaluation software version 1.00 (GE healthcare)

6.2.4 CFH functional studies

These studies were performed in two parts to see if C1QTNF5 resulted in a difference in CFH function in the fluid phase and the solid phase. The solid phase studies were performed using sheep red blood cells (RBCs) using a method that had previously been published (Morgan, 2000). One of CFH's functions is to breakdown C3b with the help of CFI. C3b has a molecular weight of 176 kDa and is composed of an alpha chain (101 kDa) and a beta chain (75 kDa) linked by a disulphide bridge. CFH acts as a co-factor so that factor I can cleave the alpha chain into fragments. Various combinations of C1QTNF5, CFI, CFH and C3b were tested. C3b (4ug) was added to CFH (1ug) and CFI (1ug) in a total volume of 15ul and incubated for 10 minutes at 37^{o}C. SDS sample buffer with reducing agent was added to the tubes at 10 minutes and heated at 95^{o}C for 5 minutes. SDS PAGE gels run under reducing conditions should reveal cleavage of the alpha chain of C3b. The gels were stained for 20 minutes using Coomassie brilliant blue and then imaged on a Licor geldock imaging device.

For the solid phase assays a RBC lysis assay was used (Pangburn, 2002). Sensitised sheep RBCs (Comptech), Briefly, a complement-containing serum sample is diluted so that the final dilutions in the assay are in the range from 1/100 to 1/500. Assay tubes were kept on ice. For the addition of CFH to depleted sera 50ug/ml was added as soon as the depleted serum thawed. The volume is brought to 1.3 mL with GVB^{++}, (0.1 % gelatin, 5 mM Veronal, 145 mM NaCl, .025 NaN_3 , pH 7.3. Containing 0.15 mM calcium chloride and 0.5 mM magnesium chloride). 0.2 mL of RBCs at 5 x 10^8 EA/mL (Comptech) were added. The mixtures were incubated at 37^{o}C for 60 minutes. The mixtures were then spun down to isolate remaining cells at 500g for 3 minutes. The absorbance of the supernatant determined at 541 nm in a 1 cm cuvette to calculate the percentage of RBC lysis.

6.3 Results

6.3.1 Comparison of wild type and mutant gC1QTNF5

The supernatant, following centrifugation, was passed through a gel filtration column and the eluents analysed by spectrophotometry. The characteristics of the proteins were markedly different (figures 6.2 and 6.3). Wild-type tagged gC1QTNF5 produced a single main peak whilst the mutant produced multiple peaks generating a number of different constituents. A Coomassie stain of the eluents revealed that the protein eluted had two molecular weights. Firstly, at approximately 16kDa and a second weight at approximately double this at 28kDA. To confirm that the protein was expressed correctly as per the plasmid design a western blot was prepared using anti-His antibody (figure 6.4). This showed that the proteins also contained His sequences as intended and

that the molecular weights corresponded to a monomer and dimer. There was also a higher order stain for potentially a trimer. Once again as in the cell studies the mutant appeared to preferentially form the monomer without higher order multimers. Eluents with similar western blot characteristics were pooled to provide an increased volume of protein. Protein was then maintained at 4ºC or frozen at -20ºC. The stability was checked after a week at these temperatures by performing a further Coomassie gel which was unchanged. This showed that the proteins were stable to be stored prior to further experiments.

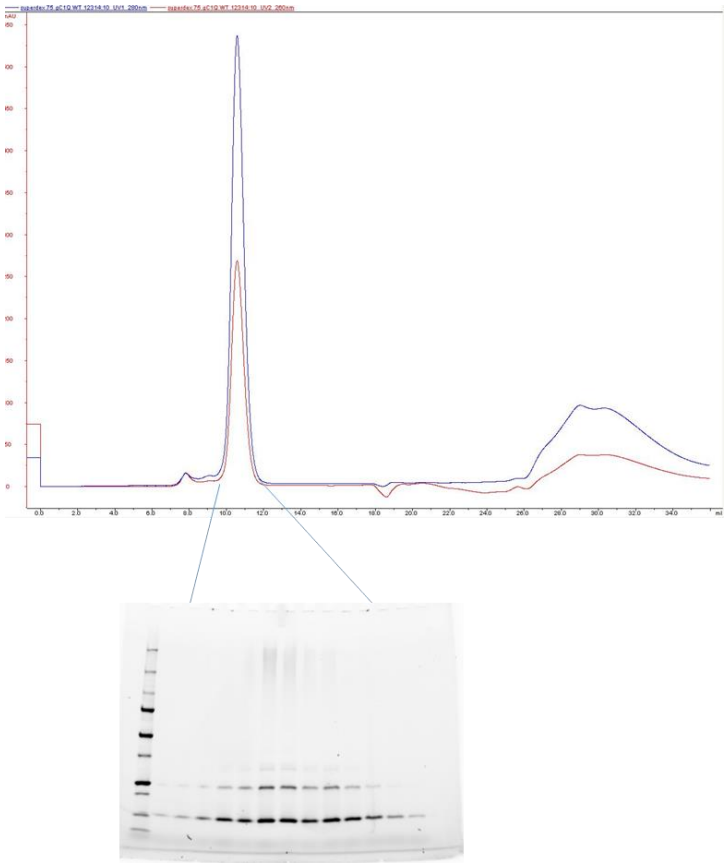

Figure 6.2 : Readout for wild-type gC1QTNF5 using spectrophotometry after gel filtration. The readout shows a clear uniform peak suggesting a pure species. When the flow through from the peak is analyzed with Coomassie staining there is a clear band at 16 kDa and a potential dimer with little else stained suggested a relatively pure extraction. The y axis of the graph is the absorbance in milli absorbance units the x-axis shows the volume of fluid in millilitres. The proteins are measured iat 260 and 280 nm wavelength.

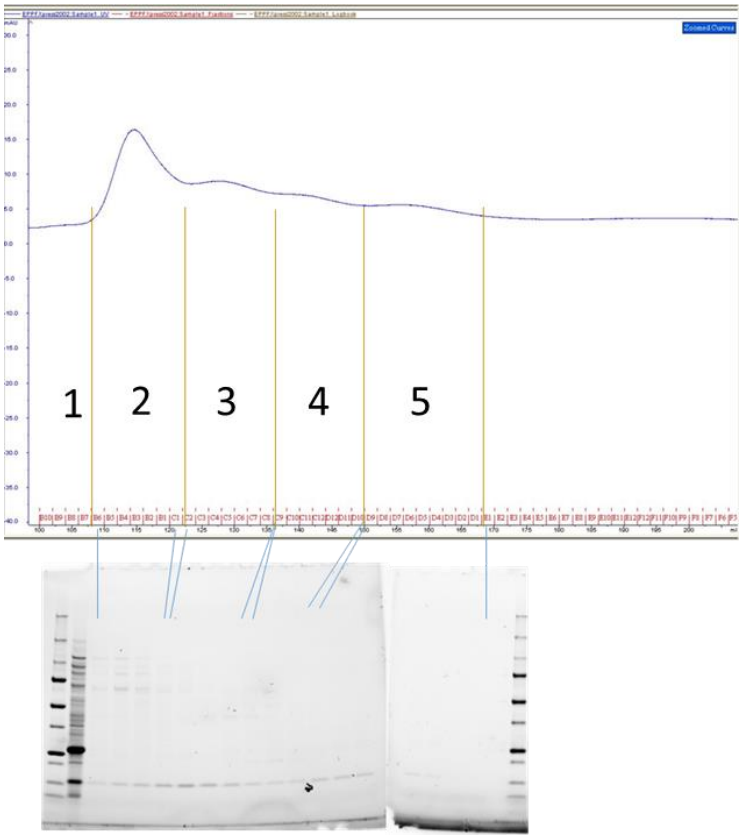

Figure 6.3 : Readout for mutant gC1QTNF5 using spectroscopy after gel filtration. The readout shows multiple peaks. When the flow through from the different peaks are analyzed on Coomassie staining gel the third and fourth follow through provide a relatively pure protein at the expected molecular weight for mutant gC1QTNF5. The y axis of the graph is the absorbance in milli absorbance units (mAU) and the x-axis shows the volume of fluid in millilitres. The proteins were measured at 260 and 280 nm wavelength.

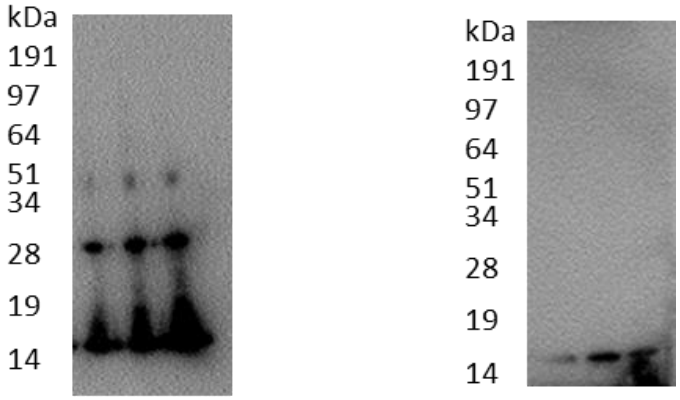

Figure 6.4: Reducing SDS-PAGE for HiS-C1QTNF5 fractions. The gel on the left shows the reducing gel for the His-gC1QTNF5 wild type. The gel shows that despite reducing conditions there is still formation of the dimer and trimer. The gel on the right shows that after reduction the His-gC1QTNF5 mutant proteins reduce to a monomeric form. The gels show three repeats from pooled samples.

The profile of mutant elution from the column revealed multiple different weighted moieties. As a result, the first eluent was discarded and groups 2, 3 and 4 were pooled pending a thermal denaturation assay (see below).

When measuring the amount of protein after pooling there was a far lower concentration of the mutant protein (mean=0.18mg/ml) than the wild type (3.3 mg/ml) prompting questions of stability in the mutant compared to the wild type. A thermal denaturation assay was also performed to check the thermal stability of the generated proteins and to test the different eluents prior to pooling (figures 6.5 and 6.6). The wild type protein was highly stable. The different eluents appeared to all denature at approximately 80^{o}C with an inflexion temperature of approximately 90^{o}C. This suggested that the wild type eluents are highly stable and relatively pure. A similar denaturation assay of the mutant protein eluents revealed a mixed picture with a variety of thermal denaturation curves (figure 6.6). In addition, the denaturation began at approximately 45^{o}C with inflexion points varying from 50 to 65^{o}C. This suggested that there was some variability in the eluents and that the mutant globular domain was more unstable. The four most unstable eluent batches were discarded at this stage.

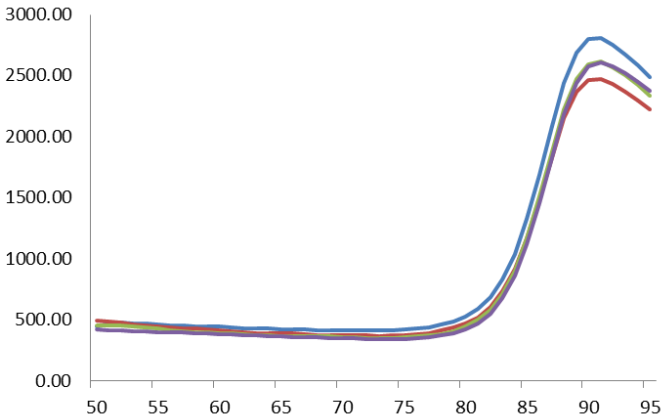

Figure 6.5. : Thermal denaturation assay for the wild-type g-C1QTNF5. The denaturation of gC1QTNF5 shows similar characteristics from different fractions suggesting that the eluted fractions from gel filtration are similar. The protein is very stable requiring 90^{o}C for denaturation.

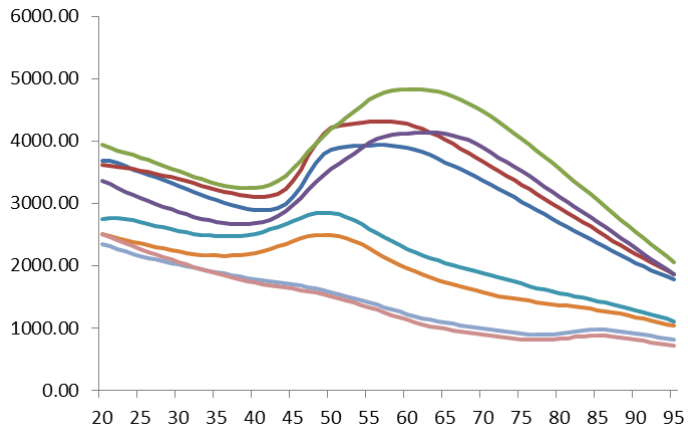

Figure 6.6 : Thermal denaturation assay for mutant g-C1QTNF5. The mutant eluted fractions show different denaturation characteristics. This suggests that there are different proteins in the different elution fractions. The bottom four fractions were discarded. The top four fractions show denaturation between 55 and 70ºC suggesting that the mutant is less thermodynamically stable than the wild-type.

6.3.2 Interaction of wild type C1QTNF5 with complement factor H (CFH)

Both the wild-type and mutant protein were found to be stably bound to the chip with less than 10% loss during the course of the initial substrate quality control stage (figure 6.7). This suggested that loss of resonance would not be secondary to loss of protein from the chip throughout the course of the experiments.

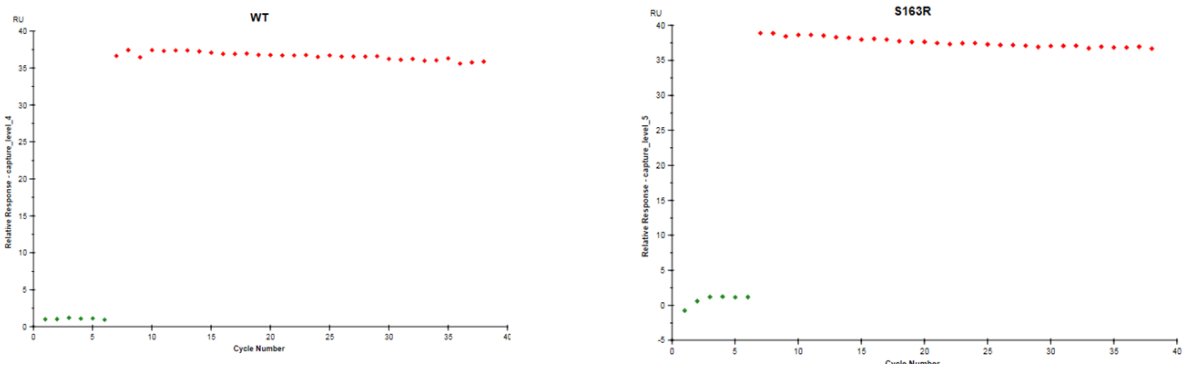

Figure 6.7 Stability of ligand binding to the chip. The wild-type and mutant gC1QTNF5 were bound to the gold plated chip. During the course of the experiment there was less than 10 percent loss of material suggesting that the system could be used for the ligand binding experiments.

The values for the kinetics were obtained after three repeats of the experiments on the same chip. The complex formation constant (Ka) and dissociation constant (Kd) were calculated using supplier provided software. Initially a 1:1 model of affinity was tested unsuccessfully. The data were eventually fitted to a heterogeneous ligand model on the basis that the ligands would contain a mixture of mainly monomers and trimers as seen in the Coomassie stains. There are several different features of binding of CFH to the wild-type (figure 6.8). There is a strong on rate Ka1 (monomer) and Ka2 (trimer) with both forms of the protein with values of $2.7x\ 10^{-5}$ M and $5.5\ x10^{-6}$ M respectively. The formation of the complex with the proposed trimeric form is greater. The dissociation constants are $6.32x10^{-7}$ and $6.68x10^{-10}$ respectively for the two forms suggesting that the trimeric form is almost 1000 fold greater average affinity than the monomeric form.

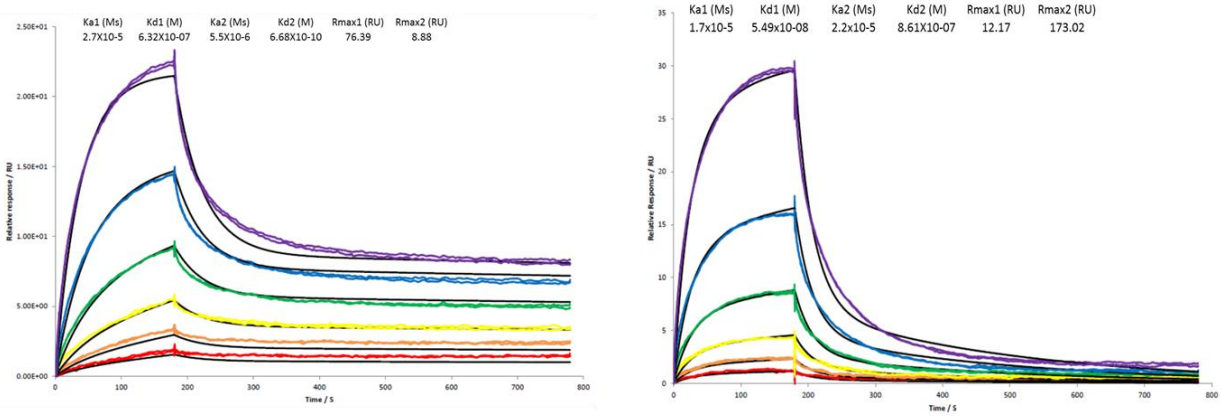

Figure 6.8: SPR sensorgrams demonstrating CFH interaction with mutant and wild type His-gC1QTNF5 Three separate experiments were performed. A heterogeneous ligand model was used to fit the affinities (Kd) and association rates (Ka). CFH is flowed over the gC1QTNF5 which is bound to the SPR chip. The lines represent different concentrations of CFH. Each line represents a twofold greater concentration of CFH than the line below. The CFH is flowed for 180 seconds. The dissociation was then measured for 600 seconds. The affinities for the monomeric and multimeric wild type are $6.32x10^{-7}$ M and $6.68x10^{-10}$ M respectively suggesting that the multimeric form has almost 1000 fold greater average affinity. The strong affinity of the multimeric form is shown by the prolonged resonance even after 600 seconds.
The affinity values for the mutant were $5.49\ x\ 10^{-8}$ M and $8.61\ x\ 10^{-7}$ M. The mutant has a similar affinity to the monomeric form of the wild type.

The mutant protein affinity fitted better to a 1:1 model (figure 6.8). However, for comparison a heterogeneous ligand model was used as the previous analysis had shown that the samples contained multiple different elements. Perhaps unsurprisingly, as the protein appeared to be mainly monomeric the Ka and Kd were similar for the different predicted ligands. With Ka values of $1.7x10^{-5}$ and $2.2\ x\ 10^{-5}$. The Kd values were $5.49\ x\ 10^{-8}$ M and $8.61\ x\ 10^{-7}$ M. The affinities were similar to the monomeric forms of wild-type protein. This suggested that the main difference

between the proteins in CFH affinity resulted from the inability of the mutant to form trimers and potentially multimers.

After establishing that CFH binds to C1TQNF5, I wanted to see if a functional role for C1QTNF5 in mediating localised complement pathway activation could be found. C1QTNF5 is secreted by the cell and we showed in chapter 4 that C1QTNF5 could be found in the media. As a result the first functional studies test the effects of C1QTNF5 on CFH function in the fluid phase.

In the biacore studies, monomeric form of the mutant was found to have a similar affinity for CFH as the monomeric form of the wild-type. Ideally, it would have been good to see if the mutant protein altered CFH function. Unfortunately, the mutant was found to degenerate over days. When the mutant was retested for protein concentration using spectrophotometry there was not sufficient concentration of the protein to perform the solid phase functional analyses. The fluid phase functional studies looked to see how the addition of wild-type and mutant C1QTNF5 altered the breakdown of C3b alpha chain into fragments (67kDa and 43 kDa). To ensure that the system was valid the system was tested without CFI or CFH (figure 6.9). There was no breakdown of C3b without all C3b, CFH and CFI being present. The addition of the wild type appeared to make little difference to breakdown. The addition of the mutant C1QTNF5 led to a minimal decrease in fragment density. Large amounts of C3b and C3b alpha chain were still present in the solution even after addition of C1QTNF5. This suggests that in the fluid phase C1QTNF5 appears to make little difference to CFH function using this system.

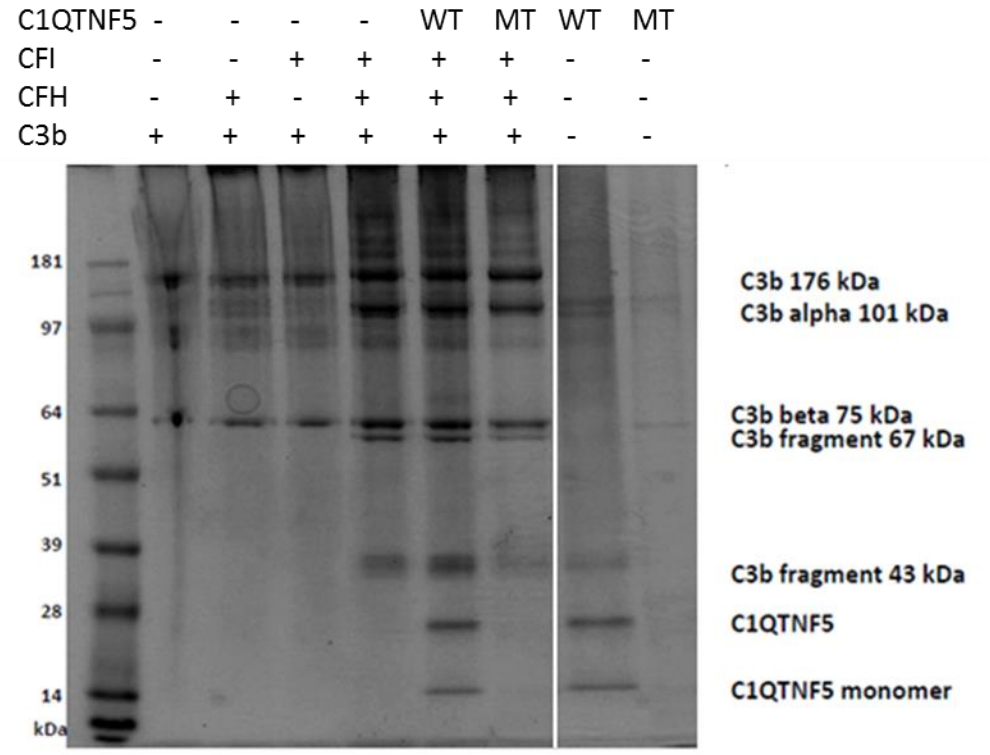

Figure 6.9 : Fluid phase CFH functional studies. CFH breaks C3b with the help of CFI. C3b has a molecular weight of 176 kDa and is composed of an alpha chain (101 kDa) and a beta chain (75 kDa) linked by a disulphide bridge. Breakdown of C3b results in a fragment at 67kDa and 43 kDa. Various combinations of C1QTNF5, CFI, CFH and C3b were tested. The gels were stained for 20 minutes using Coomassie brilliant blue and then imaged on a Licor geldock imaging device. The negative controls in the first three columns show that there is no breakdown of C3b. The addition of the wild type appears to make little difference in breakdown. The mutant appears to reduce breakdown.

The solid phase assay used sensitised sheep red blood cells to see if CFH could prevent complement mediated lysis in different quantities of serum. CFH depleted serum quickly loses complement activation as C3 is converted to C3-H_2O and/or C3b. This is shown by the lack of lysis in the CFH depleted sera (figure 6.10). However, when CFH is added back into the depleted sera it can retain near normal activity levels to normal serum (figure 6.10). The addition of C1QTNF5 to this serum appears to minimally protect RBCs from lysis. Only one concentration of C1QTNF5 was tested and a limited amount of test points in serum could be attempted due to the lack of necessary wild-type C1QTNF5 required for this experiment. It would be useful to repeat this at various concentrations of C1QTNF5 to confirm that C1QTNF5 modifies CFH function in the solid phase.

The data in these set of results showed that CFH bound to C1QTNF5. Secondly, the Biacore data also shows that there is difference in binding characteristic between the wild-type and mutant globular domains. In addition, the data suggests that there is also role for C1QTNF5 in protecting against complement mediated attack in the solid phase but not in the fluid phase.

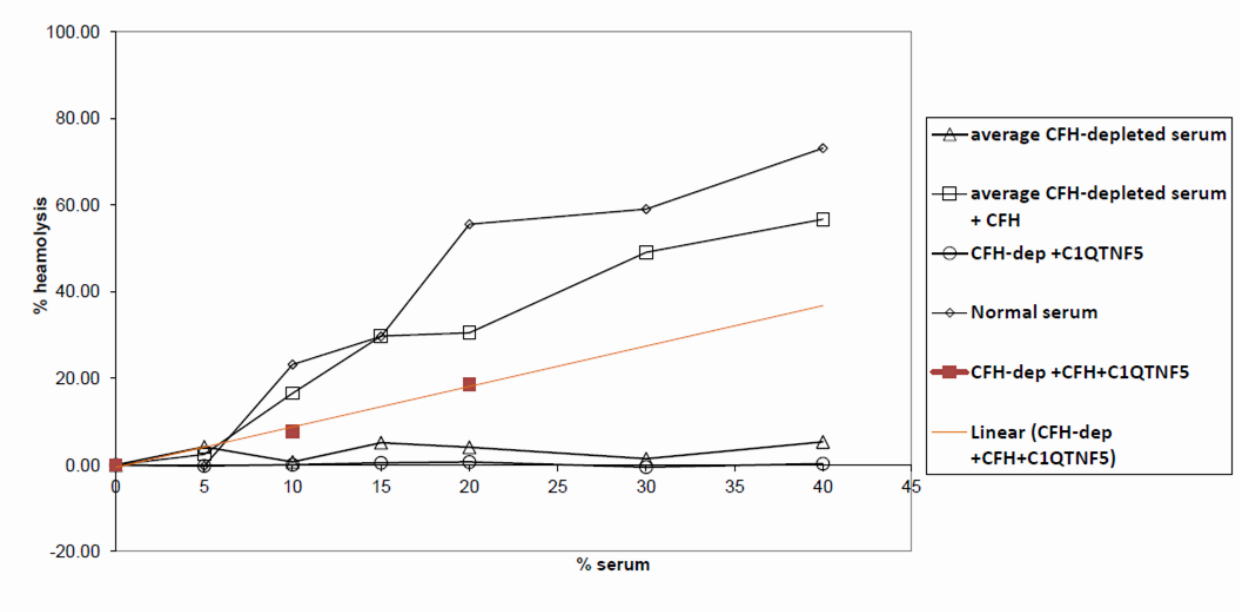

Figure 6.10 : Solid phase CFH functional study using RBC haemolysis. Sensitised sheep RBCs were placed in varying concentrations of serum with normal serum, CFH depleted serum, CFH depleted serum with gC1QTNF5, CFH depleted serum with CFH added and CFH depleted serum with C1QTNF5 and CFH added. Haemolysis did not occur in either of the CFH depleted sera conditions without addition of CFH which suggests that the media burnt out of C3 and was no longer complement active. This provided a good negative control of the system. The addition of CFH was able to maintain C3 levels within the media and maintain complement activity and is shown by an increase in haemolysis with serum concentration. The normal serum is a good positive control. The addition of gC1QTNF5 to the CFH depleted media with CFH added reduced the amount of haemolysis at the 10% and 20% serum concentrations suggesting that the addition reduced complement mediated activity at the cell surface.

6.4 Discussion

In this series of studies C1QTNF5 generated by *E.Coli* was found to bind to CFH. The wild-type protein was found to at a significantly higher affinity to CFH than mutant C1QTNF5. Previously, different regions of CFH have been shown to bind to different substances. CCPs 1-4 bind C3b and act as a cofactor for CFI to catalyse the breakdown of C3b to form iC3b. CCPs 1-4 also help decay the C3 convertase C3bBb which also negatively regulates the alternative complement pathway. C3d is essentially the buried thioester domain of C3b. Crystallography of C3d and CCP19-20 fragments of CFH show close association of the two fragments (Jokiranta et al., 2006). Affinity studies have also confirmed that 19-20 fragments bind strongly to C3d in a similar manner as to C3b (Morgan et al., 2011). This suggests that there are two binding sites on CFH for different parts of C3b. There is also evidence that CFH has some evidence of binding to CRP, annexin II, malondialdehyde acetaldehyde (MAA) and oxidised lipids (Jarva et al., 1999, Leffler et al., 2010, Weismann et al., 2011, Shaw et al., 2012). CRP is found on cells with an acute phase response and is often also found when cells become infected. MAA is known to be produced in oxidative stress. CCP 7 and 20 were found to bind to MAA. Annexin II is often a marker of apoptotic cells (Weismann et al., 2011). If binding data are true CFH may play a role in coating dead or dying cells and forming iC3b from C3b thus coating the cells in opsonising agents to assist in clearance.

The Y402H variant of CFH is associated with AMD. The variant substitutes a histidine for a tyrosine amino acid at position 402 found on CCP7 of CHF. This region has binding sites for heparin, CRP and streptococcal M protein (Giannakis et al., 2003). In the common variant the tyrosine side chain is thought to bind closely to GAG-like structures. Binding to BM was found to be reduced in the variant. Interestingly glycosylation patterns were also altered in BM with ageing. Reduced binding was shown on aged BM. In addition, the AMD associated variant has been shown to have reduced binding to RPE (Skerka et al., 2007). This suggests that CFH binds to RPE and BM. In solid phase CFH can inhibit localised complement pathway activation by inactivating C3b. We hypothesise that C1QTNF5 may also act in a similar way to GAGs. C1QTNF5 is secreted and has been found on cell membranes. C1QTNF5 on extra cellular surfaces facilitates CFH binding on cell surfaces to prevent cell surface complement activation.

In chapter 4, the studies showed that C1QTNF5 was secreted by the cells. In conditioned media there was a lack of high order polymers in the non-reduced western blot of conditioned media. This suggested that the mutant heterozygote disrupted normal C1QTNF5 multimerisation. This was similar to the findings in this chapter with the wild-type protein appearing to form dimers and trimers whilst the mutant protein remained mainly monomeric from the western blots. Tu *et al* had

generated full length C1QTNF5 and found that not only did C1QTNF5 form trimers but that the trimers formed bouquets of C1QTNF5. This structure was clearly seen using negative staining electron microscopy (Tu and Palczewski, 2014). In this set of studies, we were unable to study heterozygote trimer formation in detail or the effects that this might have on binding to CFH. In addition, we were unable to study the formation of high order multimers with wild-type protein as only the globular domain was generated.

In these studies, gC1QTNF5 was shown to bind to CFH. The wild type globular domain had a far greater affinity with CFH than the mutant. One could suggest that the lack of multimerisation would reduce the available binding sites for CFH on the cell surface. Reduced CFH binding may result in insufficiency and therefore reduce available binding sites for CFH on cell surfaces, which in turn leads to increased complement activation and TCC deposition on RPE and in the sub-RPE as seen in the L-ORMD donor retinal sections.

Chapter 7

7. Discussion

Macular degenerations are amongst the commonest causes of sight threatening ophthalmic disease (Roy, 1974, Resnikoff et al., 2004). AMD is the commonest form of macular degeneration. Although studies have highlighted key factors associated with AMD (Smith et al., 2001), they have not been able to clearly demonstrate the stepwise mechanism of pathogenesis. In particular, the initial injury and subsequent development of early disease is poorly understood. Although anti-VEGF treatments have improved the visual outcome of patients with late-stage neovascular AMD these patients continue to reduce vision after diagnosis. Additionally, treatment for geographic atrophy is currently inadequate. A lack of suitable models has hampered the development of new treatments for AMD. AMD is a complex disease resulting from genetic and environmental interactions. Inherited macular degenerations offer a potential route to understanding molecular pathways involved in disease. L-ORMD is an autosomal dominant inherited macular degeneration which shares many clinical and pathological characteristics with AMD (Kuntz et al., 1996, Milam et al., 2000, Ayyagari et al., 2005).

This study aimed to develop a model of macular degeneration using L-ORMD. In the first instance, the aim was to see if clinical characteristics of our cohort of patients conformed to previous reports of L-ORMD patients. A secondary aim was to use newer retinal investigation techniques and histopathology to see if L-ORMD patients exhibited features described for AMD patients.

HiPSCs had previously been used to model inherited retinal disease (Li et al., 2014, Lukovic et al., 2015, Meyer et al., 2011, Singh et al., 2013b). Using a similar approach the aim was to model L-ORMD using hiPSCs. The first aim was to reprogram patient somatic cells to hiPSCs. Subsequently the study aimed to differentiate hiPSCs to disease-causing RPE. The study sought to investigate cell autonomous vulnerabilities in the generated hiPSC-RPE. Subsequently, the study aimed to investigate differences identified during histopathological studies in particular those with reference to the complement pathway. In the final chapter, the dissertation looked to see if the differences in the complement pathway activation found were due to an interaction of C1QTNF5 with complement factor H.

The next part of the dissertation aimed to develop an *in vitro* model for L-ORMD using hiPSCs. The aim was to see whether the cells showed any cell autonomous differences from those of control cell lines. Secondly, the aim was to see if the model could be used to study localised complement dysfunction *in vitro*.

Finally investigations targeted CFH to see if C1QTNF5 showed altered activation of the alternative complement pathway through a direct interaction with this regulator of the alternative complement pathway.

7.1 Summary of the principal findings and suggestions for future studies

The clinical studies in chapter 2 of this dissertation demonstrated that the L-ORMD patients in this cohort shared characteristics with previously described cohorts of L-ORMD. (Vincent et al., 2012, Soumplis et al., 2013, Jacobson et al., 2014). In particular, the patients were shown to develop a thick sub-retinal deposit which extended from the far-periphery to the fovea. These findings are similar to the histopathological reports for L-ORMD (Kuntz et al., 1996, Duvall et al., 1986). The SLO studies identified that the region temporal to the fovea appears to the first to develop neuro-retinal changes and that this region was the most sensitive region for deterioration in functional studies including microperimetry and multifocal ERG. Again these findings correspond with previous reports of delayed dark adaptation which are most sensitive at 15 degrees temporal to the fovea (Jacobson et al., 2001).

Previously, patients with L-ORMD had been described to have features similar to AMD. These included drusenoid white spots, sub-retinal deposit, retinal pigment epithelial loss and neuro-retinal atrophy and choroidal neovascularisation (Kuntz et al., 1996, Milam et al., 2000, Ayyagari et al., 2005). This study revealed that patients with L-ORMD also demonstrated other features of AMD including cuticular drusen, reticular pseudodrusen and choroidal thinning. Recent studies of macular degeneration have demonstrated that choroidal thinning appears to be associated with cuticular drusen (Garg et al., 2013). In this study we show that choroidal thinning occurs prior to neuro-retinal loss, suggesting that initial disease may involve the RPE-Bruchs' and choroid complex prior to the neuro-retina in L-ORMD. Recently, the choroid has also been attracting attention as a site for initial injury in macular degeneration (Mullins et al., 2014b). Additionally, methods used to monitor AMD including measurement of atrophy using SLO could also be used to monitor L-ORMD progression in stage 2 disease. In chapter 2, this study also identified complement staining in the deposit and choriocapillaris in L-ORMD histopathology samples. Therefore choroidal complement activation could also be involved early in L-ORMD pathogenesis. Mullins *et al.* also showed TCC deposition in the choroid in their histopathology study suggesting a similar mechanism in AMD (Mullins et al., 2014b). A similar process could be confirmed in L-ORMD if younger donor material was available. In addition, it would be interesting to investigate the serum of patients with L-ORMD to see if they have raised complement components as has been found in AMD patients (Stanton et al., 2011).

Dark adaptation delay is reported as one of the earliest clinical features of L-ORMD (Jacobson et al., 2001). Although dark adaptation delay is also a feature of AMD, it is less commonly reported (Haimovici et al., 2002). It was unclear why this feature was so prominent in L-ORMD patients. However, these studies have shown that in the peri-fovea and the temporal macula there are marked changes suggestive of reticular pseudodrusen in L-ORMD patients. This is the region of retina with the highest concentration of rods (Jonas et al., 1992). Reticular pseudodrusen are located above the RPE layer and are in contact with the photoreceptor layer (figure 2.2). Therefore unlike traditional drusen, pseudodrusen can induce direct damage to photoreceptors. Since the pseudodrusen are especially concentrated in the rod-rich areas it is likely that the rod function deteriorates prior to cone function. This may result in early marked dark adaptation delay. When looking at AMD cases, those with pseudodrusen were found to have a significantly greater dark adaptation delay (Flamendorf et al., 2015). It is still unclear why these changes occur more prominently in rod-rich areas initially sparing cone-rich regions such as the fovea. It would be interesting to investigate these differences further by co-culturing either rods or cones with case hiPSC-RPE. The hypothesis being that co00culturing with rods would lead to increased RPE damage when compared to co-culturing in cone-rich media.

In chapter 3, hiPSCs were successfully reprogrammed from patient and control fibroblasts. The hiPSCs could be differentiated into functional RPE. Thus far there have been no published reports of hiPSC-RPE derived from L-ORMD patients. There have however, been other reports of hiPSC-RPE generation in a small number of inherited diseases (Sun et al., 2015, Li et al., 2014, Yang et al., 2014a, Singh et al., 2013a, Singh et al., 2013b, Li et al., 2012, Carr et al., 2009, Buchholz et al., 2009). The baseline characteristics of the hiPSC-RPE were similar to those previously described in terms of gene expression, TER and phagocytosis. However, the RPE were also stained with phalloidin which binds to F-actin (Vandekerckhove et al., 1985). The findings in the case lines differs to the suggestions in previous reports which suggest a role for C1QTNF5 and MFRP in binding to actin and an imbalance resulting in actin disorganisation (Li et al., 2014). The phalloidin staining for the hiPSC-RPE case and control lines in chapter 5 showed no observable differences.

In chapter 4, the study described findings from cell–autonomous studies between case and control hiPSC-RPE. Findings differed from those previously reports using transfected cell lines. Shu *et al.* had found that in cells transfected with mutant C1QTNF5, that mutant C1QTNF5 was not secreted. Instead it accumulated intracellularly within the ER forming aggregates (Shu et al., 2006b). In this study, there was heavy immunostaining particularly of the inner deposit for C1QTNF5 in both human and mouse histopathology specimens with little staining intracellularly. C1QTNF5

expression was noted in hiPSC-RPE and immunostaining noted staining within the RPE. Conditioned media from case and control hiPSC did reveal a reduction in secretion of C1QTNF5 in case lines when compared to control lines. IN addition, there was a marked reduction in multimer formation. Markers of ER stress from protein folding were only variably altered in expression in the hiPSC case lines when compared with control hiPSC lines. *HSPA2* and *HSPA6* showed a greater than 2 fold increased expression in the case line when compared to a control line. However, *HSPA4* showed a greater than two fold reduced expression in the case compared to the control lines. *GRP78* expression showed no significant change between case and control lines. Other markers of ER stress including *BiP, ATF3* and *CHOP* were not examined during these transcript analyses. Taken together the evidence for these studies suggests that mutant C1QTNF5 is secreted and forms part of the deposit leading to a gain of function. This is also supported by studies in mice which showed only a 20 percent decrease in *C1QTNF5* expression in C1QTNF5 +/- compared to the wild type making a dominant negative effect unlikely (Chavali et al., 2011). In addition, study of the knockout mouse in the studies presented here showed no deposit formation or complement activation pointing against a dominant negative effect from C1QTNF5 insufficiency. The studies presented in this dissertation are limited because the antibodies used were not specific for mutant C1QTNF5. Additionally, previous studies have shown evidence for an interaction between mutant and wild type C1QTNF5. This was not investigated further in these studies. With new gene editing techniques (Cong et al., 2013b), it would be possible to knock in a double mutant C1QTNF5 gene into human cell lines. The prediction would be that phenotypes would be worse with a gain of function mutation. Alternatively, a knockout of both alleles of the C1QTNF5 would be predicted to result in a worse phenotype if the disease was due to heterozygote insufficiency.

In chapter 5, when investigating differences between case and control hiPSC-RPE the case lines were also found to be vulnerable to oxidative stress. In addition, case lines expressed increased catalase and haem oxygenase1 suggesting that even at baseline, cells were under oxidative stress. Haem oxygenase and caeruloplasmin were also found to be significantly raised in the serum of C1QTNF5 mutant heterozygote knock in mice at 12 months of age (Chavali et al., 2011). This suggests that oxidative stress may play a part in L-ORMD. The exact role of C1QTNF5 is still unclear from this or previous studies. As yet no role for mediating cellular redox state has been shown for C1QTNF5. The case cells did not appear do to undergo apoptotic cell death with no Caspase-3 staining after being subjected to oxidative stress. However, they were sensitive to membrane permeability markers suggesting necrotic cell death. Chavali *et al.* noted similar changes *in vivo* in the knockout mouse model with signs of RPE damage through necrosis (Chavali, 2012). This points to a potential role for C1QTNF5 protecting against oxidative stress on

the cell membrane. Only a targeted screen of cellular stress related gene expression was performed here. Additionally, the findings regarding gene expression are limited as only one case line and one control line was used for the expression analyses. A clearer role may be apparent with whole transcriptome screening comparing several case and control lines using RNA sequencing for oxidative stress across more than one case line. This may reveal changes in pathway gene expression involving oxidative stress.

In non-cell autonomous experiments in chapter 5, the model demonstrated increased complement activation in case lines when compared to control cell lines with increased TCC deposition on case cells and membrane inserts. The increased immunostaining with antibodies to TCC is similar to that seen in the histopathology samples. In this model, TCC deposition mainly occurred on the cells. However, there was also deeper staining within the membrane which would be similar to staining within Bruch's membrane or the choriocapillaris. In a similar manner to complement component staining seen in AMD, this study shows that complement dysregulation is seen in L-ORMD. However, what causes differential complement activation is not clear. The mutant protein may cause complement activation.

In chapter 6, I showed that mutant gC1QTNF5 was relatively unstable compared to the wild type gC1QTNF5. Thus, the degradation or breakdown of the mutant protein could be a potential trigger for pathogenesis. A simple experiment of adding mutant protein to the media of wild type cells or adding conditioned media to wild type cells could show that the mutant protein may be involved in early pathogenesis. This is supported by the lack of deposit formation in the C1QTNF5 knockout mouse.
I would predict that conditioned media would induce increased C5b-9 deposition in wild type cells lines. An antibody specific to the mutant was not developed during the course of this thesis. However, if a validated antibody could be generated a co-immunostaining or precipitation could be performed with C5b-9 to see if complement activation occurred directly on the mutant protein.

A recent study of another inherited deposit degeneration, Malattia Leventinese, revealed the mutant protein in this condition Efemp1 was also found in the deposit (Fernandez-Godino et al., 2015). Mutant Efemp1 was found to induce abnormal ECM turnover and cause complement activation which was C3 mediated. Complement activation also resulted in increased IL-6 and IL-1β both of which were found to be important in deposit formation. A similar role in altered ECM is suggested for mutant C1QTNF5. C1QTNF5 is composed of a globular C1Q head with a collagen like domain and a nitrile end (Tu and Palczewski, 2014). Electron microscopy of L-ORMD donor retina has revealed that the deposit is composed of wide-spaced collagen. The deposit resembles

BLamD (Sarks et al., 2007) BlamD are known to contain ECM components and wide-spaced collagen (Sarks, 1976). BlamD has also been shown to harbour complement components in a similar manner to drusen (Hageman and Mullins, 1999a, Anderson et al., 2002). Development of BLamD changes in a mouse model ceased with the absence of an active complement system suggesting that propagation of the deposit results from complement activation (Garland et al., 2014a). This study showed marked C3d staining of the deposit suggesting that there is C3 activation and C3b breakdown in the deposit (figure 7.1). In AMD basal laminar deposits form early in the disease process. It has been suggested that these are produced secondary to RPE stress (van der Schaft et al., 1994). In addition, there is some evidence that oxidative stress may also plays a part in AMD. Hollyfield *et al.* used a carboxyethylpyrrole (CEP), a downstream product of oxidised docosahexaenoic acid (DHA) on cell membranes. These mice developed BLamD (Hollyfield et al., 2008). A similar process may initiate AMD with released protein components causing the localised activation of the complement pathway. It is not clear from AMD studies what component of the deposits could initiate a complement response. Drusen and basal laminar deposits have been studied in molecular and proteomic studies (Hageman and Mullins, 1999b). Serum amyloid P, vitronectin, APOE, immunoglobulin light chains, Factor X, and C5 and C5b-9 have been identified as the only common components of all types of drusen and basal laminar deposit (Mullins et al., 2000b). In this dissertation, I have shown that the case lines express markers of oxidative stress even under basal conditions and are vulnerable to oxidative damage when compared to the control cell lines. Both the complement model study and the oxidative stress study showed increased staining in case cell lines with cell death and membrane permeability markers in the relative absence of apoptosis. This points to a vulnerability cell membrane mediated necrosis in the case lines and suggests that C1QTNF5 plays a key role in stabilising the cell membrane against necrotic attack.

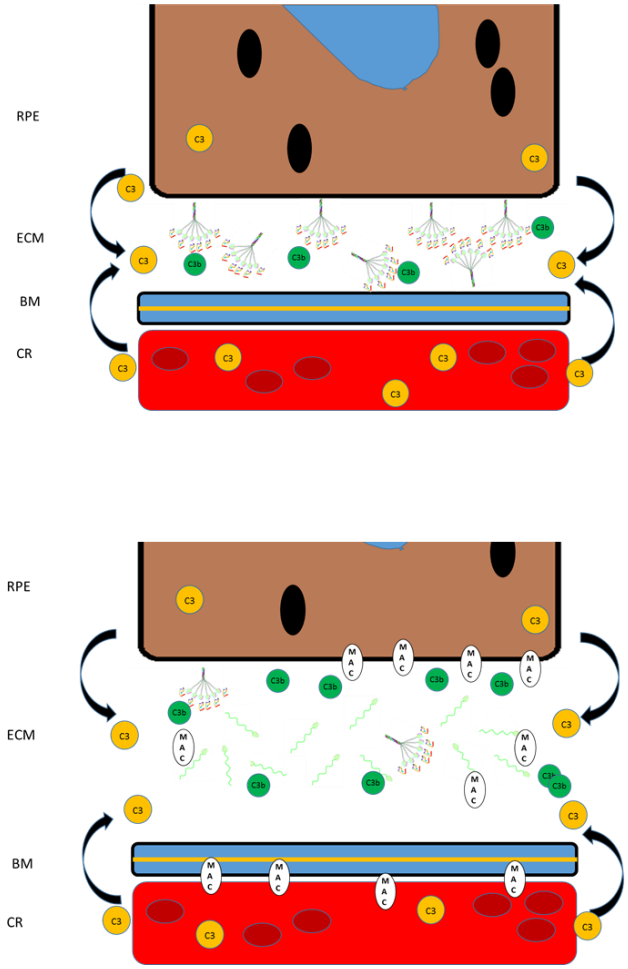

Figure 7.1: A schematic of C1QTNF5 function in health and disease. The upper diagram represents potential C1QTNF5 function in health. It acts as an anchor for multiple species on the cell membrane and the extra-cellular matrix. The figure shows that wild type C1QTNF5 is secreted and forms multimers binding multiple CFH molecules onto the cell surface and in the extracellular matrix (ECM). This assists local regulation of C3 tickover.

The bottom diagram shows the possible role of C1QTNF5 in L-ORMD. C1QTNF5 is secreted but mainly forms monomers which do not bind CFH well. This leaves the RPE cell membrane and choroid prone to attack from the complement pathway with no regulation of C3 activity. It also makes the RPE vulnerable to other stress such as oxidative stress. The monomeric species accumulate in the ECM. This causes further complement pathway activation preventing clearance and resulting in a thick basal laminar like deposit forming. CR=choroid

C1QTNF5 has already been shown to bind to MITF and to form high order polymers (Tu and Palczewski, 2014). In chapter 6, this study showed that C1QTNF5 also bound to CFH, a key regulator of the alternative complement pathway. Polymorphisms of CFH have been associated with AMD. An attempt was made to see if there were functional changes with CFH. These showed a trend towards functional changes in the solid state but not in fluid phase. However, the

experiments were limited by the lack of available C1QTNF5 protein. CFH is also known to bind to ECM products including heparin sulphate and GAGS. The Y402H polymorphism of CFH results in an increased risk of AMD. This polymorphism results in a change to CCP 7 which alters GAG binding. All of the deposit forming macular degenerations show some form of disruption to ECM turnover (Weber et al., 1994, Garland et al., 2014b, Kortvely et al., 2010). CFH may also have a role in helping ECM turnover. CFH has been found to coat drusen in AMD and has been shown to bind with reduced affinity in Y402H variant and reduced binding to aged Bruch's (Clark et al., 2010). CFH has also been shown to clear iC3b (Paixão-Cavalcante et al., 2009). CFH is also known to bind to apoptotic and necrotic cells and is thought to prevent complement activation with differential affinity of the Y402H variant (Sjöberg et al., 2007). Why complement downregulation is important when apoptosis and necrosis occurs in the sub-retina is still not clear.

In these experiments, we noted activation of complement on necrotic cells in the case hiPSC-RPE cell lines. Failure of downregulation of the complement pathway may lead to deposit formation (Garland et al., 2014a). Recently, another component of necrotic cell membranes was found to bind to CFH (Weismann et al., 2011). Malondialdehyde (MDA), a lipid peroxidation product is exposed on necrotic cells, is a ligand of CFH. This could provide a role for CFH in preventing complement activation on damaged cells and regulating oxidative damage at the cell membrane and preventing cell death. MDA has been shown to increase in AMD eyes (Weismann et al., 2011). CFH has been shown to decrease oxidative stress resulting from MDA. MDA has previously been shown to increase at the cell surface with hydrogen peroxide administration (Sheridan et al., 1996). The role of MDA was not investigated during these experiments but could simply be examined by immunostaining with progressive levels of oxidative stress and combining these experiments with complement activation studies.

The exact binding site of C1QTNF5 on CFH was not determined during this set of experiments. This could quite easily be tested by assessing individual CCP regions for C1QTNF5. Another potential method by which mutant C1QTNF5 could result in pathology is the modulation of localised complement activity. In these studies, I provided evidence that the mutant appears to reduce the formation of multimeric C1QTNF5. I showed that C1QTNF5 binds to CFH. Reduced multimerisation of C1QTNF5 on the cell membrane may lead to reduced CFH binding and therefore reduced downregulation of complement activity making the cell membranes vulnerable to complement mediated attack as shown by the cell model. This could be tested by increasing CFH concentration in the cell model and comparing this with increasing functional C1QTNF5 and CFH levels in the model. I predict that this would reduce C5b-9 activation.

The normal physiological role for C1QTNF5 is still unclear from this study however, it may play a role in binding mediators of the ECM on the cell membrane including CFH and MITF. C1QTNF5 has previously been shown to interact with other molecules of C1QTNF5 forming high order polymers. Recently, Tu *et al.* generated full length C1QTNF5 using a bacterial expression system (Tu and Palczewski, 2014). Using negative staining electron microscopy they noted multimeric bouquets of C1QTNF5. They suggested that the nitrile and collagen domains lay in the cell membrane exposing the globular domains. Together this suggests that C1QTNF5 plays a complex role in the ECM helping bind a number of modifiers of the ECM to cell membranes.

There are several limitations when making conclusions about macular degeneration from the model. The first is that the model is developed from L-ORMD cell lines and not AMD. Differences between L-ORMD and AMD have already been highlighted and these include an earlier age of onset and increased severity of disease which eventually affects the whole retina. In addition, there may be other differences in the diseases. For instance, L-ORMD patients demonstrate long anterior zonules (Ayyagari et al., 2005). Long anterior zonules have also been reported in a number of other conditions (Moroi et al., 2003). C1QTNF5 is also expressed by the ciliary body. It is thought that expression of the mutant here may bring about these changes however the exact mechanism is unclear. However, this does highlight that changes are not limited to the macula in L-ORMD. I have also shown that L-ORMD appears to start in the temporal macula unlike AMD which usually begins at or near the fovea. So whilst the model appears to provide a reliable replication of certain aspects of AMD the inferences are limited and any findings would have to be confirmed in AMD itself.

Chapter 1 also highlights a number of limitations with using hiPSCs to model human disease. Amongst the biggest obstacles to using hiPSCs is the variability. Firstly, hiPSCs retain some epigenetic memory from the cell of origin which may skew some of the *in vitro* findings (Bar-Nur et al., 2011). In addition, reprogramming can alter gene expression with the insertion or deletion of the host genome. This means that the phenotype does not only result from the mutation but could results from a number of other differences in gene expression. Gene expression beyond the mutant gene of interest may also be important when case and control lines are from different sources. In this study, I used cells from siblings or close relatives to reduce the variation in gene expression. However, newer methods have recently become available. Using gene editing it is possible to create isogenic lines from diseased cell lines (Soldner et al., 2011). These corrected control cell lines have an identical genome to the case lines except for the gene of interest. Therefore any differences in the cell lines could be more confidently attributed to the gene of interest. In addition, the majority of the lines have been derived using integration free methods therefore reducing the

risk of unintentional insertions or deletions. In order to validate my findings, I also used *in vivo* findings which appeared to replicate the complement activation found in the model in the disease itself.

There remain a number of unanswered questions which I plan to answer with upcoming studies. Firstly, it is still unclear whether L-ORMD results form a gain of function resulting from the damaging effect of a mutant protein or whether L-ORMD results from a loss of function from the lack of two alleles resulting in haploinsufficiency. I plan to address this question with gene editing studies firstly by knocking out C1QTNF5 from control hiPSCs to test loss of function. To test whether the phenotype results from a gain of function I will use CRISPR-CAS gene editing on the mutant lines to see if there is an increase in severity of the phenotype which suggests a gain of function.

In addition, it is not clear what pathway is involved in increasing complement activation in the model. I plan to use RNAseq to provide an unbiased screen of pathways comparing case cell lines prior to and after the serum stress tests. This work will provide the foundation of further validation studies.

Future studies	Aim of studies	Relevance of studies
CRISPR-CAS knockout line generation	A human C1QTNF5 knockout line will be generated by using CRISPR-CAS targeting removal of the whole C1QTNF5 gene.	To see if the disease results from loss of function the same serum stress tests will be performed with this edited line when compared with mutant lines.
CRISPR-CAS mutant allele knock in line generation	The aim is to create a homozygous mutant line with CRISPR CAS-guide to target the wild-type allele and a DNA template used to insert the mutant base pair change.	To see if the disease results from gain of function from the mutant allele the double knock in lines will be tested using the serum stress tests to see if there is any difference when compared to heterozygote lines.
RNA sequencing	3 case lines will be sequenced as treatment naïve. A further 3 case lines will also be analysed after being incubated 12 hours in serum.	To identify key pathways causing differences in c5b-9 deposition in the mutant cell lines.

Table 7.1 A summary of future planned work

7.2 Implications for the treatment of L-ORMD

The ultimate aim of this dissertation is to develop treatments for patients with macular degeneration. Degenerative eye diseases progress through a range of stages (figure 7.2). Prior to clinical disease the patients are asymptomatic and there may be no signs of disease. Developments in genetic testing now enable the identification of patients at this stage. The genetic elements of disease can potentially be treated at this stage with gene editing or gene therapy. This study highlights a potential gain of function from the mutant protein. Recently, gene editing technology has provided a platform for the silencing of gene expression *in vivo* including retinal disease (Ousterout et al., 2015, Bakondi et al., 2015). Using a similar approach with guide RNA encoded alongside CRISPR-Cas with a plasmid encased within an AAV capsid it would potentially be possible to truncate the mutant C1QTNF5 whilst leaving the wild type allele unaffected. This would leave only wild type C1QTNF5 expressed and potentially resolve any effect from the mutant protein. The potential efficiency of this technique are relatively high (Bakondi et al., 2015). Ultimately complete gene correction of the mutant allele would yield normal expression of wild type protein without the potential effect from a truncated mutant protein. This would also potentially be possible however, the efficiency of this technique would be relatively low (Cong et al., 2013a). In addition, the efficiency would be lowered further in non-dividing cells. If a loss of function is due to a dominant negative effect then AAV gene replacement therapy may be an option as has previously been used to treat other inherited eye conditions (Bainbridge et al., 2008).

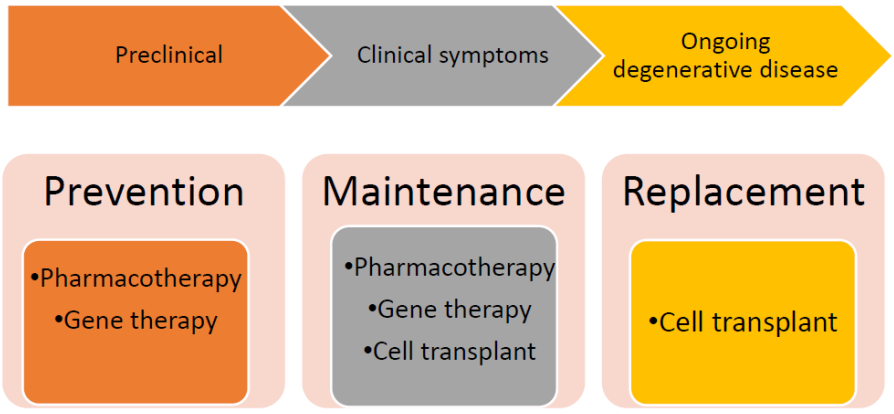

Figure 7.2: Diagram of treatments for stages of degenerative disease

In early stages when structure and function is maintained, preventative treatments including pharmacological and gene therapeutic treatments could provide useful in preventing disease or slowing progression. As degeneration occurs the structure, function and number of cells is affected. In later disease, cell replacement may be effective in restoring function.

In early clinical disease, the structure and integrity of the retina may be largely maintained. Therefore disease modifiers may be important. Pharmacotherapy may play a part. In this study we showed that the depletion of both C3 and C5 resulted in abolishing the phenotype. C3 or C5 inhibitors could be used to modify the disease. There is already a clinical grade monoclonal antibody against C5 known as eculizumab. Eculizumab has already been used to treat paroxysmal nocturnal haematuria (Hillmen et al., 2006). A trial of eculizumab was attempted with systemic dosing (Yehoshua et al., 2014). However, we show in this study that the RPE also expresses C5 and therefore systemic administration alone may not be adequate in reducing C5 activity within the eye. The trial looking at the treatment of GA showed no difference in progression between cases and controls. Symptomatic but non disease-modifying features of disease could also be treated at this stage. There is evidence from dark adaptation studies that there is a deficiency of retinoid regeneration in L-ORMD patients in stage 2 (Papastavrou et al., 2015). This may result from the development of the thick sub-retinal deposit which results in a barrier between the RPE and the choroid. The addition of high dose vitamin A has shown an improvement in dark adaptation kinetics in some patients (Jacobson et al., 2001).

In late stage disease there is marked cell loss. Cell replacement strategies may potentially benefit patients at this stage. Recently, RPE derived from hESCs was transplanted sub-retinally in macular degeneration patients. The RPE became pigmented and formed in the correct layer. The transplants had relatively few side effects. At present there is little evidence of RPE function or an improvement in clinical function however if timed correctly this could potentially form part of a cell replacement strategy to rescue photoreceptors. Recently, photoreceptors with outer segments have also been generated from hiPSCs (Zhong et al., 2014). The replacement of multiple cell lines of the outer retina offers the hope of recovery of outer retinal function however many of the techniques are as yet untested *in vivo*. Importantly, C1QTNF5 is conserved between mammalian species. The development of a mouse model for L-ORMD offers the possibility to test a number of strategies at various stages of disease before embarking on clinical translation trials in our cohort of patients.

References

ADAMIS, A. P., SHIMA, D. T., YEO, K. T., YEO, T. K., BROWN, L. F., BERSE, B., D'AMORE, P. A. & FOLKMAN, J. 1993. Synthesis and secretion of vascular permeability factor/vascular endothelial growth factor by human retinal pigment epithelial cells. *Biochem Biophys Res Commun,* 193**,** 631-8.

AISENBREY, S., ZHANG, M., BACHER, D., YEE, J., BRUNKEN, W. J. & HUNTER, D. D. 2006. Retinal pigment epithelial cells synthesize laminins, including laminin 5, and adhere to them through alpha3- and alpha6-containing integrins. *Invest Ophthalmol Vis Sci,* 47**,** 5537-44.

ALCENDOR, R. R., GAO, S., ZHAI, P., ZABLOCKI, D., HOLLE, E., YU, X., TIAN, B., WAGNER, T., VATNER, S. F. & SADOSHIMA, J. 2007. Sirt1 regulates aging and resistance to oxidative stress in the heart. *Circ Res,* 100**,** 1512-21.

ALLIKMETS, R., WASSERMAN, W. W., HUTCHINSON, A., SMALLWOOD, P., NATHANS, J., ROGAN, P. K., SCHNEIDER, T. D. & DEAN, M. 1998. Organization of the ABCR gene: analysis of promoter and splice junction sequences. *Gene,* 215**,** 111-22.

AMBATI, J., ANAND, A., FERNANDEZ, S., SAKURAI, E., LYNN, B. C., KUZIEL, W. A., ROLLINS, B. J. & AMBATI, B. K. 2003. An animal model of age-related macular degeneration in senescent Ccl-2- or Ccr-2-deficient mice. *Nat Med,* 9**,** 1390-7.

AMIN, S., CHONG, N. H., BAILEY, T. A., ZHANG, J., KNUPP, C., CHEETHAM, M. E., GREENWOOD, J. & LUTHERT, P. J. 2004. Modulation of Sub-RPE deposits in vitro: a potential model for age-related macular degeneration. *Invest Ophthalmol Vis Sci,* 45**,** 1281-8.

ANDERSON, D. H., MULLINS, R. F., HAGEMAN, G. S. & JOHNSON, L. V. 2002. A role for local inflammation in the formation of drusen in the aging eye. *Am J Ophthalmol,* 134**,** 411-31.

ANDERSON, D. H., RADEKE, M. J., GALLO, N. B., CHAPIN, E. A., JOHNSON, P. T., CURLETTI, C. R., HANCOX, L. S., HU, J., EBRIGHT, J. N., MALEK, G., HAUSER, M. A., RICKMAN, C. B., BOK, D., HAGEMAN, G. S. & JOHNSON, L. V. 2010. The pivotal role of the complement system in aging and age-related macular degeneration: hypothesis re-visited. *Prog Retin Eye Res,* 29**,** 95-112.

ARNOLD, J. J., QUARANTA, M., SOUBRANE, G., SARKS, S. H. & COSCAS, G. 1997. Indocyanine green angiography of drusen. *Am J Ophthalmol,* 124**,** 344-56.

ASLAM, T., MAHMOOD, S., BALASKAS, K., PATTON, N., TANAWADE, R. G., TAN, S. Z., ROBERTS, S. A., PARKES, J. & BISHOP, P. N. 2014. Repeatability of visual function measures in age-related macular degeneration. *Graefes Arch Clin Exp Ophthalmol,* 252**,** 201-6.

AUGOOD, C. A., VINGERLING, J. R., DE JONG, P. T., CHAKRAVARTHY, U., SELAND, J., SOUBRANE, G., TOMAZZOLI, L., TOPOUZIS, F., BENTHAM, G., RAHU, M., VIOQUE, J.,

YOUNG, I. S. & FLETCHER, A. E. 2006. Prevalence of age-related maculopathy in older Europeans: the European Eye Study (EUREYE). *Arch Ophthalmol,* 124**,** 529-35.
AYE, K. H., GUPTA, R., TALKS, S. J. & BROWNING, A. C. 2010. Treatment of a choroidal neovascular membrane in a patient with late-onset retinal degeneration (L-ORD) with intravitreal ranibizumab. *Eye (Lond),* 24**,** 1528-30.
AYYAGARI, R., GRIESINGER, I. B., BINGHAM, E., LARK, K. K., MOROI, S. E. & SIEVING, P. A. 2000. Autosomal dominant hemorrhagic macular dystrophy not associated with the TIMP3 gene. *Arch Ophthalmol,* 118**,** 85-92.
AYYAGARI, R., MANDAL, M. N., KAROUKIS, A. J., CHEN, L., MCLAREN, N. C., LICHTER, M., WONG, D. T., HITCHCOCK, P. F., CARUSO, R. C., MOROI, S. E., MAUMENEE, I. H. & SIEVING, P. A. 2005. Late-onset macular degeneration and long anterior lens zonules result from a CTRP5 gene mutation. *Invest Ophthalmol Vis Sci,* 46**,** 3363-71.
BAILEY, I. L. & LOVIE, J. E. 1980. The design and use of a new near-vision chart. *Am J Optom Physiol Opt,* 57**,** 378-87.
BAINBRIDGE, J. W., SMITH, A. J., BARKER, S. S., ROBBIE, S., HENDERSON, R., BALAGGAN, K., VISWANATHAN, A., HOLDER, G. E., STOCKMAN, A. & TYLER, N. 2008. Effect of gene therapy on visual function in Leber's congenital amaurosis. *New England Journal of Medicine,* 358**,** 2231-2239.
BAIRATI, A., JR. & ORZALESI, N. 1963. The Ultrastructure of the Pigment Epithelium and of the Photoreceptor-Pigment Epithelium Junction in the Human Retina. *J Ultrastruct Res,* 41**,** 484-96.
BAIRD, P. N., GUIDA, E., CHU, D. T., VU, H. T. & GUYMER, R. H. 2004. The epsilon2 and epsilon4 alleles of the apolipoprotein gene are associated with age-related macular degeneration. *Invest Ophthalmol Vis Sci,* 45**,** 1311-5.
BAIRD, P. N., ISLAM, F. M., RICHARDSON, A. J., CAIN, M., HUNT, N. & GUYMER, R. 2006. Analysis of the Y402H variant of the complement factor H gene in age-related macular degeneration. *Invest Ophthalmol Vis Sci,* 47**,** 4194-8.
BAKONDI, B., LV, W., LU, B., JONES, M. K., TSAI, Y., KIM, K. J., LEVY, R., AKHTAR, A. A., BREUNIG, J. J. & SVENDSEN, C. N. 2015. In Vivo CRISPR/Cas9 Gene Editing Corrects Retinal Dystrophy in the S334ter-3 Rat Model of Autosomal Dominant Retinitis Pigmentosa. *Molecular Therapy*.
BANITO, A., RASHID, S. T., ACOSTA, J. C., LI, S., PEREIRA, C. F., GETI, I., PINHO, S., SILVA, J. C., AZUARA, V., WALSH, M., VALLIER, L. & GIL, J. 2009. Senescence impairs successful reprogramming to pluripotent stem cells. *Genes Dev,* 23**,** 2134-9.

BAR-NUR, O., RUSS, H. A., EFRAT, S. & BENVENISTY, N. 2011. Epigenetic memory and preferential lineage-specific differentiation in induced pluripotent stem cells derived from human pancreatic islet beta cells. *Cell Stem Cell,* 9**,** 17-23.

BAZAN, N. G., GORDON, W. C. & RODRIGUEZ DE TURCO, E. B. 1992. Docosahexaenoic acid uptake and metabolism in photoreceptors: retinal conservation by an efficient retinal pigment epithelial cell-mediated recycling process. *Adv Exp Med Biol,* 318**,** 295-306.

BELLIN, M., MARCHETTO, M. C., GAGE, F. H. & MUMMERY, C. L. 2012. Induced pluripotent stem cells: the new patient? *Nat Rev Mol Cell Biol,* 13**,** 713-26.

BELLMANN, C., HOLZ, F. G., SCHAPP, O., VOLCKER, H. E. & OTTO, T. P. 1997. [Topography of fundus autofluorescence with a new confocal scanning laser ophthalmoscope]. *Ophthalmologe,* 94**,** 385-91.

BEN-DAVID, U., MAYSHAR, Y. & BENVENISTY, N. 2011. Large-scale analysis reveals acquisition of lineage-specific chromosomal aberrations in human adult stem cells. *Cell Stem Cell,* 9**,** 97-102.

BERMAN, K. & BRODATY, H. 2006. Psychosocial effects of age-related macular degeneration. *Int Psychogeriatr,* 18**,** 415-28.

BERNER, A., MOHAN, K., LOU, D.-Y., BROWN, J., WEST, J., KONO, R., SUGINO, I. K., ZARBIN, M. A., AMBATI, J. & KLEINMAN, M. E. 2014. RPE Cytotoxicity and Caspase Activation after Treatment with Valproic Acid. *Investigative Ophthalmology & Visual Science,* 55**,** 5991-5991.

BILL, A., SPERBER, G. & UJIIE, K. 1983. Physiology of the choroidal vascular bed. *Int Ophthalmol,* 6**,** 101-7.

BINDEWALD, A., SCHMITZ-VALCKENBERG, S., JORZIK, J. J., DOLAR-SZCZASNY, J., SIEBER, H., KEILHAUER, C., WEINBERGER, A. W., DITHMAR, S., PAULEIKHOFF, D., MANSMANN, U., WOLF, S. & HOLZ, F. G. 2005. Classification of abnormal fundus autofluorescence patterns in the junctional zone of geographic atrophy in patients with age related macular degeneration. *Br J Ophthalmol,* 89**,** 874-8.

BLENKINSOP, T. A., SAINI, J. S., MAMINISHKIS, A., BHARTI, K., WAN, Q., BANZON, T., LOTFI, M., DAVIS, J., SINGH, D., RIZZOLO, L. J., MILLER, S., TEMPLE, S. & STERN, J. H. 2015. Human Adult Retinal Pigment Epithelial Stem Cell-Derived RPE Monolayers Exhibit Key Physiological Characteristics of Native Tissue. *Invest Ophthalmol Vis Sci,* 56**,** 7085-99.

BONOMINI, F., FILIPPINI, F., HAYEK, T., AVIRAM, M., KEIDAR, S., RODELLA, L. F., COLEMAN, R. & REZZANI, R. 2010. Apolipoprotein E and its role in aging and survival. *Exp Gerontol,* 45**,** 149-57.

BOROOAH, S., COLLINS, C., WRIGHT, A. & DHILLON, B. 2009. Late-onset retinal macular degeneration: clinical insights into an inherited retinal degeneration. *Br J Ophthalmol,* 93**,** 284-9.

BOTTONI, F. G., AANDEKERK, A. L. & DEUTMAN, A. F. 1994. Clinical application of digital indocyanine green videoangiography in senile macular degeneration. *Graefes Arch Clin Exp Ophthalmol,* 232**,** 458-68.

BOUCHENAKI, N., CIMINO, L., AUER, C., TAO TRAN, V. & HERBORT, C. P. 2002. Assessment and classification of choroidal vasculitis in posterior uveitis using indocyanine green angiography. *Klin Monbl Augenheilkd,* 219**,** 243-9.

BROWN, D. I. & GRIENDLING, K. K. 2009. Nox proteins in signal transduction. *Free Radic Biol Med,* 47**,** 1239-53.

BUCHHOLZ, D. E., HIKITA, S. T., ROWLAND, T. J., FRIEDRICH, A. M., HINMAN, C. R., JOHNSON, L. V. & CLEGG, D. O. 2009. Derivation of functional retinal pigmented epithelium from induced pluripotent stem cells. *Stem Cells,* 27**,** 2427-34.

BUNT-MILAM, A. H. & SAARI, J. C. 1983. Immunocytochemical localization of two retinoid-binding proteins in vertebrate retina. *J Cell Biol,* 97**,** 703-12.

BURNS, M. S. & HARTZ, M. J. 1992. The retinal pigment epithelium induces fenestration of endothelial cells in vivo. *Curr Eye Res,* 11**,** 863-73.

CAMPION, D., DUMANCHIN, C., HANNEQUIN, D., DUBOIS, B., BELLIARD, S., PUEL, M., THOMAS-ANTERION, C., MICHON, A., MARTIN, C., CHARBONNIER, F., RAUX, G., CAMUZAT, A., PENET, C., MESNAGE, V., MARTINEZ, M., CLERGET-DARPOUX, F., BRICE, A. & FREBOURG, T. 1999. Early-onset autosomal dominant Alzheimer disease: prevalence, genetic heterogeneity, and mutation spectrum. *Am J Hum Genet,* 65**,** 664-70.

CAMPOCHIARO, P. A., HACKETT, S. F., VINORES, S. A., FREUND, J., CSAKY, C., LAROCHELLE, W., HENDERER, J., JOHNSON, M., RODRIGUEZ, I. R., FRIEDMAN, Z. & ET AL. 1994. Platelet-derived growth factor is an autocrine growth stimulator in retinal pigmented epithelial cells. *J Cell Sci,* 107 (Pt 9)**,** 2459-69.

CANO, M., WANG, L., WAN, J., BARNETT, B. P., EBRAHIMI, K., QIAN, J. & HANDA, J. T. 2014. Oxidative stress induces mitochondrial dysfunction and a protective unfolded protein response in RPE cells. *Free Radic Biol Med,* 69**,** 1-14.

CAO, W., TOMBRAN-TINK, J., ELIAS, R., SEZATE, S., MRAZEK, D. & MCGINNIS, J. F. 2001. In vivo protection of photoreceptors from light damage by pigment epithelium-derived factor. *Invest Ophthalmol Vis Sci,* 42**,** 1646-52.

CAO, W., WEN, R., LI, F., LAVAIL, M. M. & STEINBERG, R. H. 1997. Mechanical injury increases bFGF and CNTF mRNA expression in the mouse retina. *Exp Eye Res,* 65**,** 241-8.

CARR, A. J., VUGLER, A. A., HIKITA, S. T., LAWRENCE, J. M., GIAS, C., CHEN, L. L., BUCHHOLZ, D. E., AHMADO, A., SEMO, M., SMART, M. J., HASAN, S., DA CRUZ, L., JOHNSON, L. V., CLEGG, D. O. & COFFEY, P. J. 2009. Protective effects of human iPS-derived retinal pigment epithelium cell transplantation in the retinal dystrophic rat. *PLoS One,* 4**,** e8152.

CERESO, N., PEQUIGNOT, M. O., ROBERT, L., BECKER, F., DE LUCA, V., NABHOLZ, N., RIGAU, V., DE VOS, J., HAMEL, C. P. & KALATZIS, V. 2014. Proof of concept for AAV2/5-mediated gene therapy in iPSC-derived retinal pigment epithelium of a choroideremia patient. *Mol Ther Methods Clin Dev,* 1**,** 14011.

CHAKRAVARTHY, U., WONG, T. Y., FLETCHER, A., PIAULT, E., EVANS, C., ZLATEVA, G., BUGGAGE, R., PLEIL, A. & MITCHELL, P. 2010. Clinical risk factors for age-related macular degeneration: a systematic review and meta-analysis. *BMC Ophthalmol,* 10**,** 31.

CHAMBERS, S. M., FASANO, C. A., PAPAPETROU, E. P., TOMISHIMA, M., SADELAIN, M. & STUDER, L. 2009. Highly efficient neural conversion of human ES and iPS cells by dual inhibition of SMAD signaling. *Nat Biotechnol,* 27**,** 275-80.

CHANG, B., HURD, R., WANG, J. & NISHINA, P. 2013. Survey of common eye diseases in laboratory mouse strains. *Invest Ophthalmol Vis Sci,* 54**,** 4974-81.

CHAVALI, V. R., KHAN, N. W., CUKRAS, C. A., BARTSCH, D. U., JABLONSKI, M. M. & AYYAGARI, R. 2011. A CTRP5 gene S163R mutation knock-in mouse model for late-onset retinal degeneration. *Hum Mol Genet,* 20**,** 2000-14.

CHAVALI, V. R., SAHU, B., BARTSCH,D., BANSAL, T., CURCIO, C.A., MILLER, S., JABLONKSI, M., AYYAGARI, R. 2012. Absence Of Ctrp5/c1qtnf5 Leads To RPE Degeneration In Ctrp5 Gene Knock-out Mice. *IOVS,* 53**,** 308.

CHAVALI, V. R., VASIREDDY, V. & AYYAGARI, R. 2012. Silencing the expression of CTRP5/C1QTNF5 and ELOVL4 genes by small interfering RNA. *Adv Exp Med Biol,* 723**,** 225-33.

CHEN, Y., HU, Y., LU, K., FLANNERY, J. G. & MA, J. X. 2007. Very low density lipoprotein receptor, a negative regulator of the wnt signaling pathway and choroidal neovascularization. *J Biol Chem,* 282**,** 34420-8.

CHEW, E. Y., CLEMONS, T. E., AGRON, E., SPERDUTO, R. D., SANGIOVANNI, J. P., DAVIS, M. D., FERRIS, F. L., 3RD & AGE-RELATED EYE DISEASE STUDY RESEARCH, G. 2014. Ten-year follow-up of age-related macular degeneration in the age-related eye disease study: AREDS report no. 36. *JAMA Ophthalmol,* 132**,** 272-7.

CHIHARA, E. & NAO-I, N. 1985. Resorption of subretinal fluid by transepithelial flow of the retinal pigment epithelium. *Graefes Arch Clin Exp Ophthalmol,* 223**,** 202-4.

CHONG, N. H., KEONIN, J., LUTHERT, P. J., FRENNESSON, C. I., WEINGEIST, D. M., WOLF, R. L., MULLINS, R. F. & HAGEMAN, G. S. 2005. Decreased thickness and integrity of the macular elastic layer of Bruch's membrane correspond to the distribution of lesions associated with age-related macular degeneration. *Am J Pathol,* 166**,** 241-51.

CHURCHILL, A. J., CARTER, J. G., LOVELL, H. C., RAMSDEN, C., TURNER, S. J., YEUNG, A., ESCARDO, J. & ATAN, D. 2006. VEGF polymorphisms are associated with neovascular age-related macular degeneration. *Hum Mol Genet,* 15**,** 2955-61.

CLARK, S. J., HIGMAN, V. A., MULLOY, B., PERKINS, S. J., LEA, S. M., SIM, R. B. & DAY, A. J. 2006. His-384 allotypic variant of factor H associated with age-related macular degeneration has different heparin binding properties from the non-disease-associated form. *J Biol Chem,* 281**,** 24713-20.

CLARK, S. J., PERVEEN, R., HAKOBYAN, S., MORGAN, B. P., SIM, R. B., BISHOP, P. N. & DAY, A. J. 2010. Impaired binding of the age-related macular degeneration-associated complement factor H 402H allotype to Bruch's membrane in human retina. *Journal of Biological Chemistry,* 285**,** 30192-30202.

CLAUSEN, T., KAISER, M., HUBER, R. & EHRMANN, M. 2011. HTRA proteases: regulated proteolysis in protein quality control. *Nat Rev Mol Cell Biol,* 12**,** 152-62.

COFFEY, P. J., GIAS, C., MCDERMOTT, C. J., LUNDH, P., PICKERING, M. C., SETHI, C., BIRD, A., FITZKE, F. W., MAASS, A., CHEN, L. L., HOLDER, G. E., LUTHERT, P. J., SALT, T. E., MOSS, S. E. & GREENWOOD, J. 2007. Complement factor H deficiency in aged mice causes retinal abnormalities and visual dysfunction. *Proc Natl Acad Sci U S A,* 104**,** 16651-6.

CONG, L., RAN, F. A., COX, D., LIN, S., BARRETTO, R., HABIB, N., HSU, P. D., WU, X., JIANG, W. & MARRAFFINI, L. A. 2013a. Multiplex genome engineering using CRISPR/Cas systems. *Science,* 339**,** 819-823.

CONG, L., RAN, F. A., COX, D., LIN, S., BARRETTO, R., HABIB, N., HSU, P. D., WU, X., JIANG, W., MARRAFFINI, L. A. & ZHANG, F. 2013b. Multiplex genome engineering using CRISPR/Cas systems. *Science,* 339**,** 819-23.

CRABB, J. W., MIYAGI, M., GU, X., SHADRACH, K., WEST, K. A., SAKAGUCHI, H., KAMEI, M., HASAN, A., YAN, L., RAYBORN, M. E., SALOMON, R. G. & HOLLYFIELD, J. G. 2002. Drusen proteome analysis: an approach to the etiology of age-related macular degeneration. *Proc Natl Acad Sci U S A,* 99**,** 14682-7.

CRISWELL, M. H., CIULLA, T. A., HILL, T. E., SMALL, W., DANIS, R. P., SNYDER, W. J., LOWSETH, L. A. & CARSON, D. L. 2004. The squirrel monkey: characterization of a new-world primate model of experimental choroidal neovascularization and comparison with the macaque. *Invest Ophthalmol Vis Sci,* 45**,** 625-34.

CURCIO, C. A., MEDEIROS, N. E. & MILLICAN, C. L. 1996. Photoreceptor loss in age-related macular degeneration. *Invest Ophthalmol Vis Sci,* 37**,** 1236-49.

CURCIO, C. A., MESSINGER, J. D., SLOAN, K. R., MCGWIN, G., MEDEIROS, N. E. & SPAIDE, R. F. 2013. Subretinal drusenoid deposits in non-neovascular age-related macular degeneration: morphology, prevalence, topography, and biogenesis model. *Retina,* 33**,** 265-76.

CURCIO, C. A. & MILLICAN, C. L. 1999. Basal linear deposit and large drusen are specific for early age-related maculopathy. *Arch Ophthalmol,* 117**,** 329-39.

DAGHESTANI, H. N. & DAY, B. W. 2010. Theory and applications of surface plasmon resonance, resonant mirror, resonant waveguide grating, and dual polarization interferometry biosensors. *Sensors (Basel),* 10**,** 9630-46.
DAVIS, M. D., GANGNON, R. E., LEE, L. Y., HUBBARD, L. D., KLEIN, B. E., KLEIN, R., FERRIS, F. L., BRESSLER, S. B., MILTON, R. C. & AGE-RELATED EYE DISEASE STUDY, G. 2005. The Age-Related Eye Disease Study severity scale for age-related macular degeneration: AREDS Report No. 17. *Arch Ophthalmol,* 123**,** 1484-98.
DAWSON, D. W., VOLPERT, O. V., GILLIS, P., CRAWFORD, S. E., XU, H., BENEDICT, W. & BOUCK, N. P. 1999. Pigment epithelium-derived factor: a potent inhibitor of angiogenesis. *Science,* 285**,** 245-8.
DE BATS, F., WOLFF, B., MAUGET-FAYSSE, M., MEUNIER, I., DENIS, P. & KODJIKIAN, L. 2013. Association of reticular pseudodrusen and early onset drusen. *ISRN Ophthalmol,* 2013**,** 273085.
DEANGELIS, M. M., JI, F., KIM, I. K., ADAMS, S., CAPONE, A., JR., OTT, J., MILLER, J. W. & DRYJA, T. P. 2007. Cigarette smoking, CFH, APOE, ELOVL4, and risk of neovascular age-related macular degeneration. *Arch Ophthalmol,* 125**,** 49-54.
DELORI, F. C., DOREY, C. K., STAURENGHI, G., AREND, O., GOGER, D. G. & WEITER, J. J. 1995. In vivo fluorescence of the ocular fundus exhibits retinal pigment epithelium lipofuscin characteristics. *Invest Ophthalmol Vis Sci,* 36**,** 718-29.
DHILLON, B., WRIGHT, A. F., TUFAIL, A., PAPPWORTH, I., HAYWARD, C., MOORE, I., STRAIN, L., KAVANAGH, D., BARLOW, P. N., HERBERT, A. P., SCHMIDT, C. Q., ARMBRECHT, A. M., LAUDE, A., DEARY, I. J., STANIFORTH, S. J., HOLMES, L. V., GOODSHIP, T. H. & MARCHBANK, K. J. 2010. Complement factor h autoantibodies and age-related macular degeneration. *Invest Ophthalmol Vis Sci,* 51**,** 5858-63.
DI GIORGIO, F. P., CARRASCO, M. A., SIAO, M. C., MANIATIS, T. & EGGAN, K. 2007. Non-cell autonomous effect of glia on motor neurons in an embryonic stem cell-based ALS model. *Nat Neurosci,* 10**,** 608-14.
DINCULESCU, A., MIN, S. H., DYKA, F. M., DENG, W. T., STUPAY, R. M., CHIODO, V., SMITH, W. C. & HAUSWIRTH, W. W. 2015. Pathological Effects of Mutant C1QTNF5 (S163R) Expression in Murine Retinal Pigment Epithelium. *Invest Ophthalmol Vis Sci,* 56**,** 6971-80.
DITHMAR, S., SHARARA, N. A., CURCIO, C. A., LE, N. A., ZHANG, Y., BROWN, S. & GROSSNIKLAUS, H. E. 2001. Murine high-fat diet and laser photochemical model of basal deposits in Bruch membrane. *Arch Ophthalmol,* 119**,** 1643-9.
DIXON, S. J. & STOCKWELL, B. R. 2014. The role of iron and reactive oxygen species in cell death. *Nat Chem Biol,* 10**,** 9-17.

DOREY, C. K., WU, G., EBENSTEIN, D., GARSD, A. & WEITER, J. J. 1989. Cell loss in the aging retina. Relationship to lipofuscin accumulation and macular degeneration. *Invest Ophthalmol Vis Sci,* 30**,** 1691-9.
DUVALL, J., MCKECHNIE, N. M., LEE, W. R., ROTHERY, S. & MARSHALL, J. 1986. Extensive subretinal pigment epithelial deposit in two brothers suffering from dominant retinitis pigmentosa. A histopathological study. *Graefes Arch Clin Exp Ophthalmol,* 224**,** 299-309.
EBRAHIMI, K. B., FIJALKOWSKI, N., CANO, M. & HANDA, J. T. 2013. Decreased membrane complement regulators in the retinal pigmented epithelium contributes to age-related macular degeneration. *J Pathol,* 229**,** 729-42.
EDWARDS, A. O., RITTER, R., 3RD, ABEL, K. J., MANNING, A., PANHUYSEN, C. & FARRER, L. A. 2005. Complement factor H polymorphism and age-related macular degeneration. *Science,* 308**,** 421-4.
EDWARDS, R. B. & FLAHERTY, P. M. 1986. Association of changes in intracellular cyclic AMP with changes in phagocytosis in cultured rat pigment epithelium. *Curr Eye Res,* 5**,** 19-26.
ELIZABETH RAKOCZY, P., YU, M. J., NUSINOWITZ, S., CHANG, B. & HECKENLIVELY, J. R. 2006. Mouse models of age-related macular degeneration. *Exp Eye Res,* 82**,** 741-52.
ENNIS, S., JOMARY, C., MULLINS, R., CREE, A., CHEN, X., MACLEOD, A., JONES, S., COLLINS, A., STONE, E. & LOTERY, A. 2008. Association between the SERPING1 gene and age-related macular degeneration: a two-stage case-control study. *Lancet,* 372**,** 1828-34.
EVANS, J. & WORMALD, R. 1996. Is the incidence of registrable age-related macular degeneration increasing? *Br J Ophthalmol,* 80**,** 9-14.
FARKAS, T. G., SYLVESTER, V., ARCHER, D. & ALTONA, M. 1971. The histochemistry of drusen. *Am J Ophthalmol,* 71**,** 1206-15.
FEENEY-BURNS, L., BERMAN, E. R. & ROTHMAN, H. 1980. Lipofuscin of human retinal pigment epithelium. *Am J Ophthalmol,* 90**,** 783-91.
FERNANDEZ-GODINO, R., GARLAND, D. L. & PIERCE, E. A. 2015. A local complement response by RPE causes early-stage macular degeneration. *Hum Mol Genet,* 24**,** 5555-69.
FERRIS, F. L., 3RD, KASSOFF, A., BRESNICK, G. H. & BAILEY, I. 1982. New visual acuity charts for clinical research. *Am J Ophthalmol,* 94**,** 91-6.
FERRIS, F. L., DAVIS, M. D., CLEMONS, T. E., LEE, L. Y., CHEW, E. Y., LINDBLAD, A. S., MILTON, R. C., BRESSLER, S. B., KLEIN, R. & AGE-RELATED EYE DISEASE STUDY RESEARCH, G. 2005. A simplified severity scale for age-related macular degeneration: AREDS Report No. 18. *Arch Ophthalmol,* 123**,** 1570-4.
FINGER, R. P., WU, Z., LUU, C. D., KEARNEY, F., AYTON, L. N., LUCCI, L. M., HUBBARD, W. C., HAGEMAN, J. L., HAGEMAN, G. S. & GUYMER, R. H. 2014. Reticular

pseudodrusen: a risk factor for geographic atrophy in fellow eyes of individuals with unilateral choroidal neovascularization. *Ophthalmology,* 121**,** 1252-6.
FINNEMANN, S. C., BONILHA, V. L., MARMORSTEIN, A. D. & RODRIGUEZ-BOULAN, E. 1997. Phagocytosis of rod outer segments by retinal pigment epithelial cells requires alpha(v)beta5 integrin for binding but not for internalization. *Proc Natl Acad Sci U S A,* 94**,** 12932-7.
FINNEMANN, S. C., LEUNG, L. W. & RODRIGUEZ-BOULAN, E. 2002. The lipofuscin component A2E selectively inhibits phagolysosomal degradation of photoreceptor phospholipid by the retinal pigment epithelium. *Proc Natl Acad Sci U S A,* 99**,** 3842-7.
FLAMENDORF, J., AGRON, E., WONG, W. T., THOMPSON, D., WILEY, H. E., DOSS, E. L., AL-HOLOU, S., FERRIS, F. L., 3RD, CHEW, E. Y. & CUKRAS, C. 2015. Impairments in Dark Adaptation Are Associated with Age-Related Macular Degeneration Severity and Reticular Pseudodrusen. *Ophthalmology,* 122**,** 2053-62.
FLECKENSTEIN, M., ADRION, C., SCHMITZ-VALCKENBERG, S., GOBEL, A. P., BINDEWALD-WITTICH, A., SCHOLL, H. P., MANSMANN, U., HOLZ, F. G. & GROUP, F. A. M. S. 2010. Concordance of disease progression in bilateral geographic atrophy due to AMD. *Invest Ophthalmol Vis Sci,* 51**,** 637-42.
FLECKENSTEIN, M., SCHMITZ-VALCKENBERG, S., ADRION, C., VISVALINGAM, S., GOBEL, A. P., MOSSNER, A., VON STRACHWITZ, C. N., MACKENSEN, F., PAULEIKHOFF, D., WOLF, S., MANSMANN, U., HOLZ, F. G. & GROUP, F. A. M. S. 2011. Progression of age-related geographic atrophy: role of the fellow eye. *Invest Ophthalmol Vis Sci,* 52**,** 6552-7.
FONG, S. L., LIOU, G. I., LANDERS, R. A., ALVAREZ, R. A. & BRIDGES, C. D. 1984. Purification and characterization of a retinol-binding glycoprotein synthesized and secreted by bovine neural retina. *J Biol Chem,* 259**,** 6534-42.
FRIEDMAN, D. S., O'COLMAIN, B. J., MUNOZ, B., TOMANY, S. C., MCCARTY, C., DE JONG, P. T., NEMESURE, B., MITCHELL, P., KEMPEN, J. & EYE DISEASES PREVALENCE RESEARCH, G. 2004. Prevalence of age-related macular degeneration in the United States. *Arch Ophthalmol,* 122**,** 564-72.
FRITSCHE, L. G., IGL, W., BAILEY, J. N., GRASSMANN, F., SENGUPTA, S., BRAGG-GRESHAM, J. L., BURDON, K. P., HEBBRING, S. J., WEN, C., GORSKI, M., KIM, I. K., CHO, D., ZACK, D., SOUIED, E., SCHOLL, H. P., BALA, E., LEE, K. E., HUNTER, D. J., SARDELL, R. J., MITCHELL, P., MERRIAM, J. E., CIPRIANI, V., HOFFMAN, J. D., SCHICK, T., LECHANTEUR, Y. T., GUYMER, R. H., JOHNSON, M. P., JIANG, Y., STANTON, C. M., BUITENDIJK, G. H., ZHAN, X., KWONG, A. M., BOLEDA, A., BROOKS, M., GIESER, L., RATNAPRIYA, R., BRANHAM, K. E., FOERSTER, J. R., HECKENLIVELY, J. R., OTHMAN, M. I., VOTE, B. J., LIANG, H. H., SOUZEAU, E., MCALLISTER, I. L., ISAACS, T., HALL, J.,

LAKE, S., MACKEY, D. A., CONSTABLE, I. J., CRAIG, J. E., KITCHNER, T. E., YANG, Z., SU, Z., LUO, H., CHEN, D., OUYANG, H., FLAGG, K., LIN, D., MAO, G., FERREYRA, H., STARK, K., VON STRACHWITZ, C. N., WOLF, A., BRANDL, C., RUDOLPH, G., OLDEN, M., MORRISON, M. A., MORGAN, D. J., SCHU, M., AHN, J., SILVESTRI, G., TSIRONI, E. E., PARK, K. H., FARRER, L. A., ORLIN, A., BRUCKER, A., LI, M., CURCIO, C. A., MOHAND-SAID, S., SAHEL, J. A., AUDO, I., BENCHABOUNE, M., CREE, A. J., RENNIE, C. A., GOVERDHAN, S. V., GRUNIN, M., HAGBI-LEVI, S., CAMPOCHIARO, P., KATSANIS, N., HOLZ, F. G., BLOND, F., BLANCHE, H., DELEUZE, J. F., IGO, R. P., JR., TRUITT, B., PEACHEY, N. S., MEUER, S. M., MYERS, C. E., MOORE, E. L., KLEIN, R., et al. 2016. A large genome-wide association study of age-related macular degeneration highlights contributions of rare and common variants. *Nat Genet,* 48**,** 134-43.

FRITSCHE, L. G., LOENHARDT, T., JANSSEN, A., FISHER, S. A., RIVERA, A., KEILHAUER, C. N. & WEBER, B. H. 2008. Age-related macular degeneration is associated with an unstable ARMS2 (LOC387715) mRNA. *Nat Genet,* 40**,** 892-6.

FU, L., GARLAND, D., YANG, Z., SHUKLA, D., RAJENDRAN, A., PEARSON, E., STONE, E. M., ZHANG, K. & PIERCE, E. A. 2007. The R345W mutation in EFEMP1 is pathogenic and causes AMD-like deposits in mice. *Hum Mol Genet,* 16**,** 2411-22.

GABORIAUD, C., THIELENS, N. M., GREGORY, L. A., ROSSI, V., FONTECILLA-CAMPS, J. C. & ARLAUD, G. J. 2004. Structure and activation of the C1 complex of complement: unraveling the puzzle. *Trends Immunol,* 25**,** 368-73.

GAMM, D. M., WRIGHT, L. S., CAPOWSKI, E. E., SHEARER, R. L., MEYER, J. S., KIM, H. J., SCHNEIDER, B. L., MELVAN, J. N. & SVENDSEN, C. N. 2008. Regulation of prenatal human retinal neurosphere growth and cell fate potential by retinal pigment epithelium and Mash1. *Stem Cells,* 26**,** 3182-93.

GARCIA, T. Y., GUTIERREZ, M., REYNOLDS, J. & LAMBA, D. A. 2015. Modeling the Dynamic AMD-Associated Chronic Oxidative Stress Changes in Human ESC and iPSC-Derived RPE Cells. *Invest Ophthalmol Vis Sci,* 56**,** 7480-8.

GARG, A., OLL, M., YZER, S., CHANG, S., BARILE, G. R., MERRIAM, J. C., TSANG, S. H. & BEARELLY, S. 2013. Reticular pseudodrusen in early age-related macular degeneration are associated with choroidal thinning. *Invest Ophthalmol Vis Sci,* 54**,** 7075-81.

GARLAND, D. L., FERNANDEZ-GODINO, R., KAUR, I., SPEICHER, K. D., HARNLY, J. M., LAMBRIS, J. D., SPEICHER, D. W. & PIERCE, E. A. 2014a. Mouse genetics and proteomic analyses demonstrate a critical role for complement in a model of DHRD/ML, an inherited macular degeneration. *Hum Mol Genet,* 23**,** 52-68.

GARLAND, D. L., FERNANDEZ-GODINO, R., KAUR, I., SPEICHER, K. D., HARNLY, J. M., LAMBRIS, J. D., SPEICHER, D. W. & PIERCE, E. A. 2014b. Mouse genetics and proteomic

analyses demonstrate a critical role for complement in a model of DHRD/ML, an inherited macular degeneration. *Human molecular genetics,* 23**,** 52-68.
GASS, J. D. 1972. Drusen and disciform macular detachment and degeneration. *Trans Am Ophthalmol Soc,* 70**,** 409-36.
GEORGIANNAKIS, A., BURGOYNE, T., LUECK, K., FUTTER, C., GREENWOOD, J. & MOSS, S. E. 2015. Retinal Pigment Epithelial Cells Mitigate the Effects of Complement Attack by Endocytosis of C5b-9. *J Immunol,* 195**,** 3382-9.
GIANNAKIS, E., JOKIRANTA, T. S., MALE, D. A., RANGANATHAN, S., ORMSBY, R. J., FISCHETTI, V. A., MOLD, C. & GORDON, D. L. 2003. A common site within factor H SCR 7 responsible for binding heparin, C-reactive protein and streptococcal M protein. *European journal of immunology,* 33**,** 962-969.
GOLD, B., MERRIAM, J. E., ZERNANT, J., HANCOX, L. S., TAIBER, A. J., GEHRS, K., CRAMER, K., NEEL, J., BERGERON, J., BARILE, G. R., SMITH, R. T., GROUP, A. M. D. G. C. S., HAGEMAN, G. S., DEAN, M. & ALLIKMETS, R. 2006. Variation in factor B (BF) and complement component 2 (C2) genes is associated with age-related macular degeneration. *Nat Genet,* 38**,** 458-62.
GONZALEZ-CORDERO, A., WEST, E. L., PEARSON, R. A., DURAN, Y., CARVALHO, L. S., CHU, C. J., NAEEM, A., BLACKFORD, S. J., GEORGIADIS, A., LAKOWSKI, J., HUBANK, M., SMITH, A. J., BAINBRIDGE, J. W., SOWDEN, J. C. & ALI, R. R. 2013. Photoreceptor precursors derived from three-dimensional embryonic stem cell cultures integrate and mature within adult degenerate retina. *Nat Biotechnol,* 31**,** 741-7.
GOURAS, P., IVERT, L., LANDAUER, N., MATTISON, J. A., INGRAM, D. K. & NEURINGER, M. 2008. Drusenoid maculopathy in rhesus monkeys (Macaca mulatta): effects of age and gender. *Graefes Arch Clin Exp Ophthalmol,* 246**,** 1395-402.
GREEN, W. R. & ENGER, C. 1993. Age-related macular degeneration histopathologic studies. The 1992 Lorenz E. Zimmerman Lecture. *Ophthalmology,* 100**,** 1519-35.
GROSSNIKLAUS, H. E. & GREEN, W. R. 2004. Choroidal neovascularization. *Am J Ophthalmol,* 137**,** 496-503.
GURDON, J. B. 1962. The developmental capacity of nuclei taken from intestinal epithelium cells of feeding tadpoles. *J Embryol Exp Morphol,* 10**,** 622-40.
GURNE, D. H., TSO, M. O., EDWARD, D. P. & RIPPS, H. 1991. Antiretinal antibodies in serum of patients with age-related macular degeneration. *Ophthalmology,* 98**,** 602-7.
HAGEMAN, G. S., ANDERSON, D. H., JOHNSON, L. V., HANCOX, L. S., TAIBER, A. J., HARDISTY, L. I., HAGEMAN, J. L., STOCKMAN, H. A., BORCHARDT, J. D., GEHRS, K. M., SMITH, R. J., SILVESTRI, G., RUSSELL, S. R., KLAVER, C. C., BARBAZETTO, I., CHANG, S., YANNUZZI, L. A., BARILE, G. R., MERRIAM, J. C., SMITH, R. T., OLSH, A. K.,

BERGERON, J., ZERNANT, J., MERRIAM, J. E., GOLD, B., DEAN, M. & ALLIKMETS, R. 2005. A common haplotype in the complement regulatory gene factor H (HF1/CFH) predisposes individuals to age-related macular degeneration. *Proc Natl Acad Sci U S A,* 102**,** 7227-32.

HAGEMAN, G. S., HANCOX, L. S., TAIBER, A. J., GEHRS, K. M., ANDERSON, D. H., JOHNSON, L. V., RADEKE, M. J., KAVANAGH, D., RICHARDS, A., ATKINSON, J., MERI, S., BERGERON, J., ZERNANT, J., MERRIAM, J., GOLD, B., ALLIKMETS, R., DEAN, M. & GROUP, A. M. D. C. S. 2006. Extended haplotypes in the complement factor H (CFH) and CFH-related (CFHR) family of genes protect against age-related macular degeneration: characterization, ethnic distribution and evolutionary implications. *Ann Med,* 38**,** 592-604.

HAGEMAN, G. S., LUTHERT, P. J., VICTOR CHONG, N. H., JOHNSON, L. V., ANDERSON, D. H. & MULLINS, R. F. 2001. An integrated hypothesis that considers drusen as biomarkers of immune-mediated processes at the RPE-Bruch's membrane interface in aging and age-related macular degeneration. *Prog Retin Eye Res,* 20**,** 705-32.

HAGEMAN, G. S. & MULLINS, R. F. 1999a. Molecular composition of drusen as related to substructural phenotype. *Mol Vis,* 5**,** 28.

HAGEMAN, G. S. & MULLINS, R. F. 1999b. Molecular composition of drusen as related to substructural phenotype. *Mol Vis,* 5**,** b71.

HAIMOVICI, R., OWENS, S. L., FITZKE, F. W. & BIRD, A. C. 2002. Dark adaptation in age-related macular degeneration: relationship to the fellow eye. *Graefes Arch Clin Exp Ophthalmol,* 240**,** 90-5.

HAINES, J. L., HAUSER, M. A., SCHMIDT, S., SCOTT, W. K., OLSON, L. M., GALLINS, P., SPENCER, K. L., KWAN, S. Y., NOUREDDINE, M., GILBERT, J. R., SCHNETZ-BOUTAUD, N., AGARWAL, A., POSTEL, E. A. & PERICAK-VANCE, M. A. 2005. Complement factor H variant increases the risk of age-related macular degeneration. *Science,* 308**,** 419-21.

HAINES, J. L., SCHNETZ-BOUTAUD, N., SCHMIDT, S., SCOTT, W. K., AGARWAL, A., POSTEL, E. A., OLSON, L., KENEALY, S. J., HAUSER, M., GILBERT, J. R. & PERICAK-VANCE, M. A. 2006. Functional candidate genes in age-related macular degeneration: significant association with VEGF, VLDLR, and LRP6. *Invest Ophthalmol Vis Sci,* 47**,** 329-35.

HAKOBYAN, S., HARRIS, C. L., TORTAJADA, A., GOICOCHEA DE JORGE, E., GARCIA-LAYANA, A., FERNANDEZ-ROBREDO, P., RODRIGUEZ DE CORDOBA, S. & MORGAN, B. P. 2008. Measurement of factor H variants in plasma using variant-specific monoclonal antibodies: application to assessing risk of age-related macular degeneration. *Invest Ophthalmol Vis Sci,* 49**,** 1983-90.

HAMANN, S., LA COUR, M., LUI, G. M., BUNDGAARD, M. & ZEUTHEN, T. 2000. Transport of protons and lactate in cultured human fetal retinal pigment epithelial cells. *Pflugers Arch,* 440**,** 84-92.

HAMEL, C. P., TSILOU, E., PFEFFER, B. A., HOOKS, J. J., DETRICK, B. & REDMOND, T. M. 1993. Molecular cloning and expression of RPE65, a novel retinal pigment epithelium-specific microsomal protein that is post-transcriptionally regulated in vitro. *J Biol Chem,* 268**,** 15751-7.
HARGRAVE, P. A. 2001. Rhodopsin structure, function, and topography the Friedenwald lecture. *Invest Ophthalmol Vis Sci,* 42**,** 3-9.
HASEGAWA, K., WAKINO, S., YOSHIOKA, K., TATEMATSU, S., HARA, Y., MINAKUCHI, H., WASHIDA, N., TOKUYAMA, H., HAYASHI, K. & ITOH, H. 2008. Sirt1 protects against oxidative stress-induced renal tubular cell apoptosis by the bidirectional regulation of catalase expression. *Biochem Biophys Res Commun,* 372**,** 51-6.
HAYREH, S. S. 1975. Segmental nature of the choroidal vasculature. *Br J Ophthalmol,* 59**,** 631-48.
HAYWARD, C., SHU, X., CIDECIYAN, A. V., LENNON, A., BARRAN, P., ZAREPARSI, S., SAWYER, L., HENDRY, G., DHILLON, B., MILAM, A. H., LUTHERT, P. J., SWAROOP, A., HASTIE, N. D., JACOBSON, S. G. & WRIGHT, A. F. 2003. Mutation in a short-chain collagen gene, CTRP5, results in extracellular deposit formation in late-onset retinal degeneration: a genetic model for age-related macular degeneration. *Hum Mol Genet,* 12**,** 2657-67.
HECKER, L. A., EDWARDS, A. O., RYU, E., TOSAKULWONG, N., BARATZ, K. H., BROWN, W. L., CHARBEL ISSA, P., SCHOLL, H. P., POLLOK-KOPP, B., SCHMID-KUBISTA, K. E., BAILEY, K. R. & OPPERMANN, M. 2010. Genetic control of the alternative pathway of complement in humans and age-related macular degeneration. *Hum Mol Genet,* 19**,** 209-15.
HEINEMANN-VERNALEKEN, B., PALMOWSKI, A. M., ALLGAYER, R. & RUPRECHT, K. W. 2001. Comparison of different high resolution multifocal electroretinogram recordings in patients with age-related maculopathy. *Graefes Arch Clin Exp Ophthalmol,* 239**,** 556-61.
HEINEN, S., HARTMANN, A., LAUER, N., WIEHL, U., DAHSE, H. M., SCHIRMER, S., GROPP, K., ENGHARDT, T., WALLICH, R., HALBICH, S., MIHLAN, M., SCHLOTZER-SCHREHARDT, U., ZIPFEL, P. F. & SKERKA, C. 2009. Factor H-related protein 1 (CFHR-1) inhibits complement C5 convertase activity and terminal complex formation. *Blood,* 114**,** 2439-47.
HELB, H. M., CHARBEL ISSA, P., FLECKENSTEIN, M., SCHMITZ-VALCKENBERG, S., SCHOLL, H. P., MEYER, C. H., ETER, N. & HOLZ, F. G. 2010. Clinical evaluation of simultaneous confocal scanning laser ophthalmoscopy imaging combined with high-resolution, spectral-domain optical coherence tomography. *Acta Ophthalmol,* 88**,** 842-9.
HILLMEN, P., YOUNG, N. S., SCHUBERT, J., BRODSKY, R. A., SOCIE, G., MUUS, P., ROTH, A., SZER, J., ELEBUTE, M. O., NAKAMURA, R., BROWNE, P., RISITANO, A. M., HILL, A., SCHREZENMEIER, H., FU, C. L., MACIEJEWSKI, J., ROLLINS, S. A., MOJCIK, C.

F., ROTHER, R. P. & LUZZATTO, L. 2006. The complement inhibitor eculizumab in paroxysmal nocturnal hemoglobinuria. *N Engl J Med,* 355**,** 1233-43.
HIRAMI, Y., OSAKADA, F., TAKAHASHI, K., OKITA, K., YAMANAKA, S., IKEDA, H., YOSHIMURA, N. & TAKAHASHI, M. 2009. Generation of retinal cells from mouse and human induced pluripotent stem cells. *Neurosci Lett,* 458**,** 126-31.
HOGAN, M. J. 1972. Role of the retinal pigment epithelium in macular disease. *Trans Am Acad Ophthalmol Otolaryngol,* 76**,** 64-80.
HOLEKAMP, N. M., BOUCK, N. & VOLPERT, O. 2002. Pigment epithelium-derived factor is deficient in the vitreous of patients with choroidal neovascularization due to age-related macular degeneration. *Am J Ophthalmol,* 134**,** 220-7.
HOLLYFIELD, J. G., BONILHA, V. L., RAYBORN, M. E., YANG, X., SHADRACH, K. G., LU, L., UFRET, R. L., SALOMON, R. G. & PEREZ, V. L. 2008. Oxidative damage-induced inflammation initiates age-related macular degeneration. *Nat Med,* 14**,** 194-8.
HOLZ, F. G., BINDEWALD-WITTICH, A., FLECKENSTEIN, M., DREYHAUPT, J., SCHOLL, H. P., SCHMITZ-VALCKENBERG, S. & GROUP, F. A.-S. 2007. Progression of geographic atrophy and impact of fundus autofluorescence patterns in age-related macular degeneration. *Am J Ophthalmol,* 143**,** 463-72.
HOLZ, F. G., SCHUTT, F., KOPITZ, J., ELDRED, G. E., KRUSE, F. E., VOLCKER, H. E. & CANTZ, M. 1999. Inhibition of lysosomal degradative functions in RPE cells by a retinoid component of lipofuscin. *Invest Ophthalmol Vis Sci,* 40**,** 737-43.
HSIUNG, J., ZHU, D. & HINTON, D. R. 2015. Polarized human embryonic stem cell-derived retinal pigment epithelial cell monolayers have higher resistance to oxidative stress-induced cell death than nonpolarized cultures. *Stem Cells Transl Med,* 4**,** 10-20.
HSU, S. C. & MOLDAY, R. S. 1994. Glucose metabolism in photoreceptor outer segments. Its role in phototransduction and in NADPH-requiring reactions. *J Biol Chem,* 269**,** 17954-9.
HU, D. N., SIMON, J. D. & SARNA, T. 2008. Role of ocular melanin in ophthalmic physiology and pathology. *Photochem Photobiol,* 84**,** 639-44.
HU, J. & BOK, D. 2001. A cell culture medium that supports the differentiation of human retinal pigment epithelium into functionally polarized monolayers. *Mol Vis,* 7**,** 14-9.
HUGHES, B. A., MILLER, S. S. & MACHEN, T. E. 1984. Effects of cyclic AMP on fluid absorption and ion transport across frog retinal pigment epithelium. Measurements in the open-circuit state. *J Gen Physiol,* 83**,** 875-99.
IDELSON, M., ALPER, R., OBOLENSKY, A., BEN-SHUSHAN, E., HEMO, I., YACHIMOVICH-COHEN, N., KHANER, H., SMITH, Y., WISER, O., GROPP, M., COHEN, M. A., EVEN-RAM, S., BERMAN-ZAKEN, Y., MATZRAFI, L., RECHAVI, G., BANIN, E. &

REUBINOFF, B. 2009. Directed differentiation of human embryonic stem cells into functional retinal pigment epithelium cells. *Cell Stem Cell,* 5**,** 396-408.
IMAMURA, Y., NODA, S., HASHIZUME, K., SHINODA, K., YAMAGUCHI, M., UCHIYAMA, S., SHIMIZU, T., MIZUSHIMA, Y., SHIRASAWA, T. & TSUBOTA, K. 2006. Drusen, choroidal neovascularization, and retinal pigment epithelium dysfunction in SOD1-deficient mice: a model of age-related macular degeneration. *Proc Natl Acad Sci U S A,* 103**,** 11282-7.
INAL, J. M., HUI, K. M., MIOT, S., LANGE, S., RAMIREZ, M. I., SCHNEIDER, B., KRUEGER, G. & SCHIFFERLI, J. A. 2005. Complement C2 receptor inhibitor trispanning: a novel human complement inhibitory receptor. *J Immunol,* 174**,** 356-66.
ISHIBASHI, T., SORGENTE, N., PATTERSON, R. & RYAN, S. J. 1986. Pathogenesis of drusen in the primate. *Invest Ophthalmol Vis Sci,* 27**,** 184-93.
ISHIDA, O., OKU, H., IKEDA, T., NISHIMURA, M., KAWAGOE, K. & NAKAMURA, K. 2003. Is Chlamydia pneumoniae infection a risk factor for age related macular degeneration? *Br J Ophthalmol,* 87**,** 523-4.
ITZHAKI, I., MAIZELS, L., HUBER, I., ZWI-DANTSIS, L., CASPI, O., WINTERSTERN, A., FELDMAN, O., GEPSTEIN, A., ARBEL, G., HAMMERMAN, H., BOULOS, M. & GEPSTEIN, L. 2011. Modelling the long QT syndrome with induced pluripotent stem cells. *Nature,* 471**,** 225-9.
JACOBSON, S. G., CIDECIYAN, A. V., SUMAROKA, A., ROMAN, A. J. & WRIGHT, A. F. 2014. Late-onset retinal degeneration caused by C1QTNF5 mutation: sub-retinal pigment epithelium deposits and visual consequences. *JAMA Ophthalmol,* 132**,** 1252-5.
JACOBSON, S. G., CIDECIYAN, A. V., WRIGHT, E. & WRIGHT, A. F. 2001. Phenotypic marker for early disease detection in dominant late-onset retinal degeneration. *Invest Ophthalmol Vis Sci,* 42**,** 1882-90.
JARVA, H., JOKIRANTA, T. S., HELLWAGE, J., ZIPFEL, P. F. & MERI, S. 1999. Regulation of complement activation by C-reactive protein: targeting the complement inhibitory activity of factor H by an interaction with short consensus repeat domains 7 and 8–11. *The Journal of Immunology,* 163**,** 3957-3962.
JIN, Z. B., OKAMOTO, S., OSAKADA, F., HOMMA, K., ASSAWACHANANONT, J., HIRAMI, Y., IWATA, T. & TAKAHASHI, M. 2011. Modeling retinal degeneration using patient-specific induced pluripotent stem cells. *PLoS One,* 6**,** e17084.
JIN, Z. B., OKAMOTO, S., XIANG, P. & TAKAHASHI, M. 2012. Integration-free induced pluripotent stem cells derived from retinitis pigmentosa patient for disease modeling. *Stem Cells Transl Med,* 1**,** 503-9.
JOHNSON, A. A., BACHMAN, L. A., GILLES, B. J., CROSS, S. D., STELZIG, K. E., RESCH, Z. T., MARMORSTEIN, L. Y., PULIDO, J. S. & MARMORSTEIN, A. D. 2015. Autosomal

Recessive Bestrophinopathy Is Not Associated With the Loss of Bestrophin-1 Anion Channel Function in a Patient With a Novel BEST1 Mutation. *Invest Ophthalmol Vis Sci,* 56**,** 4619-30.
JOHNSON, L. V., FOREST, D. L., BANNA, C. D., RADEKE, C. M., MALONEY, M. A., HU, J., SPENCER, C. N., WALKER, A. M., TSIE, M. S., BOK, D., RADEKE, M. J. & ANDERSON, D. H. 2011. Cell culture model that mimics drusen formation and triggers complement activation associated with age-related macular degeneration. *Proc Natl Acad Sci U S A,* 108**,** 18277-82.
JOHNSON, L. V., LEITNER, W. P., STAPLES, M. K. & ANDERSON, D. H. 2001. Complement activation and inflammatory processes in Drusen formation and age related macular degeneration. *Exp Eye Res,* 73**,** 887-96.
JOHNSON, L. V., OZAKI, S., STAPLES, M. K., ERICKSON, P. A. & ANDERSON, D. H. 2000. A potential role for immune complex pathogenesis in drusen formation. *Exp Eye Res,* 70**,** 441-9.
JOKIRANTA, T. S., JAAKOLA, V. P., LEHTINEN, M. J., PÄREPALO, M., MERI, S. & GOLDMAN, A. 2006. Structure of complement factor H carboxyl-terminus reveals molecular basis of atypical haemolytic uremic syndrome. *The EMBO journal,* 25**,** 1784-1794.
JONAS, J. B., SCHNEIDER, U. & NAUMANN, G. O. 1992. Count and density of human retinal photoreceptors. *Graefes Arch Clin Exp Ophthalmol,* 230**,** 505-10.
JOSEPH, K., KULIK, L., COUGHLIN, B., KUNCHITHAPAUTHAM, K., BANDYOPADHYAY, M., THIEL, S., THIELENS, N. M., HOLERS, V. M. & ROHRER, B. 2013. Oxidative stress sensitizes retinal pigmented epithelial (RPE) cells to complement-mediated injury in a natural antibody-, lectin pathway-, and phospholipid epitope-dependent manner. *J Biol Chem,* 288**,** 12753-65.
JOZSI, M., OPPERMANN, M., LAMBRIS, J. D. & ZIPFEL, P. F. 2007. The C-terminus of complement factor H is essential for host cell protection. *Mol Immunol,* 44**,** 2697-706.
JUSTILIEN, V., PANG, J. J., RENGANATHAN, K., ZHAN, X., CRABB, J. W., KIM, S. R., SPARROW, J. R., HAUSWIRTH, W. W. & LEWIN, A. S. 2007. SOD2 knockdown mouse model of early AMD. *Invest Ophthalmol Vis Sci,* 48**,** 4407-20.
KALAYOGLU, M. V., BULA, D., ARROYO, J., GRAGOUDAS, E. S., D'AMICO, D. & MILLER, J. W. 2005. Identification of Chlamydia pneumoniae within human choroidal neovascular membranes secondary to age-related macular degeneration. *Graefes Arch Clin Exp Ophthalmol,* 243**,** 1080-90.
KANDA, A., CHEN, W., OTHMAN, M., BRANHAM, K. E., BROOKS, M., KHANNA, R., HE, S., LYONS, R., ABECASIS, G. R. & SWAROOP, A. 2007. A variant of mitochondrial protein LOC387715/ARMS2, not HTRA1, is strongly associated with age-related macular degeneration. *Proc Natl Acad Sci U S A,* 104**,** 16227-32.
KANEMURA, H., GO, M. J., SHIKAMURA, M., NISHISHITA, N., SAKAI, N., KAMAO, H., MANDAI, M., MORINAGA, C., TAKAHASHI, M. & KAWAMATA, S. 2014. Tumorigenicity

studies of induced pluripotent stem cell (iPSC)-derived retinal pigment epithelium (RPE) for the treatment of age-related macular degeneration. *PLoS One,* 9**,** e85336.
KARLSSON, R. & FALT, A. 1997. Experimental design for kinetic analysis of protein-protein interactions with surface plasmon resonance biosensors. *J Immunol Methods,* 200**,** 121-33.
KATOH, M. 2001. Molecular cloning and characterization of MFRP, a novel gene encoding a membrane-type Frizzled-related protein. *Biochem Biophys Res Commun,* 282**,** 116-23.
KATZ, M. L. 2002. Potential role of retinal pigment epithelial lipofuscin accumulation in age-related macular degeneration. *Arch Gerontol Geriatr,* 34**,** 359-70.
KAVANAGH, D., PAPPWORTH, I. Y., ANDERSON, H., HAYES, C. M., MOORE, I., HUNZE, E. M., BENNACEUR, K., ROVERSI, P., LEA, S., STRAIN, L., WARD, R., PLANT, N., NAILESCU, C., GOODSHIP, T. H. & MARCHBANK, K. J. 2012. Factor I autoantibodies in patients with atypical hemolytic uremic syndrome: disease-associated or an epiphenomenon? *Clin J Am Soc Nephrol,* 7**,** 417-26.
KHALIQ, A., PATEL, B., JARVIS-EVANS, J., MORIARTY, P., MCLEOD, D. & BOULTON, M. 1995. Oxygen modulates production of bFGF and TGF-beta by retinal cells in vitro. *Exp Eye Res,* 60**,** 415-23.
KIM, K., DOI, A., WEN, B., NG, K., ZHAO, R., CAHAN, P., KIM, J., ARYEE, M. J., JI, H., EHRLICH, L. I., YABUUCHI, A., TAKEUCHI, A., CUNNIFF, K. C., HONGGUANG, H., MCKINNEY-FREEMAN, S., NAVEIRAS, O., YOON, T. J., IRIZARRY, R. A., JUNG, N., SEITA, J., HANNA, J., MURAKAMI, P., JAENISCH, R., WEISSLEDER, R., ORKIN, S. H., WEISSMAN, I. L., FEINBERG, A. P. & DALEY, G. Q. 2010. Epigenetic memory in induced pluripotent stem cells. *Nature,* 467**,** 285-90.
KIM, M. H., CHUNG, J., YANG, J. W., CHUNG, S. M., KWAG, N. H. & YOO, J. S. 2003. Hydrogen peroxide-induced cell death in a human retinal pigment epithelial cell line, ARPE-19. *Korean J Ophthalmol,* 17**,** 19-28.
KIM, S. Y., SADDA, S., HUMAYUN, M. S., DE JUAN, E., JR., MELIA, B. M. & GREEN, W. R. 2002. Morphometric analysis of the macula in eyes with geographic atrophy due to age-related macular degeneration. *Retina,* 22**,** 464-70.
KISHORE, U., GABORIAUD, C., WATERS, P., SHRIVE, A. K., GREENHOUGH, T. J., REID, K. B., SIM, R. B. & ARLAUD, G. J. 2004. C1q and tumor necrosis factor superfamily: modularity and versatility. *Trends Immunol,* 25**,** 551-61.
KITA, M. & MARMOR, M. F. 1992. Effects on retinal adhesive force in vivo of metabolically active agents in the subretinal space. *Invest Ophthalmol Vis Sci,* 33**,** 1883-7.
KLEIN, R., PETO, T., BIRD, A. & VANNEWKIRK, M. R. 2004. The epidemiology of age-related macular degeneration. *Am J Ophthalmol,* 137**,** 486-95.

KLEIN, R. J., ZEISS, C., CHEW, E. Y., TSAI, J. Y., SACKLER, R. S., HAYNES, C., HENNING, A. K., SANGIOVANNI, J. P., MANE, S. M., MAYNE, S. T., BRACKEN, M. B., FERRIS, F. L., OTT, J., BARNSTABLE, C. & HOH, J. 2005. Complement factor H polymorphism in age-related macular degeneration. *Science,* 308**,** 385-9.

KLETTNER, A. 2012. Oxidative stress induced cellular signaling in RPE cells. *Front Biosci (Schol Ed),* 4**,** 392-411.

KLIMANSKAYA, I., HIPP, J., REZAI, K. A., WEST, M., ATALA, A. & LANZA, R. 2004. Derivation and comparative assessment of retinal pigment epithelium from human embryonic stem cells using transcriptomics. *Cloning Stem Cells,* 6**,** 217-45.

KNIGHT, K. K., OLSON, D. R., ZHOU, R. & SNYDER, P. M. 2006. Liddle's syndrome mutations increase Na+ transport through dual effects on epithelial Na+ channel surface expression and proteolytic cleavage. *Proc Natl Acad Sci U S A,* 103**,** 2805-8.

KOKKINAKI, M., SAHIBZADA, N. & GOLESTANEH, N. 2011. Human induced pluripotent stem-derived retinal pigment epithelium (RPE) cells exhibit ion transport, membrane potential, polarized vascular endothelial growth factor secretion, and gene expression pattern similar to native RPE. *Stem Cells,* 29**,** 825-35.

KONARI, K., SAWADA, N., ZHONG, Y., ISOMURA, H., NAKAGAWA, T. & MORI, M. 1995. Development of the blood-retinal barrier in vitro: formation of tight junctions as revealed by occludin and ZO-1 correlates with the barrier function of chick retinal pigment epithelial cells. *Exp Eye Res,* 61**,** 99-108.

KORTVELY, E., HAUCK, S. M., DUETSCH, G., GLOECKNER, C. J., KREMMER, E., ALGE-PRIGLINGER, C. S., DEEG, C. A. & UEFFING, M. 2010. ARMS2 is a constituent of the extracellular matrix providing a link between familial and sporadic age-related macular degenerations. *Investigative ophthalmology & visual science,* 51**,** 79-88.

KUNTZ, C. A., JACOBSON, S. G., CIDECIYAN, A. V., LI, Z. Y., STONE, E. M., POSSIN, D. & MILAM, A. H. 1996. Sub-retinal pigment epithelial deposits in a dominant late-onset retinal degeneration. *Invest Ophthalmol Vis Sci,* 37**,** 1772-82.

KUZMENKIN, A., LIANG, H., XU, G., PFANNKUCHE, K., EICHHORN, H., FATIMA, A., LUO, H., SARIC, T., WERNIG, M., JAENISCH, R. & HESCHELER, J. 2009. Functional characterization of cardiomyocytes derived from murine induced pluripotent stem cells in vitro. *FASEB J,* 23**,** 4168-80.

LAINE, M., JARVA, H., SEITSONEN, S., HAAPASALO, K., LEHTINEN, M. J., LINDEMAN, N., ANDERSON, D. H., JOHNSON, P. T., JARVELA, I., JOKIRANTA, T. S., HAGEMAN, G. S., IMMONEN, I. & MERI, S. 2007. Y402H polymorphism of complement factor H affects binding affinity to C-reactive protein. *J Immunol,* 178**,** 3831-6.

LAKKARAJU, A., FINNEMANN, S. C. & RODRIGUEZ-BOULAN, E. 2007. The lipofuscin fluorophore A2E perturbs cholesterol metabolism in retinal pigment epithelial cells. *Proc Natl Acad Sci U S A,* 104**,** 11026-31.
LAMBA, D. A., KARL, M. O., WARE, C. B. & REH, T. A. 2006. Efficient generation of retinal progenitor cells from human embryonic stem cells. *Proc Natl Acad Sci U S A,* 103**,** 12769-74.
LAMBA, D. A., MCUSIC, A., HIRATA, R. K., WANG, P. R., RUSSELL, D. & REH, T. A. 2010. Generation, purification and transplantation of photoreceptors derived from human induced pluripotent stem cells. *PLoS One,* 5**,** e8763.
LAURENT, L. C., ULITSKY, I., SLAVIN, I., TRAN, H., SCHORK, A., MOREY, R., LYNCH, C., HARNESS, J. V., LEE, S., BARRERO, M. J., KU, S., MARTYNOVA, M., SEMECHKIN, R., GALAT, V., GOTTESFELD, J., IZPISUA BELMONTE, J. C., MURRY, C., KEIRSTEAD, H. S., PARK, H. S., SCHMIDT, U., LASLETT, A. L., MULLER, F. J., NIEVERGELT, C. M., SHAMIR, R. & LORING, J. F. 2011. Dynamic changes in the copy number of pluripotency and cell proliferation genes in human ESCs and iPSCs during reprogramming and time in culture. *Cell Stem Cell,* 8**,** 106-18.
LEDERMANN, H. M. 1995. Is maturity onset diabetes at young age (MODY) more common in Europe than previously assumed? *Lancet,* 345**,** 648.
LEFFLER, J., HERBERT, A. P., NORSTRÖM, E., SCHMIDT, C. Q., BARLOW, P. N., BLOM, A. M. & MARTIN, M. 2010. Annexin-II, DNA, and histones serve as factor H ligands on the surface of apoptotic cells. *Journal of biological chemistry,* 285**,** 3766-3776.
LENG, T., ROSENFELD, P. J., GREGORI, G., PULIAFITO, C. A. & PUNJABI, O. S. 2009. Spectral domain optical coherence tomography characteristics of cuticular drusen. *Retina,* 29**,** 988-93.
LI, C., HUANG, Z., KINGSLEY, R., ZHOU, X., LI, F., PARKE, D. W., 2ND & CAO, W. 2007. Biochemical alterations in the retinas of very low-density lipoprotein receptor knockout mice: an animal model of retinal angiomatous proliferation. *Arch Ophthalmol,* 125**,** 795-803.
LI, M., ATMACA-SONMEZ, P., OTHMAN, M., BRANHAM, K. E., KHANNA, R., WADE, M. S., LI, Y., LIANG, L., ZAREPARSI, S., SWAROOP, A. & ABECASIS, G. R. 2006. CFH haplotypes without the Y402H coding variant show strong association with susceptibility to age-related macular degeneration. *Nat Genet,* 38**,** 1049-54.
LI, Y., TSAI, Y. T., HSU, C. W., EROL, D., YANG, J., WU, W. H., DAVIS, R. J., EGLI, D. & TSANG, S. H. 2012. Long-term safety and efficacy of human-induced pluripotent stem cell (iPS) grafts in a preclinical model of retinitis pigmentosa. *Mol Med,* 18**,** 1312-9.
LI, Y., WU, W. H., HSU, C. W., NGUYEN, H. V., TSAI, Y. T., CHAN, L., NAGASAKI, T., MAUMENEE, I. H., YANNUZZI, L. A., HOANG, Q. V., HUA, H., EGLI, D. & TSANG, S. H.

2014. Gene therapy in patient-specific stem cell lines and a preclinical model of retinitis pigmentosa with membrane frizzled-related protein defects. *Mol Ther,* 22**,** 1688-97.
LIAO, J. L., YU, J., HUANG, K., HU, J., DIEMER, T., MA, Z., DVASH, T., YANG, X. J., TRAVIS, G. H., WILLIAMS, D. S., BOK, D. & FAN, G. 2010. Molecular signature of primary retinal pigment epithelium and stem-cell-derived RPE cells. *Hum Mol Genet,* 19**,** 4229-38.
LILES, M. R., NEWSOME, D. A. & OLIVER, P. D. 1991. Antioxidant enzymes in the aging human retinal pigment epithelium. *Arch Ophthalmol,* 109**,** 1285-8.
LIM, S., CHOI, S. H., KOO, B. K., KANG, S. M., YOON, J. W., JANG, H. C., CHOI, S. M., LEE, M. G., LEE, W., SHIN, H., KIM, Y. B., LEE, H. K. & PARK, K. S. 2012. Effects of aerobic exercise training on C1q tumor necrosis factor alpha-related protein isoform 5 (myonectin): association with insulin resistance and mitochondrial DNA density in women. *J Clin Endocrinol Metab,* 97**,** E88-93.
LIN, J. M., WAN, L., TSAI, Y. Y., LIN, H. J., TSAI, Y., LEE, C. C., TSAI, C. H., TSENG, S. H. & TSAI, F. J. 2008. Pigment epithelium-derived factor gene Met72Thr polymorphism is associated with increased risk of wet age-related macular degeneration. *Am J Ophthalmol,* 145**,** 716-721.
LIN, M. Y., GUTIERREZ, P. R., STONE, K. L., YAFFE, K., ENSRUD, K. E., FINK, H. A., SARKISIAN, C. A., COLEMAN, A. L., MANGIONE, C. M. & STUDY OF OSTEOPOROTIC FRACTURES RESEARCH, G. 2004. Vision impairment and combined vision and hearing impairment predict cognitive and functional decline in older women. *J Am Geriatr Soc,* 52**,** 1996-2002.
LIU, J., ITAGAKI, Y., BEN-SHABAT, S., NAKANISHI, K. & SPARROW, J. R. 2000. The biosynthesis of A2E, a fluorophore of aging retina, involves the formation of the precursor, A2-PE, in the photoreceptor outer segment membrane. *J Biol Chem,* 275**,** 29354-60.
LIU, J., VERMA, P. J., EVANS-GALEA, M. V., DELATYCKI, M. B., MICHALSKA, A., LEUNG, J., CROMBIE, D., SARSERO, J. P., WILLIAMSON, R., DOTTORI, M. & PEBAY, A. 2011. Generation of induced pluripotent stem cell lines from Friedreich ataxia patients. *Stem Cell Rev,* 7**,** 703-13.
LOFFLER, K. U. & LEE, W. R. 1986. Basal linear deposit in the human macula. *Graefes Arch Clin Exp Ophthalmol,* 224**,** 493-501.
LOMMATZSCH, A., HERMANS, P., MULLER, K. D., BORNFELD, N., BIRD, A. C. & PAULEIKHOFF, D. 2008. Are low inflammatory reactions involved in exudative age-related macular degeneration? Morphological and immunhistochemical analysis of AMD associated with basal deposits. *Graefes Arch Clin Exp Ophthalmol,* 246**,** 803-10.
LOYET, K. M., DEFORGE, L. E., KATSCHKE, K. J., JR., DIEHL, L., GRAHAM, R. R., PAO, L., STURGEON, L., LEWIN-KOH, S. C., HOLLYFIELD, J. G. & VAN LOOKEREN

CAMPAGNE, M. 2012. Activation of the alternative complement pathway in vitreous is controlled by genetics in age-related macular degeneration. *Invest Ophthalmol Vis Sci,* 53**,** 6628-37.
LU, L., HACKETT, S. F., MINCEY, A., LAI, H. & CAMPOCHIARO, P. A. 2006. Effects of different types of oxidative stress in RPE cells. *J Cell Physiol,* 206**,** 119-25.
LUECK, K., BUSCH, M., MOSS, S. E., GREENWOOD, J., KASPER, M., LOMMATZSCH, A., PAULEIKHOFF, D. & WASMUTH, S. 2015. Complement Stimulates Retinal Pigment Epithelial Cells to Undergo Pro-Inflammatory Changes. *Ophthalmic Res,* 54**,** 195-203.
LUHMANN, U. F., ROBBIE, S., MUNRO, P. M., BARKER, S. E., DURAN, Y., LUONG, V., FITZKE, F. W., BAINBRIDGE, J. W., ALI, R. R. & MACLAREN, R. E. 2009. The drusenlike phenotype in aging Ccl2-knockout mice is caused by an accelerated accumulation of swollen autofluorescent subretinal macrophages. *Invest Ophthalmol Vis Sci,* 50**,** 5934-43.
LUKOVIC, D., ARTERO CASTRO, A., DELGADO, A. B., BERNAL MDE, L., LUNA PELAEZ, N., DIEZ LLORET, A., PEREZ ESPEJO, R., KAMENAROVA, K., FERNANDEZ SANCHEZ, L., CUENCA, N., CORTON, M., AVILA FERNANDEZ, A., SORKIO, A., SKOTTMAN, H., AYUSO, C., ERCEG, S. & BHATTACHARYA, S. S. 2015. Human iPSC derived disease model of MERTK-associated retinitis pigmentosa. *Sci Rep,* 5**,** 12910.
MALAN, D., FRIEDRICHS, S., FLEISCHMANN, B. K. & SASSE, P. 2011. Cardiomyocytes obtained from induced pluripotent stem cells with long-QT syndrome 3 recapitulate typical disease-specific features in vitro. *Circ Res,* 109**,** 841-7.
MALEK, G., JOHNSON, L. V., MACE, B. E., SALOUPIS, P., SCHMECHEL, D. E., RICKMAN, D. W., TOTH, C. A., SULLIVAN, P. M. & BOWES RICKMAN, C. 2005. Apolipoprotein E allele-dependent pathogenesis: a model for age-related retinal degeneration. *Proc Natl Acad Sci U S A,* 102**,** 11900-5.
MALEK, G., LI, C. M., GUIDRY, C., MEDEIROS, N. E. & CURCIO, C. A. 2003. Apolipoprotein B in cholesterol-containing drusen and basal deposits of human eyes with age-related maculopathy. *Am J Pathol,* 162**,** 413-25.
MAMINISHKIS, A., CHEN, S., JALICKEE, S., BANZON, T., SHI, G., WANG, F. E., EHALT, T., HAMMER, J. A. & MILLER, S. S. 2006. Confluent monolayers of cultured human fetal retinal pigment epithelium exhibit morphology and physiology of native tissue. *Invest Ophthalmol Vis Sci,* 47**,** 3612-24.
MANDAL, M. N., VASIREDDY, V., JABLONSKI, M. M., WANG, X., HECKENLIVELY, J. R., HUGHES, B. A., REDDY, G. B. & AYYAGARI, R. 2006a. Spatial and temporal expression of MFRP and its interaction with CTRP5. *Invest Ophthalmol Vis Sci,* 47**,** 5514-21.
MANDAL, M. N., VASIREDDY, V., REDDY, G. B., WANG, X., MOROI, S. E., PATTNAIK, B. R., HUGHES, B. A., HECKENLIVELY, J. R., HITCHCOCK, P. F., JABLONSKI, M. M. & AYYAGARI, R. 2006b. CTRP5 is a membrane-associated and secretory protein in the RPE and

ciliary body and the S163R mutation of CTRP5 impairs its secretion. *Invest Ophthalmol Vis Sci,* 47**,** 5505-13.
MANDERSON, A. P., BOTTO, M. & WALPORT, M. J. 2004. The role of complement in the development of systemic lupus erythematosus. *Annu Rev Immunol,* 22**,** 431-56.
MAO, Y. & FINNEMANN, S. C. 2013. Analysis of photoreceptor outer segment phagocytosis by RPE cells in culture. *Methods Mol Biol,* 935**,** 285-95.
MARMOR, M. F., WOLFENSBERGER, T.J. 1998. *The retinal pigment epithelium,* New York, Oxford University press.
MARSHALL, J. 1987. The ageing retina: physiology or pathology. *Eye (Lond),* 1 (Pt 2)**,** 282-95.
MARTINEZ-BARRICARTE, R., HEURICH, M., VALDES-CANEDO, F., VAZQUEZ-MARTUL, E., TORREIRA, E., MONTES, T., TORTAJADA, A., PINTO, S., LOPEZ-TRASCASA, M., MORGAN, B. P., LLORCA, O., HARRIS, C. L. & RODRIGUEZ DE CORDOBA, S. 2010. Human C3 mutation reveals a mechanism of dense deposit disease pathogenesis and provides insights into complement activation and regulation. *J Clin Invest,* 120**,** 3702-12.
MCCARTHY, M. I. 2004. Progress in defining the molecular basis of type 2 diabetes mellitus through susceptibility-gene identification. *Hum Mol Genet,* 13 Spec No 1**,** R33-41.
MCCLURE, M. E., HART, P. M., JACKSON, A. J., STEVENSON, M. R. & CHAKRAVARTHY, U. 2000. Macular degeneration: do conventional measurements of impaired visual function equate with visual disability? *Br J Ophthalmol,* 84**,** 244-50.
MCKAY, G. J., PATTERSON, C. C., CHAKRAVARTHY, U., DASARI, S., KLAVER, C. C., VINGERLING, J. R., HO, L., DE JONG, P. T., FLETCHER, A. E., YOUNG, I. S., SELAND, J. H., RAHU, M., SOUBRANE, G., TOMAZZOLI, L., TOPOUZIS, F., VIOQUE, J., HINGORANI, A. D., SOFAT, R., DEAN, M., SAWITZKE, J., SEDDON, J. M., PETER, I., WEBSTER, A. R., MOORE, A. T., YATES, J. R., CIPRIANI, V., FRITSCHE, L. G., WEBER, B. H., KEILHAUER, C. N., LOTERY, A. J., ENNIS, S., KLEIN, M. L., FRANCIS, P. J., STAMBOLIAN, D., ORLIN, A., GORIN, M. B., WEEKS, D. E., KUO, C. L., SWAROOP, A., OTHMAN, M., KANDA, A., CHEN, W., ABECASIS, G. R., WRIGHT, A. F., HAYWARD, C., BAIRD, P. N., GUYMER, R. H., ATTIA, J., THAKKINSTIAN, A. & SILVESTRI, G. 2011. Evidence of association of APOE with age-related macular degeneration: a pooled analysis of 15 studies. *Hum Mutat,* 32**,** 1407-16.
MEKALA, S. R., VAUHINI, V., NAGARAJAN, U., MADDILETI, S., GADDIPATI, S. & MARIAPPAN, I. 2013. Derivation, characterization and retinal differentiation of induced pluripotent stem cells. *J Biosci,* 38**,** 123-34.
MELLOUGH, C. B., SERNAGOR, E., MORENO-GIMENO, I., STEEL, D. H. & LAKO, M. 2012. Efficient stage-specific differentiation of human pluripotent stem cells toward retinal photoreceptor cells. *Stem Cells,* 30**,** 673-86.

MEYER, J. S., HOWDEN, S. E., WALLACE, K. A., VERHOEVEN, A. D., WRIGHT, L. S., CAPOWSKI, E. E., PINILLA, I., MARTIN, J. M., TIAN, S., STEWART, R., PATTNAIK, B., THOMSON, J. A. & GAMM, D. M. 2011. Optic vesicle-like structures derived from human pluripotent stem cells facilitate a customized approach to retinal disease treatment. *Stem Cells,* 29**,** 1206-18.

MEYER, J. S., SHEARER, R. L., CAPOWSKI, E. E., WRIGHT, L. S., WALLACE, K. A., MCMILLAN, E. L., ZHANG, S. C. & GAMM, D. M. 2009. Modeling early retinal development with human embryonic and induced pluripotent stem cells. *Proc Natl Acad Sci U S A,* 106**,** 16698-703.

MIDENA, E., VUJOSEVIC, S., CONVENTO, E., MANFRE, A., CAVARZERAN, F. & PILOTTO, E. 2007. Microperimetry and fundus autofluorescence in patients with early age-related macular degeneration. *Br J Ophthalmol,* 91**,** 1499-503.

MILAM, A. H., CURCIO, C. A., CIDECIYAN, A. V., SAXENA, S., JOHN, S. K., KRUTH, H. S., MALEK, G., HECKENLIVELY, J. R., WELEBER, R. G. & JACOBSON, S. G. 2000. Dominant late-onset retinal degeneration with regional variation of sub-retinal pigment epithelium deposits, retinal function, and photoreceptor degeneration. *Ophthalmology,* 107**,** 2256-66.

MINASSIAN, D. C., REIDY, A., LIGHTSTONE, A. & DESAI, P. 2011. Modelling the prevalence of age-related macular degeneration (2010-2020) in the UK: expected impact of anti-vascular endothelial growth factor (VEGF) therapy. *Br J Ophthalmol,* 95**,** 1433-6.

MISHIMA, H. & KONDO, K. 1981. Extrusion of lysosomal bodies from apical mouse retinal pigment epithelium. *Albrecht Von Graefes Arch Klin Exp Ophthalmol,* 216**,** 209-17.

MOGRIDGE, J. 2004. Using light scattering to determine the stoichiometry of protein complexes. *Protein-Protein Interactions: Methods and Applications***,** 113-118.

MOISEYEV, G., TAKAHASHI, Y., CHEN, Y., GENTLEMAN, S., REDMOND, T. M., CROUCH, R. K. & MA, J. X. 2006. RPE65 is an iron(II)-dependent isomerohydrolase in the retinoid visual cycle. *J Biol Chem,* 281**,** 2835-40.

MONTES, T., TORTAJADA, A., MORGAN, B. P., RODRIGUEZ DE CORDOBA, S. & HARRIS, C. L. 2009. Functional basis of protection against age-related macular degeneration conferred by a common polymorphism in complement factor B. *Proc Natl Acad Sci U S A,* 106**,** 4366-71.

MOON, S., KIM, D. J., KIM, K., KIM, D., LEE, H., LEE, K. & HAAM, S. 2010. Surface-enhanced plasmon resonance detection of nanoparticle-conjugated DNA hybridization. *Appl Opt,* 49**,** 484-91.

MORGAN, B. P. 2000. *Complement methods and protocols,* Springer Science & Business Media.

MORGAN, H. P., SCHMIDT, C. Q., GUARIENTO, M., BLAUM, B. S., GILLESPIE, D., HERBERT, A. P., KAVANAGH, D., MERTENS, H. D., SVERGUN, D. I. & JOHANSSON, C.

M. 2011. Structural basis for engagement by complement factor H of C3b on a self surface. *Nature structural & molecular biology,* 18**,** 463-470.
MORI, K., GEHLBACH, P. L., KABASAWA, S., KAWASAKI, I., OOSAKI, M., IIZUKA, H., KATAYAMA, S., AWATA, T. & YONEYA, S. 2007. Coding and noncoding variants in the CFH gene and cigarette smoking influence the risk of age-related macular degeneration in a Japanese population. *Invest Ophthalmol Vis Sci,* 48**,** 5315-9.
MOROI, S. E., LARK, K. K., SIEVING, P. A., NOURI-MAHDAVI, K., SCHLÖTZER-SCHREHARDT, U., KATZ, G. J. & RITCH, R. 2003. Long anterior zonules and pigment dispersion. *American journal of ophthalmology,* 136**,** 1176-1178.
MOSCHOS, M. M., PANAYOTIDIS, D., THEODOSSIADIS, G. & MOSCHOS, M. 2004. Assessment of macular function by multifocal electroretinogram in age-related macular degeneration before and after photodynamic therapy. *J Fr Ophtalmol,* 27**,** 1001-6.
MULLINS, R. F., APTSIAURI, N. & HAGEMAN, G. S. 2001. Structure and composition of drusen associated with glomerulonephritis: implications for the role of complement activation in drusen biogenesis. *Eye (Lond),* 15**,** 390-5.
MULLINS, R. F., KHANNA, A., SCHOO, D. P., TUCKER, B. A., SOHN, E. H., DRACK, A. V. & STONE, E. M. 2014a. Is age-related macular degeneration a microvascular disease? *Adv Exp Med Biol,* 801**,** 283-9.
MULLINS, R. F., RUSSELL, S. R., ANDERSON, D. H. & HAGEMAN, G. S. 2000a. Drusen associated with aging and age-related macular degeneration contain proteins common to extracellular deposits associated with atherosclerosis, elastosis, amyloidosis, and dense deposit disease. *FASEB J,* 14**,** 835-46.
MULLINS, R. F., RUSSELL, S. R., ANDERSON, D. H. & HAGEMAN, G. S. 2000b. Drusen associated with aging and age-related macular degeneration contain proteins common to extracellular deposits associated with atherosclerosis, elastosis, amyloidosis, and dense deposit disease. *The FASEB Journal,* 14**,** 835-846.
MULLINS, R. F., SCHOO, D. P., SOHN, E. H., FLAMME-WIESE, M. J., WORKAMELAHU, G., JOHNSTON, R. M., WANG, K., TUCKER, B. A. & STONE, E. M. 2014b. The membrane attack complex in aging human choriocapillaris: relationship to macular degeneration and choroidal thinning. *Am J Pathol,* 184**,** 3142-53.
MUNOZ-SANJUAN, I. & BRIVANLOU, A. H. 2002. Neural induction, the default model and embryonic stem cells. *Nat Rev Neurosci,* 3**,** 271-80.
NAUTA, A. J., TROUW, L. A., DAHA, M. R., TIJSMA, O., NIEUWLAND, R., SCHWAEBLE, W. J., GINGRAS, A. R., MANTOVANI, A., HACK, E. C. & ROOS, A. 2002. Direct binding of C1q to apoptotic cells and cell blebs induces complement activation. *Eur J Immunol,* 32**,** 1726-36.

NEWSOME, D. A., HEWITT, A. T., HUH, W., ROBEY, P. G. & HASSELL, J. R. 1987. Detection of specific extracellular matrix molecules in drusen, Bruch's membrane, and ciliary body. *Am J Ophthalmol,* 104**,** 373-81.

OHKUMA, H. & RYAN, S. J. 1983. Experimental subretinal neovascularization in the monkey. Permeability of new vessels. *Arch Ophthalmol,* 101**,** 1102-10.

OHTA, K., WIGGERT, B., TAYLOR, A. W. & STREILEIN, J. W. 1999. Effects of experimental ocular inflammation on ocular immune privilege. *Invest Ophthalmol Vis Sci,* 40**,** 2010-8.

OHTA, K., YAMAGAMI, S., TAYLOR, A. W. & STREILEIN, J. W. 2000. IL-6 antagonizes TGF-beta and abolishes immune privilege in eyes with endotoxin-induced uveitis. *Invest Ophthalmol Vis Sci,* 41**,** 2591-9.

OKITA, K., MATSUMURA, Y., SATO, Y., OKADA, A., MORIZANE, A., OKAMOTO, S., HONG, H., NAKAGAWA, M., TANABE, K., TEZUKA, K., SHIBATA, T., KUNISADA, T., TAKAHASHI, M., TAKAHASHI, J., SAJI, H. & YAMANAKA, S. 2011. A more efficient method to generate integration-free human iPS cells. *Nat Methods,* 8**,** 409-12.

OKUBO, A., ROSA, R. H., JR., BUNCE, C. V., ALEXANDER, R. A., FAN, J. T., BIRD, A. C. & LUTHERT, P. J. 1999. The relationships of age changes in retinal pigment epithelium and Bruch's membrane. *Invest Ophthalmol Vis Sci,* 40**,** 443-9.

OOTO, S., ELLABBAN, A. A., UEDA-ARAKAWA, N., OISHI, A., TAMURA, H., YAMASHIRO, K., TSUJIKAWA, A. & YOSHIMURA, N. 2013. Reduction of retinal sensitivity in eyes with reticular pseudodrusen. *Am J Ophthalmol,* 156**,** 1184-1191 e2.

ORMSBY, R. J., RANGANATHAN, S., TONG, J. C., GRIGGS, K. M., DIMASI, D. P., HEWITT, A. W., BURDON, K. P., CRAIG, J. E., HOH, J. & GORDON, D. L. 2008. Functional and structural implications of the complement factor H Y402H polymorphism associated with age-related macular degeneration. *Invest Ophthalmol Vis Sci,* 49**,** 1763-70.

OSAKADA, F., IKEDA, H., MANDAI, M., WATAYA, T., WATANABE, K., YOSHIMURA, N., AKAIKE, A., SASAI, Y. & TAKAHASHI, M. 2008. Toward the generation of rod and cone photoreceptors from mouse, monkey and human embryonic stem cells. *Nat Biotechnol,* 26**,** 215-24.

OSAKADA, F., IKEDA, H., SASAI, Y. & TAKAHASHI, M. 2009a. Stepwise differentiation of pluripotent stem cells into retinal cells. *Nat Protoc,* 4**,** 811-24.

OSAKADA, F., JIN, Z. B., HIRAMI, Y., IKEDA, H., DANJYO, T., WATANABE, K., SASAI, Y. & TAKAHASHI, M. 2009b. In vitro differentiation of retinal cells from human pluripotent stem cells by small-molecule induction. *J Cell Sci,* 122**,** 3169-79.

OTTO, A. 1968. Excitation of nonradiative surface plasma waves in silver by the method of frustrated total reflection. *Zeitschrift für Physik,* 216**,** 398-410.

OUSTEROUT, D. G., KABADI, A. M., THAKORE, P. I., MAJOROS, W. H., REDDY, T. E. & GERSBACH, C. A. 2015. Multiplex CRISPR/Cas9-based genome editing for correction of dystrophin mutations that cause Duchenne muscular dystrophy. *Nature communications,* 6.

PAIXÃO-CAVALCANTE, D., HANSON, S., BOTTO, M., COOK, H. T. & PICKERING, M. C. 2009. Factor H facilitates the clearance of GBM bound iC3b by controlling C3 activation in fluid phase. *Molecular immunology,* 46**,** 1942-1950.

PALMOWSKI, A. M., SUTTER, E. E., BEARSE, M. A., JR. & FUNG, W. 1999. [Multifocal electroretinogram (MF-ERG) in diagnosis of macular changes. Example: senile macular degeneration]. *Ophthalmologe,* 96**,** 166-73.

PANGBURN, M. K. 2002. Cutting edge: localization of the host recognition functions of complement factor H at the carboxyl-terminal: implications for hemolytic uremic syndrome. *The Journal of Immunology,* 169**,** 4702-4706.

PANGBURN, M. K., SCHREIBER, R. D. & MULLER-EBERHARD, H. J. 1981. Formation of the initial C3 convertase of the alternative complement pathway. Acquisition of C3b-like activities by spontaneous hydrolysis of the putative thioester in native C3. *J Exp Med,* 154**,** 856-67.

PAPASTAVROU, V. T., BRADSHAW, K. R., AYE, K. H., TURNEY, C. & BROWNING, A. C. 2015. Improvement of retinal function in L-ORD after prolonged dark adaptation. *Canadian Journal of Ophthalmology/Journal Canadien d'Ophtalmologie,* 50**,** 112-118.

PARK, J. Y., KIM, S. H., PARK, T. K. & OHN, Y. H. 2011. Multifocal electroretinogram findings after intravitreal bevacizumab injection in choroidal neovascularization of age-related macular degeneration. *Korean J Ophthalmol,* 25**,** 161-5.

PARK, S. Y., CHOI, J. H., RYU, H. S., PAK, Y. K., PARK, K. S., LEE, H. K. & LEE, W. 2009. C1q tumor necrosis factor alpha-related protein isoform 5 is increased in mitochondrial DNA-depleted myocytes and activates AMP-activated protein kinase. *J Biol Chem,* 284**,** 27780-9.

PARKS, S., KEATING, D., WILLIAMSON, T. H., EVANS, A. L., ELLIOTT, A. T. & JAY, J. L. 1996. Functional imaging of the retina using the multifocal electroretinograph: a control study. *Br J Ophthalmol,* 80**,** 831-4.

PASCOLINI, D., MARIOTTI, S. P., POKHAREL, G. P., PARARAJASEGARAM, R., ETYA'ALE, D., NEGREL, A. D. & RESNIKOFF, S. 2004. 2002 global update of available data on visual impairment: a compilation of population-based prevalence studies. *Ophthalmic Epidemiol,* 11**,** 67-115.

PELLI, D. G. & BEX, P. 2013. Measuring contrast sensitivity. *Vision Res,* 90**,** 10-4.

PENFOLD, P. L., KILLINGSWORTH, M. C. & SARKS, S. H. 1985. Senile macular degeneration: the involvement of immunocompetent cells. *Graefes Arch Clin Exp Ophthalmol,* 223**,** 69-76.

PENFOLD, P. L., KILLINGSWORTH, M. C. & SARKS, S. H. 1986. Senile macular degeneration. The involvement of giant cells in atrophy of the retinal pigment epithelium. *Invest Ophthalmol Vis Sci,* 27**,** 364-71.

PENG, S., LACERDA, A. E., KIRSCH, G. E., BROWN, A. M. & BRUENING-WRIGHT, A. 2010. The action potential and comparative pharmacology of stem cell-derived human cardiomyocytes. *J Pharmacol Toxicol Methods,* 61**,** 277-86.

PERSSON, B. D., SCHMITZ, N. B., SANTIAGO, C., ZOCHER, G., LARVIE, M., SCHEU, U., CASASNOVAS, J. M. & STEHLE, T. 2010. Structure of the extracellular portion of CD46 provides insights into its interactions with complement proteins and pathogens. *PLoS Pathog,* 6**,** e1001122.

PICARD, E., HOUSSIER, M., BUJOLD, K., SAPIEHA, P., LUBELL, W., DORFMAN, A., RACINE, J., HARDY, P., FEBBRAIO, M., LACHAPELLE, P., ONG, H., SENNLAUB, F. & CHEMTOB, S. 2010. CD36 plays an important role in the clearance of oxLDL and associated age-dependent sub-retinal deposits. *Aging (Albany NY),* 2**,** 981-9.

PILOTTO, E., GUIDOLIN, F., CONVENTO, E., SPEDICATO, L., VUJOSEVIC, S., CAVARZERAN, F. & MIDENA, E. 2013. Fundus autofluorescence and microperimetry in progressing geographic atrophy secondary to age-related macular degeneration. *Br J Ophthalmol,* 97**,** 622-6.

PILOTTO, E., GUIDOLIN, F., CONVENTO, E., STEFANON, F. G., PARROZZANI, R. & MIDENA, E. 2015. Progressing geographic atrophy: choroidal thickness and retinal sensitivity identify two clinical phenotypes. *Br J Ophthalmol,* 99**,** 1082-6.

POMP, O., DREESEN, O., LEONG, D. F., MELLER-POMP, O., TAN, T. T., ZHOU, F. & COLMAN, A. 2011. Unexpected X chromosome skewing during culture and reprogramming of human somatic cells can be alleviated by exogenous telomerase. *Cell Stem Cell,* 9**,** 156-65.

PRAJAPATI, S. C., BERNER, A., MOHAN, K., JUNG, K., RONEY, J., LOU, D., BROWN, J. & KLEINMAN, M. E. 2015. Histone deacetylase expression and acetylation in the aging retinal pigment epithelium. *Investigative Ophthalmology & Visual Science,* 56**,** 801-801.

QUERQUES, G., GUIGUI, B., LEVEZIEL, N., QUERQUES, L., BANDELLO, F. & SOUIED, E. H. 2013. Multimodal morphological and functional characterization of Malattia Leventinese. *Graefes Arch Clin Exp Ophthalmol,* 251**,** 705-14.

QUERQUES, G., MASSAMBA, N., SROUR, M., BOULANGER, E., GEORGES, A. & SOUIED, E. H. 2014. Impact of reticular pseudodrusen on macular function. *Retina,* 34**,** 321-9.

QUINN, R. H. & MILLER, S. S. 1992. Ion transport mechanisms in native human retinal pigment epithelium. *Invest Ophthalmol Vis Sci,* 33**,** 3513-27.

RABIN, D. M., RABIN, R. L., BLENKINSOP, T. A., TEMPLE, S. & STERN, J. H. 2013. Chronic oxidative stress upregulates Drusen-related protein expression in adult human RPE stem cell-derived RPE cells: a novel culture model for dry AMD. *Aging (Albany NY),* 5**,** 51-66.
RADHAKRISHNAN, S., LUNN, A., KIRSCHFINK, M., THORNER, P., HEBERT, D., LANGLOIS, V., PLUTHERO, F. & LICHT, C. 2012. Eculizumab and refractory membranoproliferative glomerulonephritis. *N Engl J Med,* 366**,** 1165-6.
RADU, R. A., HU, J., JIANG, Z. & BOK, D. 2014. Bisretinoid-mediated complement activation on retinal pigment epithelial cells is dependent on complement factor H haplotype. *J Biol Chem,* 289**,** 9113-20.
RAFTERY, J., CLEGG, A., JONES, J., TAN, S. C. & LOTERY, A. 2007. Ranibizumab (Lucentis) versus bevacizumab (Avastin): modelling cost effectiveness. *Br J Ophthalmol,* 91**,** 1244-6.
RAHNER, C., FUKUHARA, M., PENG, S., KOJIMA, S. & RIZZOLO, L. J. 2004. The apical and basal environments of the retinal pigment epithelium regulate the maturation of tight junctions during development. *J Cell Sci,* 117**,** 3307-18.
RAMKUMAR, H. L., ZHANG, J. & CHAN, C. C. 2010. Retinal ultrastructure of murine models of dry age-related macular degeneration (AMD). *Prog Retin Eye Res,* 29**,** 169-90.
RAMRATTAN, R. S., VAN DER SCHAFT, T. L., MOOY, C. M., DE BRUIJN, W. C., MULDER, P. G. & DE JONG, P. T. 1994. Morphometric analysis of Bruch's membrane, the choriocapillaris, and the choroid in aging. *Invest Ophthalmol Vis Sci,* 35**,** 2857-64.
RAPOSO, G. & MARKS, M. S. 2007. Melanosomes--dark organelles enlighten endosomal membrane transport. *Nat Rev Mol Cell Biol,* 8**,** 786-97.
RASHID, S. T., CORBINEAU, S., HANNAN, N., MARCINIAK, S. J., MIRANDA, E., ALEXANDER, G., HUANG-DORAN, I., GRIFFIN, J., AHRLUND-RICHTER, L., SKEPPER, J., SEMPLE, R., WEBER, A., LOMAS, D. A. & VALLIER, L. 2010. Modeling inherited metabolic disorders of the liver using human induced pluripotent stem cells. *J Clin Invest,* 120**,** 3127-36.
RATTNER, A., SMALLWOOD, P. M. & NATHANS, J. 2000. Identification and characterization of all-trans-retinol dehydrogenase from photoreceptor outer segments, the visual cycle enzyme that reduces all-trans-retinal to all-trans-retinol. *J Biol Chem,* 275**,** 11034-43.
REICHMAN, S., TERRAY, A., SLEMBROUCK, A., NANTEAU, C., ORIEUX, G., HABELER, W., NANDROT, E. F., SAHEL, J. A., MONVILLE, C. & GOUREAU, O. 2014. From confluent human iPS cells to self-forming neural retina and retinal pigmented epithelium. *Proc Natl Acad Sci U S A,* 111**,** 8518-23.
RESNIKOFF, S., PASCOLINI, D., ETYA'ALE, D., KOCUR, I., PARARAJASEGARAM, R., POKHAREL, G. P. & MARIOTTI, S. P. 2004. Global data on visual impairment in the year 2002. *Bull World Health Organ,* 82**,** 844-51.

REUBINOFF, B. E., ITSYKSON, P., TURETSKY, T., PERA, M. F., REINHARTZ, E., ITZIK, A. & BEN-HUR, T. 2001. Neural progenitors from human embryonic stem cells. *Nat Biotechnol,* 19**,** 1134-40.

REYNOLDS, R., HARTNETT, M. E., ATKINSON, J. P., GICLAS, P. C., ROSNER, B. & SEDDON, J. M. 2009. Plasma complement components and activation fragments: associations with age-related macular degeneration genotypes and phenotypes. *Invest Ophthalmol Vis Sci,* 50**,** 5818-27.

RIVERA, A., FISHER, S. A., FRITSCHE, L. G., KEILHAUER, C. N., LICHTNER, P., MEITINGER, T. & WEBER, B. H. 2005. Hypothetical LOC387715 is a second major susceptibility gene for age-related macular degeneration, contributing independently of complement factor H to disease risk. *Hum Mol Genet,* 14**,** 3227-36.

RIZZOLO, L. J. 2007. Development and role of tight junctions in the retinal pigment epithelium. *Int Rev Cytol,* 258**,** 195-234.

ROCCA, W. A., HOFMAN, A., BRAYNE, C., BRETELER, M. M., CLARKE, M., COPELAND, J. R., DARTIGUES, J. F., ENGEDAL, K., HAGNELL, O., HEEREN, T. J. & ET AL. 1991. Frequency and distribution of Alzheimer's disease in Europe: a collaborative study of 1980-1990 prevalence findings. The EURODEM-Prevalence Research Group. *Ann Neurol,* 30**,** 381-90.

ROONEY, P., WANG, M., KUMAR, P. & KUMAR, S. 1993. Angiogenic oligosaccharides of hyaluronan enhance the production of collagens by endothelial cells. *J Cell Sci,* 105 (Pt 1)**,** 213-8.

ROVNER, B. W., CASTEN, R. J. & TASMAN, W. S. 2002. Effect of depression on vision function in age-related macular degeneration. *Arch Ophthalmol,* 120**,** 1041-4.

ROY, F. H. 1974. World blindness: definition, incidence and major treatable causes. *Ann Ophthalmol,* 6**,** 1049-50.

RUIZ, A., WINSTON, A., LIM, Y. H., GILBERT, B. A., RANDO, R. R. & BOK, D. 1999. Molecular and biochemical characterization of lecithin retinol acyltransferase. *J Biol Chem,* 274**,** 3834-41.

RYAN, S. J. 1979. The development of an experimental model of subretinal neovascularization in disciform macular degeneration. *Trans Am Ophthalmol Soc,* 77**,** 707-45.

RYAN, S. J. 1982. Subretinal neovascularization. Natural history of an experimental model. *Arch Ophthalmol,* 100**,** 1804-9.

RZECHORZEK, N. M., CONNICK, P., LIVESEY, M. R., BOROOAH, S., PATANI, R., BURR, K., STORY, D., WYLLIE, D. J., HARDINGHAM, G. E. & CHANDRAN, S. 2016. Hypothermic Preconditioning Reverses Tau Ontogenesis in Human Cortical Neurons and is Mimicked by Protein Phosphatase 2A Inhibition. *EBioMedicine,* 3**,** 141-54.

SAHU, B., CHAVALI, V. R., ALAPATI, A., SUK, J., BARTSCH, D. U., JABLONSKI, M. M. & AYYAGARI, R. 2015. Presence of rd8 mutation does not alter the ocular phenotype of late-onset retinal degeneration mouse model. *Mol Vis,* 21**,** 273-84.

SAITO, Y., NISHIO, K., OGAWA, Y., KIMATA, J., KINUMI, T., YOSHIDA, Y., NOGUCHI, N. & NIKI, E. 2006. Turning point in apoptosis/necrosis induced by hydrogen peroxide. *Free Radic Res,* 40**,** 619-30.

SANDOVAL, A., AI, R., OSTRESH, J. M. & OGATA, R. T. 2000. Distal recognition site for classical pathway convertase located in the C345C/netrin module of complement component C5. *J Immunol,* 165**,** 1066-73.

SARKS, S., CHEREPANOFF, S., KILLINGSWORTH, M. & SARKS, J. 2007. Relationship of Basal laminar deposit and membranous debris to the clinical presentation of early age-related macular degeneration. *Invest Ophthalmol Vis Sci,* 48**,** 968-77.

SARKS, S. H. 1976. Ageing and degeneration in the macular region: a clinico-pathological study. *Br J Ophthalmol,* 60**,** 324-41.

SARKS, S. H., ARNOLD, J. J., KILLINGSWORTH, M. C. & SARKS, J. P. 1999. Early drusen formation in the normal and aging eye and their relation to age related maculopathy: a clinicopathological study. *Br J Ophthalmol,* 83**,** 358-68.

SARKS, S. H., VAN DRIEL, D., MAXWELL, L. & KILLINGSWORTH, M. 1980. Softening of drusen and subretinal neovascularization. *Trans Ophthalmol Soc U K,* 100**,** 414-22.

SCHMID, A., KOPP, A., ASLANIDIS, C., WABITSCH, M., MULLER, M. & SCHAFFLER, A. 2013. Regulation and function of C1Q/TNF-related protein-5 (CTRP-5) in the context of adipocyte biology. *Exp Clin Endocrinol Diabetes,* 121**,** 310-7.

SCHMIDT, S., HAUSER, M. A., SCOTT, W. K., POSTEL, E. A., AGARWAL, A., GALLINS, P., WONG, F., CHEN, Y. S., SPENCER, K., SCHNETZ-BOUTAUD, N., HAINES, J. L. & PERICAK-VANCE, M. A. 2006. Cigarette smoking strongly modifies the association of LOC387715 and age-related macular degeneration. *Am J Hum Genet,* 78**,** 852-64.

SCHMITZ-VALCKENBERG, S., FLECKENSTEIN, M., GOBEL, A. P., SEHMI, K., FITZKE, F. W., HOLZ, F. G. & TUFAIL, A. 2008. Evaluation of autofluorescence imaging with the scanning laser ophthalmoscope and the fundus camera in age-related geographic atrophy. *Am J Ophthalmol,* 146**,** 183-92.

SCHMITZ-VALCKENBERG, S., FLECKENSTEIN, M., HELB, H. M., CHARBEL ISSA, P., SCHOLL, H. P. & HOLZ, F. G. 2009. In vivo imaging of foveal sparing in geographic atrophy secondary to age-related macular degeneration. *Invest Ophthalmol Vis Sci,* 50**,** 3915-21.

SCHOLL, H. P., BELLMANN, C., DANDEKAR, S. S., BIRD, A. C. & FITZKE, F. W. 2004. Photopic and scotopic fine matrix mapping of retinal areas of increased fundus autofluorescence in patients with age-related maculopathy. *Invest Ophthalmol Vis Sci,* 45**,** 574-83.

SCHOLL, H. P., CHARBEL ISSA, P., WALIER, M., JANZER, S., POLLOK-KOPP, B., BORNCKE, F., FRITSCHE, L. G., CHONG, N. V., FIMMERS, R., WIENKER, T., HOLZ, F. G., WEBER, B. H. & OPPERMANN, M. 2008. Systemic complement activation in age-related macular degeneration. *PLoS One,* 3**,** e2593.

SEDDON, J. M., REYNOLDS, R., YU, Y., DALY, M. J. & ROSNER, B. 2011. Risk models for progression to advanced age-related macular degeneration using demographic, environmental, genetic, and ocular factors. *Ophthalmology,* 118**,** 2203-11.

SENNLAUB, F., AUVYNET, C., CALIPPE, B., LAVALETTE, S., POUPEL, L., HU, S. J., DOMINGUEZ, E., CAMELO, S., LEVY, O., GUYON, E., SAEDERUP, N., CHARO, I. F., ROOIJEN, N. V., NANDROT, E., BOURGES, J. L., BEHAR-COHEN, F., SAHEL, J. A., GUILLONNEAU, X., RAOUL, W. & COMBADIERE, C. 2013. CCR2(+) monocytes infiltrate atrophic lesions in age-related macular disease and mediate photoreceptor degeneration in experimental subretinal inflammation in Cx3cr1 deficient mice. *EMBO Mol Med,* 5**,** 1775-93.

SHAW, P. X., ZHANG, L., ZHANG, M., DU, H., ZHAO, L., LEE, C., GROB, S., LIM, S. L., HUGHES, G. & LEE, J. 2012. Complement factor H genotypes impact risk of age-related macular degeneration by interaction with oxidized phospholipids. *Proceedings of the National Academy of Sciences,* 109**,** 13757-13762.

SHERIDAN, A. M., FITZPATRICK, S., WANG, C., WHEELER, D. C. & LIEBERTHAL, W. 1996. Lipid peroxidation contributes to hydrogen peroxide induced cytotoxicity in renal epithelial cells. *Kidney international,* 49**,** 88-93.

SHU, X., TULLOCH, B., LENNON, A., HAYWARD, C., O'CONNELL, M., CIDECIYAN, A. V., JACOBSON, S. G. & WRIGHT, A. F. 2006a. Biochemical characterisation of the C1QTNF5 gene associated with late-onset retinal degeneration. A genetic model of age-related macular degeneration. *Adv Exp Med Biol,* 572**,** 41-8.

SHU, X., TULLOCH, B., LENNON, A., VLACHANTONI, D., ZHOU, X., HAYWARD, C. & WRIGHT, A. F. 2006b. Disease mechanisms in late-onset retinal macular degeneration associated with mutation in C1QTNF5. *Hum Mol Genet,* 15**,** 1680-9.

SIM, D. A., KEANE, P. A., MEHTA, H., FUNG, S., ZARRANZ-VENTURA, J., FRUTTIGER, M., PATEL, P. J., EGAN, C. A. & TUFAIL, A. 2013. Repeatability and reproducibility of choroidal vessel layer measurements in diabetic retinopathy using enhanced depth optical coherence tomography. *Invest Ophthalmol Vis Sci,* 54**,** 2893-901.

SIMON, J. D., HONG, L. & PELES, D. N. 2008. Insights into melanosomes and melanin from some interesting spatial and temporal properties. *J Phys Chem B,* 112**,** 13201-17.

SINGH, R., KUAI, D., GUZIEWICZ, K. E., MEYER, J., WILSON, M., LU, J., SMITH, M., CLARK, E., VERHOEVEN, A., AGUIRRE, G. D. & GAMM, D. M. 2015. Pharmacological

Modulation of Photoreceptor Outer Segment Degradation in a Human iPS Cell Model of Inherited Macular Degeneration. *Mol Ther,* 23**,** 1700-11.
SINGH, R., PHILLIPS, M. J., KUAI, D., MEYER, J., MARTIN, J. M., SMITH, M. A., PEREZ, E. T., SHEN, W., WALLACE, K. A., CAPOWSKI, E. E., WRIGHT, L. S. & GAMM, D. M. 2013a. Functional analysis of serially expanded human iPS cell-derived RPE cultures. *Invest Ophthalmol Vis Sci,* 54**,** 6767-78.
SINGH, R., SHEN, W., KUAI, D., MARTIN, J. M., GUO, X., SMITH, M. A., PEREZ, E. T., PHILLIPS, M. J., SIMONETT, J. M., WALLACE, K. A., VERHOEVEN, A. D., CAPOWSKI, E. E., ZHANG, X., YIN, Y., HALBACH, P. J., FISHMAN, G. A., WRIGHT, L. S., PATTNAIK, B. R. & GAMM, D. M. 2013b. iPS cell modeling of Best disease: insights into the pathophysiology of an inherited macular degeneration. *Hum Mol Genet,* 22**,** 593-607.
SJÖBERG, A. P., TROUW, L. A., CLARK, S. J., SJÖLANDER, J., HEINEGÅRD, D., SIM, R. B., DAY, A. J. & BLOM, A. M. 2007. The factor H variant associated with age-related macular degeneration (His-384) and the non-disease-associated form bind differentially to C-reactive protein, fibromodulin, DNA, and necrotic cells. *Journal of Biological Chemistry,* 282**,** 10894-10900.
SKERKA, C., LAUER, N., WEINBERGER, A. A., KEILHAUER, C. N., SÜHNEL, J., SMITH, R., SCHLÖTZER–SCHREHARDT, U., FRITSCHE, L., HEINEN, S. & HARTMANN, A. 2007. Defective complement control of factor H (Y402H) and FHL-1 in age-related macular degeneration. *Molecular immunology,* 44**,** 3398-3406.
SMITH, A. F. 2010. The growing importance of pharmacoeconomics: the case of age-related macular degeneration. *Br J Ophthalmol,* 94**,** 1116-7.
SMITH, W., ASSINK, J., KLEIN, R., MITCHELL, P., KLAVER, C. C., KLEIN, B. E., HOFMAN, A., JENSEN, S., WANG, J. J. & DE JONG, P. T. 2001. Risk factors for age-related macular degeneration: Pooled findings from three continents. *Ophthalmology,* 108**,** 697-704.
SNYDER, P. M. 2002. The epithelial Na+ channel: cell surface insertion and retrieval in Na+ homeostasis and hypertension. *Endocr Rev,* 23**,** 258-75.
SOLDNER, F., HOCKEMEYER, D., BEARD, C., GAO, Q., BELL, G. W., COOK, E. G., HARGUS, G., BLAK, A., COOPER, O., MITALIPOVA, M., ISACSON, O. & JAENISCH, R. 2009. Parkinson's disease patient-derived induced pluripotent stem cells free of viral reprogramming factors. *Cell,* 136**,** 964-77.
SOLDNER, F., LAGANIÈRE, J., CHENG, A. W., HOCKEMEYER, D., GAO, Q., ALAGAPPAN, R., KHURANA, V., GOLBE, L. I., MYERS, R. H. & LINDQUIST, S. 2011. Generation of isogenic pluripotent stem cells differing exclusively at two early onset Parkinson point mutations. *Cell,* 146**,** 318-331.

SONODA, S., SPEE, C., BARRON, E., RYAN, S. J., KANNAN, R. & HINTON, D. R. 2009. A protocol for the culture and differentiation of highly polarized human retinal pigment epithelial cells. *Nat Protoc,* 4**,** 662-73.

SOUIED, E. H., BENLIAN, P., AMOUYEL, P., FEINGOLD, J., LAGARDE, J. P., MUNNICH, A., KAPLAN, J., COSCAS, G. & SOUBRANE, G. 1998. The epsilon4 allele of the apolipoprotein E gene as a potential protective factor for exudative age-related macular degeneration. *Am J Ophthalmol,* 125**,** 353-9.

SOUIED, E. H., LEVEZIEL, N., QUERQUES, G., DARMON, J., COSCAS, G. & SOUBRANE, G. 2006. Indocyanine green angiography features of Malattia leventinese. *Br J Ophthalmol,* 90**,** 296-300.

SOUMPLIS, V., SERGOUNIOTIS, P. I., ROBSON, A. G., MICHAELIDES, M., MOORE, A. T., HOLDER, G. E. & WEBSTER, A. R. 2013. Phenotypic findings in C1QTNF5 retinopathy (late-onset retinal degeneration). *Acta Ophthalmol,* 91**,** e191-5.

SPAIDE, R. F. & CURCIO, C. A. 2010. Drusen characterization with multimodal imaging. *Retina,* 30**,** 1441-54.

SPARROW, J. R. & BOULTON, M. 2005. RPE lipofuscin and its role in retinal pathobiology. *Exp Eye Res,* 80**,** 595-606.

SPARROW, J. R. & CAI, B. 2001. Blue light-induced apoptosis of A2E-containing RPE: involvement of caspase-3 and protection by Bcl-2. *Invest Ophthalmol Vis Sci,* 42**,** 1356-62.

SPITZNAS, M. & HOGAN, M. J. 1970. Outer segments of photoreceptors and the retinal pigment epithelium. Interrelationship in the human eye. *Arch Ophthalmol,* 84**,** 810-9.

SPRAUL, C. W., LANG, G. E., GROSSNIKLAUS, H. E. & LANG, G. K. 1999. Histologic and morphometric analysis of the choroid, Bruch's membrane, and retinal pigment epithelium in postmortem eyes with age-related macular degeneration and histologic examination of surgically excised choroidal neovascular membranes. *Surv Ophthalmol,* 44 Suppl 1**,** S10-32.

STANTON, C. M., YATES, J. R., DEN HOLLANDER, A. I., SEDDON, J. M., SWAROOP, A., STAMBOLIAN, D., FAUSER, S., HOYNG, C., YU, Y., ATSUHIRO, K., BRANHAM, K., OTHMAN, M., CHEN, W., KORTVELY, E., CHALMERS, K., HAYWARD, C., MOORE, A. T., DHILLON, B., UEFFING, M. & WRIGHT, A. F. 2011. Complement factor D in age-related macular degeneration. *Invest Ophthalmol Vis Sci,* 52**,** 8828-34.

STEINBERG, J. S., AUGE, J., JAFFE, G. J., FLECKENSTEIN, M., HOLZ, F. G., SCHMITZ-VALCKENBERG, S. & GROUP, G. A. P. S. 2013. Longitudinal analysis of reticular drusen associated with geographic atrophy in age-related macular degeneration. *Invest Ophthalmol Vis Sci,* 54**,** 4054-60.

STREETEN, B. W. 1969. Development of the human retinal pigment epithelium and the posterior segment. *Arch Ophthalmol,* 81**,** 383-94.

SUBRAYAN, V., MORRIS, B., ARMBRECHT, A. M., WRIGHT, A. F. & DHILLON, B. 2005. Long anterior lens zonules in late-onset retinal degeneration (L-ORD). *Am J Ophthalmol,* 140**,** 1127-9.

SUI, G. Y., LIU, G. C., LIU, G. Y., GAO, Y. Y., DENG, Y., WANG, W. Y., TONG, S. H. & WANG, L. 2013. Is sunlight exposure a risk factor for age-related macular degeneration? A systematic review and meta-analysis. *Br J Ophthalmol,* 97**,** 389-94.

SUN, C., ZHAO, M. & LI, X. 2012. CFB/C2 gene polymorphisms and risk of age-related macular degeneration: a systematic review and meta-analysis. *Curr Eye Res,* 37**,** 259-71.

SUN, J., MANDAI, M., KAMAO, H., HASHIGUCHI, T., SHIKAMURA, M., KAWAMATA, S., SUGITA, S. & TAKAHASHI, M. 2015. Protective Effects of Human iPS-Derived Retinal Pigmented Epithelial Cells in Comparison with Human Mesenchymal Stromal Cells and Human Neural Stem Cells on the Degenerating Retina in rd1 mice. *Stem Cells,* 33**,** 1543-53.

SUNNESS, J. S. 1999. The natural history of geographic atrophy, the advanced atrophic form of age-related macular degeneration. *Mol Vis,* 5**,** 25.

TAKAHASHI, K., TANABE, K., OHNUKI, M., NARITA, M., ICHISAKA, T., TOMODA, K. & YAMANAKA, S. 2007. Induction of pluripotent stem cells from adult human fibroblasts by defined factors. *Cell,* 131**,** 861-72.

TAKAHASHI, K. & YAMANAKA, S. 2006. Induction of pluripotent stem cells from mouse embryonic and adult fibroblast cultures by defined factors. *Cell,* 126**,** 663-76.

TANG, N. P., ZHOU, B., WANG, B. & YU, R. B. 2009. HTRA1 promoter polymorphism and risk of age-related macular degeneration: a meta-analysis. *Ann Epidemiol,* 19**,** 740-5.

TARALLO, V., HIRANO, Y., GELFAND, B. D., DRIDI, S., KERUR, N., KIM, Y., CHO, W. G., KANEKO, H., FOWLER, B. J., BOGDANOVICH, S., ALBUQUERQUE, R. J., HAUSWIRTH, W. W., CHIODO, V. A., KUGEL, J. F., GOODRICH, J. A., PONICSAN, S. L., CHAUDHURI, G., MURPHY, M. P., DUNAIEF, J. L., AMBATI, B. K., OGURA, Y., YOO, J. W., LEE, D. K., PROVOST, P., HINTON, D. R., NUNEZ, G., BAFFI, J. Z., KLEINMAN, M. E. & AMBATI, J. 2012. DICER1 loss and Alu RNA induce age-related macular degeneration via the NLRP3 inflammasome and MyD88. *Cell,* 149**,** 847-59.

TATE, D. J., JR., MICELI, M. V. & NEWSOME, D. A. 1995. Phagocytosis and H2O2 induce catalase and metallothionein gene expression in human retinal pigment epithelial cells. *Invest Ophthalmol Vis Sci,* 36**,** 1271-9.

TCHIEU, J., KUOY, E., CHIN, M. H., TRINH, H., PATTERSON, M., SHERMAN, S. P., AIMIUWU, O., LINDGREN, A., HAKIMIAN, S., ZACK, J. A., CLARK, A. T., PYLE, A. D., LOWRY, W. E. & PLATH, K. 2010. Female human iPSCs retain an inactive X chromosome. *Cell Stem Cell,* 7**,** 329-42.

THAKKINSTIAN, A., BOWE, S., MCEVOY, M., SMITH, W. & ATTIA, J. 2006. Association between apolipoprotein E polymorphisms and age-related macular degeneration: A HuGE review and meta-analysis. *Am J Epidemiol,* 164**,** 813-22.

THIEL, S. 2007. Complement activating soluble pattern recognition molecules with collagen-like regions, mannan-binding lectin, ficolins and associated proteins. *Mol Immunol,* 44**,** 3875-88.

THOMSON, J. A., ITSKOVITZ-ELDOR, J., SHAPIRO, S. S., WAKNITZ, M. A., SWIERGIEL, J. J., MARSHALL, V. S. & JONES, J. M. 1998. Embryonic stem cell lines derived from human blastocysts. *Science,* 282**,** 1145-7.

TROPEPE, V., HITOSHI, S., SIRARD, C., MAK, T. W., ROSSANT, J. & VAN DER KOOY, D. 2001. Direct neural fate specification from embryonic stem cells: a primitive mammalian neural stem cell stage acquired through a default mechanism. *Neuron,* 30**,** 65-78.

TU, X. & PALCZEWSKI, K. 2012. Crystal structure of the globular domain of C1QTNF5: Implications for late-onset retinal macular degeneration. *J Struct Biol,* 180**,** 439-46.

TU, X. & PALCZEWSKI, K. 2014. The macular degeneration-linked C1QTNF5 (S163) mutation causes higher-order structural rearrangements. *J Struct Biol,* 186**,** 86-94.

TUCKER, B. A., CRANSTON, C. M., ANFINSON, K. A., SHRESTHA, S., STREB, L. M., LEON, A., MULLINS, R. F. & STONE, E. M. 2015. Using patient-specific induced pluripotent stem cells to interrogate the pathogenicity of a novel retinal pigment epithelium-specific 65 kDa cryptic splice site mutation and confirm eligibility for enrollment into a clinical gene augmentation trial. *Transl Res,* 166**,** 740-749 e1.

UMEDA, S., SUZUKI, M. T., OKAMOTO, H., ONO, F., MIZOTA, A., TERAO, K., YOSHIKAWA, Y., TANAKA, Y. & IWATA, T. 2005. Molecular composition of drusen and possible involvement of anti-retinal autoimmunity in two different forms of macular degeneration in cynomolgus monkey (Macaca fascicularis). *FASEB J,* 19**,** 1683-5.

URBACH, A., BAR-NUR, O., DALEY, G. Q. & BENVENISTY, N. 2010. Differential modeling of fragile X syndrome by human embryonic stem cells and induced pluripotent stem cells. *Cell Stem Cell,* 6**,** 407-11.

VALLIER, L., ALEXANDER, M. & PEDERSEN, R. A. 2005. Activin/Nodal and FGF pathways cooperate to maintain pluripotency of human embryonic stem cells. *J Cell Sci,* 118**,** 4495-509.

VAN DER SCHAFT, T. L., MOOY, C. M., DE BRUIJN, W. C., BOSMAN, F. T. & DE JONG, P. T. 1994. Immunohistochemical light and electron microscopy of basal laminar deposit. *Graefes Arch Clin Exp Ophthalmol,* 232**,** 40-6.

VANDEKERCKHOVE, J., DEBOBEN, A., NASSAL, M. & WIELAND, T. 1985. The phalloidin binding site of F-actin. *EMBO J,* 4**,** 2815-8.

VINCENT, A., MUNIER, F. L., VANDENHOVEN, C. C., WRIGHT, T., WESTALL, C. A. & HEON, E. 2012. The characterization of retinal phenotype in a family with C1QTNF5-related late-onset retinal degeneration. *Retina,* 32**,** 1643-51.
VIVARELLI, M., PASINI, A. & EMMA, F. 2012. Eculizumab for the treatment of dense-deposit disease. *N Engl J Med,* 366**,** 1163-5.
VOGT, S. D., CURCIO, C. A., WANG, L., LI, C. M., MCGWIN, G., JR., MEDEIROS, N. E., PHILP, N. J., KIMBLE, J. A. & READ, R. W. 2011. Retinal pigment epithelial expression of complement regulator CD46 is altered early in the course of geographic atrophy. *Exp Eye Res,* 93**,** 413-23.
VON RUCKMANN, A., FITZKE, F. W. & BIRD, A. C. 1995. Distribution of fundus autofluorescence with a scanning laser ophthalmoscope. *Br J Ophthalmol,* 79**,** 407-12.
VUGLER, A., CARR, A. J., LAWRENCE, J., CHEN, L. L., BURRELL, K., WRIGHT, A., LUNDH, P., SEMO, M., AHMADO, A., GIAS, C., DA CRUZ, L., MOORE, H., ANDREWS, P., WALSH, J. & COFFEY, P. 2008. Elucidating the phenomenon of HESC-derived RPE: anatomy of cell genesis, expansion and retinal transplantation. *Exp Neurol,* 214**,** 347-61.
WALPORT, M. J. 2001. Complement. First of two parts. *N Engl J Med,* 344**,** 1058-66.
WEBER, B. H., VOGT, G., PRUETT, R. C., STÖHR, H. & FELBOR, U. 1994. Mutations in the tissue inhibitor of metalloproteinases-3 (TIMP3) in patients with Sorsby's fundus dystrophy. *Nature genetics,* 8**,** 352-356.
WEISMANN, D., HARTVIGSEN, K., LAUER, N., BENNETT, K. L., SCHOLL, H. P., ISSA, P. C., CANO, M., BRANDSTÄTTER, H., TSIMIKAS, S. & SKERKA, C. 2011. Complement factor H binds malondialdehyde epitopes and protects from oxidative stress. *Nature,* 478**,** 76-81.
WESTENSKOW, P. D., MORENO, S. K., KROHNE, T. U., KURIHARA, T., ZHU, S., ZHANG, Z. N., ZHAO, T., XU, Y., DING, S. & FRIEDLANDER, M. 2012. Using flow cytometry to compare the dynamics of photoreceptor outer segment phagocytosis in iPS-derived RPE cells. *Invest Ophthalmol Vis Sci,* 53**,** 6282-90.
WHITMORE, S. S., SOHN, E. H., CHIRCO, K. R., DRACK, A. V., STONE, E. M., TUCKER, B. A. & MULLINS, R. F. 2015. Complement activation and choriocapillaris loss in early AMD: implications for pathophysiology and therapy. *Prog Retin Eye Res,* 45**,** 1-29.
WHITMORE, S. S., WAGNER, A. H., DELUCA, A. P., DRACK, A. V., STONE, E. M., TUCKER, B. A., ZENG, S., BRAUN, T. A., MULLINS, R. F. & SCHEETZ, T. E. 2014. Transcriptomic analysis across nasal, temporal, and macular regions of human neural retina and RPE/choroid by RNA-Seq. *Exp Eye Res,* 129**,** 93-106.
WILMUT, I., SCHNIEKE, A. E., MCWHIR, J., KIND, A. J. & CAMPBELL, K. H. 1997. Viable offspring derived from fetal and adult mammalian cells. *Nature,* 385**,** 810-3.

WONG, G. W., KRAWCZYK, S. A., KITIDIS-MITROKOSTAS, C., REVETT, T., GIMENO, R. & LODISH, H. F. 2008. Molecular, biochemical and functional characterizations of C1q/TNF family members: adipose-tissue-selective expression patterns, regulation by PPAR-gamma agonist, cysteine-mediated oligomerizations, combinatorial associations and metabolic functions. *Biochem J,* 416**,** 161-77.

WONG, W. L., SU, X., LI, X., CHEUNG, C. M., KLEIN, R., CHENG, C. Y. & WONG, T. Y. 2014. Global prevalence of age-related macular degeneration and disease burden projection for 2020 and 2040: a systematic review and meta-analysis. *Lancet Glob Health,* 2**,** e106-16.

WU, Z., AYTON, L. N., MAKEYEVA, G., GUYMER, R. H. & LUU, C. D. 2015. Impact of reticular pseudodrusen on microperimetry and multifocal electroretinography in intermediate age-related macular degeneration. *Invest Ophthalmol Vis Sci,* 56**,** 2100-6.

YAHATA, N., ASAI, M., KITAOKA, S., TAKAHASHI, K., ASAKA, I., HIOKI, H., KANEKO, T., MARUYAMA, K., SAIDO, T. C., NAKAHATA, T., ASADA, T., YAMANAKA, S., IWATA, N. & INOUE, H. 2011. Anti-Abeta drug screening platform using human iPS cell-derived neurons for the treatment of Alzheimer's disease. *PLoS One,* 6**,** e25788.

YANG, J., LI, Y., CHAN, L., TSAI, Y. T., WU, W. H., NGUYEN, H. V., HSU, C. W., LI, X., BROWN, L. M., EGLI, D., SPARROW, J. R. & TSANG, S. H. 2014a. Validation of genome-wide association study (GWAS)-identified disease risk alleles with patient-specific stem cell lines. *Hum Mol Genet,* 23**,** 3445-55.

YANG, P., BACIU, P., KERRIGAN, B. C., ETHERIDGE, M., SUNG, E., TOIMIL, B. A., BERCHUCK, J. E. & JAFFE, G. J. 2014b. Retinal pigment epithelial cell death by the alternative complement cascade: role of membrane regulatory proteins, calcium, PKC, and oxidative stress. *Invest Ophthalmol Vis Sci,* 55**,** 3012-21.

YANG, P., BACIU, P., KERRIGAN, B. C. P., ETHERIDGE, M., SUNG, E., TOIMIL, B. A., BERCHUCK, J. E. & JAFFE, G. J. 2014c. Retinal Pigment Epithelial Cell Death by the Alternative Complement Cascade: Role of Membrane Regulatory Proteins, Calcium, PKC, and Oxidative StressComplement-Mediated RPE Cell Death. *Investigative ophthalmology & visual science,* 55**,** 3012-3021.

YANG, Z., CAMP, N. J., SUN, H., TONG, Z., GIBBS, D., CAMERON, D. J., CHEN, H., ZHAO, Y., PEARSON, E., LI, X., CHIEN, J., DEWAN, A., HARMON, J., BERNSTEIN, P. S., SHRIDHAR, V., ZABRISKIE, N. A., HOH, J., HOWES, K. & ZHANG, K. 2006. A variant of the HTRA1 gene increases susceptibility to age-related macular degeneration. *Science,* 314**,** 992-3.

YANG, Z., STRATTON, C., FRANCIS, P. J., KLEINMAN, M. E., TAN, P. L., GIBBS, D., TONG, Z., CHEN, H., CONSTANTINE, R., YANG, X., CHEN, Y., ZENG, J., DAVEY, L., MA, X., HAU, V. S., WANG, C., HARMON, J., BUEHLER, J., PEARSON, E., PATEL, S., KAMINOH, Y., WATKINS, S., LUO, L., ZABRISKIE, N. A., BERNSTEIN, P. S., CHO, W.,

SCHWAGER, A., HINTON, D. R., KLEIN, M. L., HAMON, S. C., SIMMONS, E., YU, B., CAMPOCHIARO, B., SUNNESS, J. S., CAMPOCHIARO, P., JORDE, L., PARMIGIANI, G., ZACK, D. J., KATSANIS, N., AMBATI, J. & ZHANG, K. 2008. Toll-like receptor 3 and geographic atrophy in age-related macular degeneration. *N Engl J Med,* 359**,** 1456-63.

YEHOSHUA, Z., DE AMORIM GARCIA FILHO, C. A., NUNES, R. P., GREGORI, G., PENHA, F. M., MOSHFEGHI, A. A., ZHANG, K., SADDA, S., FEUER, W. & ROSENFELD, P. J. 2014. Systemic complement inhibition with eculizumab for geographic atrophy in age-related macular degeneration: the COMPLETE study. *Ophthalmology,* 121**,** 693-701.

YOUNG, R. W. & BOK, D. 1969. Participation of the retinal pigment epithelium in the rod outer segment renewal process. *J Cell Biol,* 42**,** 392-403.

YOUNG, R. W. & DROZ, B. 1968. The renewal of protein in retinal rods and cones. *J Cell Biol,* 39**,** 169-84.

YU, H., MUNOZ, E. M., EDENS, R. E. & LINHARDT, R. J. 2005. Kinetic studies on the interactions of heparin and complement proteins using surface plasmon resonance. *Biochimica et Biophysica Acta (BBA)-General Subjects,* 1726**,** 168-176.

YU, Y., BHANGALE, T. R., FAGERNESS, J., RIPKE, S., THORLEIFSSON, G., TAN, P. L., SOUIED, E. H., RICHARDSON, A. J., MERRIAM, J. E., BUITENDIJK, G. H., REYNOLDS, R., RAYCHAUDHURI, S., CHIN, K. A., SOBRIN, L., EVANGELOU, E., LEE, P. H., LEE, A. Y., LEVEZIEL, N., ZACK, D. J., CAMPOCHIARO, B., CAMPOCHIARO, P., SMITH, R. T., BARILE, G. R., GUYMER, R. H., HOGG, R., CHAKRAVARTHY, U., ROBMAN, L. D., GUSTAFSSON, O., SIGURDSSON, H., ORTMANN, W., BEHRENS, T. W., STEFANSSON, K., UITTERLINDEN, A. G., VAN DUIJN, C. M., VINGERLING, J. R., KLAVER, C. C., ALLIKMETS, R., BRANTLEY, M. A., JR., BAIRD, P. N., KATSANIS, N., THORSTEINSDOTTIR, U., IOANNIDIS, J. P., DALY, M. J., GRAHAM, R. R. & SEDDON, J. M. 2011. Common variants near FRK/COL10A1 and VEGFA are associated with advanced age-related macular degeneration. *Hum Mol Genet,* 20**,** 3699-709.

YUAN, X., GU, X., CRABB, J. S., YUE, X., SHADRACH, K., HOLLYFIELD, J. G. & CRABB, J. W. 2010. Quantitative proteomics: comparison of the macular Bruch membrane/choroid complex from age-related macular degeneration and normal eyes. *Mol Cell Proteomics,* 9**,** 1031-46.

ZAREPARSI, S., BURACZYNSKA, M., BRANHAM, K. E., SHAH, S., ENG, D., LI, M., PAWAR, H., YASHAR, B. M., MOROI, S. E., LICHTER, P. R., PETTY, H. R., RICHARDS, J. E., ABECASIS, G. R., ELNER, V. M. & SWAROOP, A. 2005. Toll-like receptor 4 variant D299G is associated with susceptibility to age-related macular degeneration. *Hum Mol Genet,* 14**,** 1449-55.

ZEISS, C. J. 2010. Animals as models of age-related macular degeneration: an imperfect measure of the truth. *Vet Pathol,* 47**,** 396-413.

ZHONG, X., GUTIERREZ, C., XUE, T., HAMPTON, C., VERGARA, M. N., CAO, L.-H., PETERS, A., PARK, T. S., ZAMBIDIS, E. T. & MEYER, J. S. 2014. Generation of three-dimensional retinal tissue with functional photoreceptors from human iPSCs. *Nature communications,* 5.

ZOU, J., MALI, P., HUANG, X., DOWEY, S. N. & CHENG, L. 2011. Site-specific gene correction of a point mutation in human iPS cells derived from an adult patient with sickle cell disease. *Blood,* 118**,** 4599-608.

ZWEIFEL, S. A., SPAIDE, R. F., CURCIO, C. A., MALEK, G. & IMAMURA, Y. 2010. Reticular pseudodrusen are subretinal drusenoid deposits. *Ophthalmology,* 117**,** 303-12 e1.

Appendix I Media

MEF medium (510ml)

DMEM (Gibco 10829) 450ml
2mM Glutamine (Invitrogen25030024) 5ml
FBS (Biosera S1818) 50ml (10%)
P/S (Gibco 15140) 5ml

HiPSC media and EB media

E8 media Thermofisher (A1517001) minus FGF for EB

Neural induction media (500mls)

DMEM/F12 485mls (Gibco 12500-062)

N2 supplement 5mls (Invitrogen 17504044)

MEM 5mls (Invitrogen 12634-010)

2 g/mL heparin

1% penicillin/streptomycin 5mls (Gibco 152140)

Retinal differentiation media (500mls)

DMEM (340ml) (Gibco 11965-118)

F12 (145ml) (Gibco 11765-062)

10ml B27 minus retinoic acid (Gibco 12587010)

15ml Penicillin/streptomycin ((Gibco 152140)

Complement serum

Sera	Company	Catalogue number
Human complement sera	Quidel	A113
C1Q depleted	Comptech	A300
C4 depleted	Comptech	A308
Factor B depleted	Comptech	A335
Factor D depleted	Comptech	A336
C3 depleted	Comptech	A314
C5 depleted	Comptech	A320
CFH depleted	Comptech	A337

Appendix II Materials

Equipment

Equipment	Make	Catalogue number
15ml centrifuge tubes	Corning	430790
50ml centrifuge tubes	Corning	430828
100mm dishes	Corning	430167
6 well plates	Corning	3516
24 well plate	Corning	3524
96 well plates	TPP	92696
Filters	Nalgene	566-0020
2ml pipette	Corning	4486
5ml pipette	Corning	4051
10 ml pipette	Corning	4101
Roller mixer	Stuart	SRT6
Orbital shaker	Stuart	SSL4
Block heater	Stuart	SBH130DC
Microscope immunofluorescence	Zeiss	Axiocam
Confocal microscope	Zeiss	
Western blot	Bio-Rad	
PCR	Bio-Rad	C1000 thermal cycler
Western imaging	LiCOR	Odyssey
Protein quantification	Nanodrop	ND-1000 spectrophotometer
Centrifuge	Eppendorf	5702
Incubator	Panasonic	MCO-1BAC-PE

Appendix III Primers

Standard PCR conditions

Material	Company	Volume
Optimized DyNAzyme EXT buffer 10x	ThermoFisher Scientific, F-511L	1.6 µl
Betaine, 5M	Sigma, B0300	7.2 µl
HPE dNTP mix	Scientific Lab Supplies, 28406551	0.3 µl
F2 primer, 5µM		2.0 µl
Repeat R primer, 5µM		1.0 µl
Tail R		3.0 µl
DyNAzyme DNA Polymerase 1U/µl	ThermoFisher Scientific, F505-L	2.4 µl
H_2O		1.5 µl
DNA, 200ng/ µl		1.0 µl

Step	Temperature (^oC)	Duration
1	95	45 seconds
2	98	10 seconds
3	61	30 seconds
4	78	5 seconds (slow ramp, 0.6°C/second)
5	78	2 seconds
6	86	2 seconds
7	78	2 seconds
8	90	2 seconds
9	78	10 minutes

Steps 3 to 8 were repeated 35 times. Steps 5 and 6 and steps 7 and 8 were repeated 2 times

every cycle.

qRT-PCR cycling conditions

Temperature (°C)	Duration	Cycles
95	7 minutes	
95	15 seconds	40
59	30 seconds	
65	0.5C/5seconds (melt curve)	
95		

Pluripotency primers

β-Actin TGAAGTGTGACGTGGACATC GGAGGAGCAATGATCTTGAT
Endo-Oct4 CCTCACTTCACTGCATGTA CAGGTTTTCTTTCCCTAGCT
Endo-Sox2 CCCGCAGACTTCACATGT CCTCCCATTTCCCTCGTTTT
Endo-Myc GCGTCCTGGGAAGGGAGATCCGGAGC
TTGAGGGGCATCGTCGCGGGAGGCTG
Endo-Klf4 GATGAACTGACCAGGCACTA GTGGGTCATATCCACTGTCT

Complement sequencing

Seq CFH original F TGAGGGTTTCTTCTTGAAAATCA
Seq CFH original R TTGGTGTGAGATAACGAACCTC

Seq HTRA1 snp2 F AGCCGCTTCCTAGGCTCTCT
Seq HTRA1 snp2 R GGGGAAAGTTCCTGCAAATC

Seq ARMS2HTRA1 F TACCCAGGACCGATGGTAAC
Seq ARMS2HTRA1 R AGGCTGGTTAAAATGCAAGC

Seq C3 F CTCGCACCTCCTTCACATGC
Seq C3 R GACAAAGAGGCCTCGTGAGA

Seq C2CFB F GGACTTCCGAAACACATTCG
Seq C2CFB R CAACTGGTCCCAAAGGAGAG

L-ORMD sequencing

LORD seqF: ACG AGC AGG GAC ATT ACG AC

LORD seqR: AGA AAT CCG GAG AAG GTG CT

Appendix IV Antibodies

Pluripotency

NANOG	Goat	R&D Systems, AF-1997	1:250
SOX2	Mouse	Millipore, AB5603	1:250
TRA-1-60	Mouse	Santa Cruz, SC-21705	1:250
OCT3/4	Mouse	Santa Cruz, SC-5279	1:250

Three germ layer differentiation

Antibody	Host	Company	Concentration
SOX1	Goat polyclonal	R&D systems	1:100
Nestin	Mouse monoclonal	Milipore	1:100
Brachyury	Goat polyclonal	R&D systems	1:100
Eomes	Rabbit polyclonal	Abcam	1:600
Fox A2	Goat polyclonal	R&D systems	1:100
GATA-4	Mouse monoclonal	Santa Cruz	1:100

HiPSC-RPE staining

Antigen	Host species	Company and code	Dilutions with use
MITF	Mouse	SANTA CRUZ sc-71588	1:250
C3d	Rabbit	Abcam ab55811	1:1000
Bestrophin	Mouse	Millipore MAB5466	1:100
Ezrin	Rabbit	Cell signalling 3145	1:200
ZO-1	Rabbit	Invitrogen 61-7300	1:250
C1QTNF5	Rabbit	Lifespan LS-B1343	1:250

RPE65	Rabbit	Abcam ab150366	1:250
CRALBP	Mouse	Abcam ab15051	1:250
Ki67	Mouse monoclonal	Dako	1:200
C5b-9	Mouse monoclonal	DAKO M0777	1:100

Appendix V Published papers

The information presented in the introduction and methods was published in part in two papers:

Using human induced pluripotent stem cells to treat retinal disease. **Borooah S**, Phillips MJ, Bilican B, Wright AF, Wilmut I, Chandran S, Gamm D, Dhillon B. Progress in Retinal and Eye Research. 2013 Nov;37:163-81.

Late-onset retinal macular degeneration: clinical insights into an inherited retinal degeneration. **Borooah S**, Collins C, Wright A, Dhillon B. British Journal of Ophthalmology. 2009 Mar;93 (3):284-9

The studies presented in chapter 3 were published in part in two articles:

Human iPSC-derived motoneurons harbouring TARDBP or C9ORF72 ALS mutations are dysfunctional despite maintaining viability. Devlin AC, Burr K, **Borooah S**, Foster JD, Cleary EM, Geti I, Vallier L, Shaw CE, Chandran S, Miles GB. Nat Communications 2015 Jan 12;6:5999.

Real-time quantitative monitoring of hiPSC-based model of macular degeneration on Electric Cell-substrate Impedance Sensing microelectrodes. Gamal W, **Borooah S**,* Smith S, Underwood I, Srsen V, Chandran S, Bagnaninchi PO, Dhillon B. Biosensors and Bioelectronics 2015 Sep 15;71:445-55.

*Joint first author